

Electronic Thesis and Dissertation Repository

8-19-2013 12:00 AM

High density gas-solids circulating fluidized bed riser and downer reactors

Chengxiu Wang, *The University of Western Ontario*

Supervisor: Dr. Jesse Zhu, *The University of Western Ontario*

Joint Supervisor: Dr. Shahzad Barghi, *The University of Western Ontario*

A thesis submitted in partial fulfillment of the requirements for the Doctor of Philosophy degree in Chemical and Biochemical Engineering

© Chengxiu Wang 2013

Follow this and additional works at: <https://ir.lib.uwo.ca/etd>

 Part of the [Catalysis and Reaction Engineering Commons](#), [Petroleum Engineering Commons](#), and the [Transport Phenomena Commons](#)

Recommended Citation

Wang, Chengxiu, "High density gas-solids circulating fluidized bed riser and downer reactors" (2013). *Electronic Thesis and Dissertation Repository*. 1572.
<https://ir.lib.uwo.ca/etd/1572>

This Dissertation/Thesis is brought to you for free and open access by Scholarship@Western. It has been accepted for inclusion in Electronic Thesis and Dissertation Repository by an authorized administrator of Scholarship@Western. For more information, please contact wlsadmin@uwo.ca.

HIGH-DENSITY GAS-SOLIDS CIRCULATING FLUIDIZED BED RISER AND
DOWNER REACTORS

(Thesis Format: Integrated-Article)

By

Chengxiu Wang

Graduate Program in Chemical and Biochemical Engineering

A thesis submitted in partial fulfillment
of the requirements for the degree of
Doctor of Philosophy

The School of Graduate and Postdoctoral Studies

The University of Western Ontario

London, Ontario, Canada

© C. Wang 2013

ABSTRACT

A systematic and comprehensive study of hydrodynamics and reactor performance was conducted in a 76 mm i.d., 10 m high riser and a 76 mm i.d., 5.8 m high downer reactor under high density/flux operating conditions using fluid catalytic cracking (FCC) catalyst particles. An optical fiber probe was used to obtain a complete mapping of local solids holdup and particle velocity. Catalytic ozone decomposition reaction was employed to study the characteristics of reactor performance in the CFB riser and downer. The superficial gas velocity (U_g) and the solids circulation rate (G_s) were 3-9 m/s and 100-1000 kg/m²·s, respectively. Based on the spatial distributions of catalyst particles and gas reactant in the riser and the downer, hydrodynamics and reactor performance were fully characterized.

Solids suspension having a solids holdup of up to 0.2-0.3 could be maintained throughout the entire high flux/density riser. A homogenous axial flow structure was observed at $G_s = 1000$ kg/m²·s. When G_s exceeded about 800 kg/m²·s, the axial profile of the particle velocity became more uniform. The axial particle velocity was affected more significantly by high superficial gas velocity especially under high solids flux/density conditions. No net downward flow near the wall was one of the most important advantages of the high flux/density riser over the conventional low flux/density reactor, leading to a reduction of solids backmixing. Radial distributions of the solids holdup were nonuniform with a dilute region and a dense region. When G_s was higher than 700 kg/m²·s, the dilute core region shrank to less than 20% of the cross-sectional area. Solids holdups thereafter increased monotonically towards the wall which could be up to 0.59. Moreover, solids holdup remained higher than 0.4 over a wide cross-sectional area ($r/R = 0.7-1.0$, about 60% of the cross-sectional area) even at the top section of the riser. Radial distribution of solids holdup in the downer was much more uniform than that in the riser. Radial profiles of solids holdup were characterized by a flat value covering a wide region of the cross section and a relatively high value near the wall in the fully developed section. The uniform distribution of solids flow provided a nearly plug flow condition in the downer reactor.

As to the ozone reaction in the CFB system, the axial and radial profiles of the ozone

concentration were consistent with the corresponding profiles of the solids holdups which indicated that ozone reaction in the CFB reactors was controlled by the gas-solids flow structure. Strong interrelation was observed between the distributions of solids and reactant concentration. Higher solids holdups would give higher ozone conversions. Most conversion occurred in the entrance region, that is, the flow developing zone of the riser and downer reactors. Overall ozone conversions in CFB riser and downer deviated from plug-flow behavior indicating that hydrodynamics affected CFB reactor performance. The extent of the deviation of the conversion could be attributed to the different gas-solids contacting efficiency.

Keywords: Circulating fluidized bed riser/downer, high density, high flux, hydrodynamics, reactor performance, catalytic ozone decomposition, solids holdup, particle velocity, solids flux

CO-AUTHORSHIP

Chapter 4: Hydrodynamics in a high density CFB riser-Solids holdup and flow development

Authors: Chengxiu Wang, Jesse Zhu, Shahzad Barghi, and Chunyi Li

Chengxiu Wang carried out the experiments and data analysis under the guidance of Dr. J. Zhu and Dr. S. Barghi and in consultation with Dr. C. Li. All experimental work was conducted by Chengxiu Wang and the draft of this manuscript was written by Chengxiu Wang. Revisions were carried out under the close supervision of three advisors, Drs. J. Zhu, S. Barghi and Dr. C. Li. The final version was submitted to AIChE Journal.

Chapter 5: Hydrodynamics in a high density CFB riser-Particle velocity and solids flux

Authors: Chengxiu Wang, Jesse Zhu, Shahzad Barghi and Chunyi Li

Chengxiu Wang carried out the experiments and data analysis under the guidance of Dr. J. Zhu and Dr. S. Barghi and in consultation with Dr. C. Li. All experimental work was conducted by Chengxiu Wang and the draft of this manuscript was written by Chengxiu Wang. Revisions were carried out under the close supervision of three advisors, Drs. J. Zhu, S. Barghi and Dr. C. Li. The final version was submitted to the journal Chemical Engineering Science.

Chapter 6: Hydrodynamics in a high flux CFB downer

Authors: Chengxiu Wang, Shahzad Barghi, Jesse Zhu and Chunyi Li

Chengxiu Wang carried out the experiments and data analysis under the guidance of Dr. J. Zhu, Dr. S. Barghi and in consultation with Dr. C. Li. All experimental work was conducted by Chengxiu Wang and the draft of this manuscript was written by Chengxiu Wang. Revisions were carried out under the close supervision of three advisors, Drs. J. Zhu, S. Barghi and C. Li. The final version is ready for submission to Chemical Engineering Journal.

Chapter 7: Catalytic ozone decomposition in a high density gas-solids CFB riser

Authors: Chengxiu Wang, Gang Wang, Shahzad Barghi and Jesse Zhu

Chengxiu Wang carried out the experiments and data analysis under the guidance of two advisors, Dr. J. Zhu and Dr. S. Barghi. Dr. G. Wang assisted in some key experimental work. All experimental work was conducted by Chengxiu Wang and the draft of this manuscript was written by Chengxiu Wang. Revisions were carried out under the close supervision of two advisors, Drs. J. Zhu and S. Barghi. The final version is ready for submission to the journal Chemical Engineering Science.

Chapter 8: Catalytic ozone decomposition in a high flux gas-solids CFB downer

Authors: Chengxiu Wang, Shahzad Barghi and Jesse Zhu

Chengxiu Wang carried out the experiments and data analysis under the guidance of two advisors, Dr. J. Zhu and Dr. S. Barghi. All experimental work was conducted by Chengxiu Wang and the draft of this manuscript was written by Chengxiu Wang. Revisions were carried out under the close supervision of two advisors, Drs. J. Zhu and S. Barghi. The final version is ready for submission to Chemical Engineering Journal.

DEDICATION

This work is dedicated to my maternal grandparents and my mother.

献词

此文献给我的外祖父母和母亲

ACKNOWLEDGEMENT

The completion of this degree would not have been possible if it were not for those people who truly believed in my potential and provided me with opportunities; who landed help whenever I needed; and who unconditionally supported me. I would like to thank the many people, supervisors, instructors, family and friends, who helped me to reach this level of achievement.

I would like to express my deepest gratefulness to my chief supervisor Dr. Jesse Zhu for his encouragement, guidance, inspiration and continuous support throughout this endeavor. He encouraged me and challenged me every step of the way, professionally and personally, allowing for my own developments. His meticulous supervision not only ensured the successful fulfillment of this study but also brought great improvement to my comprehensive skills, which is invaluable for me to enjoy forever.

Much appreciation is extended to my co-supervisor Dr. Shahzad Barghi for his helpful guidance, constructive suggestions, kind encouragement during the progress of this work, generous timely support and for carefully going through the manuscripts and making the text more readable.

My special thank you is directed to Dr. Chunyi Li, my co-supervisor on China size, at China University of Petroleum, for his inspirational knowledge and providing me this excellent opportunity for coming to Canada to complete my degree. Many thanks also go to his wife Mrs. Guifen Yin for her great help during those years when I was in China.

I would like to thank Mr. Jianzhang Wen and Mr. Michael Zhu for their help in maintaining the experimental unit, and visiting professor Gang Wang for his help with some of the ozone decomposition tests. Thanks go to George Zhang, Joanna Blom, April Finkenhoefer, Kristen Hunt, Lisa Desalaiz, Mike Gaylard, Clayton Cook for their help and supports.

Thanks are also extended to my friends in the research group, Nathan Qi, Dongbing Li, Jing Xu, Long Sang, Danni Bao, Jingsi Yang, Jing Fu, Aiwei Nie, Yuanyuan Zhang, Anon Chuachuensuk, Na Zhao, Shan Gao, Jingwei Zhang, Max Wang and Louisa Wang for all the fun,

support and fond memories throughout the years. My experience in the lab was greatly enhanced through our interactions. Thanks also go to all members of the research group, Mrs. Ying Ma, Dr. Hui Zhang, the visiting professor, Dr. Hong Chen and many others for all the help, advice and friendship.

I would like to express my most sincere gratitude to my friends Ms. Huan Gao in the Department of Statistical and Actuarial Sciences, Western University and Mr. Guangbin Sun in the School of Computer Science, Carnegie Mellon University, for their invaluable encouragement and unconditional support throughout these years of sacrifice and hard work.

Finally, I want to thank my parents, who provided not only wonderful examples of hard work, but without your dedication in my education all these would not be possible.

TABLE OF CONTENTS

ABSTRACT.....	ii
CO-AUTHORSHIP	iv
DEDICATION.....	vi
ACKNOWLEDGEMENT	vii
TABLE OF CONTENTS.....	ix
LIST OF TABLES.....	xvi
LIST OF FIGURES	xvii
CHAPTER 1 Introduction.....	1
1.1 Background.....	1
1.2 Research objectives.....	4
1.3 Thesis structure	4
References.....	6
CHAPTER 2 Literature Review	9
2.1 Introduction.....	9
2.2 Hydrodynamics in CFB riser	11
2.2.1 Axial profiles of solids concentration	12
2.2.2 Radial profiles of solids concentration and particle velocity.....	15
2.3 Effects on the flow structure	18
2.3.1 Entrance and exit effect	18

2.3.2 Scale-up effect	18
2.3.3 Riser geometry effect	19
2.4 Hydrodynamics in CFB downer	20
2.4.1 Three-section axial flow structure	22
2.4.2 Radial gas and solids flow structure	24
2.5 Ozone decomposition in CFB reactors	31
2.5.1 Experimental researches with ozone decomposition	31
2.5.2 Ozone decomposition in the CFB riser reactor	35
2.5.3 Ozone decomposition in the CFB downer reactor	38
2.5.4 Contact efficiency of ozone decomposition reaction	41
2.6 Conclusions and outlook	43
Nomenclature	45
References	47
CHAPTER 3 Experimental Setup and Measurement Techniques	54
3.1 Experimental setup	54
3.2 Preparation of particles	57
3.3 Measurements of U_g and G_s	60
3.3.1 Measurement of superficial gas velocity	60
3.3.2 Measurement of solids circulation rate	60
3.4 Measurement of pressure drop	61

3.5 Measurement of solids holdup and particle velocity	63
3.6 Measurement of ozone concentration	67
3.6.1 Ozone generation	67
3.6.2 Ozone sampling	70
3.6.3 Ozone testing	71
3.6 Summary	73
Nomenclature	74
References	76
CHAPTER 4 Hydrodynamics in a HDCFB Riser-Solids Holdup and Flow Development	78
4.1 Introduction	78
4.2 Experimental details	81
4.2.1 CFB experimental setup	81
4.2.2 Measurements of solids holdup	83
4.3 Results and discussion	87
4.3.1 Achieving high flux/density operating conditions in CFB riser	87
4.3.2 Axial profiles of solids holdup	90
4.3.3 Radial profiles of solids holdup	93
4.3.4 Flow development of solids holdup	96
4.3.5 Flow fluctuation in the high flux/density riser	101
4.4 Conclusions	104

Nomenclature.....	105
References.....	106
CHAPTER 5 Hydrodynamics in a HDCFB Riser-Particle Velocity and Solids Flux.....	109
5.1 Introduction.....	109
5.2 Experimental details.....	111
5.2.1 CFB experimental setup.....	111
5.2.2 Measurements of solids holdup and particle velocity.....	114
5.3 Results and discussion	118
5.3.1 Axial profiles of cross-sectional average particle velocity	118
5.3.2 Radial profiles of particle velocity.....	120
5.3.3 Flow development profiles of solids flux	126
5.3.4 Relationship between solids holdup, particle velocity and solids flux	131
5.4 Conclusions.....	139
Nomenclature.....	140
References.....	141
CHAPTER 6 Hydrodynamics in a High Flux CFB Downer	144
6.1 Introduction.....	144
6.2 Experimental details.....	145
6.2.1 CFB experimental setup.....	145
6.2.2 Measurements of solids holdup and particle velocity.....	148

6.3 Results and discussion	152
6.3.1 Radial profiles of solids flow	152
6.3.2 Development of solids flow	159
6.3.3 Axial profiles of solids flow	163
6.4 Conclusion	167
Nomenclature	168
References	170
CHAPTER 7 Catalytic Ozone Decomposition in a High Density CFB Riser	173
7.1 Introduction	173
7.2 Experimental details	175
7.2.1 CFB experimental setup	175
7.2.2 Measurements of solids holdup	178
7.2.3 Catalyst preparation	179
7.2.4 Ozone generation and testing	180
7.3 Results and discussion	183
7.3.1 Axial and radial profiles of ozone concentration	183
7.3.2 Effect of operating conditions on ozone concentration	189
7.3.3 Relationship between ozone concentration and solids holdup	191
7.3.4 Performance of the CFB reactor	193
7.4 Conclusions	195

Nomenclature.....	196
References.....	197
CHAPTER 8 Catalytic Ozone Decomposition in a High Flux Gas-solids CFB Downer	200
8.1 Introduction.....	200
8.2 Experimental details.....	202
8.2.1 CFB experimental system.....	202
8.2.2 Measurements of solids holdup	204
8.2.3 Catalyst preparation	206
8.2.4 Ozone generation and testing.....	207
8.3 Results and discussion	210
8.3.1 Radial profiles of ozone concentration	210
8.3.2 Axial profiles of ozone concentration.....	211
8.3.3 Effect of operating conditions on ozone concentration	215
8.3.4 Relationship between solids holdup and ozone concentration	217
8.3.5 Reactor performance.....	219
8.4 Conclusions.....	221
Nomenclature.....	222
References.....	224
CHAPTER 9 Conclusions and Recommendations.....	228
9.1 Summary comments on experimental setup and measurements.....	228

9.2 Conclusions.....	230
9.3 Recommendations.....	234
Appendix 1. Raw data of solids holdup, particle velocity, and solids flux in the CFB riser	236
Appendix 2. Raw data of solids holdup, particle velocity and solids flux in the CFB downer ..	256
Appendix 3. Raw data of ozone concentration in the CFB riser	265
Appendix 4. Raw data of ozone concentration in the CFB downer.....	271
Curriculum Vitae	273

LIST OF TABLES

Table 2.1	Studies of fluidized bed reaction by using ozone decomposition. (part 1)	33
Table 2.2	Studies of fluidized bed reaction by using ozone decomposition. (part 2)	34
Table 3.1	Locations of pressure taps	62
Table 3.2	Test results for ozone generator performance	68
Table 4.1	Size distribution of the FCC particles.....	83
Table 5.1	Size distribution of the FCC particles.....	113
Table 6.1	Size distribution of the FCC particles.....	147
Table 7.1	Size distribution of the FCC particles.....	180
Table 8.1	Size distribution of the FCC particles.....	207

LIST OF FIGURES

Figure 2.1 Typical schematic of circulating fluidized bed riser (Zhu, 2005).....	12
Figure 2.2 Typical solids holdup profile (Zhu, 2005).....	13
Figure 2.3 Typical axial profiles of solids holdup for FCC particles (Issangya <i>et al.</i> , 1999).....	14
Figure 2.4 Schematic profile of radial solids flow structure (Bai <i>et al.</i> , 1995)	15
Figure 2.5 Radial solids holdup profile (Pärssinen and Zhu, 2001a)	16
Figure 2.6 Radial particle velocity profiles (Pärssinen and Zhu, 2001b)	17
Figure 2.7 Conceptual of circulating fluidized bed downer	21
Figure 2.8 Axial gas-solids flow structure in the downer (Zhu, 2005).....	22
Figure 2.9 Axial distribution of pressure (Wang <i>et al.</i> , 1992).....	23
Figure 2.10 Radial profiles of particle velocity and gas velocity in the downer and riser (Zhu <i>et al.</i> , 1999).....	24
Figure 2.11 Radial distribution of solids holdup in the downer and the riser (Zhu <i>et al.</i> , 1999)	25
Figure 2.12 Radial profiles along the riser and downer under different operating.....	27
Figure 2.13 Radial flow structures in CFB riser and downer (Bi and Zhu, 1993)	28
Figure 2.14 Effect of solids circulation rates and superficial gas velocity on the lengths of radial flow development for the riser and the downer. (Zhang <i>et al.</i> , 2001)	29
Figure 2.15 Axial ozone concentration profile (Ouyang <i>et al.</i> , 1993 and 1995).....	35
Figure 2.16 Axial profile of solids holdup in the riser (Ouyang <i>et al.</i> , 1995)	36
Figure 2.17 Radial profiles of ozone concentration in the riser reactor (Ouyang <i>et al.</i> , 1995) ...	37

Figure 2.18 Axial ozone conversion profiles in the riser (Schoenfelder <i>et al.</i> , 1996).....	38
Figure 2.19 Ozone conversions in CFB downer (Fan <i>et al.</i> , 2008).....	39
Figure 2.20 Axial profiles of solids holdup in the riser and (Zhang <i>et al.</i> , 1999)	40
Figure 2.21 Radial profiles of solids holdup in riser and downer (Zhang <i>et al.</i> , 1999).....	41
Figure 2.22 Contact efficiency as a function of Damköhler number.....	42
Figure 3.1 Schematic diagram of the multifunctional CFB system.....	55
Figure 3.2 Particles activation process.	57
Figure 3.3 SEM images of original and impregnated SFCC particles at $\times 500$ magnification. ..	58
Figure 3.4 Particles size distribution of FCC particles.	59
Figure 3.5 Schematic diagram of the novel optical fiber probe and its working principle.	63
Figure 3.6 Schematic diagram of the apparatus for solids concentration calibration of optical..... fiber probes.	64
Figure 3.7 Solids holdup calibration curve of the optical fiber probe for FCC catalyst particles	65
Figure 3.8 Stability of the inlet ozone concentration against time.	69
Figure 3.9 Ozone sampling and testing.	70
Figure 3.10 Schematic diagram of TEI 49i ozone analyzer.	72
Figure 4.1 Schematic diagram of the multifunctional CFB system.....	81
Figure 4.2 Schematic diagram of the novel optical fiber probe and its working principle.	85
Figure 4.3 Characteristics of flow structure under extremely high flux/density in a CFB riser..	87
Figure 4.4 Axial solids holdup distribution for various operating conditions.....	90

Figure 4.5 Comparison of local solids holdup profiles in a CFB riser under different operating ... conditions.....	93
Figure 4.6 Radial solids holdup distribution for various operating conditions.	95
Figure 4.7 Overall view of the solids hold up under different operating conditions.....	97
Figure 4.8 Solids holdup distribution in different radial regions for various operating conditions	98
Figure 4.9 RNI's of solids holdup the riser under different operating conditions.....	100
Figure 4.10 Radial profiles of local solids holdup, standard deviation and intermittency indices .. along the riser under different operating conditions.....	102
Figure 5.1 Schematic diagram of the multifunctional CFB system.....	111
Figure 5.2 Schematic diagram of the novel optical fiber probe and its working principle.	114
Figure 5.3 Axial profiles of average particle velocity and corresponding solids holdup	118
Figure 5.4 Radial profiles of particle velocity and corresponding solids holdup.	120
Figure 5.5 Radial particle velocity distribution for various operating conditions.....	121
Figure 5.6 Development of radial profiles of local particle velocities.	122
Figure 5.7 RNI's of particle velocity the riser under different operating conditions.	124
Figure 5.8 Variation of RNI (V_p) with (a) reduced centerline particle velocity and (b) reduced wall particle velocity in the riser at different operating conditions.....	125
Figure 5.9 Radial profiles of local solids flux under different operating conditions.....	126
Figure 5.10 Typical radial profile of solids flux under low and high flux/density.....	128
Figure 5.11 Radial profiles of (a) solids holdup, (b) particle velocity, and (c) solids flux.....	131
Figure 5.12 Relationship between solids holdup and particle velocity under low and	133

Figure 5.13 Relationship between solids holdup and particle velocity in the three axial.....	134
Figure 5.14 Relationship between cross-sectional average solids holdup and particle velocity	136
Figure 5.15 Relationship between cross-sectional average solids holdup and particle	137
Figure 6.1 Schematic diagram of the multifunctional CFB system.....	145
Figure 6.2 Schematic diagram of the novel optical fiber probe and its working principle.	149
Figure 6.3 Radial profiles of solids holdup along the downer under different.....	152
Figure 6.4 Overview of solids holdup along the downer under different.....	153
Figure 6.5 Radial profiles of particle velocity along the downer under different	155
Figure 6.6 Overview of particle velocity along the downer under different	156
Figure 6.7 Radial profiles of solids flux along the downer under different.....	157
Figure 6.8 Overview of solids flux along the downer under different	158
Figure 6.9 Axial development of radial solids holdup along the downer under.....	159
Figure 6.10 Axial development of $RNI(\varepsilon_s)$ along the downer under	161
Figure 6.11 Axial profiles of cross-sectional mean solids holdup along the downer	163
Figure 6.12 Axial profiles of cross-sectional mean particle velocity along the downer	165
Figure 7.1 Schematic diagram of the multifunctional CFB and ozone testing system.....	175
Figure 7.2 Schematic diagram of the novel optical fiber probe and its working principle.	177
Figure 7.3 Axial distributions of the average dimensionless ozone concentration	183
Figure 7.4 Axial distributions of the dimensionless ozone concentration and the corresponding .. solids holdup at different radial positions.....	185
Figure 7.5 Radial distributions of the average dimensionless ozone concentration.....	186

Figure 7.6 Overall view of the dimensionless ozone concentration under different operating conditions.....	187
Figure 7.7 The effect of solids circulation rate on the local dimensionless ozone concentration. ..	189
Figure 7.8 The effect of superficial gas velocity on the local dimensionless ozone concentration.	190
Figure 7.9 Relationship between the conversion and solids holdup.....	191
Figure 7.10 Effects of Damköhler number on overall ozone conversion.....	193
Figure 8.1 Schematic diagram of the multifunctional CFB and ozone testing system.....	202
Figure 8.2 Schematic diagram of the novel optical fiber probe and its working principle.	204
Figure 8.3 Radial profiles of dimensionless ozone concentration and the corresponding solids holdup.	210
Figure 8.4 Axial profiles of the average dimensionless ozone concentration and the corresponding solids holdup.	211
Figure 8.5 Axial profiles of dimensionless ozone concentration and the corresponding solids holdup at different radial positions.	213
Figure 8.6 Overall view of the dimensionless ozone concentration and the corresponding solids holdup at different operating conditions.....	214
Figure 8.7 Effects of superficial gas velocity on the dimensionless ozone concentration.	215
Figure 8.8 Effects of solids circulation rate on the dimensionless ozone concentration.	216
Figure 8.9 Relationship between overall ozone conversion and solids holdup.....	217
Figure 8.10 Effects of Damköhler number on overall ozone conversion.....	219

CHAPTER 1

Introduction

Hydrodynamics and reactor performance of high solids flux/density gas-solids circulating fluidized bed riser and downer reactors are studied in this work. An introduction to the research background, objectives and thesis structure are presented in this chapter.

1.1 Background

Many chemical processes such as combustion, Fischer-Tropsch synthesis, partial oxidation, and fluid-catalytic cracking (FCC) have been utilizing gas-solids fluidized bed reactors (Bi and Fan, 1992 and Zhu and Cheng, 2005). The reactor performance is influenced both by the hydrodynamics and the chemical reaction itself. Fluidization occurs when a gas is forced to flow vertically through a bed of particles at such a rate that buoyancy of the particles is completely supported by the drag force imposed by the gas (Zhu and Cheng, 2005). With increasing gas velocity, the bed behaviors are changed. There are at least six different fluidization regimes: particulate fluidization, bubbling fluidization, turbulent fluidization, slugging fluidization, fast fluidization, and pneumatic transport (Zenz, 1949; Yerushalmi *et al.*, 1976; Grace, 1986; Hirama, 1992 and Lim *et al.*, 1995). The bubbling and turbulent fluidization are collectively considered as low-velocity or conventional fluidization.

When the superficial gas velocity is increased beyond a critical value (Bi *et al.*, 1995), significant amount of particles will be entrained. The entrained solid particles must be replaced or the bed empties rapidly. A circulating fluidized bed (CFB) system is often used to maintain continuous operation, with gas-solids separation devices capturing the solids and returning them to the bottom of the reactor (often called riser) via a return system (standpipe or downcomer).

The commercial interest in CFB technology can be dated back to the 1940s, when the fluid catalytic cracking (FCC) process was first developed (Squires, 1986 and Grace, 1990). However, due to low catalyst reactivity and other technical difficulties, it was not until the 1970s when high velocity fluidized bed or CFB technology was “re-invented” (Yerushalmi *et al.*, 1976). CFB

riser reactors provide many advantages over conventional bed reactors such as higher gas-solids contacting efficiency, reduced axial dispersion for both gas and solids and higher gas/solids throughput (Berruti *et al.*, 1995 and Zhu *et al.*, 1995). On the other hand, a CFB riser still suffers from severe solids backmixing, macro segregations of gas and solids due to the non-uniform flow structure in axial and radial directions, and micro segregations caused by particle clustering. Resulting from both gas and solids flowing against gravity (Zhu *et al.*, 1995), these drawbacks reduce gas-solids contacting efficiency and lead to undesired distribution of products due to the reduced selectivity.

The disadvantages of the riser reactor caused by the hydrodynamic effects could be overcome in a new type of reactor, a CFB downer reactor (Zhu *et al.*, 1995; Bai *et al.*, 1995 and Wei and Zhu, 1996), where gas and solids flow co-currently downward, in the same direction with gravity.

In a CFB downer, particles accelerate much more quickly since they gain momentum from both the gas and gravity. Hydrodynamic studies show that the radial distribution of flow parameters such as solids holdup and particle velocity in CFB downers is more uniform than those in the CFB risers (Wei *et al.*, 1994; Zhang, 1999 and Qi *et al.*, 2008). This radial uniformity leads to nearly plug flow for both phases in the downer (Zhang, 1999 and Manyele *et al.*, 2003). With reduced axial dispersion and more uniform gas and solids residence times, CFB downer reactors become more advantageous over CFB riser reactors for reactions requiring short residence times (Wei and Zhu, 1996), especially where intermediates are the desired products, for example, fluid catalytic cracking process of heavy oil (Zhu *et al.*, 1995 and Zhang *et al.*, 1999).

In spite of the numerous advantages of the high gas velocity riser and downer reactors, a common shortcoming of the two types of reactors is the low volumetric concentration (holdup) of solids. Conventional fluidized beds are also called dense phase fluidized beds, while circulating fluidized beds are regarded as dilute phase fluidized beds. Typically, a conventional fluidized bed operates with an average solids holdup of 30%-50%. A riser, on the other hand, only contains 1-3% solids by volume in the fully developed region. The solids holdups achieved in downers as shown by the previous studies (Jin *et al.*, 1997; Herbert, 1998 and Wirth and Schiewe, 1998) are much lower (mostly below 1%). This represents a serious problem for

reactions where a high solids/gas ratio is required, since the reaction intensity is limited by the lower solids concentration. To overcome this weakness, Bi and Zhu (1993) proposed the concept of the high density circulating fluidized bed (HDCFB) riser. Subsequent studies on HDCFB have shown that solids holdups as high as 25% can be achieved in such a unit (Issangya *et al.*, 1997-2000 and Pärssinen *et al.*, 2001) with carefully controlled operation. However, few attempts have been made to achieve high flux/density in a cocurrent downflow system. Therefore, there is an urgent need to study the characteristics of the downer operating at high density/flux for understanding the flow mechanics and increasing its industrial applications.

Previous research works and practical applications have demonstrated that the CFB reactors could work with high efficiency under a very wide range of operating conditions, and hydrodynamics behavior which can significantly affect the performance of the reactors, e.g. mass and heat transfer, extent of reaction, gas and solids residence time distribution and mixing. So understanding the hydrodynamics is of prime importance for design and scale-up of efficient commercial fluidization processes. On the other hand, a study of a chemical reaction in a fluidized bed can supply more direct information on reactor performance. Grace and Bi (1997) pointed out that to better understand mass and heat transfer characteristics in reactors, to optimize the reactor design, and to develop and verify reactor models, hot-model (with reactions) studies providing axial and radial reactant concentration profiles are necessary.

Among previous hot-model studies, ozone decomposition reaction, catalyzed by Fe_2O_3 has become a surrogate reaction for the characterization of gas-solids contact in CFB reactors (Kagawa *et al.*, 1990; Jiang *et al.*, 1990 and 1991; Bi *et al.*, 1992; Pagliolico *et al.*, 1992; Ouyang *et al.*, 1993; Ouyang *et al.*, 1995; Schoenfelder *et al.*, 1996; Bolland, 1998; Bolland and Nicolai, 2001; Fan *et al.*, 2008 and Li *et al.*, 2011 and 2013). This reaction requires low concentrations of reactant, detection is rapid and accurate, and there is a measurable reaction rate at ambient temperature and pressure (Syamlal and O'Brien, 2003). To the best of our knowledge, few studies (Jiang, *et al.*, 1990 and 1991; Ouyang *et al.*, 1993 and 1995; Fan *et al.*, 2008 and Li *et al.*, 2011 and 2013) reported on ozone decomposition in CFB reactors (usually less than $200 \text{ kg/m}^2\text{s}$ in risers and $100 \text{ kg/m}^2\text{s}$ in downers). Experiments should be conducted at a wide range of air velocities and high solids circulation rates.

1.2 Research objectives

To comprehensively study hydrodynamics at high density/flux conditions in circulating fluidized beds and to map profiles of radial and axial reactant concentrations for reactor design and model development, based on literature review of previous studies on both hydrodynamics and ozone decomposition in CFB reactors, the objectives of this study are:

To modify the experimental unit to further increase the solids circulation rate, enabling high density/flux operations in the riser and downer,

To obtain the axial/radial solids holdup and particle velocity profiles in the riser under a wide range of operating conditions especially at high density/flux conditions,

To obtain the axial/radial solids holdup and particle velocity profiles in the downer under a wide range of operating conditions especially at high density/flux conditions,

To obtain the axial/radial profiles of ozone concentration in the riser under a wide range of operating conditions especially at high density/flux conditions,

To obtain the axial/radial profiles of ozone concentration in the downer under a wide range of operating conditions especially at high density/flux conditions.

1.3 Thesis structure

This thesis follows the “Integrated-Article Format” as outlined in the UWO Thesis Regulation. Chapter 1 gives a general introduction followed by a detailed literature review in Chapter 2. Chapter 3 provides detailed descriptions on experimental setup, measurement techniques, and experimental procedures.

Chapter 4 describes the experimental results on solids holdup in the high density CFB riser. Radial and axial profiles of solids holdup under various operating conditions are presented. A comparison between the flow structures in low density and high density CFB risers is provided.

Chapter 5 describes the experimental results on particle velocity in the high density CFB riser. Radial and axial profiles of solids holdup under various operating conditions are presented. A comparison between the flow structures in low density and high density CFB risers is discussed. Correlation between particle velocity and solids flux against solids holdup is also studied at low and high solids flux/density conditions.

Chapter 6 describes the hydrodynamics in the downer reactor under high solids flux up to 300 kg/m²s. A comprehensive study of solids holdup, particle velocity and solids flux is presented.

Chapter 7 describes the experimental results from catalytic ozone decomposition in the high density/flux CFB riser. Radial and axial profiles of ozone concentration at various operating conditions are presented. Reactor performance is also discussed.

Chapter 8 describes the experimental results from catalytic ozone decomposition in the high density/flux CFB downer. Radial and axial profiles of ozone concentration at various operating conditions are presented. Reactor performance is also discussed.

Chapter 9 gives conclusions of this study and recommendations for future work.

References

- Bai D., Shibuya E., Masuda Y., Nishio K., Nakagawa N. and Kato K., (1995), Distinction between upward and downward flows in circulating fluidized beds, *Powder Technology* 84(1), 75-81
- Berruti F., Pugsley TS., Godfroy, L., Chaouki, J. and Patience, GS., (1995), Hydrodynamics of circulating fluidized bed risers, A review, *The Canadian Journal of Chemical Engineering* 73(5), 579-602
- Bi HT. and Fan LS., (1991), Regime transition in gas-solid circulating fluidized beds, Paper#101e presented at the AIChE Annual Meeting, Los Angeles, Nov, 17-22
- Bi HT. and Zhu JX., (1993), Static instability analysis of circulating fluidized beds and concept of high-density risers, *AIChE Journal* 39, 1272-1280
- Bolland O. and Nicolai R., (2001), Describing mass transfer in circulating fluidized beds by ozone decomposition, *Chemical Engineering Communications* 187(1), 1-21
- Fan C., Bi, X., Lin W. and Song W., (2008a), Mass transfer and reaction performance of the downer and its hydrodynamic explanation, *The Canadian Journal of Chemical Engineering* 86(3), 436-447
- Fan C., Zhang Y., Bi X., Song W., Lin W. and Luo L., (2008b), Evaluation of downer reactor performance by catalytic ozone decomposition, *Chemical Engineering Journal* 140(1-3), 539-554
- Grace JR., (1986), Contacting modes and behaviour classification of gas-solid and other two-phase suspension, *The Canadian Journal of Chemical Engineering* 64, 353-363
- Grace JR., (1990), High-velocity fluidized bed reactors, *Chemical Engineering Science* 45(8), 1953-1966
- Grace JR. and Bi H., (1997), Introduction to circulating fluidized beds, in *Circulating Fluidized Beds* (editor(s), Grace JR., Avidan AA. & Knowlton TM.), Engineering Foundation, New York, 1-19
- Herbert PM., Gauthier, TA., Briens, CL. and Bergougnou MA., (1998), Flow study of a 0.05 m diameter downflow circulating fluidized bed. *Powder Technology* 96, 255-261
- Hirama T., Takeuchi T., Chiba T., (1992), Regime classification of macroscopic gas-solid flow in a circulating fluidized-bed riser, *Powder Technology* 70, 215-222
- Issangya AS., Bai D., Grace JR., Lim KS., and Zhu J., (1997), Flow behaviour in the riser of high-density circulating fluidized bed, *AIChE Symposium Series* 93, 25-30
- Issangya AS., (1998), Flow dynamics in high density circulating fluidized beds. PhD., Diss. Univ. of British Columbia, Vancouver, BC

- Issangya AS., Bai D., Bi HT., Lim KS., Zhu J., and Grace JR., (1999), Suspension densities in a high-density circulating fluidized bed riser, *Chemical Engineering Science* 54, 5451-5460
- Issangya AS., Grace JR., Bai DR., Zhu JX., (2000), Further measurements of flow dynamics in a high-density circulating fluidized bed riser, *Powder Technology* 111, 104-113
- Jiang P., Bi HT., Jean RH. and Fan LS., (1991), Baffle effects on performance of catalytic circulating fluidized bed reactor, *AIChE Journal* 37(9), 1392-1400
- Jiang P., Inokuchi K., Jean RH., Bi H. and Fan LS., (1990), Ozone decomposition in a catalytic circulating fluidized bed reactor, in *Circulating Fluidized Bed Technology III* (editor(s), Basu P., Horio M. and Hasatani M.), Pergamon Press, Oxford, 557-562
- Jin Y., Zhu JX. and Yu Z. (1997), Novel configuration and variants, Chapter 16 in *Circulating fluidized beds* (Eds. Grace JR., Avidan AA. and Knowlton TM.) pp. 525-567, Blackie Academic and Professional, London
- Kagawa H., Mineo H., Yamazaki R. and Yoshida K., (1990), A gas-solid contacting model for fast fluidized bed, in *Circulating Fluidized Bed Technology III* (editor(s), Basu P., Horio M. and Hasatani M.), Pergamon Press, Oxford, 551-556
- Li DB., Zhu J., Ray MB. and Ray AK., (2011), Catalytic reaction in a circulating fluidized bed downer, Ozone decomposition, *Chemical Engineering Science* 66 (20), 4615-4623
- Li DB., Ray AK., Ray MB. and Zhu J., (2013), Catalytic reaction in a circulating fluidized bed riser, Ozone decomposition, *Powder Technology* 342(15), 65-73
- Lim KS., Zhu JX., and Grace JR., (1995), Hydrodynamics of gas fluidization, *Int. J. Multiphase Flow*, 21(Suppl.), 141-193
- Manyele SV., Zhu J. and Zhang H., (2003), Analysis of the microscopic flow structure of a CFB downer reactor using solids concentration signals, *International Journal of Chemical Reactor Engineering* 1, A55
- Ouyang S., Li XG. and Potter OE., (1995), Circulating fluidized bed as a catalytic reactor, experimental study, *AIChE Journal* 41(6), 1534-1542
- Ouyang S., Lin J. and Potter OE., (1993), Ozone decomposition in a 0.254 m diameter circulating fluidized bed reactor, *Powder Technology* 74(1), 73-78
- Pärssinen JH. and Zhu JX., (2001a), Axial and radial solids distribution in a long and high-flux CFB riser, *AIChE Journal* 47, 2197-2205
- Pärssinen JH. and Zhu JX., (2001b), Particle velocity and flow development in a long and high-flux circulating fluidized bed riser, *Chemical Engineering Science* 56, 5295-5303
- Pagliolico S., Tiprigan M., Rovero G. and Gianetto A., (1992), Pseudo-homogeneous approach to CFB reactor design, *Chemical Engineering Science* 47(9-11), 2269-2274

- Qi XB., Zhang H. and Zhu J., (2008), Friction between gas-solid flow and circulating fluidized bed downer wall, *Chemical Engineering Journal* 142(3), 318-326
- Schoenfelder H., Kruse M., and Werther J., (1996), Two-dimensional model for circulating fluidized-bed reactors, *AIChE Journal* 42(7), 1875-1888
- Squires AM., (1986), The story of fluid catalytic cracking, the first circulating fluid bed, in *Circulating Fluidized Bed Technology* (editor(s), Basu, P.), Pergamon Press, Toronto, 1-19
- Syamlal M. and O'Brien TJ., (2003), Fluid dynamic simulation of O₃ decomposition in a bubbling fluidized bed, *AIChE Journal* 49(11), 2793-2801
- Wei F. and Zhu JX., (1996), Effect of flow direction on axial solids dispersion in gas-solids cocurrent upflow and downflow systems, *The Chemical Engineering Journal and the Biochemical Engineering Journal* 64(3), 345-352
- Wirth KE. and Schiewe T. (1998), Flow structure in a downer reactor, in *Fluidization IX* (Eds. Fan LS. and Knowlton TM), pp 253-260, Eng. Foundation, New York
- Yerushalmi J., Turner DH. and Squires AM., (1976), The fast fluidized bed, *Ind. Eng. Chem., Proc. Des. Dev.* 15, 47-57
- Zhang H., Zhu JX. and Bergougnou MA., (1999), Flow development in a gas-solids downer fluidized bed, *The Canadian Journal of Chemical Engineering* 77(2), 194-198
- Zenz FA., (1949), Two-phase fluidized-solid flow, *Ind. Eng Chem.* 41, 2801-2806
- Zhu JX., Yu ZQ., Jin Y., Grace JR. and Issangya A., (1995), Cocurrent downflow circulating fluidized bed (downer) reactors-A state of the art review, *The Canadian Journal of Chemical Engineering* 73(5), 662-677
- Zhu JX. and Cheng Y., (2005), Fluidized-Bed Reactors and Applications, Chapter 5.3 in *Multiphase Flow Handbook*, ed. Clayton Crowe, CRC Press, New York, pp 5.55-5.93

CHAPTER 2

Literature Review

2.1 Introduction

Particulate technology has played an important role in many industrial processes such as chemical processing, mineral processing, pharmaceutical production and energy-related process, etc and in particular, gas-solids fluidization has been extensively employed in recent decades (Grace, 1990 and Zhu and Cheng 2005). Particles contained in a column can be fluidized when gas is introduced via a gas distributor at the bottom of the column. Different hydrodynamic regime can be observed depending on the particle characteristics and the magnitude of the superficial gas velocity. With increasing gas velocity, these flow regimes are fixed bed, bubbling fluidization, slugging fluidization, turbulent fluidization, fast fluidization and pneumatic conveying regimes. The bubbling, slugging and turbulent fluidization regimes are considered as conventional fluidization. The main characteristic of the conventional fluidized beds is that the beds operate at relatively low superficial gas velocity (usually less than 1-2 m/s) with little solids entrainment.

When the superficial gas velocity is increased beyond a critical superficial gas velocity U_{sc} , significant entrainment of particles occurs and the column empties very rapidly unless the entrained solids are replaced (Issangya, 1998). A circulating fluidized bed (CFB) is usually used to maintain continuous operation, with gas-solids separation devices (e.g. cyclones) capturing the entrained solids and returning them to the bottom of the bed through a standpipe and a seal, (e.g. mechanical or non-mechanical valves). A CFB system operating in the fast fluidization flow regime is called a fast fluidized bed (Liu, 2001). Circulating fluidized beds are divided into two types: riser type, in which gas and solids flow upward, and downer type in which the two phases flow downward (Wei and Zhu, 1996). Circulating fluidized bed (CFB) riser reactors have been used successfully for several years in processes where gas-solids contact and mass transfer are of significant importance. Examples are combustion of low-grade fuels, mineral processing, and fluid catalytic cracking, etc. (Reh, 1999).

CFB risers allow a continuous operation and offer advantages with respect to mass and heat transfers. The overall efficiency of a riser is improved when a uniform distribution of the solid particles is obtained. At high solids fluxes ($G_s > 200 \text{ kg/m}^2\text{s}$, operating conditions at which most of the FCC units are operated), radial uniformity is disturbed by lateral segregation and backmixing phenomena resulting in core-annulus flow structure. Moreover, axial segregation phenomenon results in a distinctive dilute zone in the upper part and a dense zone in the bottom part of the riser (Zhu and Cheng, 2005 and van engelandt *et al.*, 2007).

The disadvantages of the riser reactor caused by the hydrodynamic effects of both gas and solids flowing against gravity can be overcome in a new type of chemical reactor - downer reactor. As both phases flow downwards in the same direction as gravity, axial solids dispersion and the non-uniformity of radial gas and solid flow are reduced (Bai *et al.*, 1995; Bolkan *et al.*, 2003 and Luo *et al.*, 2007).

Compared to a riser reactor, a downer reactor has many advantages such as much more uniform gas-solids flow with less aggregation, less gas and solids backing mixing, and shorter residence time (Wei *et al.*, 1994; Zhang *et al.*, 1999; and Qi *et al.*, 2008). These characteristics are usually beneficial to the processes that require a short and uniform residence time distribution for gas and solid phases to decrease byproducts and overreacting. Downer reactors have therefore attracted many investigations in the past decade (Zhu *et al.*, 1995).

Experimental and measurement methods have been developed to study the hydrodynamic behavior in CFB riser and downer reactors, which are crucial for the understanding of the reactor performance. Although most of the experimental work has been devoted to hydrodynamic studies without reaction taking place in the system, which is called cold-model study, some hot-model studies with reactions in CFB reactors have been done in order to obtain the reactor performance directly. Catalytic propane dehydrogenation (Gascon *et al.*, 2005), cumene hydroperoxide decomposition (Huang *et al.*, 2002), ammoxidation of propane to acrylonitrile (Fakeeha *et al.*, 2000 and Wei *et al.*, 2001), catalytic oxidation-dehydrogenation of butane to butadiene (Huang *et al.*, 1999) chlorination of rutile (Zhou and Sohn, 1996), catalytic oxidation of n-butane to maleic anhydride (Pugsley *et al.*, 1992), and catalytic ozone decomposition

(Bolland, 1998; Schoenfelder *et al.*, 1996; Ouyang *et al.*, 1995; Kagawa *et al.*, 1990; Pagliolico *et al.*, 1992 and Jiang *et al.*, 1991) are some examples of reactions in circulating fluidized bed reactors. Ozone decomposition reaction is the most widely-adopted model reaction because it takes place at ambient temperature and is of first-order kinetic reaction.

An introduction to the hydrodynamic characteristics of the CFB reactors including riser and downer and the experimental research with regard to ozone decomposition in CFB reactors are presented in the next section.

2.2 Hydrodynamics in CFB riser

Circulating fluidized bed (CFB) riser reactors have been used for a wide range of industrial applications over the past 50 years (Grace, 1990 and Zhu and Cheng, 2005). In a CFB riser system as shown in Figure 2.1, solids must be continuously fed into the bed bottom and entrained out of the reactor by high velocity gas flow to maintain the required solids holdup. Solids captured at the top are sent back to the bottom of the riser via the recirculation system. Fast fluidization is achieved and most reactions take place in the riser reactors (Zhu and Cheng, 2005).

Comprehensive reviews on fast gas-solids fluidization were reported by Grace (1990) and Lim *et al.* (1995). In recent years, extensive studies continued on the aspects of CFB risers, including flow structure (Yan and Zhu, 2005; Huang *et al.*, 2007; Yan *et al.*, 2008), gas and solids mixing (Westphalen and Glicksman, 1995; Gayán *et al.*, 1997; Sterneus *et al.*, 2000; Namkung and Kim, 2000; Teplitskii *et al.*, 2006; Johansson *et al.*, 2007; Yan *et al.*, 2009; Zhang *et al.*, 2009), heat and mass transfer (Mansoori *et al.*, 2005; Breault, 2006; Breault and Guenther, 2009), chemical reaction (Lyngfelt and Leckner, 1999; Fakeeha *et al.*, 2000; Wei *et al.*, 2001; Huang *et al.*, 2002; Kersten *et al.*, 2003; Gascon *et al.*, 2005; Deng *et al.*, 2005; Hakimelahi *et al.*, 2006; Yin *et al.*, 2007; Liu *et al.*, 2008), and numerical simulations (Lu *et al.*, 2007; van de Velden *et al.*, 2007; van engelandt *et al.*, 2007; Wang *et al.*, 2009).

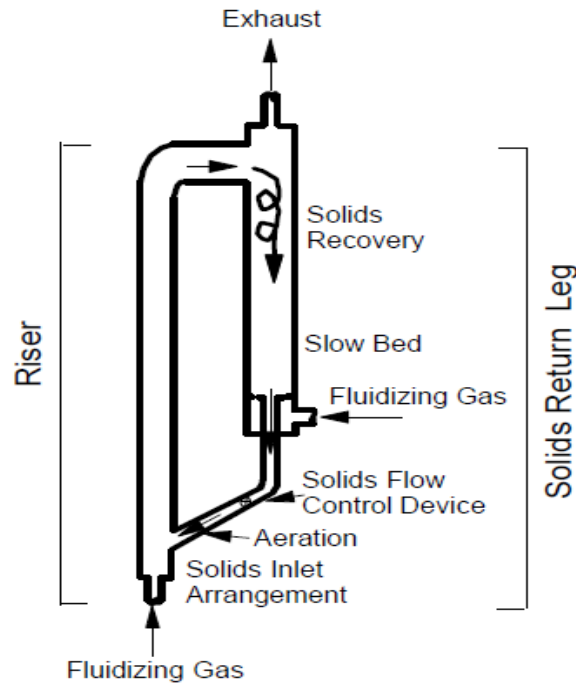


Figure 2.1 Typical schematic of circulating fluidized bed riser (Zhu, 2005)

Hydrodynamics are normally characterized by studies of solids holdup and gas and solids velocity. Knowledge of gas and solids distribution and flow behavior in CFB reactors is the key to successful design and operation of any CFB riser system as mass transfer, heat transfer, gas and solids interaction are often influenced by hydrodynamics (Grace, 1990).

2.2.1 Axial profiles of solids concentration

Previous studies demonstrate that there exists a dense phase at the bottom and a dilute phase at the top of the riser, which is called S-shape profile for bed voidage (Li and Kwauk, 1980; Schnitzlein and Weinstein, 1988 and Pärssinen and Zhu, 2001). With a transition section in-between, the riser may be divided into three regions, a dense region at the bottom portion, a dilute region at the top part and a transition between the two. From Figure 2.2, it is seen that there may be other profiles such as C-shape and exponential shape, mostly due to the entrance and exit effects as well as the operation conditions.

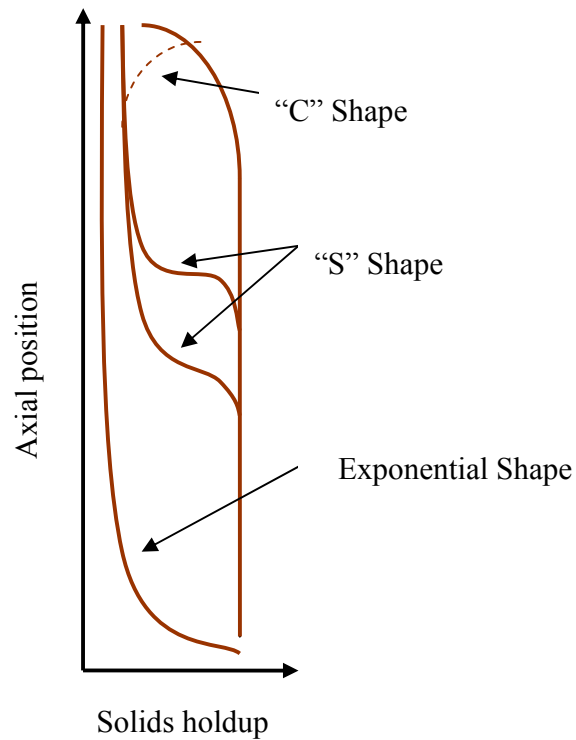


Figure 2.2 Typical solids holdup profile (Zhu, 2005)

In the exponential axial profile, the particles are being introduced into the riser and accelerated upwards by the fluidization gas very quickly to a certain point above the distributor, where the particle velocity becomes constant or to be more precise, the acceleration becomes negligible. A C-shape may be observed in a similar system with an abrupt exit. The S-shape profile is believed to be related to the high solids flux operation. Typical axial profiles in a CFB riser are shown in Figure 2.3.

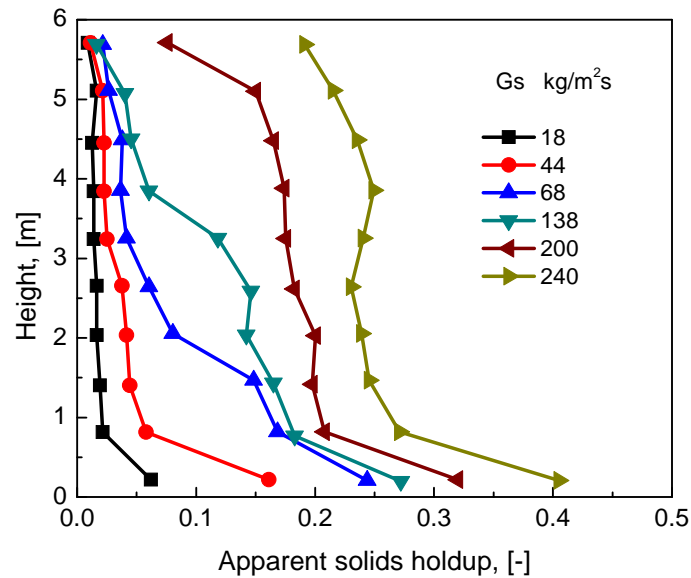


Figure 2.3 Typical axial profiles of solids holdup for FCC particles (Issangya *et al.*, 1999)

The axial voidage or holdup profile can be affected by many operating variables such as solids circulation rate, superficial gas velocity, bed diameter, particle properties, like density and size distribution, total solids inventory, solids inlet configuration, riser exit structure, secondary air injection and the solids reintroduction level into the riser. With a higher solids flux, a more dense bed can be observed and the transition region between the dense bed and dilute phase occurs higher up in the riser. The lower the solids flux, the less solids holdup exists in the riser. The superficial gas velocity also affects the solids holdup. With an increase in U_g , the solids holdup decreases, or inversely, the axial voidage increases. Increasing the bed diameter would result in a higher voidage and more uniformity. The coexistence of a bottom dense region and an upper dilute region characterizes the solids flow in a riser where the solids holdup in the dense phase zone ranges from 0.1 to 0.3, while the holdup profiles in the dilute region can be approximately 0.01 to 0.09 (Li and Kwauk, 1980, Schnitzlein and Weinstein, 1988, Pärssinen and Zhu, 2001).

There are several acceleration regions when the system is in a fast fluidization mode. The initial acceleration zone within the dense phase bottom is before the particles move somewhat constant and the second acceleration period shows up when the particles enter the dilute regime. Some

arguments based on the length of the second acceleration region make the particle velocity profile be controversial (Bai *et al.*, 1990). The experimental results that this second acceleration period is not very short but rather may extend well into the riser, while some particles may in fact still be accelerating at the top of the riser when they are forced to exit. Some experiments have shown that solids in fast fluidized beds are still in acceleration along most of the bed height, especially at low gas flow rate and high solids circulation rate (Bai *et al.*, 1990).

However, it has become widely accepted to assume the acceleration period to be very short (Bai *et al.*, 1990). This acceleration region in effect becomes the guideline to determine the transition between dense and dilute phases, since in the dense phase particle velocity is very low compared to the velocity in the dilute region. Bai *et al.* (1990) indicated that this acceleration zone may occupy from 1/3 to 2/3 of the riser height.

2.2.2 Radial profiles of solids concentration and particle velocity

A core-annular type radial solids flow with a dense particle layer in the wall region and a dilute core region is known to exist in the riser as shown in Figure 2.4.

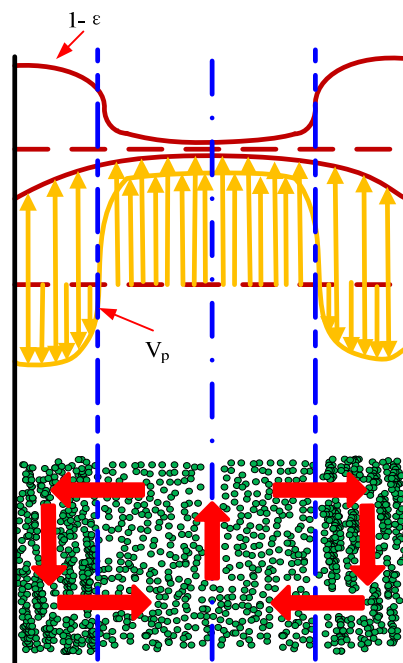


Figure 2.4 Schematic profile of radial solids flow structure (Bai *et al.*, 1988)

This can be described as a low density, high velocity gas-solids core region surrounded by slower moving or even downward flowing high solids concentration annular region (Bai *et al.*, 1995). Grace *et al.* (1997) suggested that particle exchanges occur between the dilute core and the dense wall region, as temporal and spatial accumulations of particles in the wall region form a transient dense particle layer or streamers. Non-uniform particle distributions or the presence of localized dense zones usually results from the existence of particle clusters and greatly influences the hydrodynamic characteristics of the system (Grace *et al.*, 1997).

Typical radial voidage profiles reported by Pärssinen and Zhu (2001b) are shown in Figure 2.5. A dilute central region and a denser wall region bed structures are observed. Solids holdup is seen to be low and relatively uniform in the central region up to about 70%-85% of the column radius, after which the solids concentration increases dramatically towards the wall, especially for the high solids flux conditions.

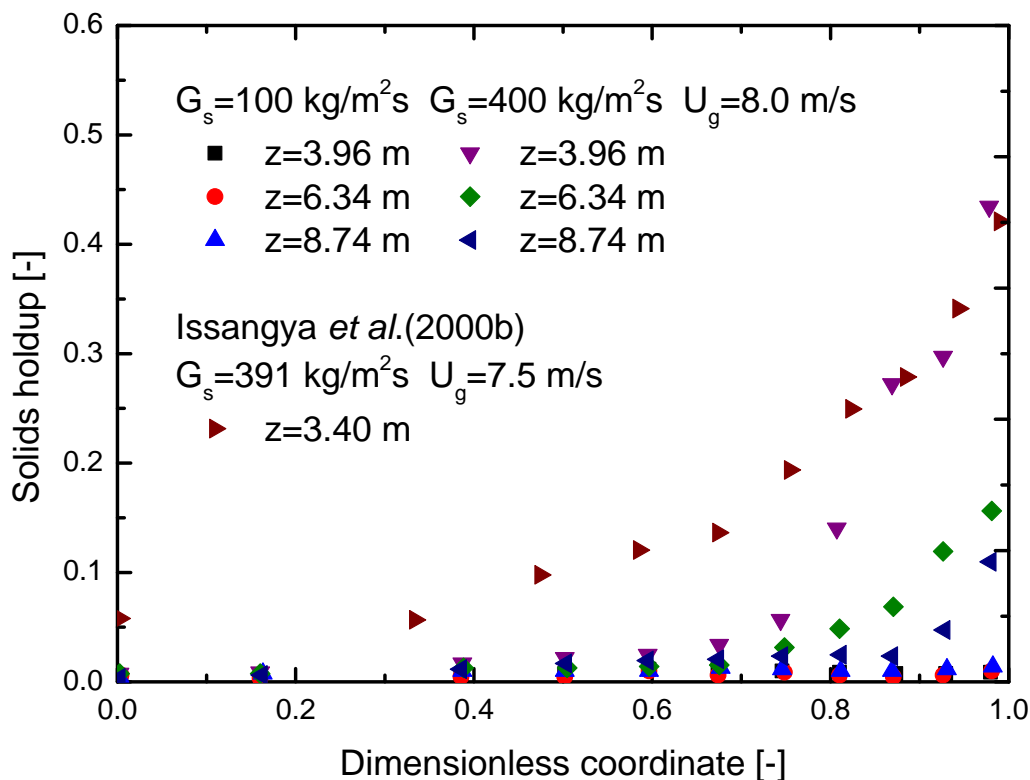


Figure 2.5 Radial solids holdup profile (Pärssinen and Zhu, 2001a)

Corresponding to the solids holdup profile, Pärssinen and Zhu (2001b) presented the particle velocity profile as seen in Figure 2.6. Particle velocities were directed upwards in the core of the column, with a magnitude similar to the superficial gas velocity at the column axis. The average velocity then fell as the radial position moves toward the wall, becoming negative in a layer adjacent to the wall. Ascending particles were dominant in the center of the column, whereas there were more descending than ascending particles near the wall. The magnitudes of the velocities of rising particles at the axis of the column were similar to the superficial gas velocity, while the magnitudes of downward velocities are significantly lower.

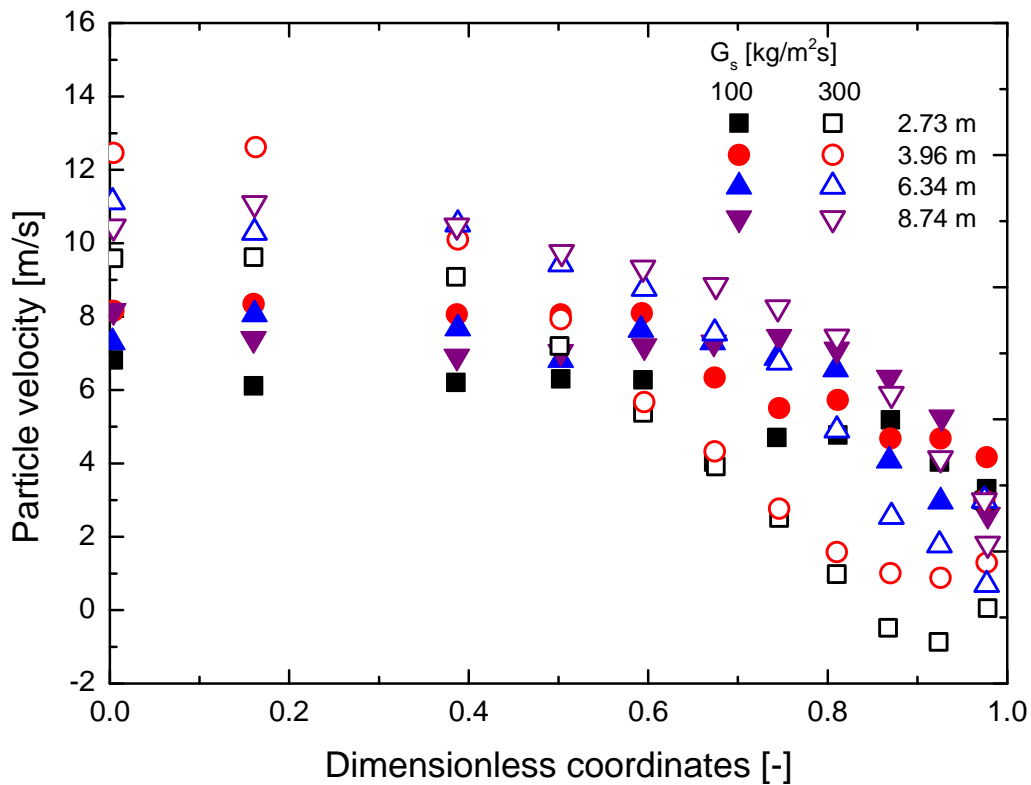


Figure 2.6 Radial particle velocity profiles (Pärssinen and Zhu, 2001b)

2.3 Effects on the flow structure

2.3.1 Entrance and exit effect

As mentioned earlier, the CFB riser, hydrodynamically, had featured by a high concentration of solids flowing near the wall with most of the gas passing through the core dilute region (Bai *et al.*, 1995). A uniform distribution of solids along the riser was of importance in the successful design of riser reactors (Yan *et al.*, 2008). Good understanding of the solids flow structure in riser reactors was critical for proper industrial design. It had been found that operating conditions (Bai *et al.*, 1992), inlet and outlet structures (Jin, 1988), and riser diameters (Yan and Zhu, 2004) impact the axial and radial solids distributions.

A large number of studies had examined the influence of entrance and exit geometry in CFB risers. Recent experimental results (Jin, 1988, Brereton and Grace, 1994, Gwyn, 1993, and Cheng *et al.*, 1998) demonstrated that the geometry of the riser exit could greatly influence the performance of CFBs, by affecting pressure and solids holdup profiles, not only close to the roof, but also at a considerable distance down the column. There were two types of exit configurations categorized as abrupt exit and smooth exit. With an abrupt exit, a relatively high solids concentration and a low particle velocity were observed, while with a smooth exit, the restriction to the solids flow was much less, and the dense suspension zone disappears. Reviews by Lim *et al.* (1995) concluded that the exit design could affect the density profile over several meters in the upper region of a riser. Bai *et al.* (1992) compared the influence exerted by different exit and inlet structures of fast fluidized beds on the axial voidage distribution. They reported that with a restrictive exit design, the voidage profile had a C-shape, while the profile was S-shape when a very weakly restrictive entrance structure was employed.

2.3.2 Scale-up effect

Although the experimental study in laboratory or pilot scale circulating fluidized bed had solved great number of issues encountered in the design and operation of CFB reactors, simplified the experimental work and reduced the expense on research, CFB application was still facing challenges in scale-up. Yerushalmi and Avidan (1985) suggested that the effect of the column

diameter on gas dispersion coefficient was probably more than linear for small-diameter tubes, approximately linear for medium-size columns, and less than linear for large risers. Their observations appeared to agree with the above cited results (Yerushalmi and Avidan, 1985) of change in the turbulent intensity as a function of d_p / l_e (l_e is length of turbulent eddies), under the assumption of l_e / D constant (Gore and Crowe, 1989). Yan and Zhu (2004) also studied the scale-up effect of riser reactors on the distributions of solids concentration, particle velocity and solids flux in a twin-riser CFB system with 0.076 and 0.203 m inner diameters. They concluded that the solids concentration increased with increasing riser diameter and the radial profiles of the solids concentration were steeper with larger-diameter risers. It had also been found that the cross-sectional average particle velocity was somewhat lower for the larger riser with a steeper radial particle velocity profile. For the radial profile of the solids flux, a parabolic shape and a flat core shape profiles were found for the two risers respectively (Yan and Zhu, 2004, 2005 and Yan *et al.*, 2005).

2.3.3 Riser geometry effect

Previous studies had indicated that the geometry of the riser has considerable influence on the hydrodynamics of circulating fluidized beds (Brereton and Grace, 1994; Brereton and Stromberg, 1986; Schnitzlein and Weinstein, 1988 and Zhou *et al.*, 1994). Almost all of the cold-model hydrodynamic research had been conducted in cylindrical column risers. However, risers of square and rectangular cross-sections were now widely employed in CFB applications such as combustor. Zhou *et al.* (1994) carried out experiments in square CFB risers to study the solids voidage and particle velocity profiles using optical fiber probes. They obtained both lateral and axial voidage profiles and also revealed the influence of the corner on the voidage profile. Their studies also indicated that the profiles of lateral and axial particle velocity were influenced by operating conditions. Comparing with the results obtained in cylindrical risers, they found that the profiles in square riser were not necessarily lowest at the axis of the riser, but may go through a minimum between the wall and the axis. As for rectangular risers, some of wide rectangular risers must be considered as 3-D risers. While the narrow rectangular riser, to some extent, can be considered as two-dimensional column, with the definition of the width being considerably greater than the thickness, and the fluidized particles were contained in the gap between two flat

transparent faces, separated by a distance which was usually in the range 10 to 25 mm (Grace and Baeyens, 1986).

Rectangular two-dimensional and the conventional three-dimensional beds differed qualitatively and quantitatively. The differences arose from bubble properties, such as bubble velocities, bubble coalescence properties, bubble shapes and wake characteristics, and solids ejection into the freeboard in bubbling or turbulent beds (Fan, 1990; Gera and Gautam, 1995; Almendros-Ibanez *et al.*, 2006; Zhou *et al.*, 2007 and Xu 2010). However, very few studies had been done in two-dimensional fluidized bed under fast fluidization conditions, in which the gas velocities are higher than 3 m/s (Xu 2010).

To clarify the effects of riser geometry on the flow behaviors, Xu (2010) compared the results of the solids distribution in both the rectangular riser and the cylindrical riser under a wide range of conditions. In their study, both axial and lateral profiles of solids holdup showed that the operating conditions played important roles in influencing the flow structure, and controlled the flow properties in the rectangular riser in the same way as that in cylindrical risers: increasing U_g and reducing G_s resulted in a lower solids holdup. The solids concentration profile, within the range of their study, remained low at the riser centre throughout the whole riser compared with the solids holdup in the wall region. Comparing the rectangular riser with the other cylindrical columns, it was found that the general shapes of the axial and lateral profile of solids holdup in rectangular riser were quite similar to that in cylindrical risers, but more uniform (Xu and Zhu, 2010; Xu *et al.*, 2010 and Xu, 2010).

2.4 Hydrodynamics in CFB downer

A co-current gas-solids downward flow circulating fluidized bed, or a downer, is a new alternative flow arrangement for a high-velocity system. A downer reactor system has similar system configurations to a riser reactor system except that both the gas and the solid particles flow downward as shown in Figure 2.7. The co-current gas-solids downflow circulating fluidized beds were proposed in recent years (Shimizu *et al.*, 1978; Gross, 1983; Wang *et al.*, 1992; Zhu *et al.*, 1995; Zhu and Wei, 1996; Johnston *et al.*, 1999 and Li *et al.*, 2012). As a relatively new gas-solids reactor, it has been drawing more and more attentions due to its advantages over the

upflow riser reactors as stated by many of the researchers (Bai, *et al.*, 1991; Wang *et al.*, 1992; Herbert *et al.*, 1994; Zhu *et al.*, 1995 and Herbert *et al.*, 1998)

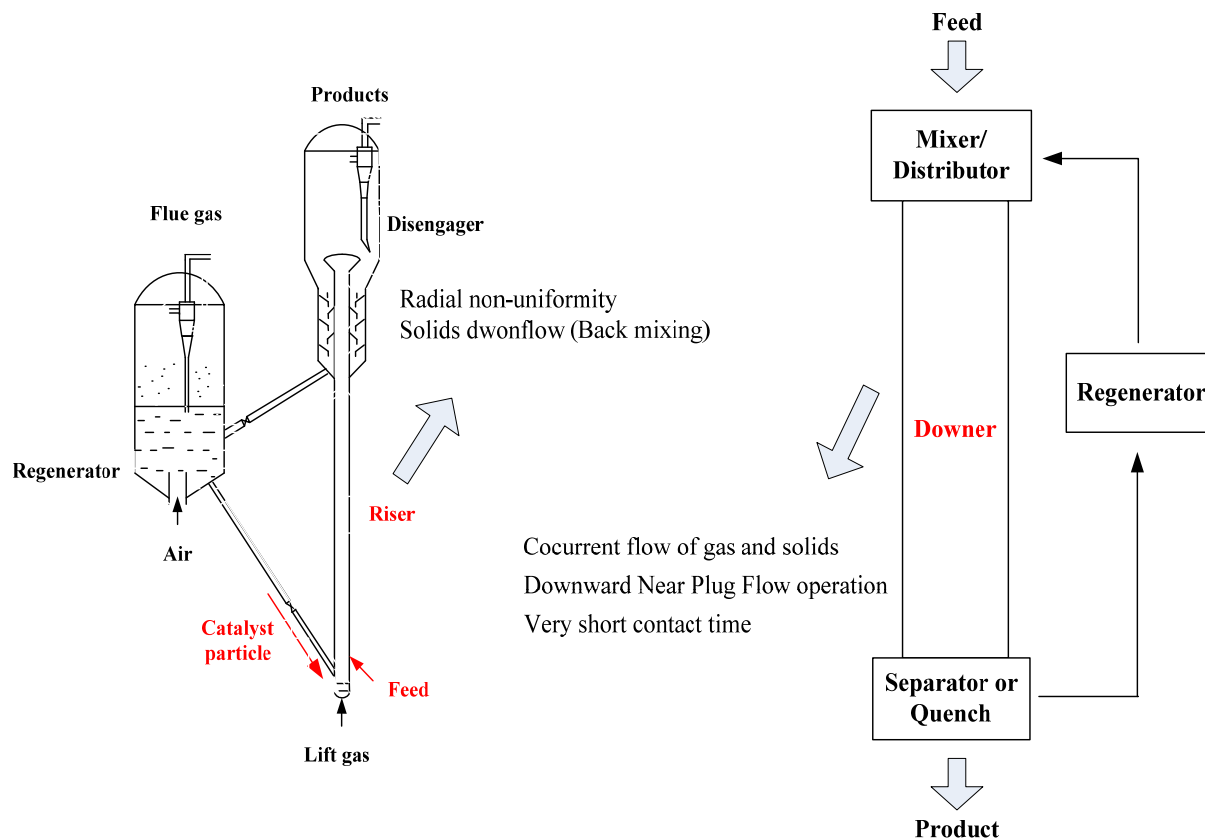


Figure 2.7 Conceptual of circulating fluidized bed downer

Cocurrent downward flow of particles and gas reduces the residence time of solid particles because the downward flow is in the same direction as gravity (Zhu *et al.*, 1995). More uniform radial gas and solids flow than those in a riser can be achieved. The downer leads to more uniform contact time between the gas and solids (Bai *et al.*, 1995; Bolkan *et al.*, 2003 and Luo *et al.*, 2007). Because the gas and solids residence time is usually very short in the downer, the initial gas and solids flow development is very important in order to control the reaction selectivity and product distribution (Luo *et al.*, 2007). With these advantages, downer reactors have been proposed for some processes such as fluid catalytic cracking (FCC), where short contacting time and uniform gas and solids residence time distribution are extremely important (Zhu *et al.*, 1995).

2.4.1 Three-section axial flow structure

In a downer reactor, gas and particles were fed from the top of the downer through separate gas and particle distributors. Upon entering the downer, gas immediately attained superficial velocity while particle velocity was initially close to zero (Zhang, 1999).

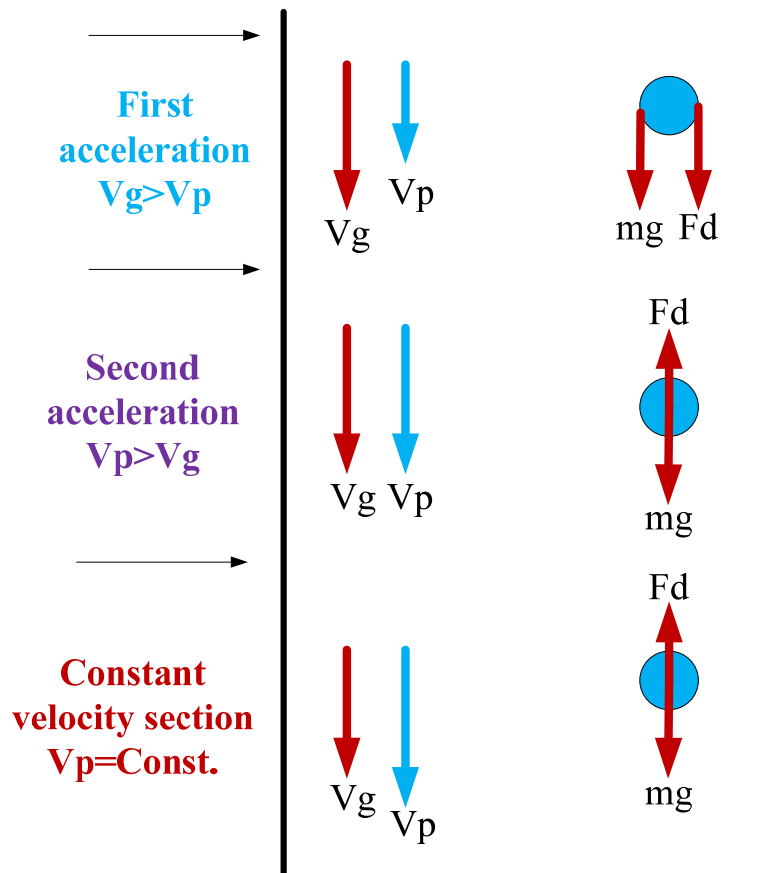


Figure 2.8 Axial gas-solids flow structure in the downer (Zhu, 2005)

As shown in Figures 2.8 and 2.9, solid particles were first accelerated both by gravity and drag force from the gas. As a consequence, pressure decreased continuously along the downer to compensate for the drag on the particles and the friction between wall and gas-solids suspension. When particle velocity became equal to the gas velocity, the gas drag acting on the particles became zero and the pressure reached a minimum. The section from the top to the position where

particle velocity was equal to the gas velocity had been referred to as the first acceleration section (Zhang, 1999).

After acquiring the same velocity as the gas phase, solids were further accelerated by gravity while encountering drag in the upward direction exerted by the now slower moving gas phase. Therefore, particle velocity increased further until the slip velocity between the gas and particles reached a value where the drag force counter-balanced the gravitational force. This section had been referred to as the second acceleration section. In this section, particle velocity continued to increase but at a lower rate than in the first acceleration zone and pressure increased gradually.

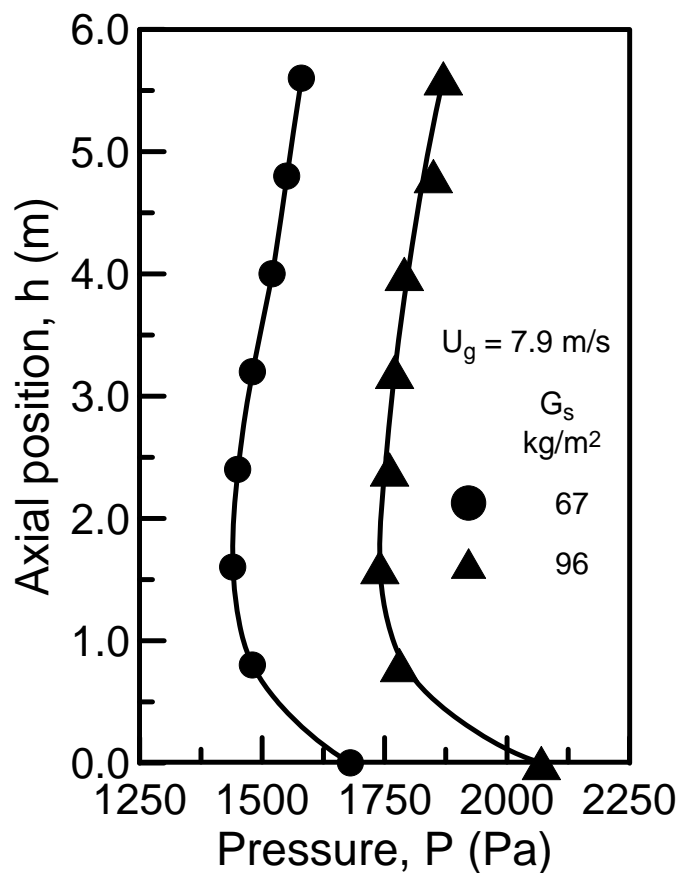


Figure 2.9 Axial distribution of pressure (Wang *et al.*, 1992)

When the drag was sufficient to balance the gravitational force, particles were not further accelerated and the remainder of the downer had been named the constant velocity section

(Wang *et al.*, 1992). In this section, particles traveled faster than gas and both particle and gas velocities remained constant. Pressure increased linearly along the downer and the pressure gradient was equal to the cross-sectional bed density, if wall friction was neglected.

This three-section axial flow structure had been confirmed by pressure and pressure drop measurements and the axial distribution of average particle velocity measured in a 140 mm downer (Wang *et al.*, 1992). This flow structure was also consistent with the prediction by Kwauk (1964) in his generalized fluidization model.

2.4.2 Radial gas and solids flow structure

Measurements for radial profiles of gas and particle velocities and solids concentration in both downers and risers had been made in the 140 mm diameter riser-downer system (Wang, *et al.*, 1992; Cao, *et al.*, 1994 and Zhu *et al.*, 1999). Typical radial profiles of gas and particle velocities measured in downer and the radial profile of solids concentration measured in both downers and risers were given in Figures 2.10 and 2.11 (Zhu *et al.*, 1999).

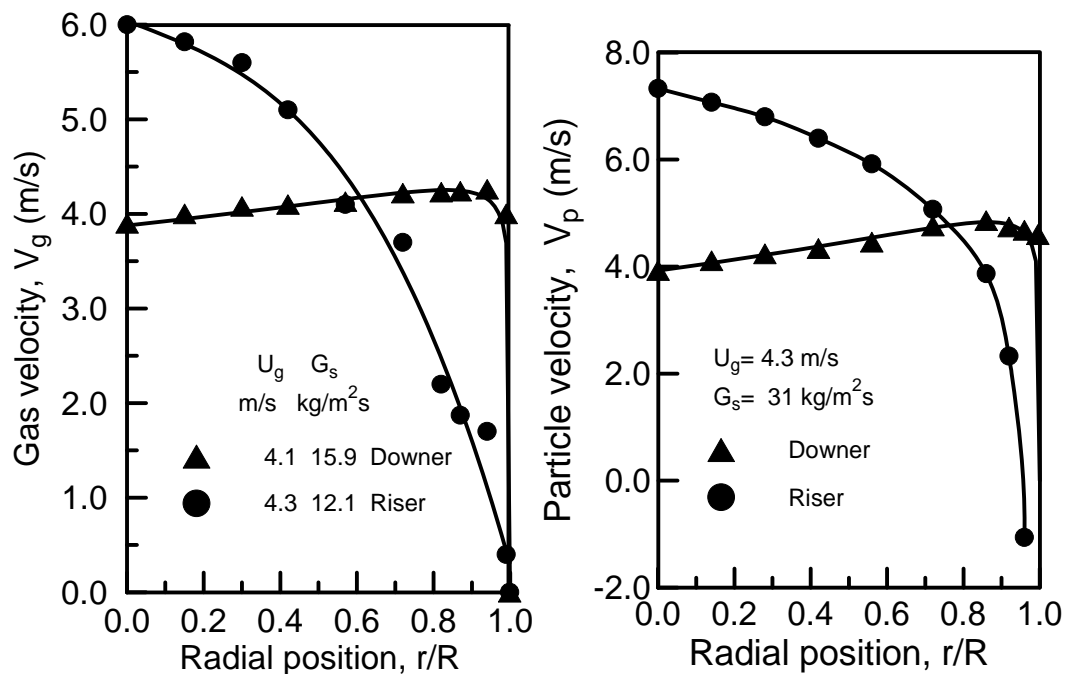


Figure 2.10 Radial profiles of particle velocity and gas velocity in the downer and riser (Zhu *et al.*, 1999)

Compared with the radial flow structure in the riser, the radial distributions of gas and particle velocities and solids concentration were all significantly more uniform in the downer. For the radial distribution of solids concentration in the downer, a similar phenomenon as that in the riser was found; the local bed voidage was a function of the radial position r/R only, with a given average voidage at any axial position, independent of the superficial gas velocity and the solids circulation rate (Wang *et al.*, 1992).

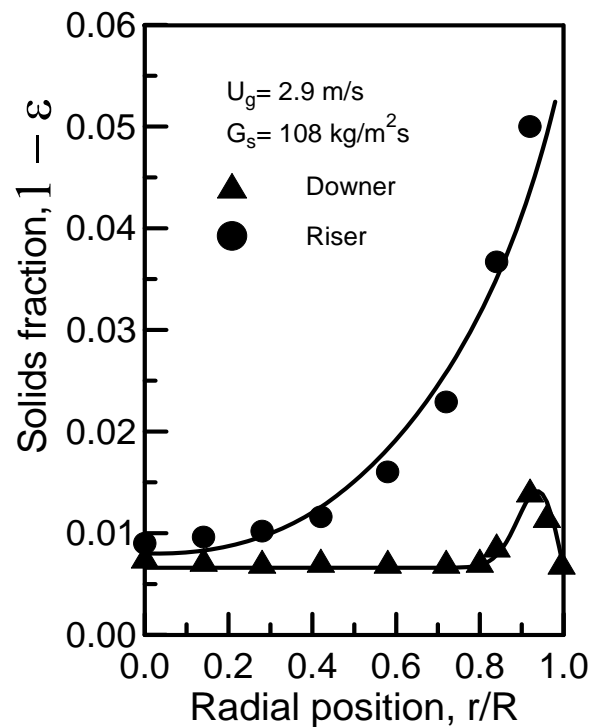
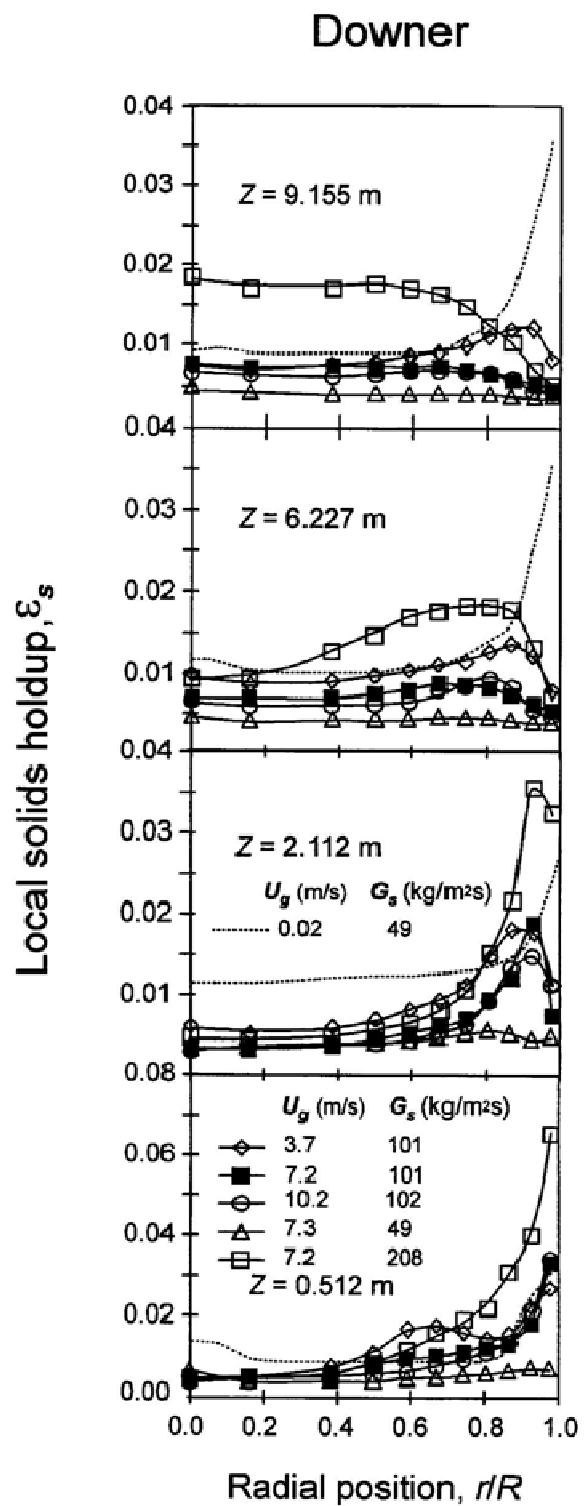
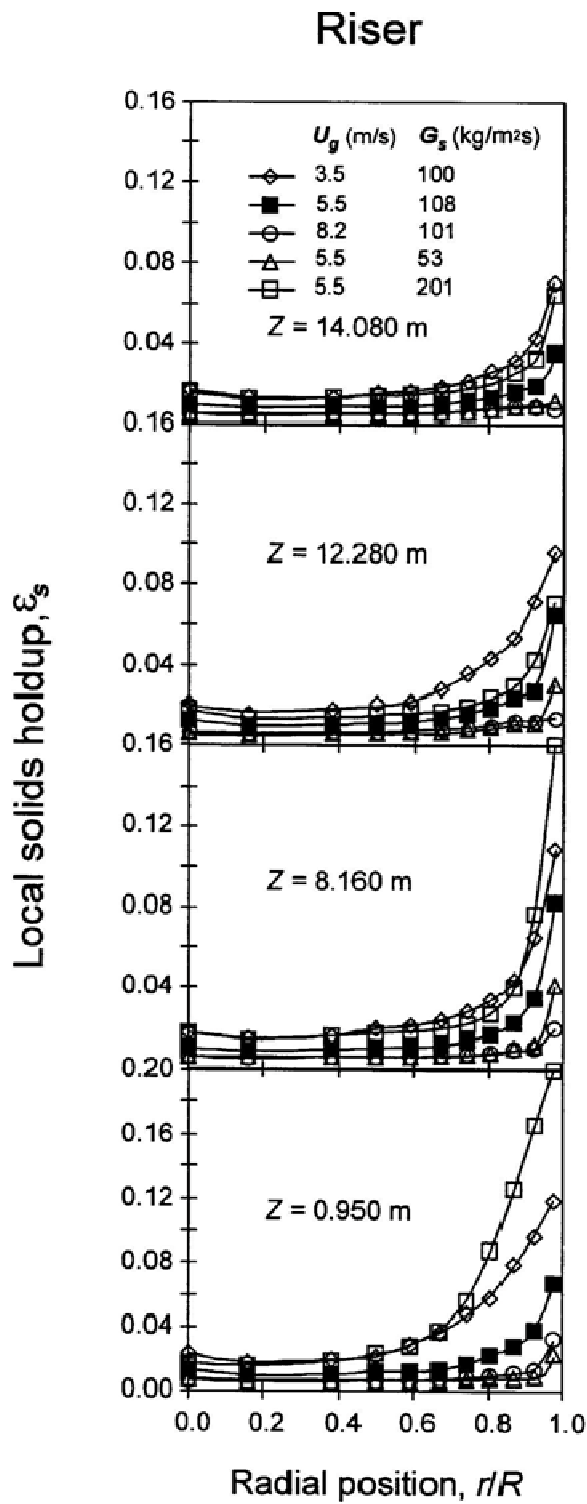


Figure 2.11 Radial distribution of solids holdup in the downer and the riser (Zhu *et al.*, 1999)

Examining the radial profiles of the gas and particle velocities and the solids concentration in the downer in Figures 2.10 and 2.11, it was found that in the downer, local particle velocity could be higher than local gas velocity and a higher local solids concentration always corresponded to higher gas and particle velocities. This was contrary to the situation in the riser, where local particle velocity was always lower than local gas velocity and a higher local solids concentration always corresponded to lower gas and particle velocities (Zhu *et al.*, 1999).



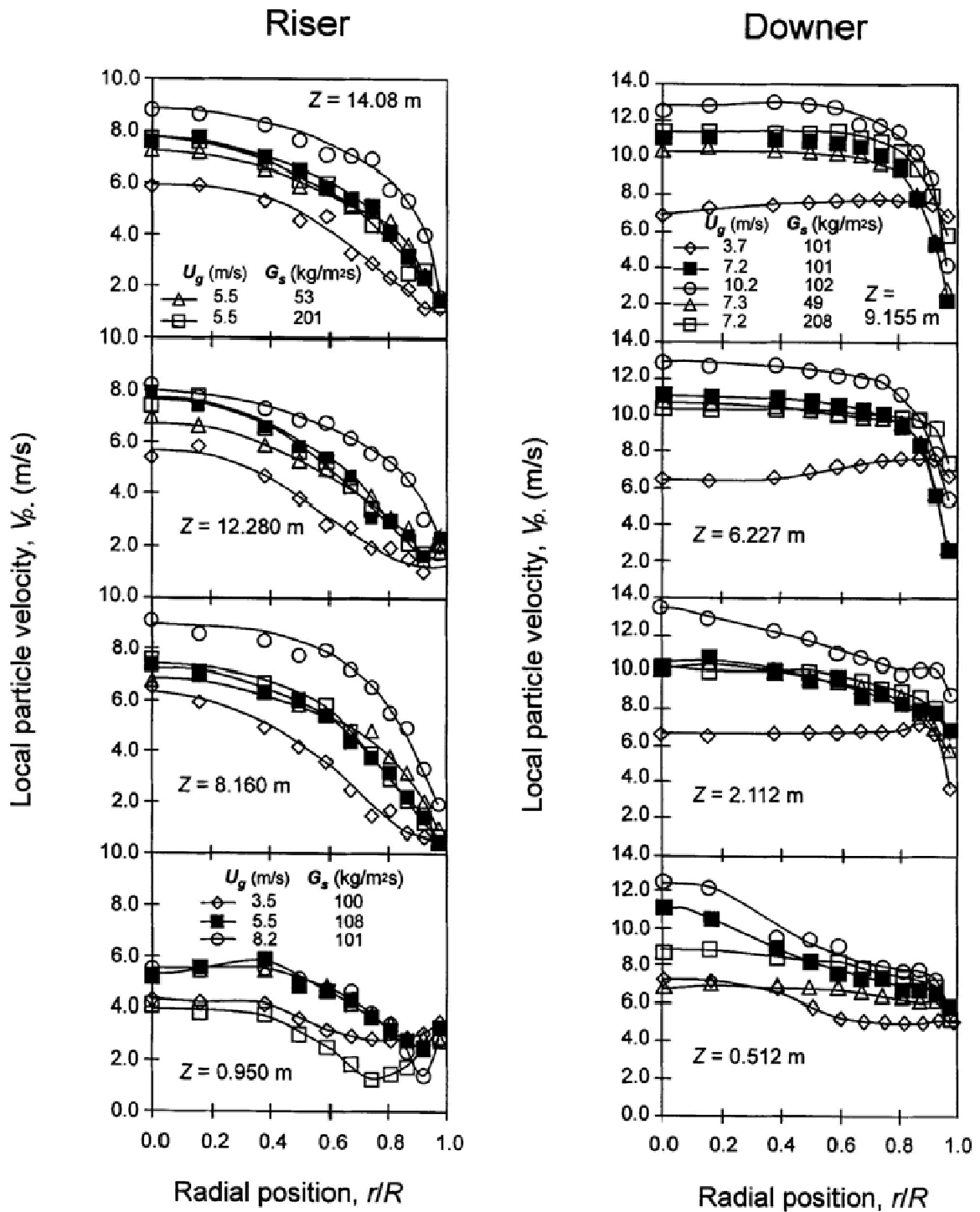


Figure 2.12 Radial profiles along the riser and downer under different operating conditions (Zhang *et al.*, 2001)

The radial distributions of time-averaged solids holdups in Figure 2.12 showed distinct differences between the riser and the downer. In the riser, the overall radial structure generally showed a non-uniform solids holdup distribution with a dilute core and a dense annulus, with the radial profile being relatively flat in the core and solids holdup increasing sharply toward the wall in the annulus with the highest solids holdup right at the wall. The radial distribution of solids holdup was affected by the operating condition. However, the shapes of the two profiles were very similar, both increasing gradually with increasing r/R , reaching a maximum value near the wall at about $r/R = 0.95$ and then decreasing towards the wall, although the gas and particle velocity profiles were quite different for the downer and the riser.

Compared to riser reactors, downer reactors had a much more uniform radial gas-solids flow pattern. This was likely due to the change of the direction of gas and solids flow from opposing gravity to following it. The following mechanism was provided to explain the more favorable radial flow structure in the downer (Bi and Zhu 1993).

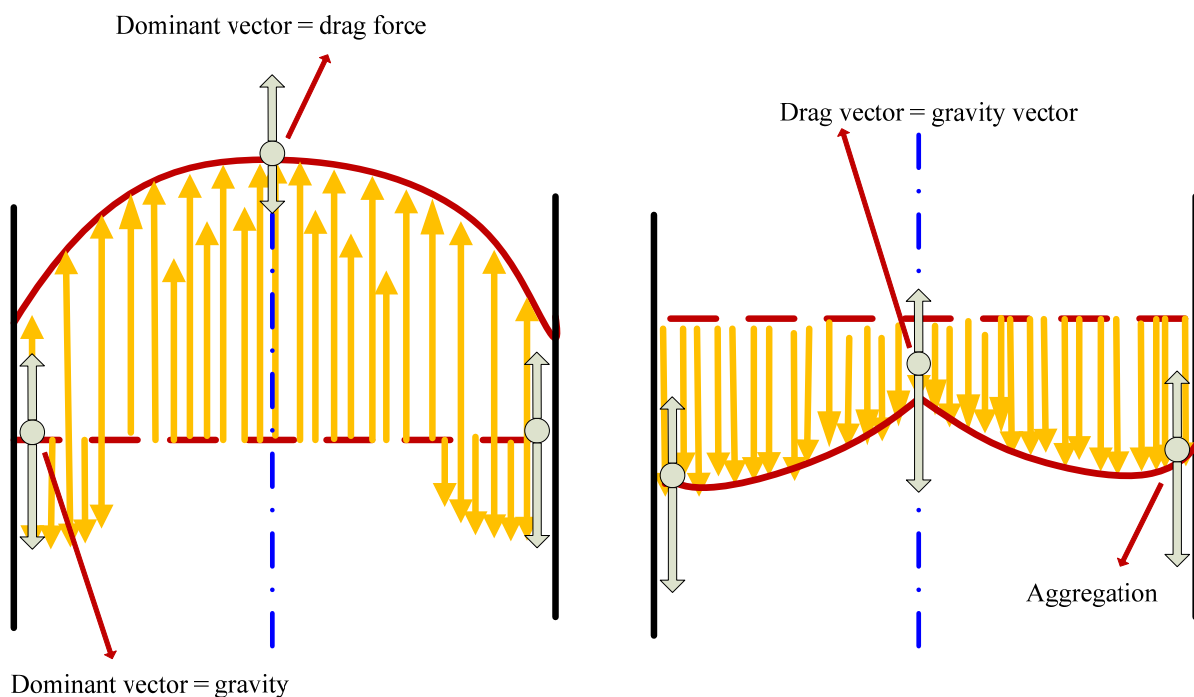


Figure 2.13 Radial flow structures in CFB riser and downer (Bi and Zhu, 1993)

As was shown in Figure 2.13, in both the downer and the riser, higher local solids concentration resulted in the reduction of drag coefficient (Zhang *et al.*, 2001). In the riser (where the drag was the driving force for particle flow) reduction of drag decreases the upwards particle velocity, which in turn increased the tendency for particle aggregation (Bi and Zhu 1993). Increased particle aggregation then further reduced the drag and the local particle velocity, leading to steeper radial profiles for both gas and particle velocity. However, in the downer (flow in the direction of gravity so that gravity was the driving force), a reduction of the upwards drag force would result in increased downwards particle velocity, which in turn led to increased gas velocity. On the other hand, increased local gas and particle velocities in the downer tended to reduce the extent of particle aggregation, thus increasing the gas drag. Therefore, the system stabilizes by itself and a more uniform radial flow structure was present in the downer.

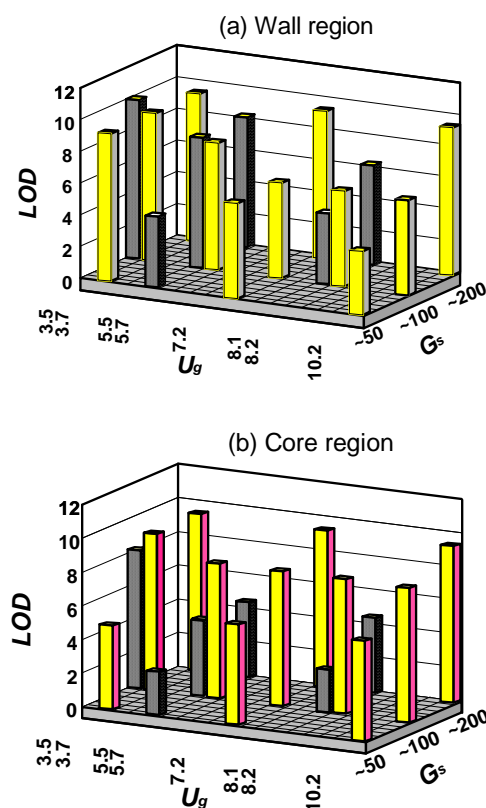


Figure 2.14 Effect of solids circulation rates and superficial gas velocity on the lengths of radial flow development for the riser and the downer. (Zhang *et al.*, 2001)

The length of the flow development (LOD) was the length that is needed for both the radial solids holdup profile and radial particle velocity to become fully developed (Zhang *et al.*, 2001). In a downer, the length of flow of development was comparable to that of a riser. In the core region of downer, the length of flow of development was longer than in the core of a riser. However, the total length of flow of development was approximately equal. Length of development in both reactors increased with increasing solids holdup and decreasing gas velocity as shown in Figure 2.14. In a downer the radial distribution of solids hold up and particle velocity was uniform than in a riser, therefore, it became a less important parameter in design compared to a riser. This LOD can be increased by increasing the solids circulation and holdup and also by decreasing the gas velocity. For catalytic or non-catalytic reactions, smaller LOD was favorable since the axial solids dispersion was less uniform in the development zone. This resulted in unfavorable flow patterns and non-uniform residence times. In the long run it may lead to over-conversion of the particle reactions and formation of undesired products in reactors with longer LOD. Therefore, downer was preferred due to smaller length of development (Zhang *et al.*, 2001).

In addition, heat transfer was generally considered to be affected by hydrodynamics. Investigations on heat transfer in the downer reactor were made by many researchers (Ma and Zhu, 1999 and 2001 and Kim *et al.*, 1999). Ma and Zhu (2001) studied the heat transfer coefficient between the suspended surface and the gas-solids flow suspension in a downer of 9.3 m high using a miniature cylindrical heat transfer probe. They found that bed suspension density was the most influential factor. The average heat transfer coefficient decreased with decreasing solids circulation rate due to the decreased solids holdup. On the other hand, the heat transfer coefficient did not always decrease with increasing the superficial gas velocity given the increased importance of gas convective heat transfer under high gas velocities and low solids holdup in downer reactors. They also compared the heat transfer coefficient in both riser and downer reactors (Ma and Zhu, 2001). In their studies, the axial heat transfer coefficient had negligible effect on the trend of the flow development. The radial heat transfer coefficient was nearly uniform but was higher at the top due to effect of the distributor on the solids distribution. The heat transfer radial distribution was uniform in the developed section compared to the riser

as the solids distribution in the downer was more uniform. In the riser, the radial heat transfer coefficient was non-uniform due to the solids holdup and formation of clusters especially at the wall.

2.5 Ozone decomposition in CFB reactors

2.5.1 Experimental researches with ozone decomposition

In order to improve the design and operation of commercial fluidized beds, studies have been conducted in conventional fluidized bed systems for both bubbling and turbulent fluidized bed conditions, where the decomposition of ozone has been used as a model reaction. Chemical reaction gives the direct information on reactor performance in contrast to any other method (Frye *et al.*, 1958 and Jiang *et al.*, 1991). Reactor performance investigations have also been carried out in CFB systems using ozone decomposition as the model reaction. Recently, high density circulating fluidized beds have become a hot research topic, especially on hydrodynamics. However, there are only a few published research studies dealing with catalytic reactions and these were in small-scale circulating fluidized bed reactors (Jiang *et al.*, 1991 and Pagliolico *et al.*, 1992).

Due to complex reaction kinetics and the accompanied heat transfer and catalyst deactivation effects involved in the fluidization bed reactors, it is hard to properly assess reaction mechanism and effects of transport parameters on the reactor performance. In 1955, Shen and Johnstone studied the kinetics of decomposition of nitrous oxide over an impregnated alumina catalyst in fixed and fluidized beds at temperatures ranging from 340°C to 430°C. A mass transfer coefficient between the two phases was used to evaluate the effectiveness of contact between the gas and solids. The reaction rate for the catalytic decomposition of nitrous oxide was determined in a fluidized bed of impregnated alumina particles and compared with the corresponding rate in a fixed bed. But this kind of knowledge of the contacting mechanism is insufficient to develop generalized correlations for reactor design. The design of large-scale fluidized bed reactors depends on empirical correlations developed based on kinetic data (Frye *et al.*, 1958).

Later, Frye *et al.* (1958) developed an experimental method using ozone to investigate the kinetics of FCC in fluidized beds. They considered that ozone experimental method had the following characteristics: low concentrations of reactant; rapid and accurate analysis by simple, well established methods; and measurable reaction rates at low pressures and temperatures. They also found ozone decomposition was a desirable substitute reaction providing reactor design data for hydrocarbon synthesis. As an economical and convenient research method on fluidization reactors, meaningful results have been obtained (shown in Table 2.1). In these studies, different riser geometries and construction materials were used. The most commonly used particles were FCC catalyst particles impregnated with ferric oxide. UV-absorption principle is widely used to detect the concentration of ozone. Axial/radial ozone concentration and axial solids concentration profiles in the CFB were obtained.

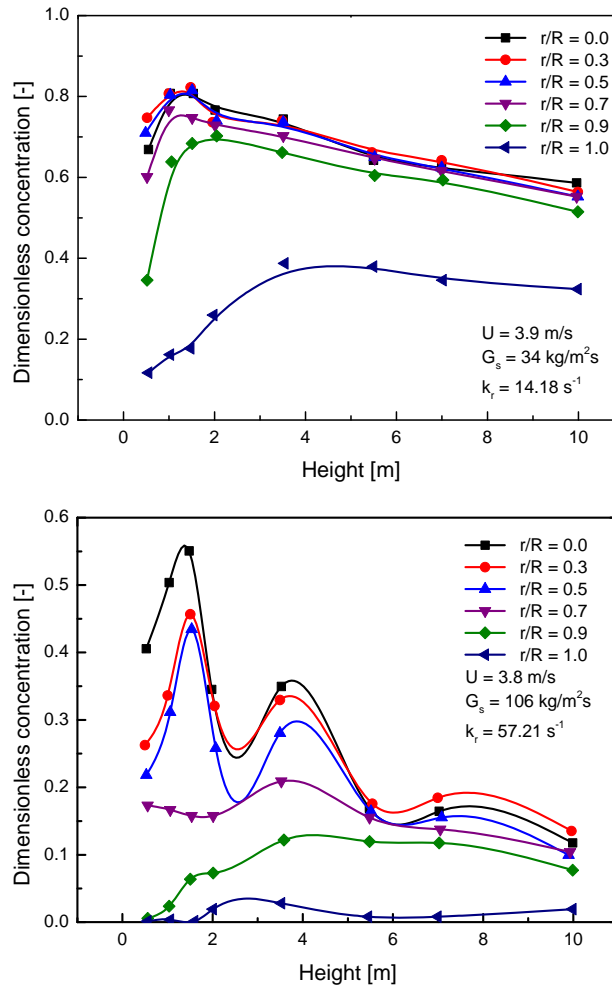
Table 2.1 Studies of fluidized bed reaction by using ozone decomposition. (part 1)

	Reactor material	Reactor diameter (mm)	Reactor height (m)	U_g (m/s)	Reactor	G_s (kg/m ² s)	Temperature (°C)	Type of FCC	Particle size (μm)	Particle density (kg/m ³)	Reaction rate (1/s)
Li <i>et al.</i> , (2013)	Aluminum	76	10	2-5	riser	50-150	20	FCC+ ferric nitrate	67	1370	4.0
Li <i>et al.</i> , (2011)	Aluminum	76	5	2-5	downer	50-150	20	FCC+ ferric nitrate	67	1370	4.0
Fan <i>et al.</i> , (2008)	Plexiglas	90	8.5	2.2-3.7	downer	8.4-28.8	-	FCC FCC+ferric nitrate	62 72	1747 1400	0.098 ml (g cat) ⁻¹ s ⁻¹
Bolland <i>et al.</i> , (2001)	Steel	411	8.5	5.6-7.2	riser	31-53	60	angular cast steel	117	3320	26-62
Schoenfelder <i>et al.</i> , (1996)	-	400	15.6	2.4-4.5	riser	9-45	20	aluminum hydro silicate +10% silica + Iron Oxide	50	1420	0.001-0.003 M ³ /(s.kg)
Ouyang <i>et al.</i> , (1995, 1996)	Steel	254	10.85	2.0-7.5	riser	10-206	20	FCC+ ferric oxide	65	1380	3.9-57.2

Table 2.2 Studies of fluidized bed reaction by using ozone decomposition. (part 2)

	Reactor material	Reactor diameter (mm)	Reactor height (m)	U_g (m/s)	Reactor	G_s (kg/m ² s)	Temperature (°C)	Type of FCC	Particle size (μm)	Particle density (kg/m ³)	Reaction rate (1/s)
Pagliolico (1992)	-	50	4.5	3.8-8.8	riser	20.4-102	15	γ-alumina+ ferric oxide	82	2970	44.71
Jiang <i>et al.</i> , (1991)	Plexiglas	102	6.32	1.5-2.5	riser+ baffle ring	5.1-28.9	23	FCC+ferric nitrate	89	1500	2.81-5.1
Sun <i>et al.</i> , (1990)	Aluminum	100	2.6	0.06-1.8	bubbling, slugging, turbulent	-	-	FCC+ferric nitrate	Wide, 60; Bimodel, 60; Narrow, 60	-	1-9
Fryer <i>et al.</i> , (1958, 1976)	Stainless steel +glass	229	2	0.024-0.017	bubbling	-	20	sand+iron oxide	117	2650	-

2.5.2 Ozone decomposition in the CFB riser reactor

Figure 2.15 Axial ozone concentration profile (Ouyang *et al.*, 1993 and 1995)

Ouyang *et al.* (1993 and 1995) investigated the ozone decomposition in CFB riser and obtained the axial ozone concentration profiles at different radial positions at different operating conditions shown in Figure 2.15. The strong up and down movements of solids observed in the bottom region contributed to the axial gas backmixing resulting in the uniform axial ozone concentration distributions. In the upper region, the gas backmixing was not as significant. The decreasing trend of the axial ozone concentration profile corresponds roughly to that of the axial voidage profile. In fully developed section, ozone concentration varied axially from low to high

with the catalyst circulating rates, corresponding to the axial profiles of the solids holdup shown in Figure 2.16, which meant that the ozone conversion was proportional to the solids concentration.

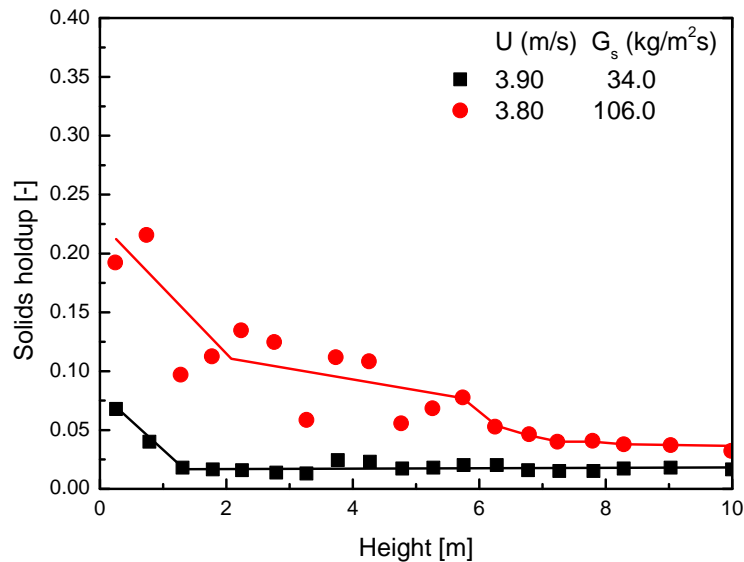


Figure 2.16 Axial profile of solids holdup in the riser (Ouyang *et al.*, 1995)

Figure 2.17 showed the radial distribution of ozone concentration in CFB riser reactors, where k_r was the apparent reaction rate constant, U_g was the superficial gas velocity, G_s was the solids circulation rate, and z was axial position of the sampling point from the gas distributor (Ouyang *et al.*, 1995).

Ozone concentration in the central region was much higher than that in the near wall region, producing a parabolic concentration profile in the radial direction at a given axial level. The radial concentration gradients persisted over the entire height of the CFB riser reactor, decreasing with increased axial positions. The suggested reason for such a radial concentration profile in the CFB riser was that in the wall region higher solids holdup resulted in higher reaction rates as compared to those in the dilute core region (Jiang *et al.*, 1990). The ozone concentration difference between the core and wall regions decreased with an increase in the axial heights, which corresponded to a decrease in solids holdup. These data indicated that the trend of the radial ozone concentration profiles was essentially dominated by the flow structure, which was

represented by the axial and radial solids holdup profiles, showing strong correlation between hydrodynamics and ozone conversion. Effects of solids circulation rate on the radial ozone concentration profile was also can be found in Figure 2.16. The ozone concentration decreased with increasing solids circulation rates. Moreover, an increase in the solids circulation rate increased the ozone concentration difference between the wall and center regions.

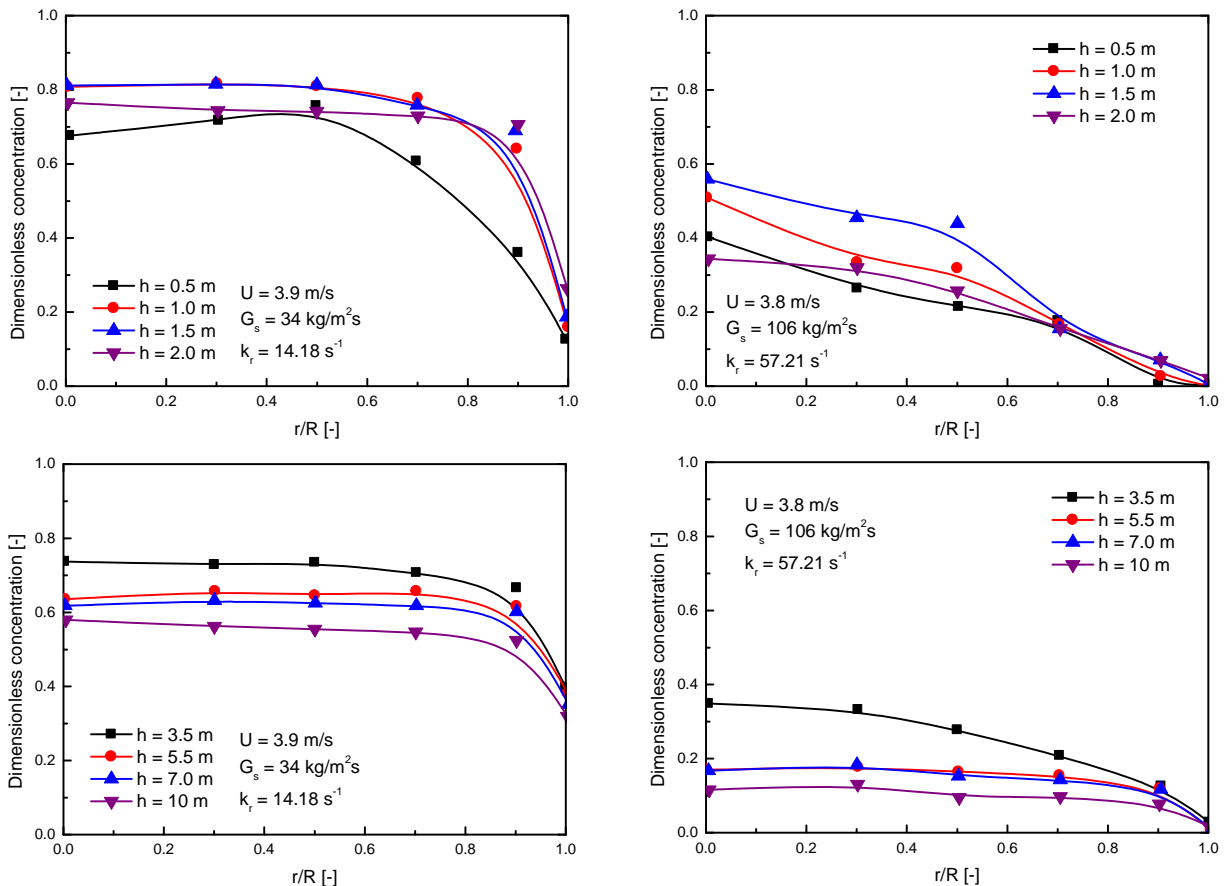


Figure 2.17 Radial profiles of ozone concentration in the riser reactor (Ouyang *et al.*, 1995)

As shown in Figure 2.17, Ouyang *et al.* (1995) found that in the case of low values of solids holdup, the radial ozone concentration gradient between the riser wall and center was relatively high, and the profile became much smoother at a higher solids holdup. When solids circulation rate was $106 \text{ kg/m}^2\text{s}$, the radial concentration gradient was much smaller than that for a solids circulation rate of $34 \text{ kg/m}^2\text{s}$. This phenomenon was also reported by other researchers

(Schoenfelder *et al.*, 1996; Jiang *et al.*, 1990 and Bi *et al.*, 1992). Higher solids circulation rate intensified radial ozone concentration gradient. Therefore, there was a factor of uncertainty in assessing how radial concentration profile correlated with solids holdup, or at different solids circulation rates.

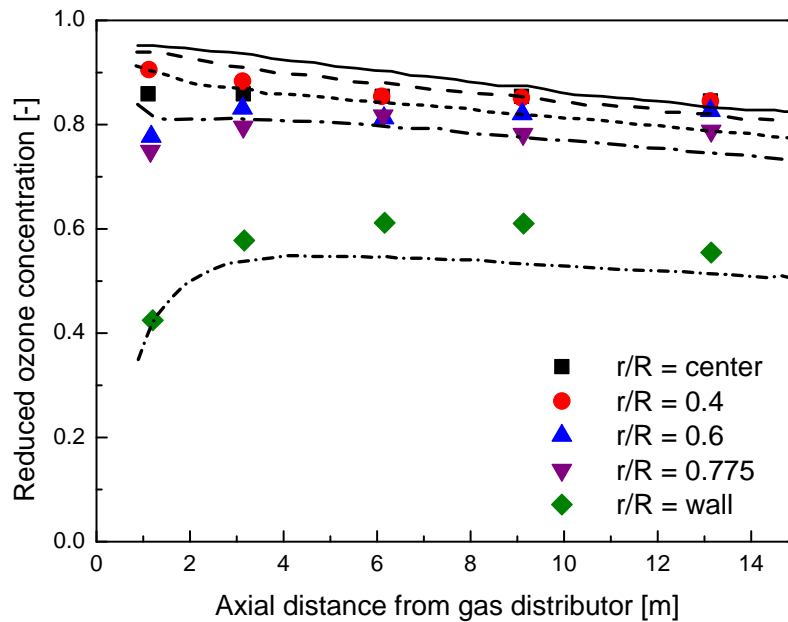


Figure 2.18 Axial ozone conversion profiles in the riser (Schoenfelder *et al.*, 1996)

In addition, Figure 2.18 showed the axial profiles of radial distributions of ozone concentration (Schoenfelder *et al.*, 1996). It was found that the ozone concentration in the centerline of the riser was almost constant with riser height. Only minor differences between the ozone concentration profiles at radial positions between $r/R = 0.0$ and $r/R = 0.775$ were found. Near the wall, a significantly lower ozone concentration had been observed. In this figure, a maximum of the ozone concentration had been measured at a medium height above the gas distributor. This result was corresponded well to the findings by Ouyang (1993) as shown in Figure 2.15.

2.5.3 Ozone decomposition in the CFB downer reactor

Downer reactors were intensively studied and widely accepted for fast selective reactions because of their uniform radial solids holdup profiles, good gas-solids contacting and no back

mixing (Zhang *et al.*, 1999 and 2000). Ozone decomposition studies were conducted by Fan *et al.* (2008) in a downer reactor as shown in Figure 2.19.

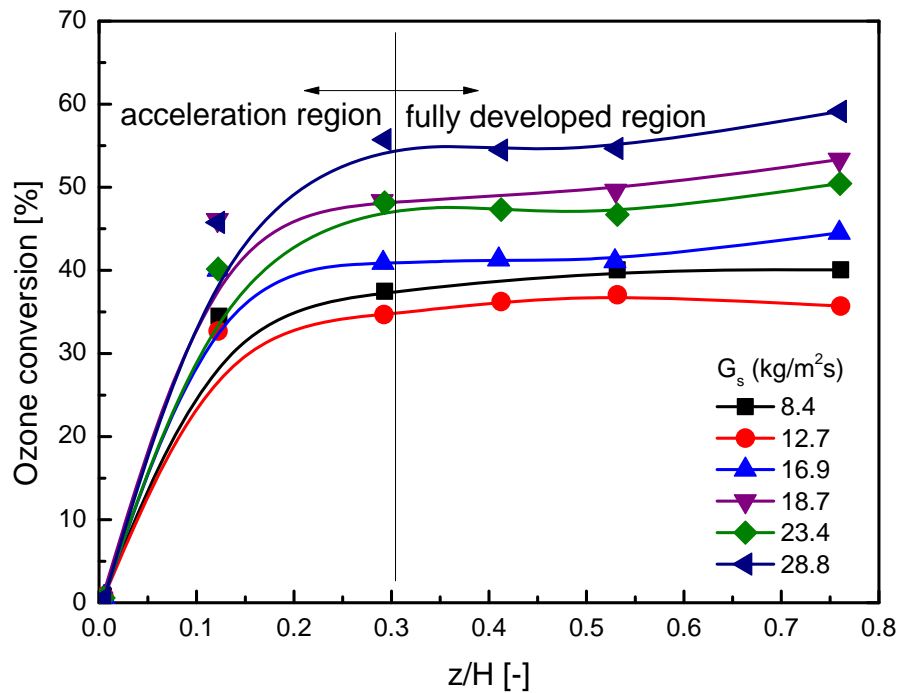


Figure 2.19 Ozone conversions in CFB downer (Fan *et al.*, 2008)

Axial ozone conversion profiles in a downer suggested that most of the ozone was decomposed in the acceleration region, and the ozone concentration varied very little in the fully developed section (below $z/H = 0.29$) in the downer. Fan *et al.* (2008) concluded that the conversion was much faster in the acceleration region than that in the developed region because of the higher solids concentration and reactant concentration which increased the reaction rate of the first order ozone decomposition reaction. Ozone was absorbed or reacted quickly on fresh catalyst particles at the acceleration or entrance zone and then at fully developed sections ozone concentration nearly reached an equilibrium state due to the balance between absorbing and desorbing molecules.

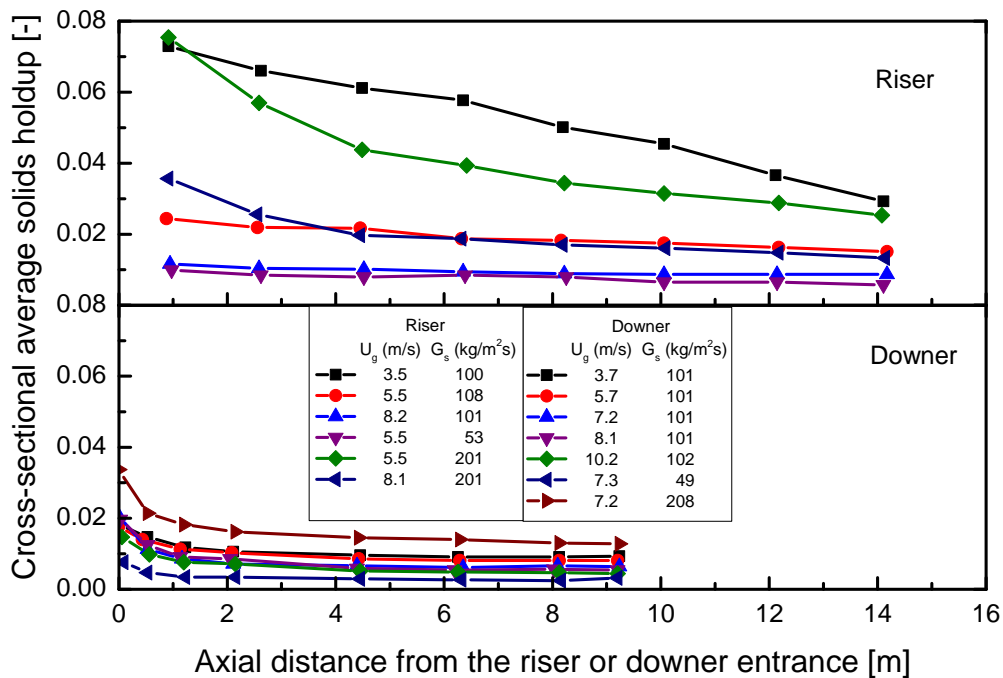


Figure 2.20 Axial profiles of solids holdup in the riser and (Zhang *et al.*, 1999)

Comparing ozone decomposition on FCC in the riser shown in Figure 2.17 with that in the downer (Figure 2.19), the axial ozone conversion profiles of the riser had the same tendency as in the downer at very close circulating solids flux. In the acceleration zone of the riser, the ozone concentrations reduced quickly and leveled off at fully developed section. Although Fan *et al.* (2008) did not report their axial solids holdup profiles, the results of solids holdup could be inferred based on the study of the downer reported by Zhu and Zhang shown in Figure 2.20 and 2.21. At entrance section gas-solids mixing was poor and became uniform and steady at fully developed section. All of these facts seemed to indicate that there was no back mixing in downers.

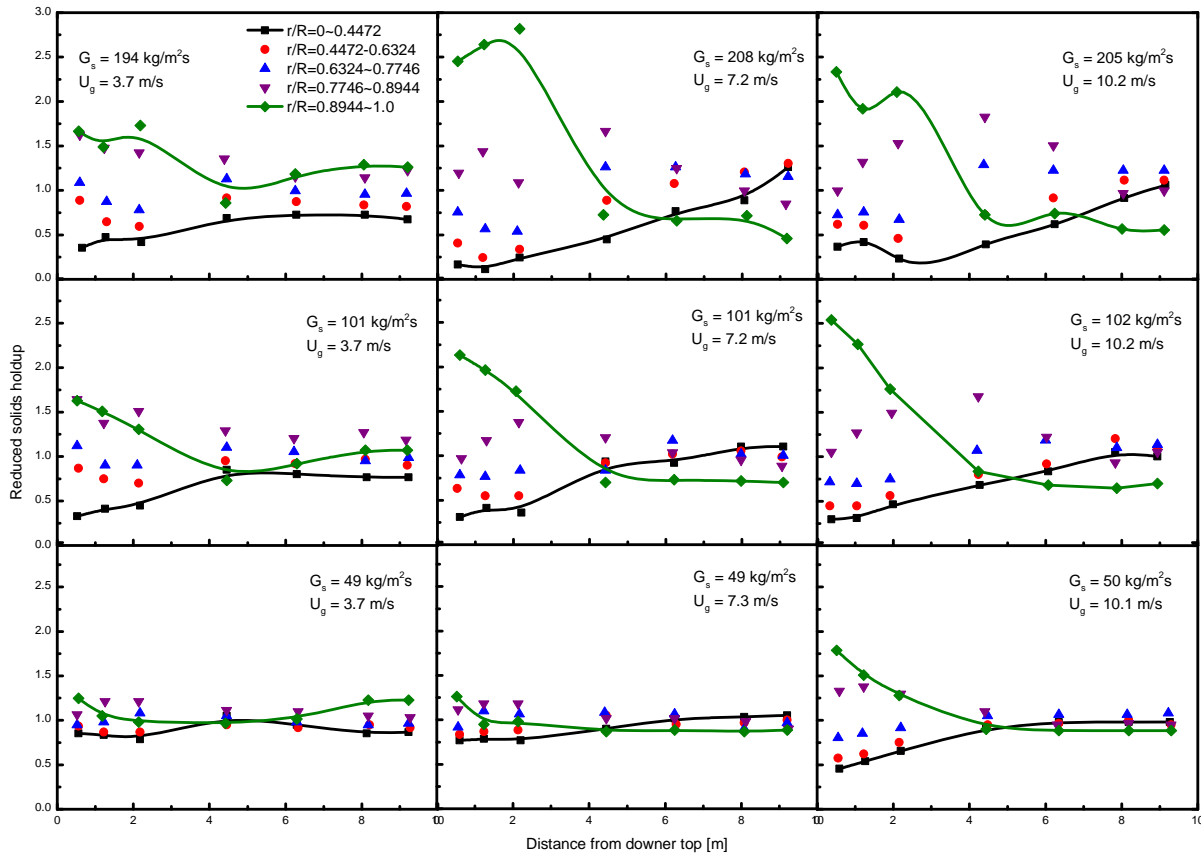


Figure 2.21 Radial profiles of solids holdup in riser and downer (Zhang *et al.*, 1999)

2.5.4 Contact efficiency of ozone decomposition reaction

Different from hydrodynamics of fluidization, one goal of ozone decomposition was the contact efficiency. Unfortunately, only a few authors report their results on this topic (Jiang *et al.*, 1991; Ouyang *et al.*, 1993 and 1995 and Li *et al.*, 2011 and 2013). Based on the pseudo-homogeneous plug-flow, the contact efficiency, α , was defined as:

$$1 - X = \exp\left[-\alpha k_r \bar{\varepsilon}_s H / U_g\right] \text{ or } 1 - X = \exp\left[-\alpha k_r'\right] \quad (2.1)$$

where $k_r' = k_r \bar{\varepsilon}_s H / U_g$ was Damköhler number, X was the conversion. Contact efficiency represented the fraction of the external surface area of the catalysts available for the diffused reactant from the gas phase (Jiang *et al.*, 1991). It can also be regarded as the utilization

efficiency of catalysts in the CFB reactor compared to that in the plug flow reactor. The lower the contact efficiency, the poorer the reactor performance, the more the reactor deviated from a fixed bed with negligible axial dispersion (Sun, 1991).

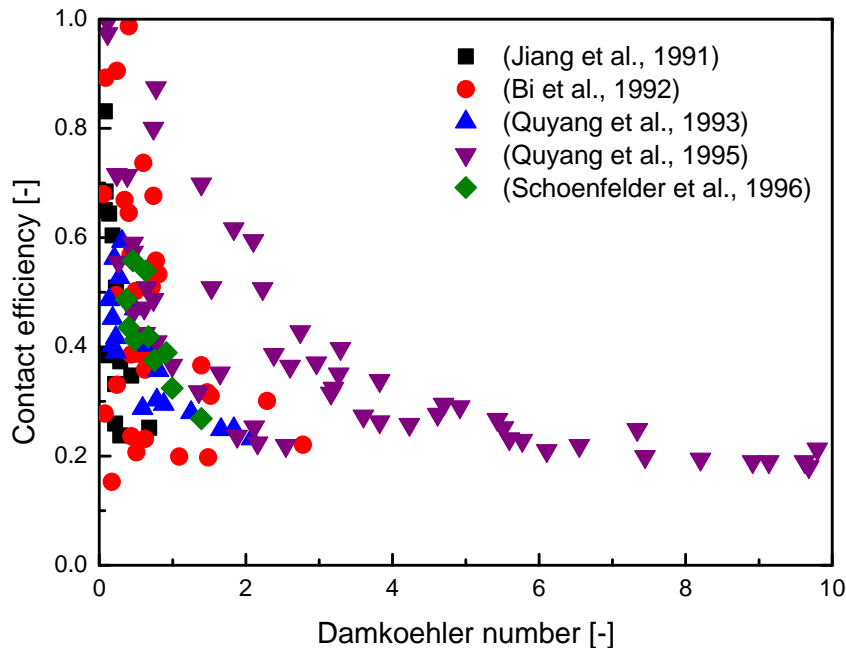


Figure 2.22 Contact efficiency as a function of Damköhler number

The contact efficiency of the reactor against Damköhler number was plotted in Figure 2.22. A typical contact efficiency value varied between 0.3-0.7 showing that the solids were not uniformly in contact with the gas stream. As shown in the Figure, the contact efficiency decreased with increasing Damköhler number. Considering the definition of the Damköhler number, it can be concluded that, the contact efficiency approached unity at very low solids holdup, indicating a good contacting conditions between gas and solids. But the general trend was that the contact efficiency of the reactor decreased as the solids holdup increased. It indicated that higher solids holdup seemed to be accompanied by a reduction in gas-solids contacting efficiency.

2.6 Conclusions and outlook

- (1) As to the axial flow structure, there exists a dense phase at the bottom and a dilute phase at the top of the riser following the so called S-shape profile for bed voidage. There is a transition section in-between, therefore the riser may be divided into three regions, a dense region at the bottom portion, a dilute region at the top part and a transition between those two parts. Other profiles such as C-shape and exponential shape have also been observed.
- (2) A core-annular type radial flow with a dense particle layer in the wall region and a dilute core region is known to exist in the riser. This can be described as a low density, high velocity gas-solids core region surrounded by slower moving or even downward flowing solid particles in the annular region.
- (3) It has been found that operating conditions, inlet and outlet structures, riser geometry and properties of the gas and solids affect the axial and radial solids distributions in the riser.
- (4) In the axial direction along the downer, there exist three sections: the first acceleration section at the top, where particles are accelerated by both gas drag and gravity; the second acceleration section where particles are accelerated by gravity but decelerated by gas drag; and the constant velocity section where both gas and particles travel downwards at constant velocities with a constant slip velocity due to the gravitational and drag forces being in equilibrium.
- (5) Radial distributions of gas and particle velocities and solids concentration are much more uniform in downers than those in risers, resulting in a more uniform gas-solids flow structure inside the downer.
- (6) In order to improve the production operation and design good commercial fluidized beds, reactor performance investigations have been carried out using ozone decomposition as the model reaction.
- (7) Nearly uniform axial profile in the bottom region, followed by a decrease in reactant concentration in the upper region was observed in some studies. More experimental studies are needed to characterize this trend in detail.

- (8) Significant radial reactant concentration gradients exist between the core and near wall regions, persisting over the entire height of the CFB riser reactor. Considering the contradictory findings, the effects of superficial gas velocity and solids circulation rate on radial reactant concentration profile are not fully understood.
- (9) Contact efficiency was proposed to account for incomplete gas-solids contact due to the effects of hydrodynamics on reactor performance. It is of interest to know the contact efficiency at different reactor heights.

Nomenclature

C	ozone (reactant) concentration [ppm]
C_0	initial ozone (reactant) concentration [ppm]
D	column diameter [m]
d_p	particle diameter [m]
G_s	solids circulation rate [$\text{kg}/(\text{m}^2 \cdot \text{s})$]
H	height of the reactor [m]
k_r	reaction rate constant [s^{-1}]
k_r'	Damköhler number, $k_r \bar{\varepsilon}_s H / U_g$ [-]
r	radial coordinate [m]
l_e	the length of the turbulent eddies
LOD	the length of the flow development
R	column radius [m]
r/R	reduced radial position [-]
U_g	superficial gas velocity [m/s]
X	conversion [-]
z	axial coordinate [m]

Greek letters

α	gas-solids contacting efficiency [-]
ε	voidage [-]
ε_s	solids holdup, $1 - \varepsilon$ [-]
$\bar{\varepsilon}_s$	cross-sectional average solids holdup [-]

Subscripts

g	gas
p	particle

r reaction

s solids

References

- Almendros-Ibanez JA, Sobrino C., de Vega M. and Santana D., (2006), A new model for ejected particle velocity from erupting bubbles in 2-D fluidized beds. *Chemical Engineering Science* 61, 5981-5990
- Bai, D.R., Jin, Y., Yu, ZQ., 1988. In: Kwauk, M., Kunii, D. eds., *Fluidization 88: Science and Technology*. Beijing: Science Press, 155-164
- Bai DR., Jin Y., Yu ZQ. and Zhu JX., (1992), The axial distribution of the cross-sectionally averaged voidage in fast fluidized beds. *Powder Technology* 71, 51-58
- Bai D., Shibuya E., Masuda Y., Nishio K., Nakagawa N. and Kato K., (1995), Distinction between upward and downward flows in circulating fluidized beds, *Powder Technology* 84(1), 75-81
- Bi H., Jiang P., Jean RH. and Fan LS., (1992), Coarse-particle effects in a multi-solids circulating fluidized bed for catalytic reactions, *Chemical Engineering Science* 47(12), 3113-3124
- Bi HT. and Zhu JX., (1993), Static instability analysis of circulating fluidized beds and concept of high-density risers. *AIChE Journal* 36, 1272-1280
- Bolkan Y., Berruti F., Zhu J. and Milne B., (2003), Hydrodynamic modeling of CFB risers and downers, *International Journal of Chemical Reactor Engineering* 1: A51, P1
- Bolland O., (1998), Describing mass transfer in circulating fluidized beds by ozone decomposition, Master's thesis, The Norwegian University of Science and Technology, Norway
- Bolland O. and Nicolai R., (2001), Describing mass transfer in circulating fluidized beds by ozone decomposition, *Chemical Engineering Communications* 187(1), 1-21
- Breault RW. (2006), A review of gas-solid dispersion and mass transfer coefficient correlations in circulating fluidized beds, *Powder Technology* 163(1-2), 9-17
- Breault RW. and Guenther CP. (2009), Mass transfer in the core-annular and fast fluidization flow regimes of a CFB, *Powder Technology* 190(3), 385-389
- Brereton C. and Stromberg L., (1986), Some aspects of the fluid behavior of fast fluidized beds. In: Basu, P. *Circulating Fluidized Bed Technology*. Toronto. pp. 133-143
- Brereton CM. H. and Grace JR., (1994), End effects in circulating fluidized bed hydrodynamics. In: Avidan AA., *Circulating Fluidized Bed Technology IV*, AIChE, New York, pp. 137-144

Cao CS., Jin Y., Yu ZQ. and Wang ZW., (1994), The gas-solids velocity profiles and slip phenomenon in a cocurrent downflow circulating fluidized bed technology IV. Avidan AA. Ed. AIChE, New York. pp 406-413

Cheng Y., Wei F., Yang G. and Jin Y., (1998), Inlet and outlet effects on flow patterns in gas-solid risers. Powder Technology 98, 151-156

Deng R.; Liu H.; Gao L.; Wang L.; Wei F. and Jin Y. (2005), Study on the FCC process in a novel riser-downer-coupling reactor (ii): Simulation and hot experiments, Industrial and Engineering Chemistry Research 44(5), 1446-1453

Fakeeha AH., Soliman MA. and Ibrahim AA., (2000), Modeling of a circulating fluidized bed for ammoxidation of propane to acrylonitrile, Chemical Engineering and Processing 39(2), 161-170

Fan C., Zhang Y., Bi XT., Song W., Lin W. and Luo L., (2008), Evaluation of downer reactor performance by catalytic ozone decomposition, Chemical Engineering Journal 140(1-3), 539-554

Fan Z., (1990), Analysis of pressure fluctuations in a 2-D fluidized bed. Powder Technology 62, 139-145

Frye CG., Lake WC. and Eckstrom HC., (1958), Gas-solid contacting with ozone decomposition reaction, AIChE Journal 4(4), 403-408

Fryer C. and Potter OE., (1976), Experimental investigation of models for fluidized bed catalytic reactors, AIChE Journal 22(1), 38-47

Gascon J., Tellez C., Herguido J. and Menendez M. (2005), A two-zone fluidized bed reactor for catalytic propane dehydrogenation, Chemical Engineering Journal 106(2), 91-96

Gayán P.; de Diego LF. and Adánez J. (1997), Radial gas mixing in a fast fluidized bed, Powder Technology 94(2), 163-171

Gera D. and Gautam M. (1995), Effect of bubble coalescence on throughflow velocity in a 2-D fluidized bed. Powder Technology 83, 49-53

Grace JR. and Baeyens J., (1986), Gas fluidization technology. In: Geldart D. Gas fluidization technology John Wiley & Sons Ltd. pp. 415-463

Grace JR., 1990. High Velocity Fluidized Bed Reactors. Chemical Engineering Science 45 1953-1966.

Grace JR. and Bi H. (1997), Introduction to circulating fluidized beds, in Circulating Fluidized Beds (editor(s): Grace, J. R., Avidan A. and Knowlton T.), Engineering Foundation, New York, 1-19

- Gore RA. and Crowe CT., (1989), Effect of particle size on modulating turbulent intensity. *International Journal of Multiphase Flow* 15(2), 279-285
- Gwyn JE., 1993. Entrance, exit and wall effects on gas/particulate solids flow regimes. In: 4th International Conf. On Circulating Fluid Beds. pp. 679
- Hakimelahi HR.; Sotudeh-Gharebagh R. and Mostoufi N. (2006), Cluster-based modeling of fluidized catalytic oxidation of n-butane to maleic anhydride, *International Journal of Chemical Reactor Engineering* 4, A23
- Herbert PM., Gauthier, TA., Briens, CL. and Bergougnou MA. (1994), Application of fiber optic reflection probes to the measurement of local particle velocity and concentration in gas-solids flow. *Powder Technology* 80, 243-252
- Herbert PM., Gauthier, TA., Briens, CL. and Bergougnou MA. (1998), Flow study of a 0.05 m diameter downflow circulating fluidized bed. *Powder Technology* 96, 255-261
- Huang D., Han M., Wang J. and Jin Y., (2002), Catalytic decomposition process of cumene hydroperoxide using sulfonic resins as catalyst, *Chemical Engineering Journal* 88(1-3), 215-223.
- Huang S., Wang Z. and Jin Y., (1999), Studies on gas-solid-solid circulating fluidized-bed reactors, *Chemical Engineering Science* 54(13-14), 2067-2075
- Jiang P., Bi H., Jean RH. and Fan LS., (1991), Baffle effects on performance of catalytic circulating fluidized bed reactor, *AIChE Journal* 37(9), 1392-1400
- Jin Y., Yu ZQ. Qi CM. and Bai DR., (1988), The influence of exit structure on the axial distribution of voidage in fast fluidized bed. In: Kunii MK., *Fluidization Science and Technology*, Science Press, Beijing, pp. 165-173
- Johansson A.; Johansson F. and Leckner B. (2007), Solids back-mixing in CFB boilers, *Chemical Engineering Science* 62(1-2), 561-573
- Kagawa H., Mineo H., Yamazaki R. and Yoshida K., (1990), A gas-solid contacting model for fast fluidized bed, in *Circulating Fluidized Bed Technology III* (editor(s): Basu P., Horio M. and Hasatani M.), Pergamon Press, Oxford, 551-556
- Kersten SRA., Prins W., van der Drift B. and van Swaaij WPM. (2003), Principles of a novel multistage circulating fluidized bed reactor for biomass gasification, *Chemical Engineering Science* 58(3-6), 725-731
- Kwauk M., (1964), Generalized fluidization II. Accelerative motion with steady profiles. *Scientia Sinica* 13, 1477-1492
- Li Y. and Kwauk M., (1980). The dynamics of fast fluidization. *Fluidization*. Grace JR. and Matsen JM. New York, Plenum Press: 537-544

- Li DB., Zhu J., Ray MB. and Ray AK., (2011), Catalytic reaction in a circulating fluidized bed downer: Ozone decomposition, *Chemical Engineering Science* 66 (20), 4615-4623
- Li DB., Ray AK., Ray MB. and Zhu J., (2013), Catalytic reaction in a circulating fluidized bed riser: Ozone decomposition, *Powder Technology* 342(15), 65-73
- Liu JZ. (2001), Particle and gas dynamics of high density circulating fluidized beds. Phd. Diss. University of British Columbia
- Liu F., Wei, F., Li G., Cheng Y., Wang, L., Luo G., Li Q., Qian Z., Zhang Q. and Jin Y., (2008), Study on the FCC process of a novel riser-downer coupling reactor (iii): industrial trial and CFD modeling, *Industrial and Engineering Chemistry Research* 47(22), 8582-8587
- Lim KS., Zhu JX. and Grace JR., (1995), Hydrodynamics of gas fluidization. *Int. J. Multiphase Flow* 21(Suppl.), 141-193
- Lu H.; Zhao, Y.; Ding J.; Gidaspow, D. and Li, W. (2007), Investigation of mixing/segregation of mixture particles in gas-solid fluidized beds, *Chemical Engineering Science* 62(1-2), 301-317
- Luo B., Yan D., Ma Y. L., Barghi S. and Zhu J., (2007), Characteristics of gas-solid mass transfer in a concurrent downflow circulating fluidized bed reactor, *Chemical Engineering Journal* 132(1-3), 9-15
- Lyngfelt A. and Leckner B. (1999), Combustion of wood-chips in circulating fluidized bed boilers – NO and CO emissions as functions of temperature and air-staging, *Fuel* 78(9), 1065-1072
- Mansoori Z.; Saffar-Avval M.; Basirat Tabrizi H.; Dabir B. and Ahmadi G. (2005), Inter-particle heat transfer in a riser of gas-solid turbulent flows, *Powder Technology* 159(1), 35-45
- Namkung W. and Kim SD., (2000), Radial gas mixing in a circulating fluidized bed, *Powder Technology* 113(1-2), 23-29
- Ouyang S., Lin J. and Potter OE., (1993), Ozone decomposition in a 0.254 m diameter circulating fluidized bed reactor, *Powder Technology* 74(1), 73-78
- Ouyang S., Li XG. and Potter OE., (1995), Circulating fluidized bed as a catalytic reactor: experimental study, *AIChE Journal* 41(6), 1534-1542
- Pärssinen JH. and Zhu JX., (2001a), Axial and radial solids distribution in a long and high-flux CFB riser. *AIChE Journal* 47(10), 2197-2205
- Pärssinen JH. and Zhu J., (2001b), Particle velocity and flow development in a long and high-flux circulating fluidized bed riser. *Chemical Engineering Science* 56, 5295-5303

- Pagliolico S., Tiprigan M., Rovero G. and Gianetto A., (1992), Pseudo-homogeneous approach to CFB reactor design, *Chemical Engineering Science* 47(9-11), 2269-2274
- Pugsley TS., Patience GS., Berruti F. and Chaouki J., (1992), Modeling the catalytic oxidation of n-butane to maleic anhydride in a circulating fluidized bed reactor, *Industrial and Engineering Chemistry Research* 31(12), 2652-2660
- Qi XB., Huang WX. and Zhu JX., (2008), Comparative study of flow structure in circulating fluidized bed risers with FCC and sand particles. *chemical Engineering Technology* 31(4), 542-553
- Reh L., (1999), Challenges of circulating fluid-bed reactors in energy and raw materials industries, *Chemical Engineering Science* 54(22), 5359-5368
- Schoenfelder H., Kruse M. and Werther J., (1996), Two-dimensional model for circulating fluidized-bed reactors, *AIChE Journal* 42(7), 1875-1888
- Schnitzlein MG. and Weinstein H., (1988), Flow characterization in high-velocity fluidized beds using pressure fluctuations. *Chemical Engineering Science* 43, 2605-2614
- Shen CY. and Johnstone HF., (1955), Gas-solid Contact in Fluidized Beds. *AIChE Journal*, 1(3), 349-354
- Sterneus J., Johnsson F. and Leckner B. (2000), Gas mixing in circulating fluidised-bed risers, *Chemical Engineering Science* 55(1), 129-148
- Sun G. and Grace JR., (1990), The effect of particle size distribution on the performance of a catalytic fluidized bed reactor, *Chemical Engineering Science* 45(8), 2187-2194
- Teplitskii Y., Kovenskii V., Nogotov E. and Borodulya V. (2006), Solids mixing in a circulating fluidized bed, *International Journal of Heat and Mass Transfer* 49(21-22), 4183-4193
- van de Velden M.; Baeyens J. and Smolders K. (2007), Solids mixing in the riser of a circulating fluidized bed, *Chemical Engineering Science* 62(8), 2139-2153
- van engelandt G., De Wilde J., Heynderickx G. and Marin G., (2007), Experimental study of inlet phenomena of 35° inclined non-aerated and aerated Y-inlets in a dilute cold-flow riser, *Chemical Engineering Science* 62(1-2), 339-355
- Wang S., Yang X., Lu H.; Yu, L., Wang S. and Ding Y., (2009), CFD studies on mass transfer of gas-to-particle cluster in a circulating fluidized bed, *Computers & Chemical Engineering* 33(2), 393-401
- Wang Y., Zhang J., Zhu J., Yin J. and Wang H., (2009), Experimental research on catalytic decomposition of nitrous oxide on supported catalysts, *Energy Conversion and Management* 50(5), 1304-1307

Wei F. and Zhu JX., (1996), Effect of flow direction on axial solids dispersion in gas-solids cocurrent upflow and downflow systems, *The Chemical Engineering Journal and the Biochemical Engineering Journal* 64(3), 345-352

Wei F., Wan X., Hu Y., Wang Z., Yang Y. and Jin Y., (2001), A pilot plant study and 2-D dispersion-reactor model for a high-density riser reactor, *Chemical Engineering Science* 56(2), 613-620

Westphalen D. and Glicksman L., (1995), Lateral solids mixing measurements in circulating fluidized beds, *Powder Technology* 82(2), 153-167

Xu J., (2010), Hydrodynamics studies on macro- and micro-Flow structure with effects of particle properties in a circulating fluidized bed. PhD Diss. Western University, London

Xu J., Peng B., Zhang C. and Zhu J., (2010), The effects of distributor design on the solids distribution in a CFB riser, *Fluidization XIII: New Paradigm in Fluidization Engineering*, 2010, 375-382

Xu J. and Zhu J., (2010), Experimental study on solids concentration distribution in a two-dimensional circulating fluidized bed, *Chemical Engineering Science* 65(20), 5447-5454

Yan A. and Zhu J., (2004), Scale-up effect of riser reactors (1): Axial and radial solids concentration distribution and flow development. *Industrial & Engineering Chemistry Research* 43(18), 5810-5819

Yan A., Ball J. and Zhu J., (2005a), Scale-up effect of riser reactors (3) axial and radial s flux distribution and flow development. *Chemical Engineering Journal* 109, 97-106

Yan A. and Zhu J., (2005b), Scale-up effect of riser reactors: Particle velocity and flow development. *AIChE Journal* 51, 2956-2964

Yan A., Huang W. and Zhu J., (2008), The influence of distributor structure on the solids distribution and flow development in circulating fluidized beds, *The Canadian Journal of Chemical Engineering* 86(6), 1023-1031

Yang YL., Jin Y., Yu ZQ., Wang ZW., and Bai DR., (1993), The radial distribution of local particle velocity in a dilute circulating fluidized bed. *AIChE Symp. Ser.* 89(296), 81-90

Yerushalmi Y. and Avidan AA., (1985). High velocity fluidization. In: Davidson, J. F., Clift R. and Harrison D., *Fluidization*, Academic Press, New York

Yin L., Wang, S., Lu H.; Ding J., Mostofi R. and Hao Z., (2007), Simulation of effect of catalyst particle cluster on dry methane reforming in circulating fluidized beds, *Chemical Engineering Journal* 131(1-3), 123-134

Zhang H., Zhu JX. and Bergougnou MA., (1999a), Hydrodynamics in downflow fluidized beds (1): solids concentration profiles and pressure gradient distributions. *Chemical Engineering Science*, 55, 4367-4377

Zhang H., Zhu JX. and Bergougnou MA., (1999b), Flow development in a gas-solids downer fluidized bed, *The Canadian Journal of Chemical Engineering* 77(2), 194-198

Zhang H., (1999c), Hydrodynamics of gas-solids downflow fluidized bed (downer) reactor, PhD thesis, The University of Western Ontario, Canada

Zhang H. and Zhu JX., (2000), Hydrodynamics in downflow fluidized beds (2): Particle velocity and solids flux profiles. *Chemical Engineering Science* 55, 4367-4377

Zhang H., Huang WX. and Zhu JX., (2001), Gas-solids flow behavior: CFB riser vs. downer. *AIChE Journal*. 47(9): 2000-2010

Zhang Y., Lu C. and Shi M., (2009), Evaluating solids dispersion in fluidized beds of fine particles by gas backmixing experiments, *Chemical Engineering Research and Design* 87(10), 1400-1408

Zhou J., Grace JR. Lim CJ. and Brereton CM., (1994a), Particle velocity profiles in a circulating fluidized bed riser of square cross-section. *Chemical Engineering Science* 50, 237-244

Zhou J., Grace JR. Qin S. Brereton CM. Lim CJ. and Zhu JX., (1994b), Voidage profiles in a circulating fluidized bed of square cross-section. *Chemical Engineering Science* 49, 3217-3226

Zhou L. and Sohn HY., (1996), Mathematical modeling of fluidized-bed chlorination of rutile, *AIChE Journal* 42(11), 3102-3112

Zhou H., Flamant G. and Gauthier G., (2007), Modelling of the turbulent gas-particle flow structure in a two-dimensional circulating fluidized bed riser. *Chemical Engineering Science* 62, 269-280

Zhu JX., Yu ZQ., Jin Y., Grace JR. and Issangya A., (1995), Cocurrent downflow circulating fluidized bed (downer) reactors - A state of the art review, *The Canadian Journal of Chemical Engineering* 73(5), 662-677

Zhu JX. and Cheng Y., (2005), Fluidized-Bed Reactors and Applications, Chapter 5.3 in *Multiphase Flow Handbook*, ed. Clayton Crowe, CRC Press, New York, pp 5.55-5.93

Zhu J., (2005). *Advanced high velocity fluidization technology*. London, Canada, The University of Western Ontario

CHAPTER 3

Experimental Setup and Measurement Techniques

3.1 Experimental setup

The circulating fluidized bed setup used in the experiments is originally designed, constructed and operated at the University of Western Ontario by Li (2010). Figure 1 shows the schematic diagram of the experimental setup. The system includes three circulating fluidized beds, the left hand fluidized bed serves as a high flux/density circulating fluidized bed riser with an inner diameter of 76 mm and 10 m in height. The right hand fluidized beds are two circulating fluidized bed downers (co-current downflow circulating fluidized beds) of different diameters (inner diameter of 76 mm and 50 mm, respectively). A large downcomer with an inner diameter of 203 mm returns solids during riser operation. At its bottom, there is a solids storage tank with an inner diameter up to 457 mm. The two are used as general solids storage for the entire system. Total solids inventory of FCC particles in the downcomer and storage tank could be up to 450 kg, equivalent to a solids height of approximately 6.0 m. This high solids level ensures high back pressure in the downcomer and enables high solids circulation rates and high solids concentrations in the CFBs.

The multifunctional circulating fluidized bed (MCFB) can be operated as a CFB riser and downer. For CFB riser operations, particles in the storage tank are fluidized by aeration air and they flow into the bottom of the riser column. The particles obtain momentum from the air passing through the riser gas distributor made of perforated plates (2 mm×176 holes, 12% opening area) and are conveyed upward along the riser column. At the top of the riser, particles and gas are separated by primary, secondary and tertiary cyclones and most of the particles returned to the downcomer and further down to the storage tank. Fine particles leaving the cyclones are trapped by the bagfilter and returned periodically to the downcomer.

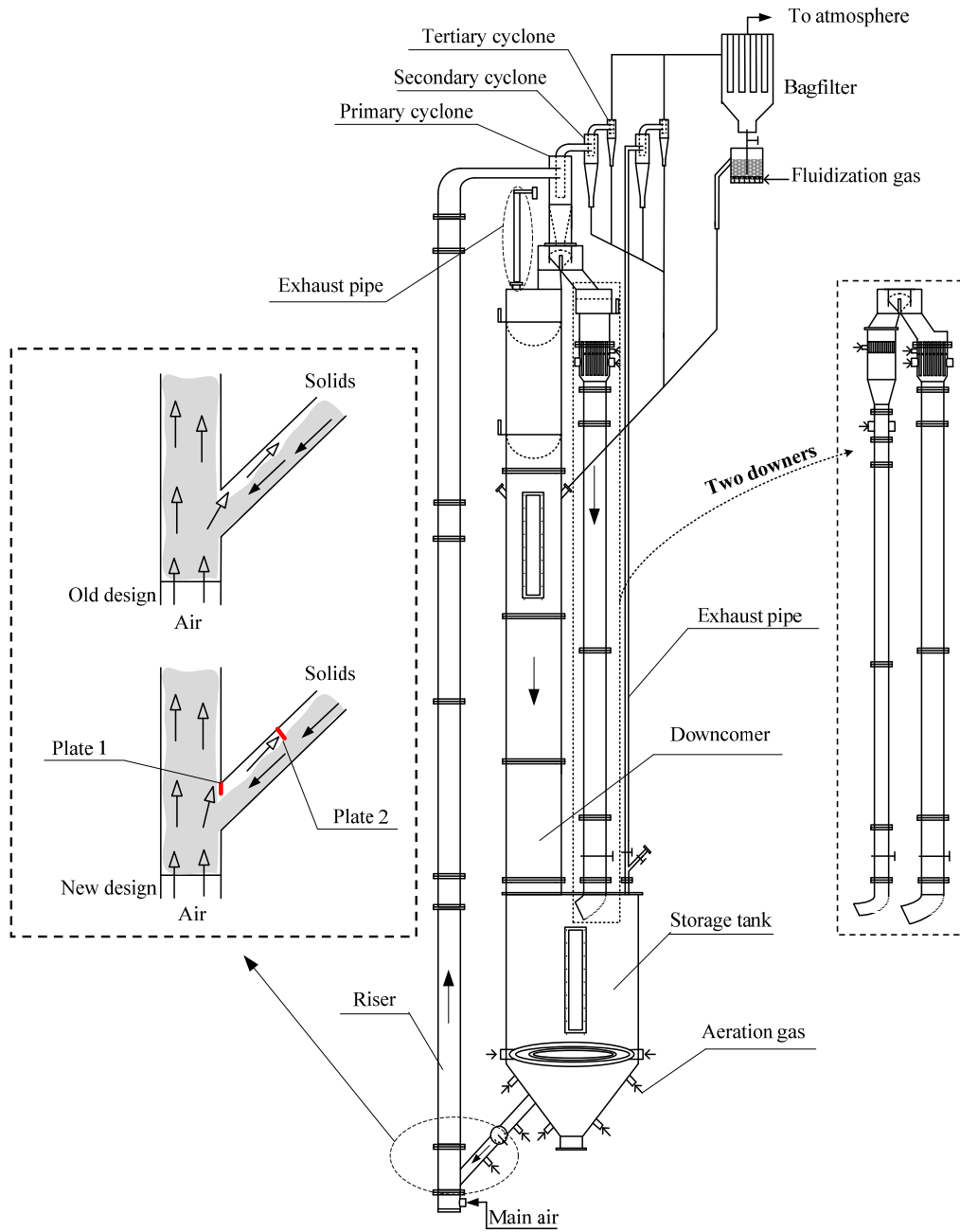


Figure 3.1 Schematic diagram of the multifunctional CFB system.

When the MCFB is under downer operating mode, solid particles are first lifted through the riser, separated by the primary cyclone fixed at the top of the downcomer and then fed into the downers. At the top of either downer is a gas-solids distributor (details shown in Figure 3.1) where the particles are uniformly distributed along with the downer air to flow down concurrently. After fast separation by gravity at the exit of either downer column, most particles are retained in the storage tank, with the remaining particles captured by two cyclones installed in series at the top of the exhaust pipeline and the common bagfilter. To eliminate the effects of solids inventory and other influencing parameters on the hydrodynamic characteristics, the whole experimental work in this study was carried out with a constant particle mass of 400 kg of FCC particles stored in the downcomer and the storage tank.

The entire fluidized bed system uses aluminum as the main construction material with small portions made of Plexiglas for visual observation. In order to minimize possible electrostatic charges formed in the columns during the experiments, the whole fluidized bed system is electrically grounded. A measuring device for solids circulation rate is installed in the top section of the downcomer. By regulating the ball valve located in the solids feeding line connecting the storage tank and the riser column, the solids circulation rate can be adjusted and maintained at the desired level during each experiment.

The original CFB system could be operated with solids circulation rates of up to about 400 kg/m²s (Li, 2010). However, some of the important industrial processes are operated at much higher solids circulation rates. For example, a typical solids circulation rate in the commercial fluid catalytic cracking can be as high as 1200 kg/m²s (Zhu and Bi, 1995). Because of the limited capacity of the gas source and the high pressure drop of the gas-solids separation systems, such high solids fluxes could not be achieved in the previous work. Modifications were made to the original CFB unit to boost the solids flux towards this lever. The main modification work was as follows:

- (1) replaced the blower with a compressor of capacity 1000 standard cubic feet per minute (SCFM) at 100 psi;

(2) installed an additional air exhaust pipe at the top of the of the downcomer to discharge majority of the air flowing upward through the downcomer, with minimum downcomer air flowing into the primary cyclone, so that the pressure drop across the cyclone is significantly reduced (which efficiently increases the available pressure for the riser to achieve higher densities);

(3) installed two small deflecting plates (see the left insert of Figure 3.1) in the solids inlet region, one vertically at the outlet of the inclined pipe covering 30% of the lower end of the inclined feed pipe joining the riser to prevent riser air from flowing into the solids feeding pipe which tends to restrict solids downflow, and the other half-way of the inclined pipe covering 30% of the cross-sectional area of the inclined pipe to direct particles downwards so as to provide a quick “exit route” for the remaining air entering into the feed pipe so that solids movement in the inclined pipe is much faster and steadier.

After modification, the riser could be operated much more steadily at solids circulation rates of up to $1000 \text{ kg/m}^2\text{s}$ much higher than $400 \text{ kg/m}^2\text{s}$ in the original system. This allowed us to operate the CFB system under a wide range of the operating conditions and obtain a comprehensive matrix of solids and gas flows.

3.2 Preparation of particles

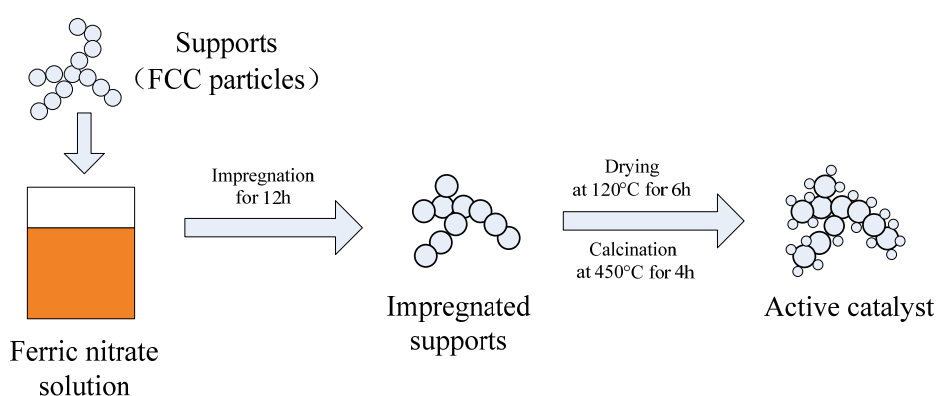
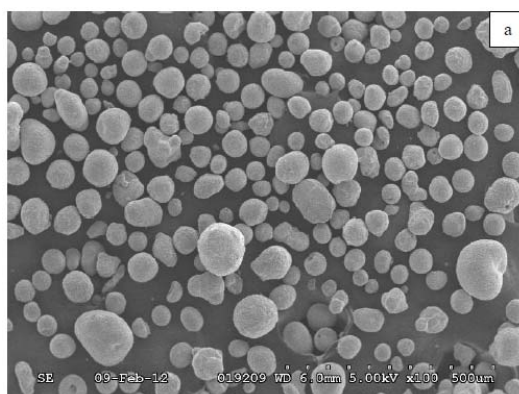


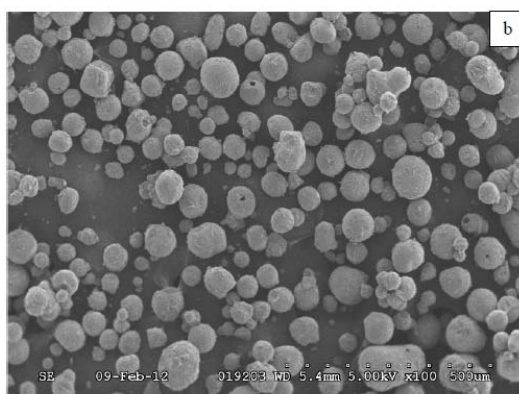
Figure 3.2 Particles activation process.

Spent fluid catalytic cracking (SFCC) particles are activated as the catalyst for ozone decomposition by being impregnated with ferric nitrate solution at room temperature. The impregnation process is shown in Figure 3.2.

FCC particles are impregnated with a 41% $\text{Fe}(\text{NO}_3)_3$ solution for about 12 hours and thereafter the wet particles are dried at 120°C for 6 hrs in the oven followed by calcination at 450°C for 4 hrs. After calcination, iron nitrate is decomposed to iron oxide as the active component loaded on the particles. After breaking up the agglomerates formed during calcination using a ball mill, the resulting particles are sifted using a sieve with pore size $250\ \mu\text{m}$. Scanning electron microscopy (SEM) images of the SFCC particles at 500 magnifications shown in Figure 3.3 suggest that, particles before and after impregnation are similar in size distribution.



SFCC particle (original)



SFCC particles (impregnated)

Figure 3.3 SEM images of original and impregnated SFCC particles at $\times 500$ magnification.

The activated and non-activated particles are mixed to control the overall activity of the particles. Chemical activity of the catalysts used in the experiments is measured before and after each run in a small fixed bed reactor. Particle size distribution shown in Figure 3.4 is measured using BT-9300s laser particle size analyzer. The mean particle size of particles' blend is determined to be 76 μm . Two kinds of particles densities, the apparent particle density, ρ_p , and the bulk particle density, ρ_b , are determined for the particle blend. The particle density, ρ_p , is measured by the “wet cake” method (Sun, 1991). The bulk density, ρ_b , is determined after the bulk volume of a loosely packed bed of a preweighted sample of particles is determined using a graduated cylinder. Apparent particle density and bulk density is 1780 kg/m^3 and 890 kg/m^3 , respectively.

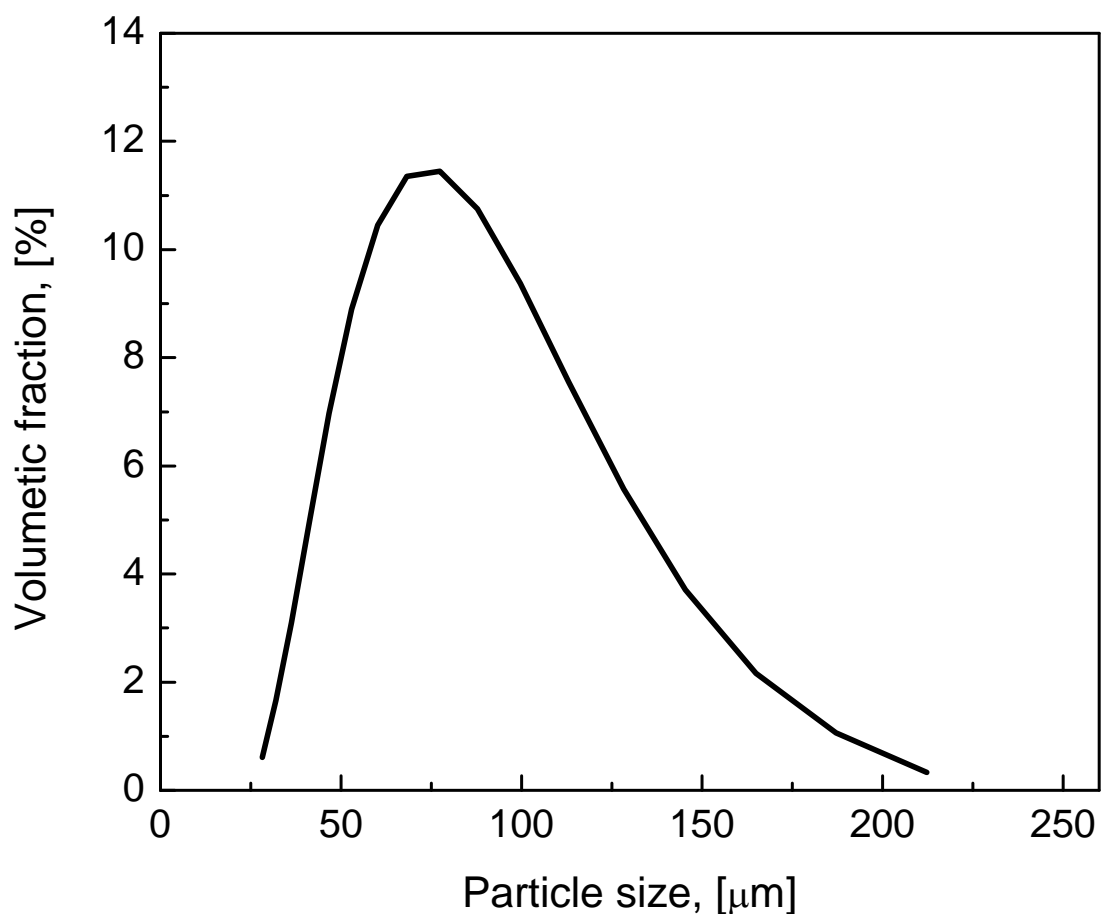


Figure 3.4 Particles size distribution of FCC particles.

3.3 Measurements of U_g and G_s

3.3.1 Measurement of superficial gas velocity

Superficial gas velocities for both riser and downers are monitored by rotameters. They have been calibrated by the manufacturer with the same fluid media (air) under standard calibration condition ($P_c = 101325$ Pa, $T_c = 293.15$ K). When the rotameter is used under different conditions, the actual flow rate can be obtained using the following equation:

$$Q_{actual} = Q_{reading} \sqrt{\frac{P_c T_a}{P_a T_c}} \quad (3.1)$$

where P_a is the actual upstream pressure of the rotameter, Pa; T_a is the actual air temperature, K.

3.3.2 Measurement of solids circulation rate

Solids circulation rate is measured by a measurement column located at the top of the downcomer. The column is divided into two halves by a central vertical plate with two flapper valves fixed at the top and the bottom. By appropriately flipping over the top valve from one side to the other, particles falling into the column are introduced to pass through the other half of the column where the bottom is sealed by the bottom valve. Therefore, solids circulated through the system can be accumulated in one side of the measurement column for a given time period. The solids circulation rate can then be obtained knowing the time period for solids accumulation and the solids packed volume. The solids circulation rate is determined using equation 3.2.:

$$G_s = \frac{\Delta V \cdot \rho_b}{A \cdot \Delta t} \quad (3.2)$$

where ΔV is the volume of the particles accumulated in the half section, ρ_b is the bulk density of the particles, A is the cross-sectional area of the column, and Δt is the time period when the particles accumulate in one side of the measurement column.

3.4 Measurement of pressure drop

To obtain pressure drops along the three beds, 20 differential pressure transducers from Omega Engineering (PX162-027D5V, 8 sets, 0~27.68 inch H₂O; PX164-010D5V, 4 sets, 0~10 inch H₂O; PX163-005BD5V, 3 sets, -5.0~5.0 inch H₂O; and PX164-005D5V, 5 sets, 0~5 inch H₂O) are installed along the riser column. Excitation voltage required for these pressure transducers is 8 VDC (at 20 mA each), giving a voltage output of 1 to 5 VDC over their respective pressure ranges.

Manometers are employed to calibrate the pressure transducers: air source of 20 psig is connected to one end of the manometer and the high-pressure pin of the unidirectional differential pressure transducer. The other end of the U-tube and the other pin of the pressure transducer are open to surrounding air. The typical calibration data are well agreeable with a linear calibration curve. Differential pressure data are acquired with an on-line personal computer via a 16-bits A/D converter. The transducer output signals are linearly proportional to the pressure drop in the range of 0 to 10 kPa. For all experiments, the signals of the differential pressure fluctuations are sampled with a frequency of 1000 Hz and stored on a hard disk of a computer. The total acquisition time is 40 s and thus the maximum length of the time series is 40,000 points. The locations of pressure taps along the fluidized bed are shown in Table 3.1.

Table 3. 1 Locations of pressure taps

Transducer No.	Measuring section (distance from distributor, [m])		
	76 mm riser	76 mm downer	50 mm downer
P01	0.11~0.57	--	--
P02	0.57~1.02	--	--
P03	1.02~1.48	--	--
P04	1.48~1.94	--	--
P05	1.94~2.39	--	--
P06	2.39~2.85	--	--
P07	2.85~3.31	--	--
P08	3.31~3.77	4.02~4.99	0.22~0.76
P09	3.77~4.78	3.26~4.02	0.76~1.27
P10	4.78~5.84	2.64~3.26	1.27~1.78
P11	5.84~6.98	2.13~2.64	1.78~2.35
P12	6.98~7.32	1.63~2.13	2.35~3.26
P13	7.32~7.78	1.12~1.63	3.26~4.18
P14	7.78~8.24	--	--
P15	--	0.61~1.12	--
P16	8.24~8.69	--	--
P17	--	0.22~0.61	--
P18	8.69~9.15	--	--
P19	9.15~9.61	--	--
P20	9.61~10.09	--	--

3.5 Measurement of solids holdup and particle velocity

The optical fiber probe used in this work is model PV6D, developed by the Institute of Processing Engineering, Chinese Academy of Sciences, Beijing, China. The probe and measurement procedure are schematically shown in Figure 3.5.

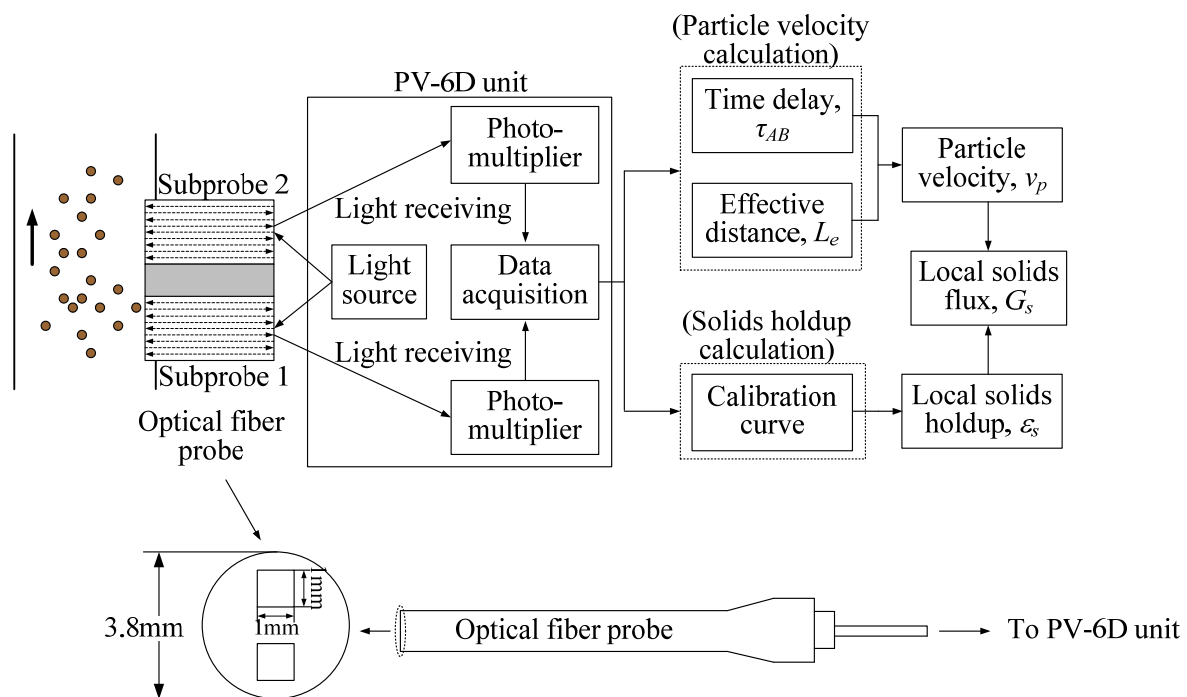


Figure 3.5 Schematic diagram of the novel optical fiber probe and its working principle.

The outer diameter of the probes is 3.8 mm with two subprobes. Each of the subprobes consists of 8000 fine quartz fibers. The effective distance (Oki et al., 1977) of the two vertically aligned subprobes is 1.51 mm, and the active tip area of each subprobe is 1×1 mm. Each subprobe consists of many quartz fibers with a diameter of 15 μm , for light-emitting and receiving, arranged in alternating arrays. In order to prevent particles from occupying the blind zone, a glass cover of 0.2 mm thickness is placed over the probe tip (the underlying theory is elaborated by Liu *et al.* (2003)). As shown in Figure 3.5, light from the source illuminates a measuring volume of particles through the light-emitting fibers. The received light reflected by the particles

is captured by light receiving fibers and processed by a photo-multiplier. The light intensity is then converted into voltage signals and the voltage signals are further amplified and fed into a PC. The voltage signal obtained by the probe is then converted into volumetric solids concentration using a calibration equation. The relationship between the output signals of the optical fiber probe and the local solids holdup (non-linear) is first established through a proper calibration.

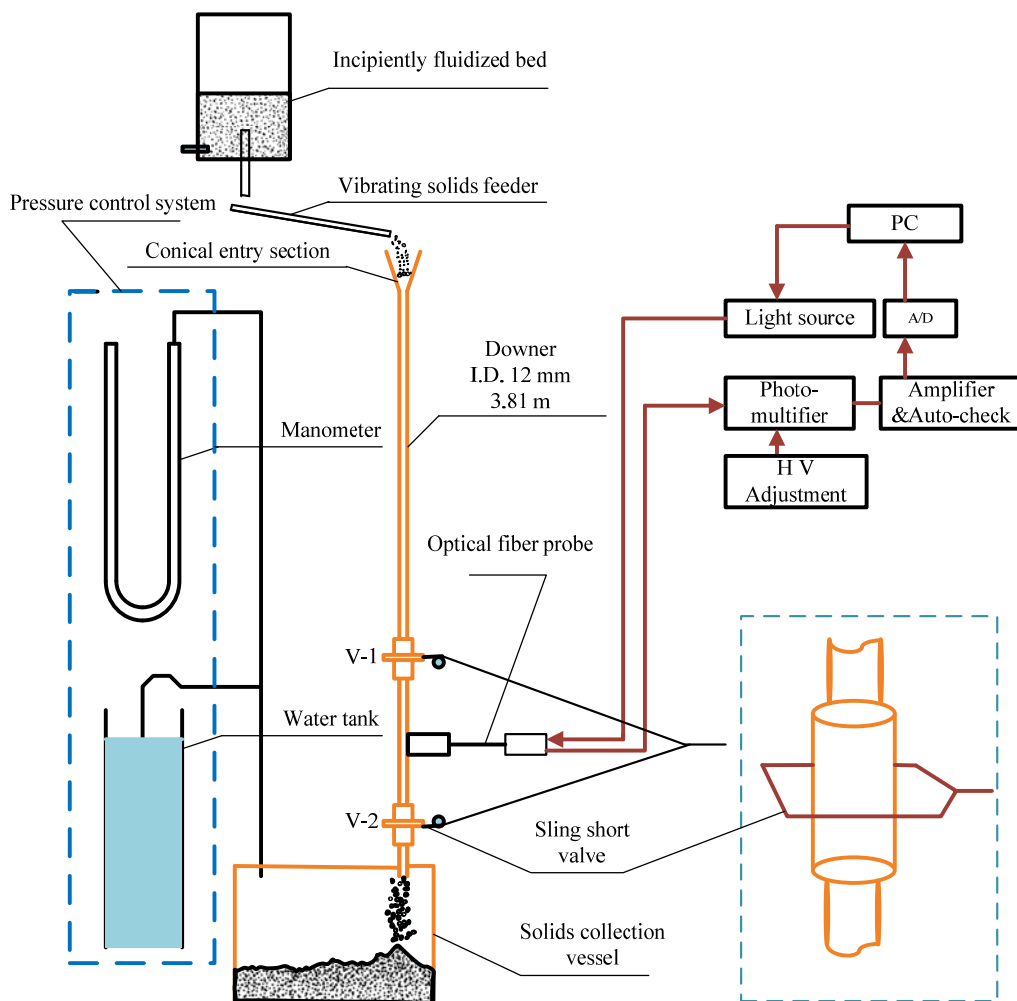


Figure 3.6 Schematic diagram of the apparatus for solids concentration calibration of optical fiber probes.

In this study, the calibration is based on the method developed by Zhang *et al.* (1998). The calibration is carried out in a downer calibration system (Figure 3.6), which can be divided into three parts: (1) the solids feed control system, (2) the solids concentration measurement system, and (3) the solids collection system (Zhang *et al.*, 1998). The falling solids fed by a vibrating solid feeder are trapped by a couple of sling shot valves. Weighing the trapped solids allows the solids concentration to be determined since the suspension density can be calculated from the solids weight and the volume of the trap section. A back pressure control system is used to enhance the back pressure of the downer column to slow down the particles velocity and increase the solids concentration in the column. By adjusting the valve installed in the vibrating solids feeder, with the help from the back pressure control system, various solids mass flow rates can be achieved to provide solids holdups in the downer all the way from dilute to very dense conditions. Under each flow rate condition, the optical fiber probe is applied to measure the solids reflecting light intensity. This is matched with the calculated solids holdup, to build up a full calibration curve. The calibration curve for particle blend is shown in Figure 3.7.

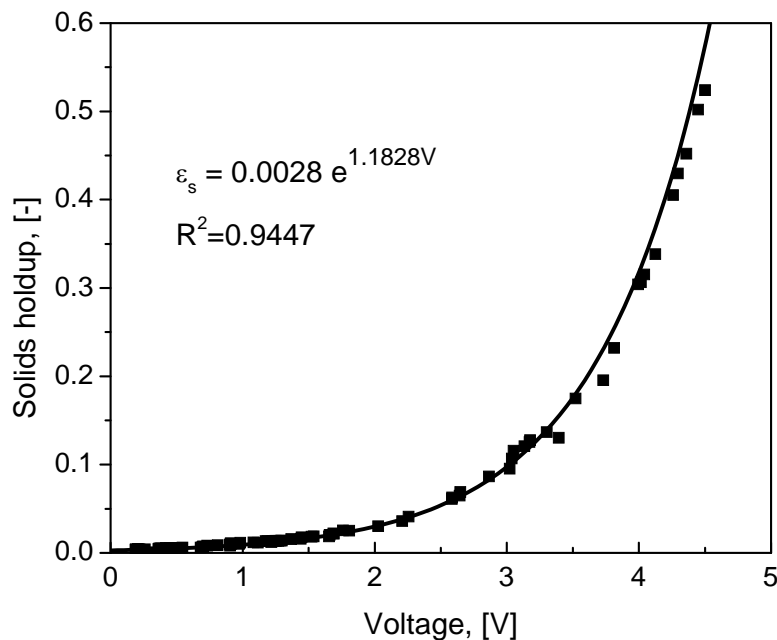


Figure 3.7 Solids holdup calibration curve of the optical fiber probe for FCC catalyst particles

From the voltage time series $V(t)$ and the calibration equation, local instantaneous solids holdup, $\varepsilon_s(t)$, can be calculated:

$$\varepsilon_s(t) = f[V(t)] \quad (3.3)$$

where, f is the calibration function. The time-mean solids concentration ε_s can be given by integrating $\varepsilon_s(t)$ over the time period, T :

$$\varepsilon_s = \frac{1}{T} \int_0^T \varepsilon_s(t) dt \quad (3.4)$$

The cross-sectional average solids holdup $\bar{\varepsilon}_s$, can be calculated as follow:

$$\bar{\varepsilon}_s = \frac{1}{\pi R^2} \int_0^R 2\pi r \varepsilon_s dr = \frac{2}{R^2} \int_0^R \varepsilon_s r dr \quad (3.5)$$

The particle velocity was measured simultaneously with the solids holdup. When particles pass through the tips of the two subprobes, they would produce two similar signals with a time delay τ , which can be calculated by cross-correlation method. Combining the time delay τ with the effective distance between two subprobes, L_e , the instantaneous particle velocity, V_p can be calculated as follow:

$$v_p = \frac{L_e}{\tau} \quad (3.6)$$

To obtain the particle velocities, an integration time of 12.80 ms is set after the optimization (Liu, *et al.*, 2003). Because of the turbulent nature of gas-solids suspension in fluidized beds, a particle passing through the upstream subprobe may not be detected by the downstream subprobes, due to possible particle-particle and/or particle-probe interactions. This may lead to low or even indeterminate cross-correlation coefficients. Such poorly or uncorrelated data need to be eliminated. The correlation coefficients are set to be higher than 0.6 as the criteria to collect the acceptable results. The direction of the particle motion is determined based on the maximum

cross-correlation coefficient from the positive and negative correlation of the two channel signals (Nieuwland *et al.*, 1996; Werther, 1999 and Zhu *et al.*, 2001).

The cross-sectional average particle velocity weighted by the local solids concentrations can be calculated as follows:

$$\bar{v}_p = \frac{2}{R^2 \bar{\varepsilon}_s} \int_0^R v_p \varepsilon_s r dr \quad (3.7)$$

3.6 Measurement of ozone concentration

3.6.1 Ozone generation

Due to its strong oxidation characteristic and the explosion hazard, ozone must be generated when used in the experiments (Kirschner, 2000). There are three main methods of ozone generation for laboratory and industrial applications: ultraviolet radiation, electrolysis and corona discharge (Wojtowicz, 2005). An ozone generator with electronic corona discharge method (Model AE15M, manufactured by Absolute Ozone Inc.) was used in this study. Using bottled oxygen as gas supply, it produces up to 30 g/h of ozone depending on the oxygen flow rate and electrical current settings. Its working pressure is 5-50 psig, with oxygen flow rate of 0.1-10 standard liter per minute (SLPM).

Generator performance test was performed at 20°C by the manufacturer, with the generator powered on for more than 30 minutes. Different oxygen flow rates and potentiometer settings were tested, with the test results presented in Table 3.2. Higher oxygen flow rate and electrical current throughput will give higher ozone production, but when oxygen flow rate reaches 5 liter per minute (LPM), the increase of the ozone production is not very significant. The output ozone concentration (4-12% by weight) decreases with increasing oxygen flow rate.

Table 3.2 Test results for ozone generator performance

Oxygen flow	Gas pressure	Current potentiometer	Ozone production	Ozone concentration
[SLPM]	[psig]	[%]	[g/h]	[% wt]
0.5	20	40	4.79	11.99
1	20	50	8.27	10.35
2	20	60	14.77	9.24
3	20	70	19.86	8.29
4	20	80	24.09	7.54
5	20	100	26.99	6.76
6	20	100	28.70	5.99
7	20	100	30.09	5.38
8	20	100	31.02	4.85
9	20	100	31.29	4.35

The O₂-O₃ mixture exiting from the ozone generator is mixed with the main fluidization air before entering the CFB riser or downer. With a fairly long flow path and several L-bends in the main air feeding lines, the mixing process is thorough. To ensure that the O₂-O₃ stream could be smoothly injected into the main air, an output pressure of 50 psig is used for the regulator installed on the oxygen gas cylinder, maintaining a much higher pressure for the O₂-O₃ flow than that of the main air with the pressure of less than 30 psig.

The resulting initial ozone concentration (C_0) with the main air before is set to 80-100 ppm, balancing various factors such as detection range of the ozone analyzer, oxygen consumption, and ozone concentration stability.

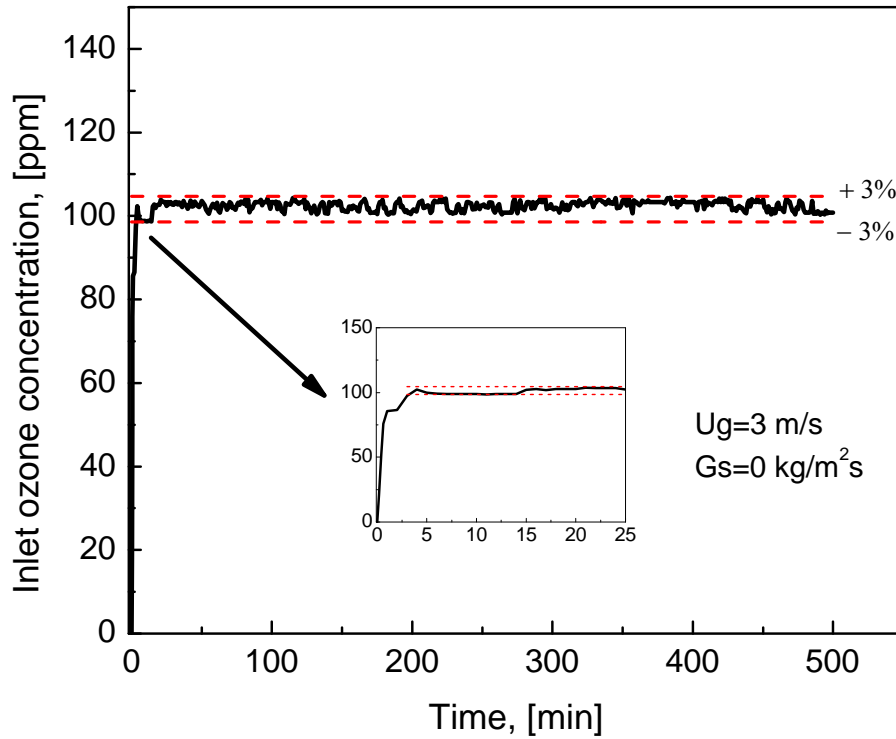


Figure 3.8 Stability of the inlet ozone concentration against time.

To ensure that the data of ozone concentration in CFB riser or downers is reliable, it is necessary to maintain a stable inlet ozone concentration during the experimental run. Three factors may affect the stability of the initial ozone concentration: ozone production by the ozone generator, main air supply, and the mixing process. The ozone analyzer is firstly warmed up for about an hour before performing the experiments. Figure 3.8 shows the change of the initial ozone concentration (CFB riser or downer inlet ozone concentration) with the time under superficial gas velocity of 5.0 m/s and solids circulation rate of 100 kg/m²s. Ozone-air samples are taken from the windbox of the 76 mm riser. As can be seen from the magnified Figure for data in the first 25 min, it takes only 5 min before the initial ozone concentration can reach a steady state. When a stable concentration is reached, the ozone concentration fluctuations are within the range

of $\pm 3\%$ around the mean value. Thereafter, this stable concentration can last for more than 3 hours, long enough for each experimental run, which typically takes less than 2 hours.

3.6.2 Ozone sampling

To reduce ozone loss by decomposition during the sampling process, ozone-inert materials (e.g. stainless steel, Teflon, copper and aluminum) are used for sampling probes. Valves were made of copper and the 3 mm i. d. and 6 mm o. d. piping lines were made of Teflon. Gas samples are continuously drawn from the CFB column through a sampling system shown in Figure 3.9 using brass tubes (6 mm o.d. and 0.36 mm wall thickness) as the sampling probes. The tip of the probe is covered with a fine stainless steel mesh to prevent particles from being entrained into the sampling system. The velocity of gas sucked for sampling is 1.5 LPM, low enough to assure minimal disturbance of the flow structure in the CFB system. A high pressure purging air stream of 100 psig is introduced to blow away any particles potentially caked in the sampling probes.

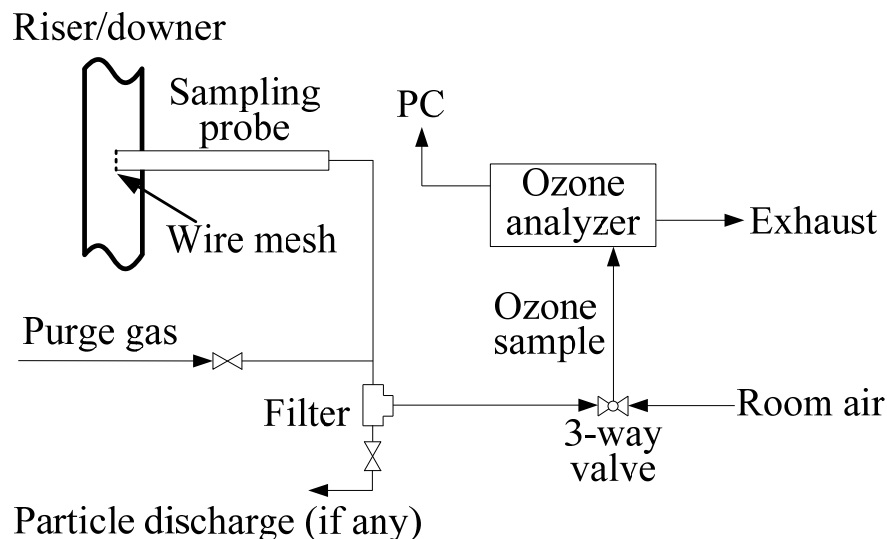


Figure 3.9 Ozone sampling and testing.

3.6.3 Ozone testing

Many methods have been reported on how to measure ozone concentration (Kirschner, 2000 and Seinfeld and Pandis, 2006). Ethylene chemiluminescence and UV absorption are the two efficient techniques (Proffitt and McLaughlin, 1983; Butkevich *et al.*, 1985; Sen *et al.*, 1996; Wilson, 2005 and Li *et al.*, 2006). Analysis of ozone by ethylene chemiluminescence is based on the gas-phase reaction between ozone and ethylene to produce formaldehyde and oxygen with emission of light. The intensity of this photoemission is proportional to the concentration of ozone, and is measured by a photomultiplier. The UV-absorption technique has been used more extensively to make in situ ozone measurements (Kirschner, 2000).

In this study, an ozone analyzer (Model 49i, Thermo Electron Inc.) that employs the UV photometric method of measurement is used to measure the amount of ozone in the sample air. It is a dual-cell photometer, having both sample and reference air flowing at the same time. Each cell has a length of 37.84 cm and an inner diameter of 0.91 cm, with the internal surfaces coated with polyvinylidene fluoride (PVDF) to ensure that ozone undergoes no decomposition upon exposure to the internal surface of the cells (Thermo Electron Inc., 2004 and 2005). The UV light source used in ozone photometers is 253.7 nm from a low-pressure Hg discharge lamp. The light intensities in the sample air and the sample-free air are used to calculate ozone concentration according to the Beer-Lambert law:

$$C = \left(10^6 \times \frac{P_0 T}{P T_0} \right) \frac{1}{\sigma l} \ln \left(\frac{I_0}{I} \right) \quad (3.8)$$

where

- I_0 intensity of the light beam with no ozone present [cd]
- I intensity of the light beam after passing through the sample [cd]
- l length of the light path through the sample [cm]
- C molar fraction of ozone in the sample [ppm]

- σ specific absorption coefficient of ozone at wavelength 253.7 nm, 308 cm^{-1}
- P pressure [mmHg]
- P_0 standard pressure, 760 mmHg
- T temperature [K]
- T_0 standard temperature, 273.15 K

Figure 3.10 shows the schematic diagram of the TEI 49i ozone analyzer. The air sample is pulled through the analyzer by an air pump at the exit of the analyzer. Ozone concentration of the air is measured in the cells using UV radiation. The solenoid valves operating under computer control allow sample gas to pass through Cell A and reference gas (with ozone depleted in an ozone scrubber) through Cell B, or vice versa, depending upon which cycle the instrument is performing. The analyzer monitors temperature (accuracy $\pm 0.2^\circ\text{C}$), pressure (accuracy $\pm 0.3 \text{ mmHg}$) and flow rates of the sample air in the cells. Temperature and pressure compensation features based on Equation (3.8).

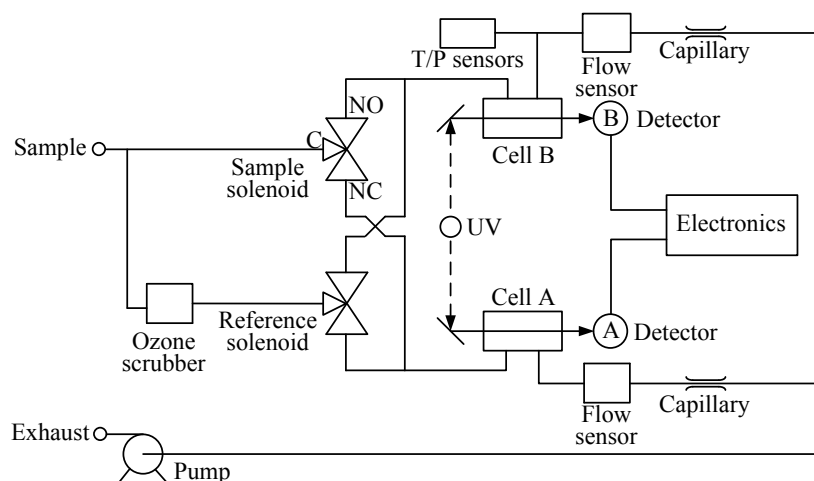


Figure 3.10 Schematic diagram of TEI 49i ozone analyzer.

3.6 Summary

A multifunctional gas-solids circulating fluidized bed system is modified in order to obtain high flux/density operating conditions. An optical fiber probe, differential pressure transducers, and a UV ozone analyzer are used to measure local solids concentration and particle velocity, pressure drop, and ozone concentration in the CFBs, respectively.

Spent FCC catalyst particles impregnated with iron oxide are employed as activated catalyst for ozone decomposition reaction in this study. The impregnation process did not change the particles density and size distribution much so that a mixture of non-activated and activated particles is used in the experiments.

Ozone sampling probes made of brass tubes covered with fine wire mesh on the tip are developed to extract ozone samples from the CFB columns, providing very good representation of the actual ozone concentration in the CFBs. A high pressure purging air stream of 100 psig is introduced to blow away any particles potentially caked in the sampling probes.

The stability check of the inlet ozone concentration over a long time period shows a stable air supply, good performance of the ozone generator, and thorough mixing of the fluidization air and the O₂-O₃ stream.

Nomenclature

A	Cross-sectional area of the column [m^2]
C	molar fraction of ozone in the sample [ppm]
C_0	inlet (initial) ozone concentration [ppm]
G_s	solids circulation rate [$\text{kg}/(\text{m}^2 \cdot \text{s})$]
I	intensity of the light beam after passing through the sample [cd]
I_0	intensity of the light beam with no ozone present [cd]
l	length of the light path through the sample [cm]
P	pressure [mmHg]
P_0	standard pressure, 760 mmHg
P_a	standard pressure of the rotameter [Pa]
P_c	actual upstream pressure of the rotameter [Pa]
Q_a	actual volumetric flowrate of the air [m^3/s]
Q_r	volumetric flowrate of the air reading from the rotameter [m^3/s]
R	radius of the column [m]
t	time [s]
T	temperature [K], or time interval [s]
T_0	standard temperature, 273.15 K
T_a	actual air temperature [K]
v_p	particle velocity [m/s]
U_g	superficial gas velocity [m/s]
V	voltage [volt]

Greek letters

ε_s	solids holdup [-]
-----------------	-------------------

- $\bar{\varepsilon}_s$ cross-sectional average solids holdup [-]
 ρ_b, ρ_p bulk density, apparent particle density [kg/m^3]
 σ specific absorption coefficient of ozone at 253.7 nm, 308 cm^{-1}
 τ transit time between light-receiving fiber 1 and 2 [s]
 ΔV volume of the particles accumulated in the measurement column

Subscripts

- $0, 1$ initial (inlet) and exit ozone concentration
 $1, 2$ subprobe of optical fiber probe
 g gas
 p particle
 r reaction
 s solids

References

- Butkevich VI., Skvortsova GV. and Shalamyanskii AM., (1985), Problems of atmospheric-ozone monitoring, *Measurement Techniques* 28(5), 447-451
- Kirschner MJ., (2000), Ozone, in *Ulmann's Encyclopedia of Industrial Chemistry*, Wiley-VCH Verlag GmbH & Co. KGaA
- Li DB., (2010), Investigation of circulating fluidized bed riser and downer reactor performance for catalytic ozone decomposition, Ph.D. Diss. The University of Western Ontario
- Li Y., Lee SR. and Wu CY., (2006), UV-absorption-based measurements of ozone and mercury, an investigation on their mutual interferences, *Aerosol and Air Quality Research* 6(4), 418-429
- Liu JZ., Grace JG., and Bi HT., (2003a), Novel multifunctional optical-fiber probe, development and validation, *AIChE Journal* 49(6), 1405-1420
- Nieuwland JJ. and Meijer R., (1996), Measurements of solids concentration and axial solids velocity in gas-solid two-phase flows, *Powder Technology* 87(2), 127-139
- Proffitt MH. and McLaughlin RJ., (1983), Fast-response dual-beam UV-absorption ozone photometer suitable for use on stratospheric balloons, *Review of Scientific Instruments* 54(12), 1719-1728
- Seinfeld JH. and Pandis SN., (2006), *Atmospheric chemistry and physics, from air pollution to climate change*, John Wiley & Sons, Inc
- Sen B., Sheldon WR. and Benbrook JR., (1996), Ultraviolet-absorption photometer for measurement of ozone on a rocket-boosted payload, *Applied Optics* 35(30), 6010-6014
- Sun GL., (1991), Influence of particle size distribution on the performance of fluidized bed reactors, PhD thesis, The University of British Columbia, Canada
- Werther J., (1999), Measurement techniques in fluidized beds, *Powder Technology* 102(1), 15-36
- Wilson KL., (2005), Water vapor interference in the UV absorption measurement of atmospheric ozone, PhD thesis, University of Colorado, the U.S
- Wojtowicz JA., (2005), Ozone, in *Kirk-Othmer Encyclopedia of Chemical Technology*, John Wiley & Sons

Zhang H., Johnston PM., Zhu JX., de Lasa HI., and Bergougnou MA., (1998), A novel calibration procedure for a fiber optic solids concentration probe, *Powder Technology* 100, 260-272

Zhu JX. and Bi HT., (1995), Distinctions between low density and high density circulating fluidized beds, *The Canadian Journal of Chemical Engineering* 73,644-649

Zhu JX. and Li GZ., (2001), Direct measurements of particle velocities in gas-solids suspension flow using a novel five-fiber optical probe, *Powder Technology* 115, 184-192

CHAPTER 4

Hydrodynamics in a HDCFB Riser-Solids Holdup and Flow Development

4.1 Introduction

Circulating fluidized beds (CFBs) have been successfully and widely used in industrial operations such as combustion, Fischer-Tropsch synthesis, partial oxidation, and fluid-catalytic cracking (FCC) (Bi and L. Fan, 1992 and Zhu and Cheng, 2005). The FCC process has been considered as one of the most successful processes which are used to convert high molecular-weight heavy oil stocks into lighter hydrocarbon products by utilizing a riser reactor, where the solids circulation rate could range from 400 kg/m²s to 1200 kg/m²s and the superficial gas velocity from 6 m/s to 28 m/s, increasing with the height (Zhu and Bi, 1995). Circulating fluidized beds operating under high solids flux and/or high solids holdup conditions can be referred to as high flux (HFCFB) and/or high density circulating fluidized beds (HDCFB), while those operating at low solids flux (e.g. 200 kg/m²s) and low suspension densities (3% in the developed region) are low density circulating fluidized beds (LDCFB) (Bi and Zhu, 1993). Good understanding of the gas and solids flow structures in CFB reactors is critical for proper industrial design and operation. Despite extensive researches dedicated to gas-solids fluidized bed over the past several decades, very limited work has been conducted under solids circulation rates beyond 500 kg/m²s (Azzi *et al.*, 1991; Martin *et al.*, 1992; Contractor *et al.*, 1994 and Knowlton, 1995).

Recently, studies under high solids flux (Issangya *et al.*, 1999; Grace, 2000; Karri and Knowlton, 1999; Parssinen and Zhu, 2001; and Yan and Zhu, 2004) have shown that the hydrodynamics are quite different compared to low flux and low density CFB risers operated with G_s of 200 kg/m²s or less. Issangya *et al.* (1999) conducted tests in a 6 m high riser under high superficial gas velocities ($U_g = 4-8$ m/s) and high solids fluxes ($G_s = 200-425$ kg/m²s) and reported that there was negligible net downflow of solids at the wall, and the cross-sectional mean solids holdups

ranged from 0.1 to 0.2, with little axial variation. Liu *et al.* (1999) studied gas dispersion in the same system used by Issangya *et al.* (1999) and found that gas backmixing became smaller for high-density operating conditions. More recently, Bi (2004) further investigated the gas and solids mixing in high density risers. His results illustrated that there existed a clear transition of both gas and solids axial mixing behavior when the operating conditions changed from LDCFB to HDCFB, corresponding to the disappearance of the solids downward flow near the wall. Grace *et al.* (1999) proposed a new flow regime named “dense suspension upflow” (DSU) to represent the flow dynamics inside a high density riser and claimed that this flow regime “clearly requires both high superficial gas velocity and high solids fluxes.” Compared to the results in DSU regime, Pärssinen *et al.* (2001) described that the axial solids holdup was clearly less than 0.1 in the upper section of the riser with a dense bottom region ($\epsilon_s \approx 0.2$) which clearly was different from solids holdups in the DSU regime. On the other hand, radial solids concentration profiles at high G_s ($>300 \text{ kg/m}^2 \text{ s}$) were less uniform than that of lower G_s ($<200 \text{ kg/m}^2 \text{ s}$) reported by Issangya *et al.* (1999). Solids holdups were found to be lower than 0.06 in the center region ($r/R < 0.5$) and increased to 0.4-0.44 at the wall region under high flux operating conditions.

Understanding the fluid and particle dynamics is evidently of importance to successful modeling of CFB reactors. Flow dynamics also influences pressure drop across the riser, heat transfer (Grace *et al.*, 1986) as well as erosion rate of surfaces (Zhu *et al.*, 1989). Improved understanding of the flow structures in high flux/density circulating fluidized bed systems should enable better comprehension of the advantages and limitations of HDCFB reactors, in turn leading to more reliable scale-up and more cost-effective units (Issangya, 1998). Moreover, further increase of the solids flux and solids suspension density will be very useful for other applications requiring even higher solids/gas ratios and higher solids concentration. In addition, extension of risers to higher density conditions would be of considerable fundamental interest. It is possible to operate well beyond conditions which are usually considered to induce choking with careful design of the equipment and for relatively fine (no-slugging) systems (Bi *et al.*, 1993 and Zhu and Bi, 1995). It has been shown that the dense region at the bottom can extend to the whole riser leading to a high density riser with overall solids holdup of 0.15-0.20 (Contractor *et al.*, 1994 and Issangya *et al.*, 1999). Based on these conditions, it is of interest to study flow

regimes, the mechanism of instability, local phase segregations and axial and radial dispersions under loading conditions and suspension densities which exceed those previous researches (Zhu and Bi, 1995).

By using an optical fiber probe system, which can take the measurements of solids holdup and particle velocity simultaneously, this study was aimed at providing improved experimental investigation in high flux/density circulating fluidized bed riser, including local solids holdup distribution and its evolution with operating conditions. The fluctuations of the local flow structures were also investigated.

4.2 Experimental details

4.2.1 CFB experimental setup

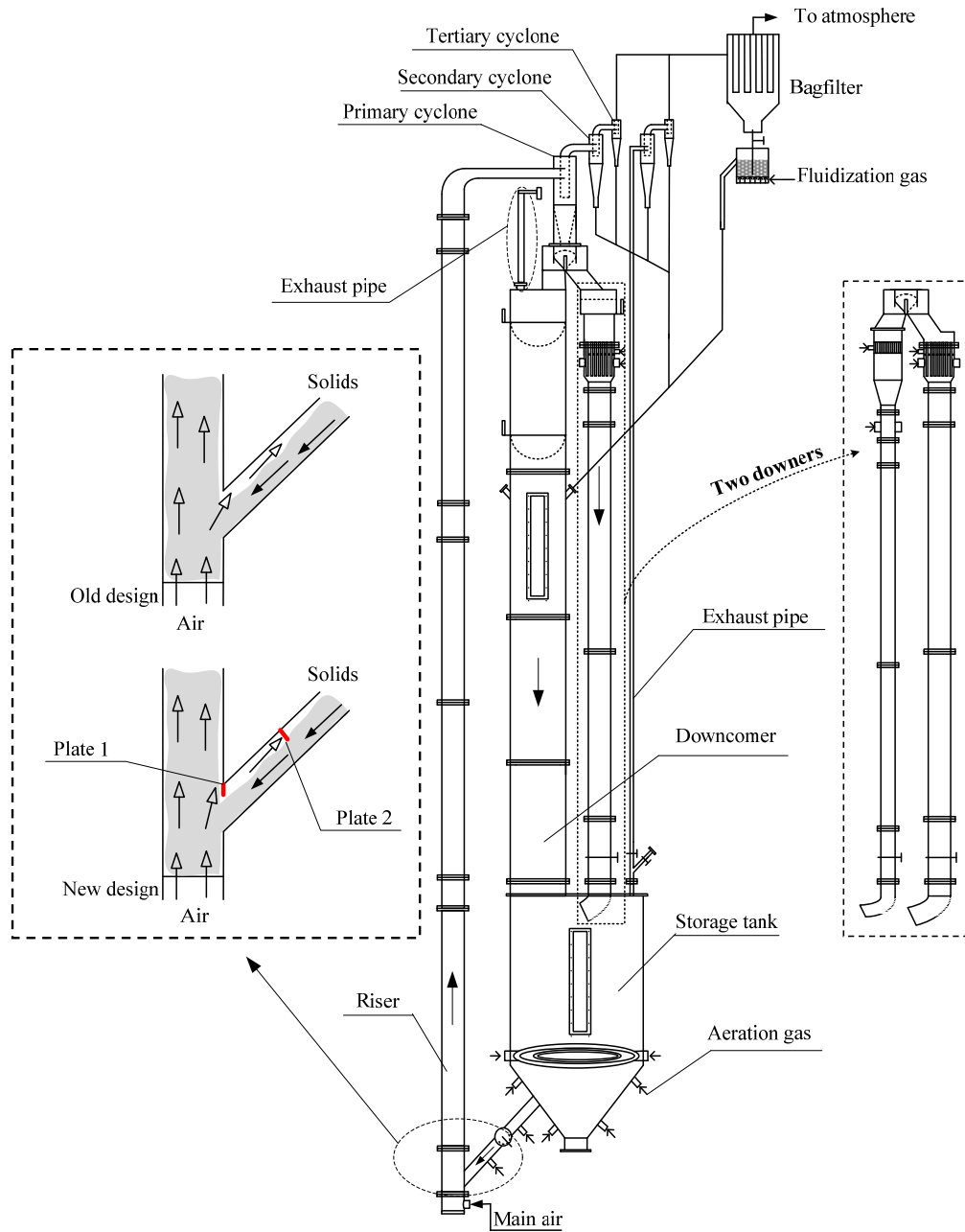


Figure 4.1 Schematic diagram of the multifunctional CFB system.

All experiments were conducted in a multifunctional circulating fluidized bed (MCFB) system, schematically shown in Figure 4.1. The system includes three circulating fluidized beds, the left hand fluidized bed serves as a high flux/density circulating fluidized bed riser (76 mm i. d. and 10 m high). The right hand fluidized beds are two circulating fluidized bed downers (co-current downflow circulating fluidized beds) of different diameters (76 mm i. d. and 5.8 m high and 50 mm and 4.9 m high, respectively). A downcomer with an inner diameter of 203 mm returns solids during riser operation. At its bottom there is a solids storage tank with an inner diameter up to 457 mm. The two are used as general solids storage for the entire system. Total solids inventory of FCC particles in the downcomer and storage tank could be up to 450 kg, equivalent to a solids height of approximately 6.0 m. This high solids level ensures high back pressure in the downcomer and enables high solids circulation rates and high solids concentrations in the CFBs.

The multifunctional circulating fluidized bed (MCFB) can be operated as a CFB riser and downers. For CFB riser operations, particles in the storage tank fluidized by aeration air and then flow into the bottom of the riser and obtained momentum from the air passing through the riser gas distributor made of perforated plates (2 mm×176 holes, 12% opening area) and are conveyed upward along the column. At the top of the riser, particles and gas are separated by primary, secondary and tertiary cyclones and most of the particles returned to the downcomer and further down to the storage tank. Fine particles leaving from the cyclones are trapped by the bagfilter and returned periodically to the downcomer. When the MCFB is under downer operating mode, solid particles are first lifted through the riser, separated by the primary cyclone fixed at the top of the downcomer and then fed into the downers. At the top of either downer is a gas-solids distributor (details shown in Figure 4.1) where the particles are uniformly distributed along with the downer air to flow down concurrently. After fast separation by gravity at the exit of either downer column, most particles are retained in the storage tank, with the remaining particles captured by two cyclones installed in series at the top of the exhaust pipeline and the common bagfilter. To eliminate the effects of solids inventory and other influencing parameters on the hydrodynamic characteristics, the whole experimental work in this study was carried out with a constant particle mass of 400 kg of FCC particles stored in the downcomer and the storage tank.

The entire fluidized bed system uses aluminum as the main construction material with small portions made of Plexiglas for visual observation. In order to minimize possible electrostatic charges formed in the columns during the experiments, the whole fluidized bed system is electrically grounded. A measuring device for solids circulation rate is installed in the top section of the downcomer. By regulating the ball valve located in the solids feeding line connecting the storage tank and the riser column, the solids circulation rate can be adjusted and maintained at the desired level during each experiment. The fluidization gas used in this study is air at ambient temperature, supplied by a large compressor capable of delivering 1000 SCFM at 100 psi. Equilibrium FCC catalyst particles impregnated with ferric oxide (Fe_2O_3) are used in this study and other catalytic ozone decomposition experiments. The Sauter mean diameter and the particle density is $76 \mu\text{m}$ and 1780 kg/m^3 respectively. The particle size distribution measured using BT-9300s laser particle size analyzer is listed in Table 4.1.

Table 4.1 Size distribution of the FCC particles.

Particle Size (μm)	Volume Fraction (%)
0-20	0.61
20-40	9.72
40-60	26.32
60-80	22.80
80-130	33.24
>130	7.31

4.2.2 Measurements of solids holdup

Experimental measurements include differential pressure, local solids concentration (solids holdup) and particle velocity. Twenty pressure taps were installed along the CFB column and

connected with 19 differential pressure transducers (Omega PX162) to measure axial profiles of pressure gradient. The pressure gradient was mainly used to double check the solids holdup measured by an optical fiber probe mentioned below. Local solids holdup and particle velocity were measured simultaneously using a novel reflective-type optical fiber probe which has been shown to be effective and accurate for measuring the local solids concentration and particle velocity in high velocity fluidized beds and thus has been widely used by many investigators (Patrose and Caram, 1982 and Zhou *et al.*, 1995). It yields high signal-to-noise ratios and is nearly free from interference by temperature, humidity, electrostatics and electromagnetic field. Moreover, its small size does not significantly disturb the overall flow structure in CFB systems with proper design. The optical fiber probe used in this work is model PV6D, developed by the Institute of Processing Engineering, Chinese Academy of Sciences, Beijing, China. The probe and measurement procedure are schematically shown in Figure 2. The outer diameter of the probes is 3.8 mm and it has two subprobes. The effective distance of the two vertically aligned subprobes is 1.51 mm, and the active tip area of each subprobe is 1×1 mm. Each subprobe consists of many quartz fibers with a diameter of 15 μm, for light-emitting and receiving, arranged in alternating arrays. In order to prevent particles from occupying the blind zone, a glass cover of 0.2 mm thickness is placed over the probe tip. The underlying theory was elaborated by Liu *et al.* (2003).

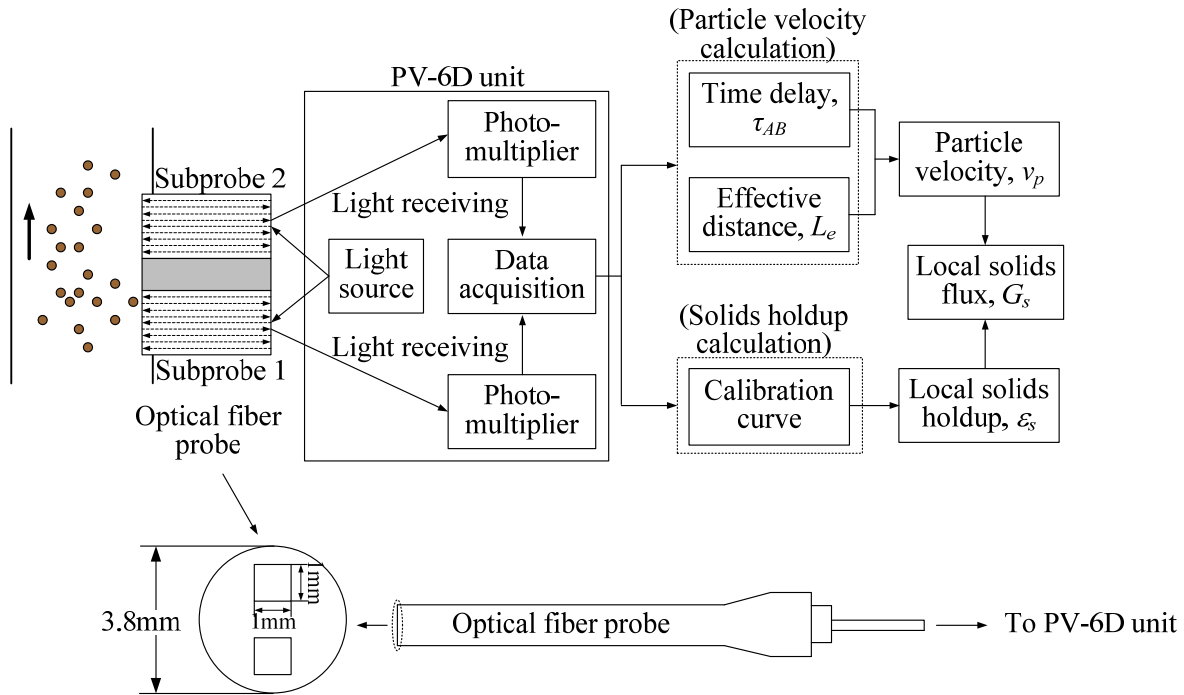


Figure 4.2 Schematic diagram of the novel optical fiber probe and its working principle.

As shown in Figure 4.2, light from the source illuminates a measuring volume of particles through the light-emitting fibers. The received light reflected by the particles is captured by light receiving fibers and processed by a photo-multiplier. The light intensity is then converted into voltage signals and the voltage signals are further amplified and fed into a PC. The voltage signal obtained by the probe is then converted into volumetric solids concentration using a calibration equation. The relationship between the output signals of the optical fiber probe and the local solids holdup (non-linear) is first established through a proper calibration based on the method developed by Zhang *et al.* (1998).

From the voltage time series $V(t)$ and the calibration equation, local instantaneous solids holdup, $\varepsilon_s(t)$, can be calculated:

$$\varepsilon_s(t) = f[V(t)] \quad (4.1)$$

where, f is the calibration function. The time-mean solids concentration ε_s can be given by integrating $\varepsilon_s(t)$ over the time period, T :

$$\varepsilon_s = \frac{1}{T} \int_0^T \varepsilon_s(t) dt \quad (4.2)$$

The cross-sectional average solids holdup $\bar{\varepsilon}_s$, can be calculated as follow:

$$\bar{\varepsilon}_s = \frac{1}{\pi R^2} \int_0^R 2\pi r \varepsilon_s dr = \frac{2}{R^2} \int_0^R \varepsilon_s r dr \quad (4.3)$$

In order to map the entire cross-section of the riser, ten axial measuring ports ($z = 0.59, 1.02, 1.94, 2.85, 3.77, 4.78, 5.84, 7.78, 9.61, \text{ and } 10.09$ m above the gas distributor) are installed along the column. Measurements are conducted at six radial positions ($r/R = 0, 0.316, 0.548, 0.707, 0.837$ and 0.950 , where r is the distance from the center and R is the riser radius) on each axial level of the CFB riser system. These positions are determined by dividing the column cross-section into five equal areas and determining the mid-point of each of these areas. For the hydrodynamic experiments in the current study, voltage signals from the optical fiber probe are sampled at a frequency of 100 kHz with 1,638,40 data points for each measurement under a wide range of operating conditions so that detailed dynamic nature of the flow structure can be fully collected. To get the valid and repeatable data, all measurements are repeated at least 5 times.

4.3 Results and discussion

4.3.1 Achieving high flux/density operating conditions in CFB riser

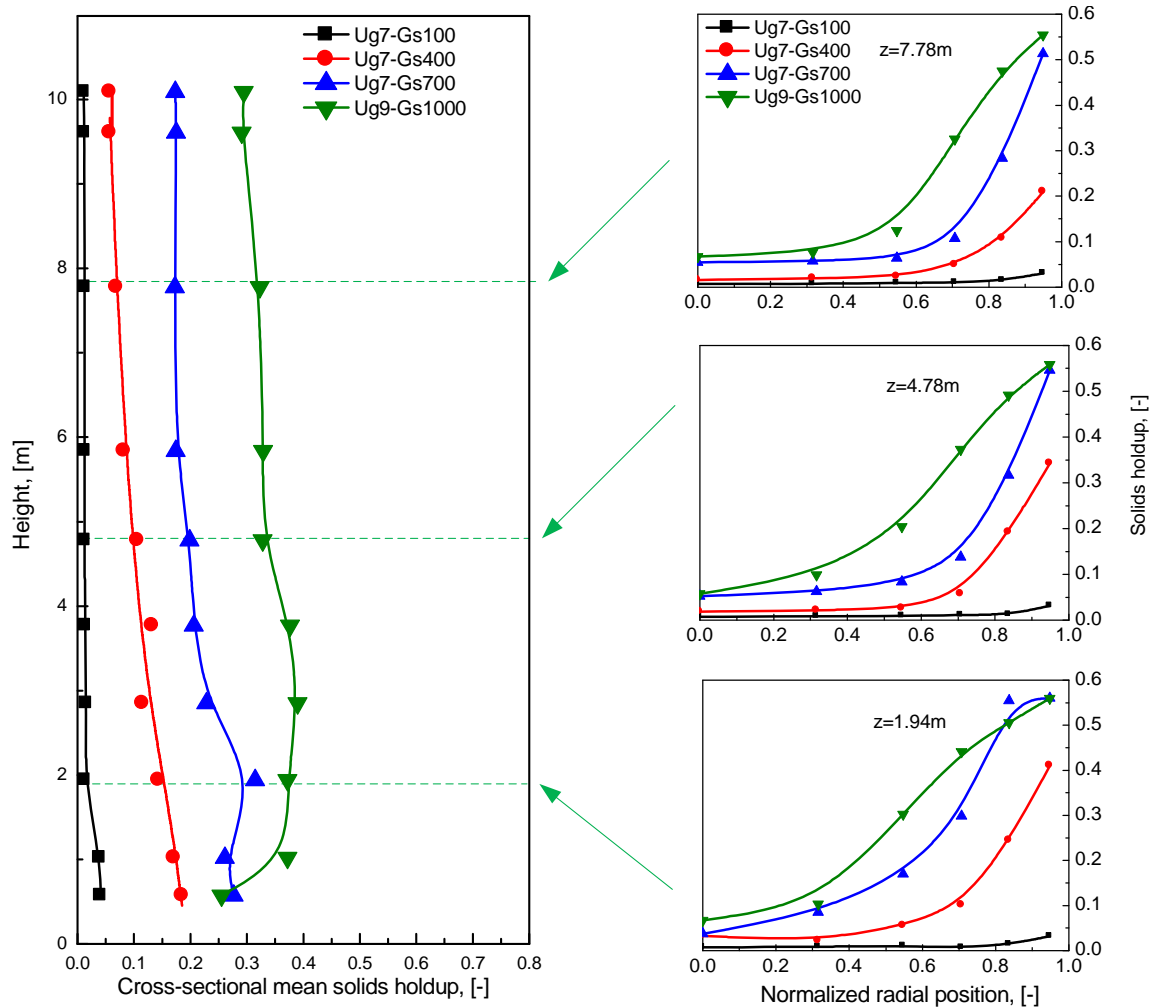


Figure 4.3 Characteristics of flow structure under extremely high flux/density in a CFB riser.

Figure 4.3 compares local and cross-sectional mean solids holdup in the CFB riser for solids circulation rates ranging between $100 \text{ kg/m}^2\text{s}$ and $1000 \text{ kg/m}^2\text{s}$. To the best of our knowledge, such a high solids flux has never been reported in a laboratory scale pilot plant experiments. Firstly, at G_s of $100 \text{ kg/m}^2\text{s}$, the axial profile is approximately exponential shape with a constant solids holdup (lower than 0.01) in the upper section of the riser. By increasing the solids

circulation rate (G_s), the axial profile became non-uniform with solids concentration (solids holdup) decreasing gradually upwards to the top of the riser. When G_s is extremely high, especially high than $700 \text{ kg/m}^2\text{s}$, the non-uniform axial flow structure is replaced by a homogenous axial profile with solids holdup higher than 0.2 in the entire riser. Interestingly, the radial distributions of the solids holdup are totally different under different operating conditions. At low solids flux, the radial profile is comparably more uniform and less sensitive to the change of the axial position. Increasing G_s the areas of the relatively dilute region continues decreasing. The solids holdup in the center of the riser is near to 0.1 under extremely high G_s . Moving outwards towards the wall, solids holdup increase monotonically. Solids holdup remained greater than 0.4 over a wide cross-sectional area ($r/R = 0.7-1.0$, about 60% of the cross-sectional area) even at the top section of the riser. Moreover, flow development was much slower under high flux as the radial profiles continued to change as seen in Figure 4.3. The above phenomenon suggests that low solids flux data has very limited usefulness to high solids flux reactor modeling and design, especially for solids fluxes within the industrial range ($400-1200 \text{ kg/m}^2\text{s}$) in FCC riser. Therefore, there is clearly a need to conduct more fundamental researches to study both axial and radial profiles of solids holdup and flow structures in CFB systems operating at higher flux and/or density.

However, achieving high flux/density in a CFB system is extremely difficult in any experimental lab. While a few (only a few) research groups (e.g. University of British Columbia, UBC, Vancouver and University of Western Ontario, UWO, Ontario) have tried to obtain high flux/density operating, the solids fluxes are still far below the practical fluxes in industrial reactor processes. Theoretically, Bi and Zhu (1993) proposed that high densities and high solids fluxes could be accomplished by a combination of high solids inventories, large downcomer-to-riser diameter ratio, a low pressure drop solids feeder, and minimizing pressure drops in solids separation devices and fittings along the CFB loop. Besides, a proper blower and suitable particle size/riser diameter combinations are also of importance. Based on their suggestion, a dual loop CFB was used to reduce total pressure drop of the recycle system at UBC which enabled a high solids flux of about $400 \text{ kg/m}^2\text{s}$ to be achieved. A twin-riser CFB with a large downcomer-to-

riser ratio was constructed at UWO which achieved high fluxes up to 500 kg/m²s. Building further upon the practical experience, we have:

- (1) installed a large diameter storage tank at the bottom of the downcomer;
- (2) replaced the blower with a compressor of capacity 1000 SCFM at 100 psi;
- (3) installed an additional air exhaust pipe at the top of the of the downcomer to discharge most of the air flowing upward through the downcomer, minimizing downcomer air flowing into the primary cyclone, so that the pressure drop across the cyclone is significantly reduced. This step increased the available pressure for the riser to achieve higher density;
- (4) installed two small deflecting plates (see the left insert of Figure 4.1) in the solids inlet region, one vertically at the outlet of the inclined pipe covering 30% of the lower end of the inclined feed pipe joining the riser to prevent the riser air from flowing into the solids feeding pipe which tends to restrict solids downflow. The other deflecting plate was half-way up in the inclined pipe covering 30% of the cross-sectional area of the inclined pipe. It directed particles downwards so as to provide a quit “exit route” for the remaining air entering the feed pipe so that the solids movement in the inclined pipe is much faster and steadier.

After modification, the riser can be operated much more steadily at solids circulation rates of up to 1000 kg/m²s, much higher than 400 kg/m²s in the original system reported by Li (2010). This allows us to operate the CFB system under a wide range of operating conditions to obtain a comprehensive map of solids flow in the new solids recycle loop. An example is the data set plotted in Figure 4.3 and discussed above.

4.3.2 Axial profiles of solids holdup

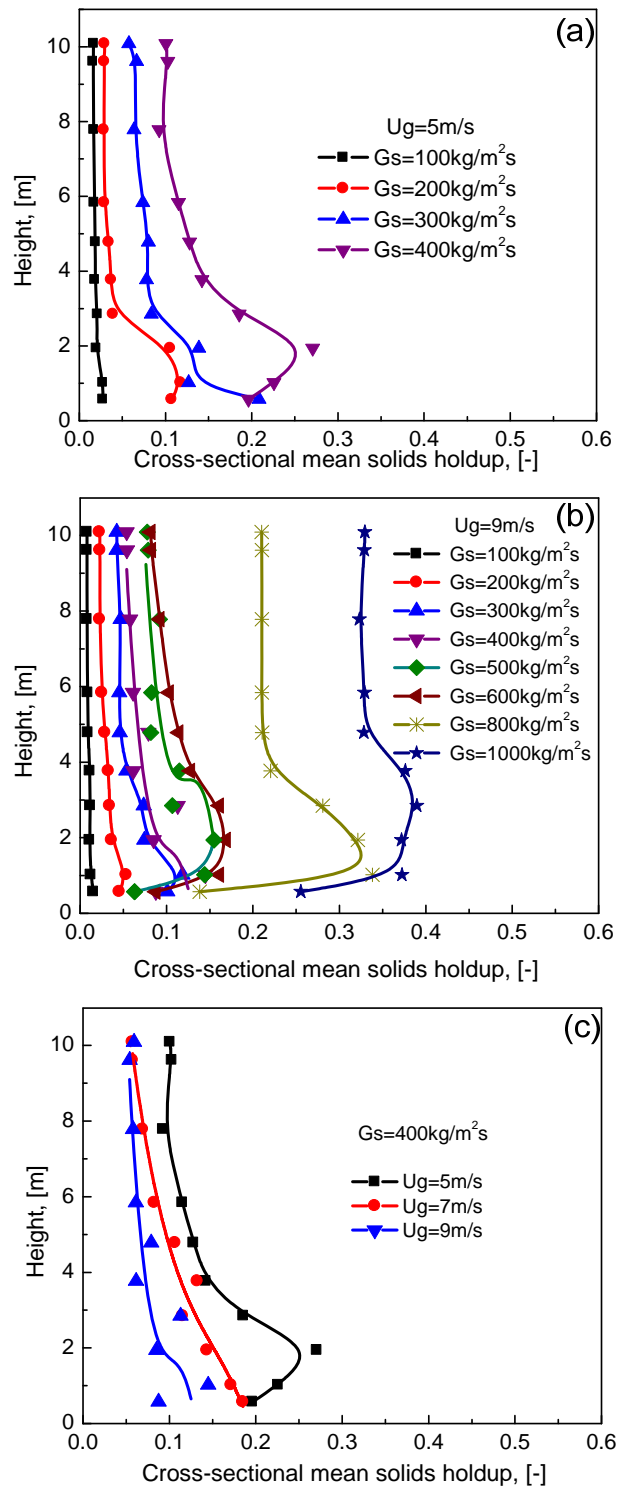


Figure 4.4 Axial solids holdup distribution for various operating conditions.

Figure 4.4 displays the axial distribution of cross-sectional mean solids holdup in the CFB riser for superficial gas velocity, U_g , of 5, 7 and 9 m/s and solids circulation rate, G_s , up to 1000 kg/m²s. The cross-sectional mean solids holdups are obtained by integrating local solids holdups measured at 5 radial positions (excluding the central region) measured by the optical fiber probe. As shown in Figure 4.4, significantly different axial profiles can be seen under various operating conditions. In general, as solids circulation rate (G_s) increases, the approximately exponential-shaped axial profile is replaced by the relatively non-uniform axial profile with a dense region at the base and a dilute region at the top of the riser and then at even higher solids fluxes, by more uniform axial profiles. In Figures 4.4 (a) and 4.4 (b), when U_g is constant the solids holdup increases with increasing G_s , while for a constant solids circulation rate the solids holdup decreases with increasing U_g as plotted in Figure 4.4 (c).

In details, relatively high solids holdups near the bottom of the riser are extensively affected by the particle acceleration and the gas distributor. Above this region, at the lowest G_s of 100 kg/m²s, the solids holdup decreases exponentially, eventually approaching a constant value up to the riser exit. This exponential shape occurs when solids entering in the riser are immediately entrained so that there is no significant particle accumulation at the riser bottom. By increasing G_s gradually, a significant dense region formed at the bottom of the riser leading to a non-uniform axial solids holdup profile. It can also be seen that the solids holdup along axial elevations is increasing with increasing G_s at a fixed superficial gas velocity. Meanwhile, the solids holdup is also increasing at each axial level with decreasing U_g when G_s is constant. The dense region occurs between 2 and 4 m heights with the high solids holdup ranging from 0.1 to 0.25. Above this region, relatively dilute regions are attained and the average solids holdup becomes independent of elevation. From this plot, it can be seen that the 2 m-elevation lies in the developing flow region with high solids holdups and a fully-developed region with relatively low solids concentrations begins at 5 m height. Interestingly, the shape of the axial profile is hardly changed with various operating conditions. It is apparent that the axial profiles move in parallel from low solids holdup towards high solids holdup with increasing G_s and/or decreasing U_g . The solids holdup and the flow development in both regions of the riser do not seem to depend on the height, but are expected to depend on gas velocity and solids loading. This may be partly

affected by the solids inventory due to the overall pressure balance in the loop of the riser and downcomer and by the configurations of the HFCFB/HDCFB system. The pressure at the riser bottom must be equal to the pressure at the bottom of the return system minus the pressure drop across the solids recycle valve. If the solids inventory is high, the pressure head in the return system would be sufficiently high. Therefore, it is easy to adjust the pressure in the return system to meet the requirement for pressure balance in the whole loop under various operating conditions. Moreover, this axial profile is different from the height-dependent S-shaped axial profile reported by other authors under high flux and/or high density operating conditions (Issangya *et al.*, 1999; Pärssinen and Zhu, 2001 and Yan and Zhu, 2004).

Further increasing G_s , significantly dense solids holdup in the entire height of the riser is achieved ranging from 0.23 to 0.38 when solids circulation rate is extremely high, particularly higher than $700 \text{ kg/m}^2\text{s}$. The uniform and dense gas-solids suspension has been achieved along the whole column if ignoring the entrance effect. This homogenous axial structure is similar to other results reported by previous researchers. Contractor *et al.* (1994) reported that volumetric solids concentrations between 0.15 and 0.2 could cover the entire riser for a solids flux up to $685 \text{ kg/m}^2\text{s}$ and gas velocity up to 5.7 m/s . Issangya *et al.* (1999) also found that the apparent solids holdup obtained from pressure drops could be maintained as high as 0.2 in the whole column at $U_g = 8 \text{ m/s}$ and $G_s = 425 \text{ kg/m}^2\text{s}$. In contrast to the non-uniformity axial profiles with solids circulation rate lower than $700 \text{ kg/m}^2\text{s}$, the dense bed at the base riser of the can persist over the entire column under such high G_s . Axial distribution of solids holdup becomes very uniform. As already noted, it is clear that being able to achieve this kind of homogenous axial profile depends on being able to provide sufficient pressure drop. If the pressure head is high enough, the homogenous axial profile appears to be robust and self-sustaining over a considerable range of superficial gas velocity and solids flux. Information about the effect of solids circulation rate on the respective axial profiles in an industrial riser is very useful since the solids flux varies widely from 400 to $1200 \text{ kg/m}^2\text{s}$ in the industrial reactors.

Bi and Zhu (1993) proposed the concept of the high-density operation to distinguish the high-flux and high-density operating conditions from those low-flux and low-density one. Solids flux of over $200 \text{ kg/m}^2\text{s}$ is used to distinguish a high-flux operation. In their following work, Zhu and

Bi (1995) used $G_s > 200 \text{ kg/m}^2\text{s}$ and $\varepsilon_s > 0.03\text{-}0.05$ in the developed section of the riser to demarcate high-density operation from the low-density one. It is clear that what we have seen here in the high flux riser does match the high flux and /or high density operating conditions suggested by Zhu and Bi (1995). In addition, the result is also comparable to the results (0.25-0.30) in C-TFB reported by Zhu and Zhu (2008) with a special mode operated at low superficial gas velocity and high solids circulation rate, resulting in a highly dense suspension and uniform axial flow structure. The uniform high density structure stresses the importance to both uniform gas-solids contacting efficiency and uniform bed-to-wall heat transfer throughout the whole reactor.

4.3.3 Radial profiles of solids holdup

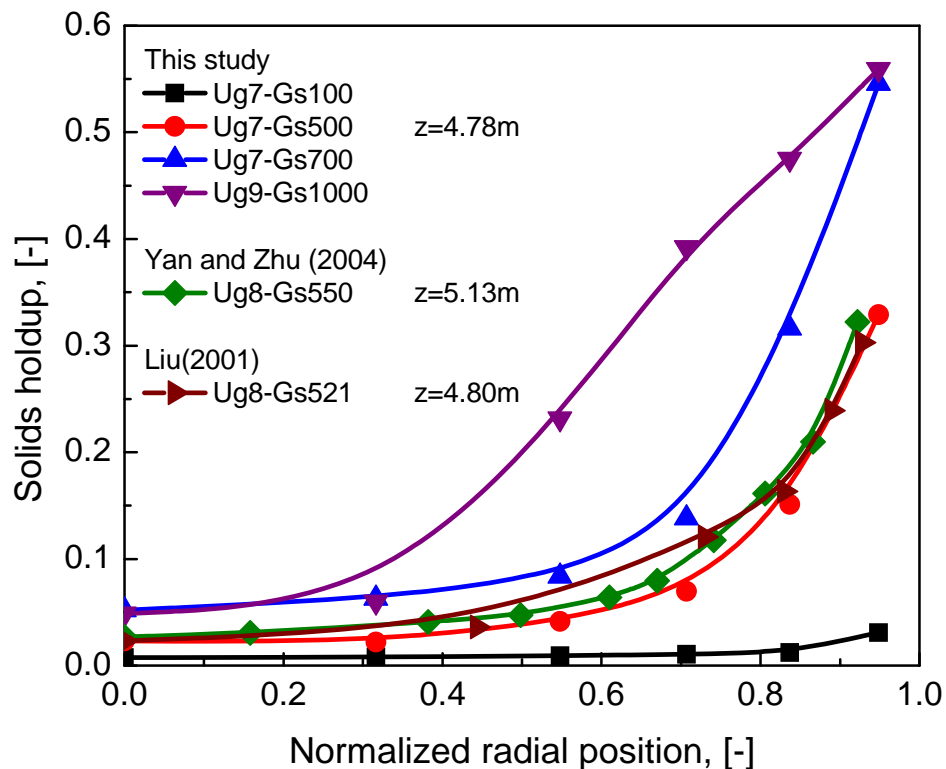


Figure 4.5 Comparison of local solids holdup profiles in a CFB riser under different operating conditions.

Typical radial profiles of solids holdup in the CFB riser are presented in Figure 4.5 where results are compared to the operating conditions (superficial gas velocity, U_g and solids circulation rate,

G_s) as well as different axial elevations. Under all operating conditions, radial distributions of the solids holdup are nonuniform with dilute and dense regions. The radial profile is relatively flat in the center of the riser and the solids holdup increased towards the wall with the maximum value right at the wall at 0.59. Operating conditions affect dramatically the radial solids holdup distribution. The riser became progressively denser away from the wall towards the center by feeding more solids at a fixed superficial velocity. The solids holdup and its radial distribution in the high density CFB riser are quite different from those in the low density systems. Obviously, the radial profile is a clear-cut “core-annulus” structure with a dilute and uniform core region surrounded by a dense annulus zone when G_s is low. The radial variation can be divided into three parts: a central region up to $r/R \approx 0.5-0.6$ with a low and fairly constant value with a slight increase towards the wall, an intermediate region between $r/R \approx 0.5-0.6$ and $r/R \approx 0.8-0.9$, where solids holdup appreciably increases, and a wall region when $r/R > 0.9$ where the solids holdup is high but not more than 0.35. The results are similar to those reported by other researchers under comparable operating conditions. As G_s increases to higher than $700 \text{ kg/m}^2\text{s}$, the dilute region shrinks ($r/R = 0-0.2$, less than 20% of the cross-sectional area). After this short region, solids holdup increase gradually towards the wall which can be up to 0.5. The “core-annulus” radial profile is replaced by the concave parabolic curve under extremely high G_s .

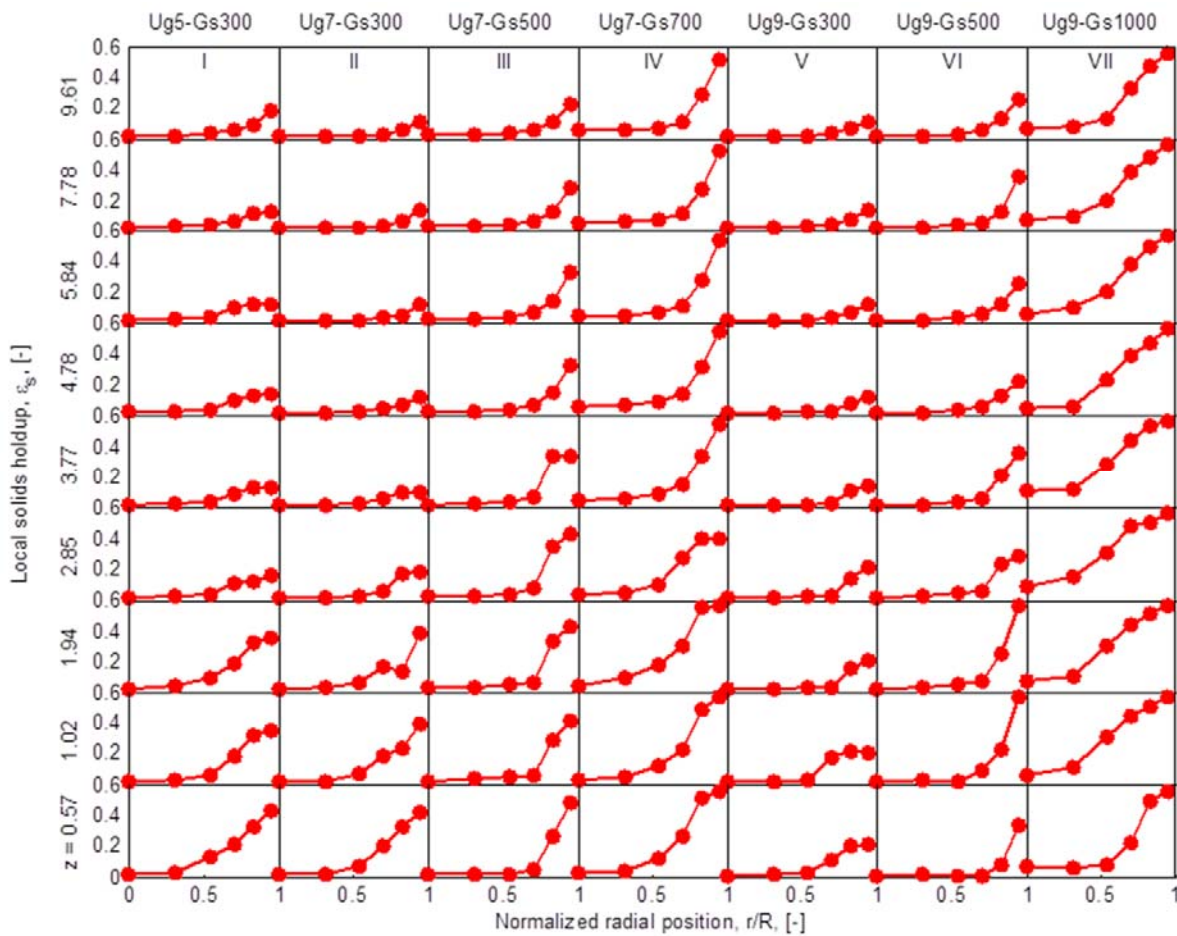


Figure 4.6 Radial solids holdup distribution for various operating conditions.

Regarding the results in columns *I*, *II* and *V* in Figure 4.6, it is clear that the superficial gas velocity plays important roles in solids distribution in radial and axial directions. It is apparent that reducing the superficial gas velocity results in an increased solids holdup and thus an increased solids holdup profile. Additionally, superficial gas velocity influences the solids holdup not only in the near wall region but also in the center of the riser. For example, when superficial gas velocity increases from 5 to 9 m/s, the solids holdup decreases in the center region at different heights and drops more rapidly in the wall region especially at the bottom of the riser. Moreover, the solids holdup distribution was less uniform at lower superficial gas velocity. Through comparison between columns *II*, *III* and *IV* and/or between *V*, *VI* and *VII*, increasing solids circulation rate led to a higher solids holdup with a less uniform profile. Under

high solids circulation rates, the effects of the walls are more confined to the near wall region generating an increased solids holdup gradient. Lower G_s make the solids holdup distribution more even with lower local solids holdup at each radial position. In addition, the solids holdup distribution becomes more uniform as the axial level increases. Furthermore, the solids holdup is higher in the lower section than the upper section at almost all the operating conditions. In the upper section of the riser, when G_s is lower than $500 \text{ kg/m}^2\text{s}$, the solids holdup in the wall region is lower than that in the bottom section. Similar phenomena are also reported by other researchers in the previous studies. Moreover, the solids holdup in the central region remains almost constant throughout the riser which had been also described by others (Yang *et al.*, (1997), Wei *et al.*, (1998), Issangya *et al.*, (2000) and Parssinen and Zhu (2001)). Again, the axial variations of radial profiles of solids holdup changed very little under extremely high solids circulating rate of $1000 \text{ kg/m}^2\text{s}$.

4.3.4 Flow development of solids holdup

The solids flow can be considered as fully developed if the radial solids distribution remains relatively unchanged with the axial location. A detailed review of Figures 4.3 and 4.6 shows that increasing the superficial gas velocity accelerates the solids flow development. When the solids circulation rate is increased from $300 \text{ kg/m}^2\text{s}$ to $500 \text{ kg/m}^2\text{s}$ and then to $700 \text{ kg/m}^2\text{s}$ at a constant superficial gas velocity ($U_g = 7 \text{ m/s}$), the flow development becomes much slower. A similar tendency is also observed when the superficial gas velocity is 9 m/s .

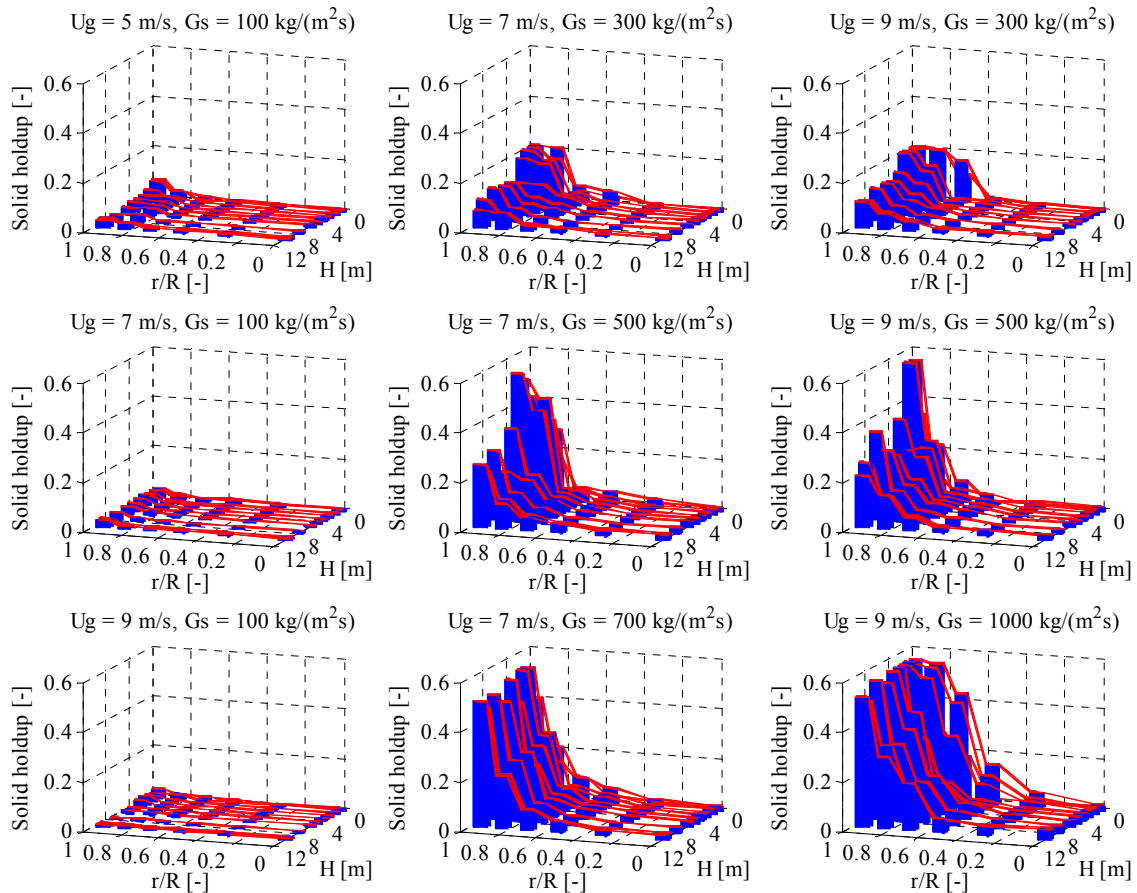


Figure 4.7 Overall view of the solids hold up under different operating conditions.

To facilitate the analysis of flow development, the three-dimensional profiles of solids holdup are given in Figure 4.7. It shows clearly that the solids concentration in the riser center remains nearly constant throughout the riser under each operating condition when $G_s < 700 \text{ kg/m}^2\text{s}$.

Figure 4.7 further expresses that, even with the change of operating conditions, the solids holdup in the riser center hardly changes with the G_s lower than $700 \text{ kg/m}^2\text{s}$. As a result, the flow development within such solids fluxes is mostly represented by the reduction of the solids holdup toward the riser top at values of r/R from about 0.50 to 1.00. Similar results are also reported by previous studies under high flux conditions (Issangya *et al.*, 2000; Parssinen and Zhu, 2001; Yan and Zhu, 2004 and Huang *et al.*, 2007). However, when G_s is up to or higher than $700 \text{ kg/m}^2\text{s}$, the flow development becomes extremely slower with a reduced core region of relatively low

solids holdups, and the solids holdup is increasing gradually from the center to the wall region. The radial solids holdup profiles are typically parabolic in shape as aforementioned.

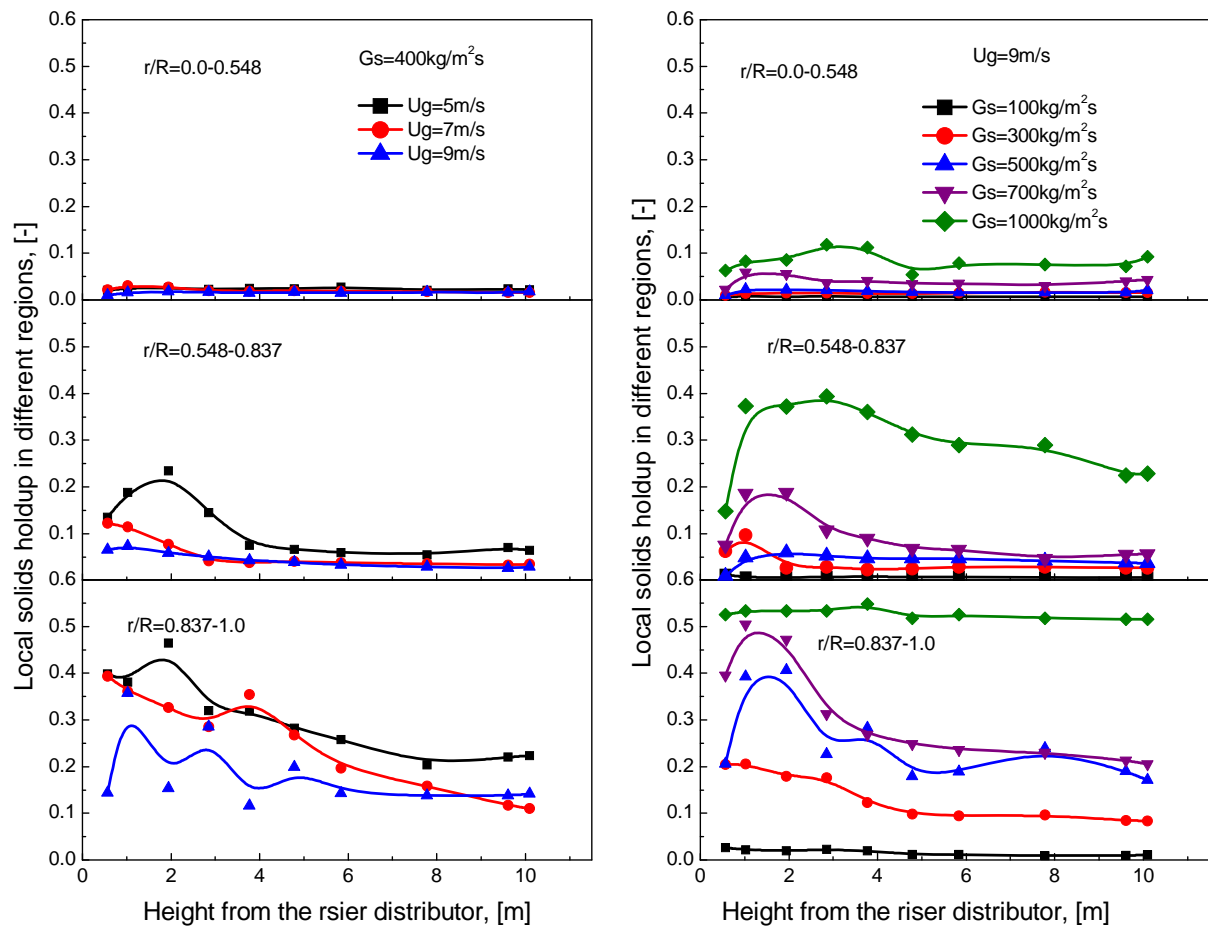


Figure 4.8 Solids holdup distribution in different radial regions for various operating conditions

In order to further examine the solids flow development, the axial profiles of the solids holdups in the three dimensionless radial regions $r/R = 0.0-0.548$, $0.548-0.837$ and $0.837-1.0$ are described in Figure 4.8. This figure describes the difference in the flow development in the three dimensionless radial regions. As is described in the left of the Figure 4.8, in the center ($r/R = 0.0-0.548$, 40% of the cross-sectional area), the solids holdup is very low and nearly constant all the way from the riser bottom to the top with no significant difference in this region at various superficial gas velocities. In the middle region ($r/R = 0.548-0.837$, 40% of the cross-sectional

area), on the other hand, the solids holdup profile varies at the entrance region up to approximately 4 m and then becomes flat toward the riser top. Compared to the middle region, developing section of the wall region at the riser bottom experienced more changes. Most significant variations of the solids holdup happen in the wall region ($r/R = 0.837-1.0$, 20% of the cross-sectional area), where the solids concentration drops sharply with increasing height until approximately 4 m above the riser distributor. The solids holdup profile then becomes relatively flat till the top of the column. The speed of the flow development mainly depends on this region.

A similar trend in flow development was observed when G_s is below $500 \text{ kg/m}^2\text{s}$ at superficial gas velocity, U_g , of 9 m/s. When G_s is higher than $700 \text{ kg/m}^2\text{s}$, the solids holdup in the central region remained at about 0.1 in the whole riser. Solids holdup in the middle region is high up to 0.4 and remains unchanged along the riser up to 4 m-level and then gradually decreases. However, the solids holdup still remained high value, up to 0.25, in this middle region. The solids holdup in the wall region is rather flat with a value up to 0.55 along all the axial elevations for $G_s = 1000 \text{ kg/m}^2\text{s}$. This insensitivity to the height levels suggests that the two-phase suspension density reaches a saturation state under extremely high solids circulation rate. In addition, Figure 4.8 also shows that increasing G_s significantly slows the flow development process whereas increasing U_g accelerates it.

The flow development can also be shown by the radial nonuniformity index (RNI) which was proposed by Zhu and Manyele (2001). The RNI is defined for each given parameter as the standard deviation of its values in the radial direction, normalized by the maximum possible standard deviation for the same parameter with the same average cross-sectional value. The RNI can be used to distinguish exactly the structure of radial profiles on a quantitative basis at different locations and/or operating conditions.

Figure 4.9 shows the RNIs ($\text{RNI}(\epsilon_s)$) in terms of the solids holdup along the axial direction in the riser. In general, all $\text{RNI}(\epsilon_s)$ profiles are showing that the value of $\text{RNI}(\epsilon_s)$ is higher at the bottom of the riser followed by a relatively flat curve along the axial direction. Obviously, higher $\text{RNI}(\epsilon_s)$ values at the bottom are due to the development of solids flow.

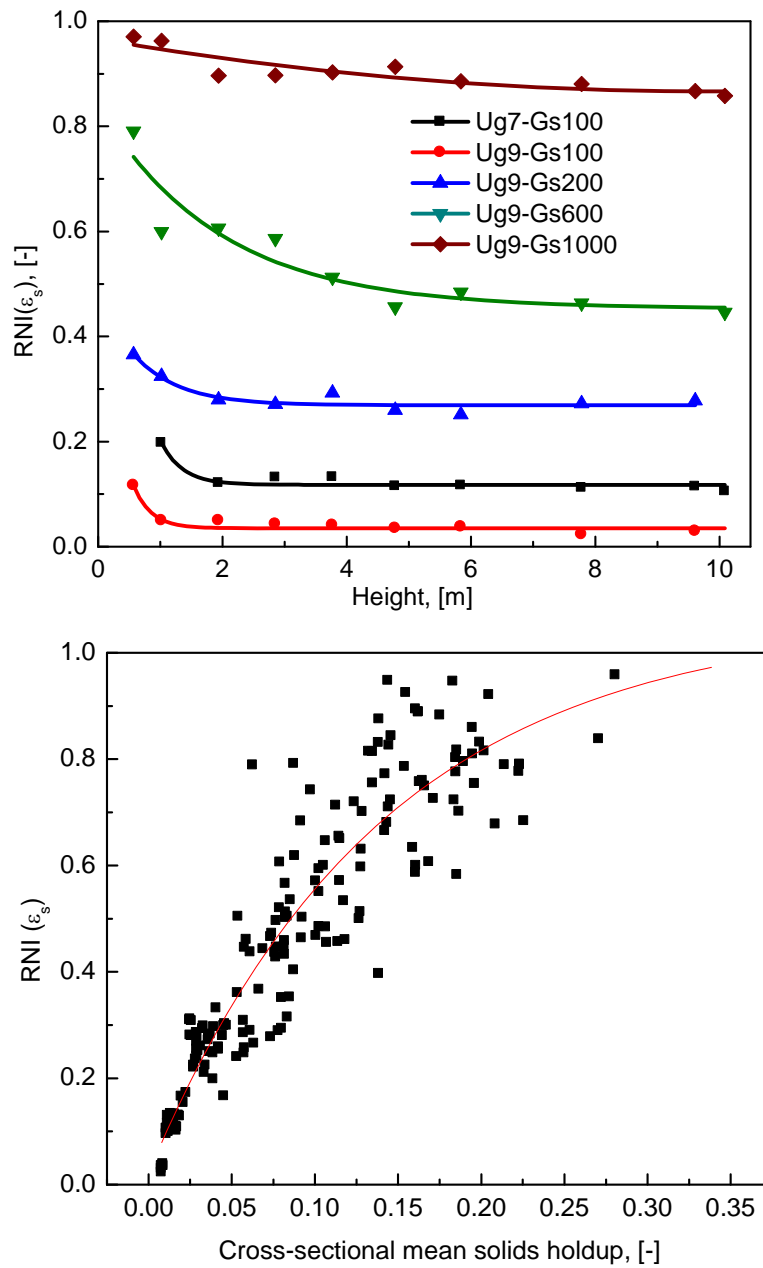


Figure 4.9 RNI's of solids holdup the riser under different operating conditions (a) RNI under different operating conditions and (b) Relationship between RNI and solids holdup.

The effect of operating conditions on the RNI (ϵ_s) can be inferred from Figure 4.9(a). RNI (ϵ_s) decreases with increasing superficial gas velocity showing that the radial profiles of solids

holdup become more uniform. High gas velocity can enhance the gas-particle interactions. Solids flow development would be accelerated by high drag force impacted by high speed gas so that the solids flow structure became more uniform. At a given superficial gas velocity, high solids circulation rate results in higher RNI (ε_s) because of the increased solids holdup. Higher solids holdup induces the preferential formation of large clusters near the wall, thus increasing the radial nonuniformity. Moreover, Figure 4.9(b) shows a relationship between the RNI (ε_s) and cross-sectional average solids holdup. It shows that the RNI (ε_s) values increase with the cross-sectional average solids holdup. This is consistent with the general understanding that radial solids concentration profiles become steepened with increased average concentration (Zhu and Manyele, 2001). It is noted the long distance for the RNI (ε_s) to become stabilized under higher G_s or lower U_g . This indicates a lengthy process for the radial flow structure to be fully developed in the riser.

4.3.5 Flow fluctuation in the high flux/density riser

From the foregoing analysis, it is clear that the local solids holdups vary against different radial positions under a wide range of operating conditions. In order to gain a better understanding of the local solids flow development, it is important to examine the flow fluctuations under different operating conditions especially in high density (HDCFB) and low density circulating fluidized beds (LDCFB). Fluctuations can be reflected quantitatively in the standard deviation and the intermittency indices (γ) of solids holdups. Definition of γ in detailed can be found in the previous paper (Brereton and Grace, 1993). Besides, the intermittency index can also be used to describe the phenomenon of segregation between gas and solids. The value of intermittency index is equal to one if the high-velocity flow in the riser consisted of “ideal cluster flow”. On the other hand, the value of intermittency index is zero if there is a “perfect core-annulus flow”. Figure 4.10 compares the radial profiles of local solids holdup, standard deviation and the corresponding intermittency index at two axial heights.

Generally, the local solids holdup is lowest and has a relatively flat radial distribution under the low flux of $100 \text{ kg/m}^2\text{s}$. With increasing solids flux or decreasing gas velocity, the solids holdup increases, and the radial distribution becomes steeper. The standard deviation and γ increase with

increasing G_s or decreasing U_g . This suggests increased flow fluctuation with the increase of G_s or decrease of U_g .

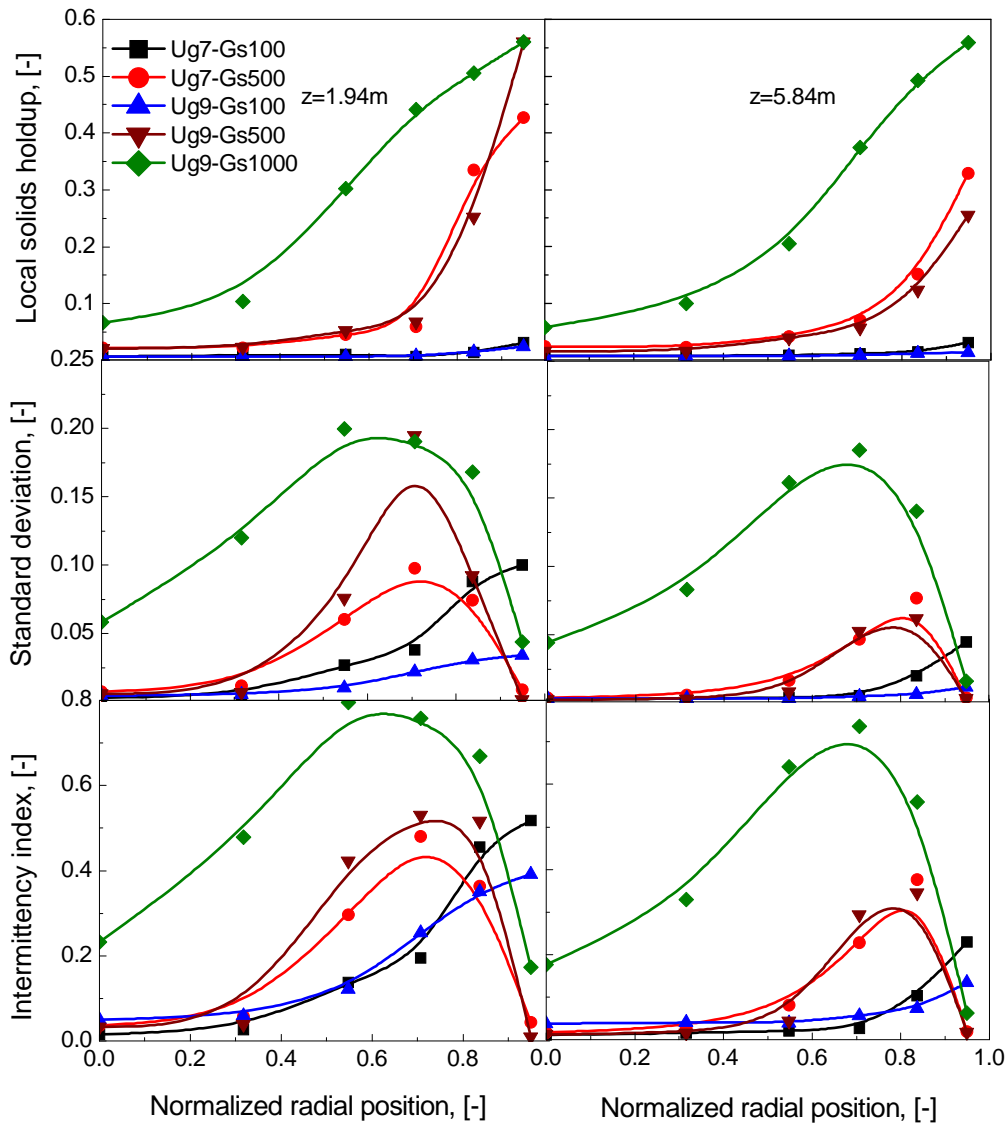


Figure 4.10 Radial profiles of local solids holdup, standard deviation and intermittency indices along the riser under different operating conditions.

The fluctuation of low flux solids holdups increases outward, reaching maxima at the outer wall. For high flux conditions, the fluctuation increases gradually to a peak at $r/R = 0.6\text{-}0.7$ and decreases thereafter towards the wall. The greatest fluctuation always occurs in the middle region of the column under high flux operating conditions which are also reported under high density

operating conditions in many papers (Grace *et al.*, 1999; Issangya *et al.*, 2000; Zhu and Zhu 2008 and Qi *et al.*, 2009). This phenomenon has been considered as an important distinguishing feature of high density CFB risers. When G_s is lower than $500 \text{ kg/m}^2\text{s}$, the standard deviation and the corresponding intermittency index remains a very low level around 0.02-0.05 up to $r/R \approx 0.4-0.6$. Considering its solids holdup profile, this indicates that a wide dilute region still occupies the center surrounded by a dense annulus region at the wall. Lower solids holdups in the center of the column and higher solids concentrations near the wall make fewer fluctuations. It is found that the standard deviations and intermittency indices under extremely high solids flux of $1000 \text{ kg/m}^2\text{s}$ are much higher than those under other low high solids flux conditions at almost all radial positions. This highest magnitude of fluctuations may due to the relatively higher solids holdup suggesting that the gas-solids and inter-particle interaction in this particularly high flux CFB are more vigorous than those in relatively low solids flux CFBs operations. The dramatic fluctuations probably induce better gas-solids contacting and mixing, improving consequently the reactor performance.

Additionally, for each solids circulation rates, there is a clear development with height, with standard deviation and γ tending to decrease with increasing axial level. This illustrates that the flow structure tends to change with increasing height from one where cluster-flow structures are more common to one where the core-annulus structure becomes predominant. The same results are also presented by Brereton *et al.* (1993).

4.4 Conclusions

The current work presented a comprehensive insight into the solids holdup and flow development phenomena in a high flux/density (up to 1000 kg/m²s) riser, using a multipurpose optical fiber probe which is capable of simultaneously measuring local solids holdup and particle velocity.

Solids suspension having a solids holdup of up to 0.2-0.3 can be maintained throughout the entire high flux/density riser. A homogenous axial flow structure is observed at $G_s = 1000$ kg/m²s.

Radial distributions of the solids holdup are nonuniform with a dilute region and a dense region. For G_s is greater than 700 kg/m²s, the dilute core region shrinks to about $r/R = 0-0.2$, less than 20% of the cross-sectional area. Solids holdups thereafter increase monotonically towards the wall reaching up to 0.59.

The radial profile of solids holdup under extremely high G_s is a concave parabolic curve. The solids holdup remains low and relatively constant at the riser center throughout the riser, suggesting very quick solids flow development in the riser center at the bottom section. In the wall region, however, the flow development is significantly slower, with the solids holdup near the wall decreasing slowly toward the riser top. Increasing solids flux prolongs the solids flow development.

Better gas-solids contacting and mixing indicated by standard deviation and intermittency index of the solids holdup over the entire cross-sectional area under extremely high solids flux can greatly lead to vigorous interactions between gas and solids phases, improving the reactor performance.

Nomenclature

f	calibration function for optical fiber probe
G_s	solids circulation rate [kg/(m ² ·s)]
L_e	effective distance between light-receiving fiber A and B [m]
t	time [s]
T	time interval [s]
U_g	superficial gas velocity [m/s]
$V(t)$	voltage time series [volt]
z	axial coordinate, or distance from gas distributor [m]

Greek letters

ε_s	solids holdup [-]
$\varepsilon_s(t)$	local instantaneous solids holdup [-]
$\bar{\varepsilon}_s$	average solids holdup in the entire column [-]
τ	lag time [s]

Subscripts

1, 2	subprobe 1 and 2 of optical fiber probe
g	Gas
p	Particle
s	Solids

References

- Azzi M., Turlier P., Bertrand JR., (1991), Mapping solids concentration in a circulating fluidized bed using gammametry, *Powder Technology* 67, 249-258
- Bi HT., Zhu JX., (1993), Static instability analysis of circulating fluidized beds and concept of high-density risers, *AIChE Journal* 39,1272-1280
- Bi HT., (2004), Gas and solid mixing in high-density CFB risers, *International Journal of Chemical Reactor Engineering* 2,A12
- Bi HT., Grace J.R., Zhu JX., (1993). Types of choking in vertical pneumatic systems, *International Journal of Multiphase Flow* 19,1077-1092.
- Berruti F., Chaouki J., (1995), Hydrodynamics of circulating fluidized bed risers, A review, *The Canadian Journal of Chemical Engineering* 73,579-602
- Brereton, CM., Grace JR., (1993), Microstructural aspects of the behavior of circulating fluidized beds, *Chemical Engineering Science* 48(14), 2565-2572
- Contractor RM., In Avidan AA., (1994), *Circulating fluidized bed technology IV*. New York: American Institute of Chemical Engineers pp387-391
- Grace JR., (1986a), Contacting modes and behavior classification of gas-solids and other two-phase suspensions, *The Canadian Journal of Chemical Engineering* 64,353-363
- Grace JR., (1986b), Heat transfer in circulating fluidized beds in *Circulating Fluidized Bed Technology*, Basu P. ed. Pergamon Press, Toronto, 63-81
- Grace JR., Issangya AS., Bai DR., Bi HT., Zhu JX., (1999), Situating the highdensity circulating fluidized bed, *AIChE Journal* 45,2108-2116
- Grace JR., (2000), Reflections on turbulent fluidization and dense suspension upflow, *Powder Technology* 113,242-248
- Huang WX., Yan AJ., Zhu JX., (2007), Hydrodynamics and flow development in a 15.1 m circulating fluidized bed riser, *Chemical Engineering Technology* 30(4), 460-466
- Issangya AS., (1998), *Flow dynamics in high density circulating fluidized beds*, PhD Diss. Univ. of British Columbia, Vancouver, BC
- Issangya AS., Bai DR., Bi HT., Lim KS., Zhu J., Grace JR., (1999), Suspension densities in a high-density circulating fluidized bed riser, *Chemical Engineering Science* 54, 5451-5460
- Issangya AS., Grace JR., Bai DR., Zhu JX., (2000), Further measurements of flow dynamics in a high-density circulating fluidized bed riser, *Powder Technology* 111, 104-113

Karri SBR., Knowlton TM. (1999), A comparison of annulus solids flow direction and radial solids mass flux profiles at low and high mass fluxes in a riser, In Werther J., (Ed.), *Circulating fluidized bed technology VI*. Frankfurt, Dechema, pp71-76

Knowlton T., (1995), Interaction of pressure and diameter on CFB pressure drop and holdup. Paper for workshop, *Modeling and control of fluidized bed systems*, Hamburg, May 22-23

Li DB., (2010), Investigation of circulating fluidized bed riser and downer reactor performance for catalytic ozone decomposition, PhD Diss, University of Western Ontario, London, ON

Liu JZ., Grace JR., Bi HT., Morikawa H., Zhu JX., (1999), Gas dispersion in fast fluidization and dense suspension upflow, *Chemical Engineering Science* 54(22), 5441-5449

Liu JZ., (2001), Particle and gas dynamics of high density circulating fluidized beds, PhD Diss, Univ. of British Columbia, Vancouver, BC

Liu JZ., Grace J.R., Bi HT., (2003), Novel multifunctional optical-fiber probe: development and validation, *AIChE Journal* 49(6), 1405-1420

Liu JZ., Grace JG., Bi HT., (2003), Novel multifunctional optical-fiber probe: high-density CFB measurements, *AIChE Journal* 49(6), 1421-1432

Martin MP., Turlier P., Bernard JR., (1992), Gas and solid behavior in cracking circulating fluidized beds, *Powder Technology* 70, 249-258

Pärssinen JH., Zhu JX., (2001a), Axial and radial solids distribution in a long and high-flux CFB riser, *AIChE Journal* 47, 2197-2205

Pärssinen JH., Zhu JX., (2001b), Particle velocity and flow development in a long and high-flux circulating fluidized bed riser, *Chemical Engineering Science* 56, 5295-5303

Qi XB., Zhu HY., Zhu J. (2009), Demarcation of a new circulating turbulent fluidization regime, *AIChE Journal* 55(3), 594-611

Reh L., (1999), Challenges of circulating fluid-bed reactors in energy and raw materials industries, *Chemical Engineering Science* 54(22), 5359-5368

Wei F., Lin HF., Cheng Y., Wang ZW., Jin Y., (1998), Profiles of particle velocity and solids fraction in a high-density riser, *Powder Technology* 100,183-189

Yan AJ., Zhu JX., (2004), Scale-up effect of riser reactors (1): Axial and radial solids concentration distribution and flow development, *Industrial & Engineering Chemistry Research* 43, 5810-5819

Yang G., Wei F., Jin Y., Yu Z.Q., (1997), Radial solids fraction profiles in inlet region of high density circulating fluidized bed, *Chemical Engineering Technology* 20, 304-308

Zhang H., Johnston PM., Zhu JX., de Lasa HI., Bergougnou MA., (1998), A novel calibration procedure for a fiber optic solids concentration probe, *Powder Technology* 100, 260-272

Zhu HY., Zhu JX., (2008a), Gas-solids flow structures in a novel circulating-turbulent fluidized bed, *AIChE Journal* 54(5), 1212-1223

Zhu HY., Zhu JX., (2008b), Comparative study of flow structures in a circulating-turbulent fluidized bed, *Chemical Engineering Science* 63, 2920-2927

Zhu JX., Grace JR., Lim CJ., (1989), Erosion-causing particle impacts on tubes in fluidized beds. In *Fluidization VI*. Grace, JR., Schemilt, LW., Bergougnou, MA., (Ed.), Engineering Foundation, New York, pp613-620

Zhu JX., Bi, HT., (1995), Distinctions between low density and high density circulating fluidized beds, *The Canadian Journal of Chemical Engineering* 73, 644-649

Zhu JX., Manyele SV., (2001), Radial nonuniformity Index (RNI) in fluidized beds and other multiphase flow systems, *The Canadian Journal of Chemical Engineering* 79, 202-211

Zhu JX., Cheng Y., (2005), Fluidized-Bed Reactors and Applications, Chapter 5.3 in *Multiphase Flow Handbook*, ed. Clayton Crowe, CRC Press, New York, pp 5.55-5.93

CHAPTER 5

Hydrodynamics in a HDCFB Riser-Particle Velocity and Solids Flux

5.1 Introduction

Circulating fluidized bed as a representative solids circulation system is utilized by chemical, metallurgical, pharmaceutical as well as energy and environmental industries. It offers advantages with respect to effective mass and heat transfer, high solids/gas throughput, flexible gas-solids flow rate control and so forth (van der Hoef *et al.*, 2004 and Kunii and Levenspiel, 1991). The performance of CFB systems deeply depends on the hydrodynamics. The major hydrodynamic features of gas-solids CFB risers have been delineated with axial dense/dilute transition solids flow and a core-annulus structure in radial direction (Li and Kwauk, 1980; Bai *et al.*, 1992; Nieuwland *et al.*, 1996 and Smolders and Baeyens, 2001). This kind of nonuniform flow structure and the relatively dilute solids holdup (usually less than 0.10) hampers the CFB systems application to processes which require high solids processing capacities and high heat transfer rates (Zhu and Bi, 1995; Grace *et al.*, 1999; Du *et al.*, 2003 and Zhu and Zhu, 2008). The overall efficiency of a riser could be improved when a uniform distribution of the solids particles was achieved. Issangya *et al.* (1997, 1999 and 2000) reported that the axial homogenous flow with no downward flow near the wall could be achieved under high superficial gas velocity and high solids circulation rate. Liu *et al.* (1999) thereafter pointed out that gas backmixing became small for the same high density operating conditions. Zhu and Zhu (2008) proposed a novel circulating-turbulent fluidized bed (C-TFB), which operated with low superficial gas velocity and high solids circulation rate, resulting in a high-density flow with cross-sectional mean volumetric solids concentration of more than 0.25 through the entire C-TFB. The axial solids distribution profile was nearly uniform ranging from 0.25-0.29, and the uniformity of radial solids distribution had also been improved with local solids holdup around 0.15 at the axis and 0.44 at the wall. There was no net downflow of solids and a good gas solids mixing was observed.

Solids holdup, particle velocity and solids flux are the key parameters of hydrodynamics in practical systems, determining the mass and energy distribution and reaction efficiency, which are the basis for modeling, optimization, and design of commercial-scale CFB systems. While there are a large number of papers reporting on the hydrodynamics only a few of them are dealing with the high solids flux/density conditions especially on particle velocities and/or solids flux (Wei *et al.*, 1998; Pärssinen *et al.*, 2001 and Qi *et al.*, 2012). To the best of our knowledge, very few researches have been directed toward particle velocity and solids flux, especially to the latter one, over a high solids flux of 500 kg/m²s due to the limitations of experimental settings or measurement techniques. A better understanding of particle velocity and solids flux distribution has an enormous impact on practical use of the high solids flux/density circulating fluidized beds, which is also highly valuable for improving the traditional CFB reactors for industrial applications. To obtain more information on solids holdups, particle velocities and solids fluxes, a multipurpose optical fiber probe, which can take the measurement of the three parameters simultaneously was used in this research. A systematic research program in risers was conducted to determine axial and radial profiles of particle velocity and solids flux and the nature of the radial profiles with regards to these two parameters in the current study. Relationships between solids holdup, particle velocity and solids flux were also investigated.

5.2 Experimental details

5.2.1 CFB experimental setup

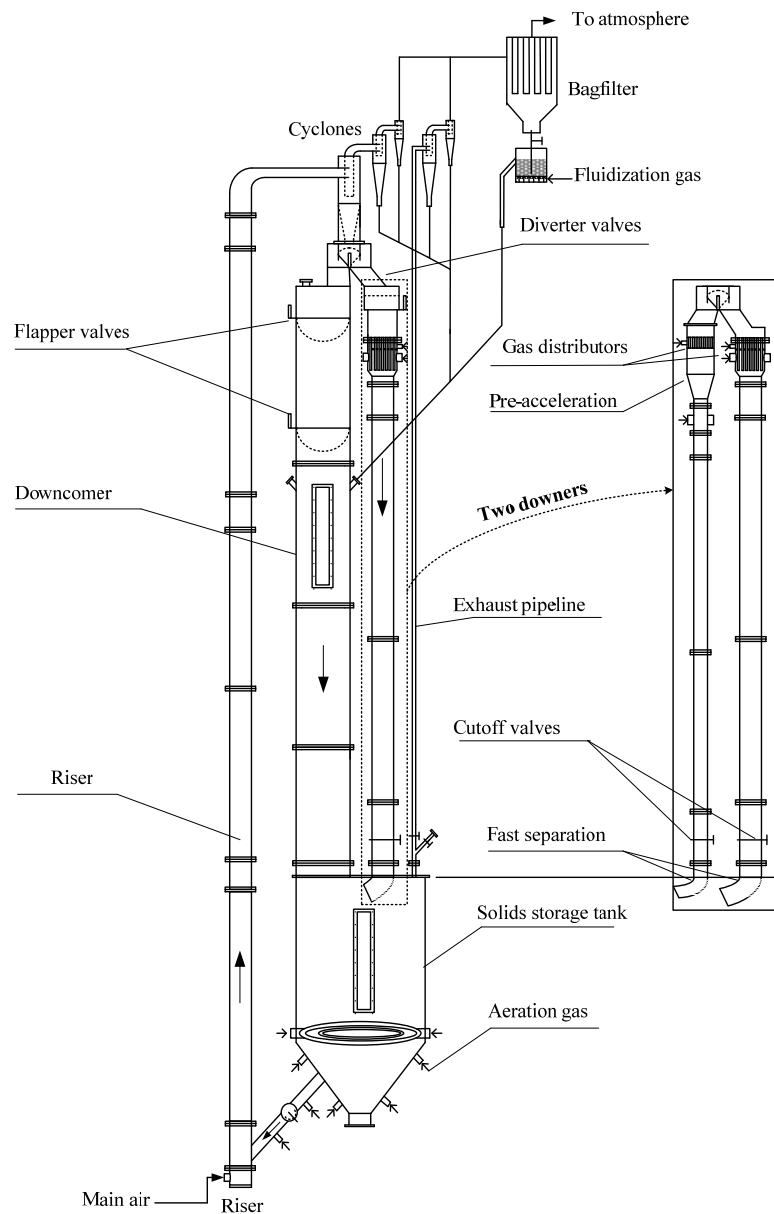


Figure 5.1 Schematic diagram of the multifunctional CFB system.

All experiments were conducted in a multifunctional circulating fluidized bed (MCFB) system, schematically shown in Figure 5.1. The system includes three circulating fluidized bed loops, the left hand fluidized bed loop serves as a high flux/density circulating fluidized bed riser with an inner diameter of 76 mm and the height of 10 m. The right hand fluidized bed loops are two circulating fluidized beds downer (co-current downflow circulating fluidized beds) of different diameters (76 mm i. d. and 5.8 m high and 50 mm i.d. and 4.9 m high, respectively). A downcomer with an inner diameter of 203 mm returns solids during riser operating and at its bottom there is a solids storage tank with an inner diameter of up to 457 mm which serves as a general solids storage for the entire system. Total solids inventory of FCC particles in the downcomer and storage tank could be up to 450 kg, equivalent to a solids height of approximately 6.0 m. This high solids level ensures high back pressure in the downcomer and enables high solids circulation rates and high solids concentrations in the CFBs. In order to obtain higher solids flux and steadier operating conditions, other modifications had been carried out in the CFB systems (details can be found in the chapter 4). The multifunctional circulating fluidized bed (MCFB) can be operated as a CFB riser and downer. For CFB riser operations, particles in the storage tank fluidized by aeration air entering into the bottom of the riser and obtained momentum from the air passing through the riser gas distributor made of perforated plates (2 mm×176 holes, 12% opening area). The particles are carried upward by the riser air along the column. At the top of the riser, particles and gas are separated by primary, secondary and tertiary cyclones and most of the particles returned to the downcomer and further down to the storage tank. Fine particles leaving from the cyclones are trapped by the bag filter and returned periodically to the downcomer.

When the MCFB is under downer operating mode, solid particles are first lifted through the riser, separated by the primary cyclone fixed at the top of the downcomer and then fed into the downers. At the top of either one of the downers is a gas-solids distributor (details shown in Fig. 5.1) where the particles are uniformly distributed along with the downer air to flow downward concurrently. After fast separation by gravity at the exit of either downer column, most particles are retained in the storage tank, with the remaining particles captured by two cyclones installed in series at the top of the exhausted pipeline and the common bag filter. To eliminate the effects

of solids inventory and other influencing parameters on the hydrodynamic characteristics, the whole experimental work in this study was carried out with a constant particle mass of 400 kg stored in the downcomer and the storage tank.

The entire fluidized bed system uses aluminum as the main construction material with small portions made of Plexiglas for visual observation. In order to minimize possible electrostatic charges formed in the columns during the experiments, the whole fluidized bed system is electrically grounded. A measuring device for solids circulation rate is installed in the top section of the downcomer. By regulating the ball valve located in the solids feeding line connecting the storage tank and the riser column, the solids circulation rate can be adjusted and maintained at the desired level during each experiment. The fluidization gas used in this study is air at ambient temperature, supplied by a compressor capable of delivering 1000 SCFM at 100 psi. Equilibrium FCC catalyst particles impregnated with ferric oxide (Fe_2O_3) are used in this study for the catalytic ozone decomposition experiments. The Sauter mean diameter and the particle density is $76 \mu\text{m}$ and 1780 kg/m^3 respectively. The particle size distribution is given in Table 5.1.

Table 5.1 Size distribution of the FCC particles

Particle Size (μm)	Volume Fraction (%)
0-20	0.61
20-40	9.72
40-60	26.32
60-80	22.80
80-130	33.24
>130	7.31

5.2.2 Measurements of solids holdup and particle velocity

Experimental measurements include differential pressure, local solids concentration (solids holdup) and particle velocity. Twenty pressure taps were installed along the CFB column and connected with 19 differential pressure transducers (Omega PX162) to measure the axial profiles of the pressure gradient. The pressure gradient is mainly used to double check the solids holdup measured by an optical fiber probe mentioned below. Local solids holdup and particle velocity are measured simultaneously using a novel reflective-type optical fiber probe which has been shown to be effective and accurate for measuring the local solid concentration and particle velocity in high velocity fluidized beds and thus has been widely used by many investigators (Herbert *et al.*, 1994; Johnson *et al.*, 2001; Liu *et al.*, 2003 and Ellis *et al.*, 2004). It yields high signal-to-noise ratios and is nearly free of interference by temperature, humidity, electrostatics and electromagnetic field. Moreover, its small size does not significantly disturb the overall flow structure in CFB systems.

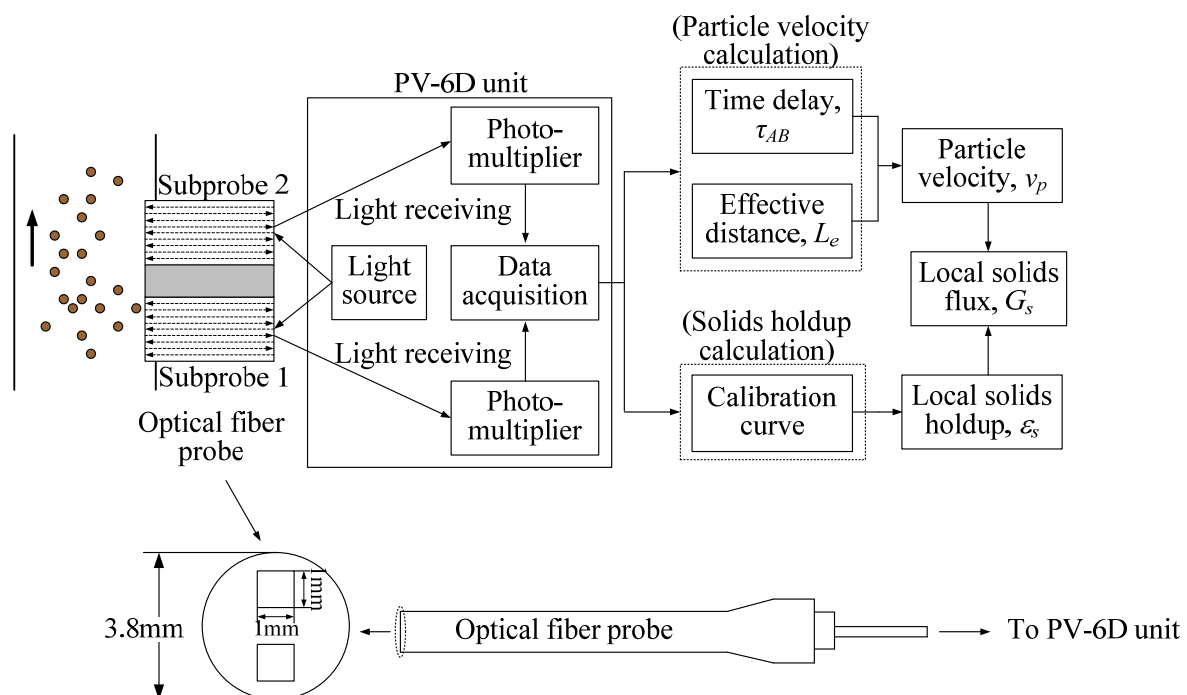


Figure 5.2 Schematic diagram of the novel optical fiber probe and its working principle.

The optical fiber probe used in this work is model PV6D, developed by the Institute of Processing Engineering, Chinese Academy of Sciences, Beijing, China. The probe and measurement procedure are schematically shown in Figure 5.2. The outer diameter of the probes is 3.8 mm. The probe has two subprobes. Each of the subprobes consists of 8000 fine quartz fibers. The effective distance of the two vertically aligned subprobes is 1.51 mm, and the active tip area of each subprobe is 1×1 mm. Each subprobe consists of many quartz fibers with a diameter of 15 μm, for light-emitting and receiving, arranged in alternating arrays. In order to prevent particles from occupying the blind zone, a glass cover of 0.2 mm thickness is placed over the probe tip. The underlying theory is elaborated by Liu *et al.* (2003).

As shown in Figure 5.2, light from the source illuminates a measuring volume of particles through the light-emitting fibers. The received light reflected by the particles is captured by light receiving fibers and processed by a photo-multiplier. The light intensity is then converted into voltage signals and the voltage signals are further amplified and fed into a PC. The voltage signal obtained by the probe is converted to volumetric concentration using a calibration equation. The relationship between the output signals of the optical fiber probe and the local solids holdup (non-linear) is first established through proper a calibration based on the method developed by Zhang *et al.* (1998).

From the voltage time series $V(t)$ and the calibration equation, local instantaneous solids holdup, $\varepsilon_s(t)$, can be calculated:

$$\varepsilon_s(t) = f[V(t)] \quad (5.1)$$

where, f is the calibration function. The time-mean solids concentration ε_s can be given by integrating $\varepsilon_s(t)$ over the time period, T :

$$\varepsilon_s = \frac{1}{T} \int_0^T \varepsilon_s(t) dt \quad (5.2)$$

The cross-sectional average solids holdup $\bar{\varepsilon}_s$, can be calculated as follow:

$$\bar{\varepsilon}_s = \frac{1}{\pi R^2} \int_0^R 2\pi r \varepsilon_s dr = \frac{2}{R^2} \int_0^R \varepsilon_s r dr \quad (5.3)$$

The particle velocity can also be measured simultaneously with solids holdups. When particles pass through the tips of the two subprobes, they would produce two similar signals with a time delay τ , which can be calculated by cross-correlation method. Combining the time delay τ with the effective distance between two subprobes, L_e , the instantaneous particle velocity, V_p can be calculated as follow:

$$v_p = \frac{L_e}{\tau} \quad (5.4)$$

To obtain the particle velocities, an integration time of 12.80 ms is set after the optimization (Liu *et al.*, 2003). Because of the turbulent nature of gas-solids suspension in fluidized beds, a particle passing through the upstream subprobe may not be detected by the downstream subprobes, due to possible particle-particle and/or particle-probe interactions. This may lead to low or even indeterminate cross-correlation coefficients. Such poorly or uncorrelated data need to be eliminated. The correlation coefficients are set to be higher than 0.6 as the criteria to collect the acceptable results. The direction of the particle motion is determined based on the maximum cross-correlation coefficient from the positive and negative correlation of the two channel signals (Nieuwland *et al.*, 1996; Werther, 1999 and Zhu *et al.*, 2001).

The cross-sectional average particle velocity weighted by the local solids concentrations can be calculated as follow:

$$\bar{v}_p = \frac{2}{R^2 \bar{\varepsilon}_s} \int_0^R v_p \varepsilon_s r dr \quad (5.5)$$

By combining the results of local solids holdup and particle velocity obtained as mentioned above, the time-mean local solids fluxes can be expressed as:

$$\bar{G}_{s,L} = \rho_p \int_0^T v_p(t) \varepsilon_s(t) dt \quad (5.6)$$

where $\bar{G}_{s,L}$ is the time-mean local solids flow rate, $V_p(t)$ is the instantaneous particle velocity and $\varepsilon_s(t)$ is the instantaneous solids holdup measured by the probe. Similarly, cross-sectional average solids fluxes can be defined as:

$$\bar{G}_s = \rho_p \int_0^R 2\pi r \bar{G}_{s,L} dr \quad (5.7)$$

By comparing the G_s measured by the flapper valves installed in the measurement tank and the \bar{G}_s calculated by Eq. (5.7), this measurement accuracy has been verified by Zhu and Zhu (2008).

In order to map the entire cross-section of the riser, ten axial measuring ports ($z = 0.59, 1.02, 1.94, 2.85, 3.77, 4.78, 5.84, 7.78, 9.61, \text{ and } 10.09$ m above the gas distributor) are installed along the column. Measurements were conducted at six radial positions ($r/R = 0, 0.316, 0.548, 0.707, 0.837$ and 0.950 , where r is the distance from the center and R is the riser radius) on each axial level of the CFB riser system. These positions are determined by dividing the column cross-section into five equal areas and determining the mid-point of each of these areas. For the hydrodynamic experiments in the current study, voltage signals from the optical fiber probe were sampled at a high frequency of 100 kHz with 1,638,40 data points for each measurement under a wide range of operating conditions so that detailed dynamic nature of the flow structure could be fully collected. To get valid and repeatable data, all measurements are repeated at least 5 times.

5.3 Results and discussion

5.3.1 Axial profiles of cross-sectional average particle velocity

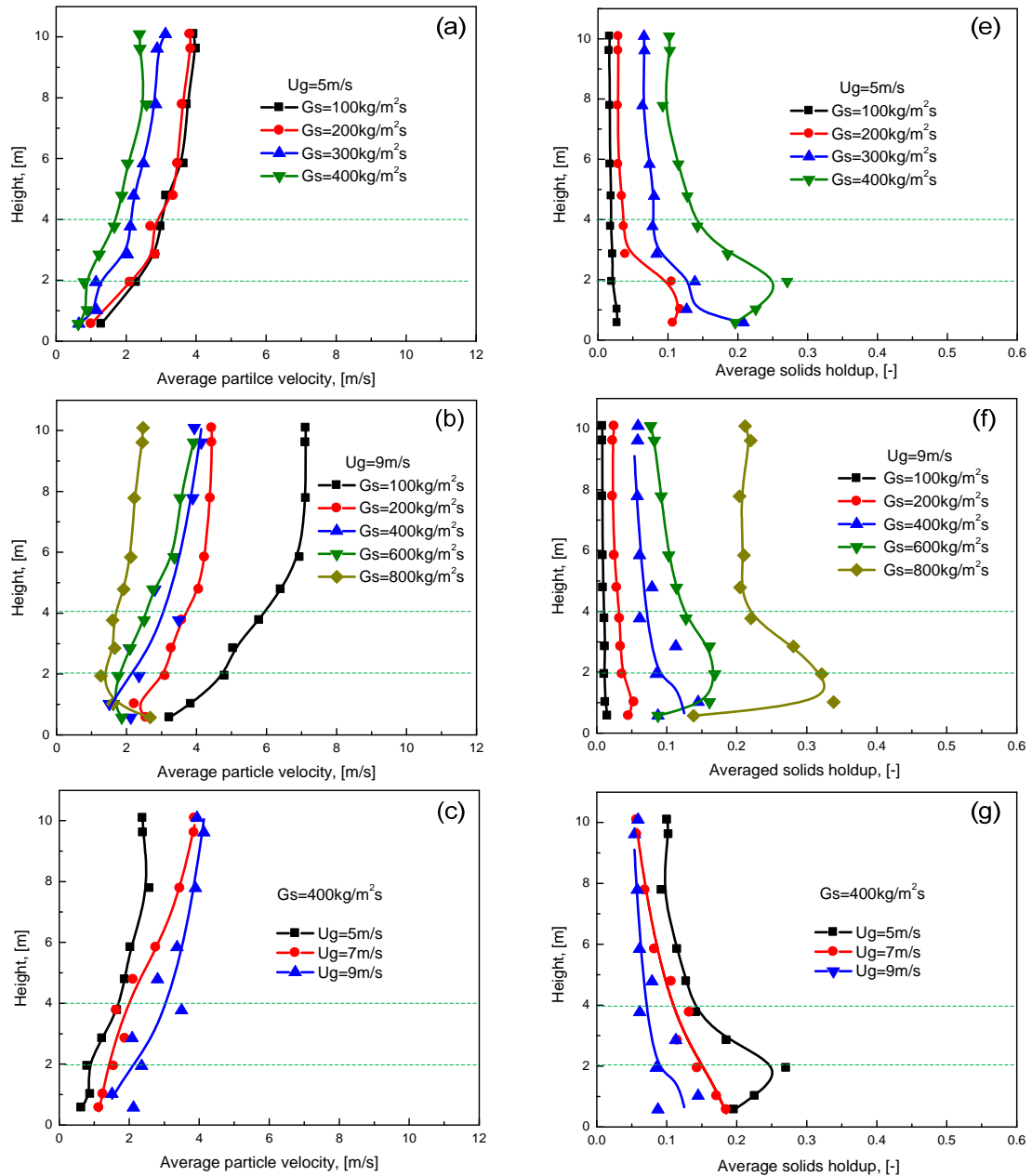


Figure 5.3 Axial profiles of average particle velocity and corresponding solids holdup under different operating conditions.

Figure 5.3 shows the cross-sectional average particle velocities and the corresponding solids holdups on ten axial elevations obtained with the same optical fiber probe. The cross-sectional average particle velocity (average particle velocity for short) is given by averaging the local particle velocity weighted with the solids holdup at six radial positions. Overall, the particle velocities are lower at the bottom of the riser and increase gradually in the upper sections. Higher superficial gas velocity results in higher average particle velocity while higher solids circulation rate leads to lower average particle velocity in each axial position. The development of axial particle velocity is also described in Figure 5.3. When G_s is lower than $700 \text{ kg/m}^2\text{s}$, there is no significant change of the shape of the axial profiles. Along the riser, these axial profiles could be divided into three sections. Firstly, the very bottom region with a short length of 2 m is the “distributor controlled” section where the average particle velocity is different under various operating conditions due to the entrance effect. Secondly, the middle section is around 2-4 m where there is a clear solids acceleration and particle velocity increased significantly especially at relatively low solids fluxes (lower than $300 \text{ kg/m}^2\text{s}$). In this region, particle velocity ranges from 1-6 m/s depending on the operating conditions. The third is the top section where the particle velocities along the riser are nearly constant. Similar results were also reported by Pärssinen and Zhu (2001) with G_s up to $550 \text{ kg/m}^2\text{s}$. It is noted that the shape of axial profiles under high flux conditions is different from that under relatively low flux conditions. Under extremely high solids circulation rate of $800 \text{ kg/m}^2\text{s}$, the axial distribution of particle velocity becomes more uniform. In other words, the average particle velocity has almost no change along all axial levels if ignoring the entrance effecting region under such high solids flux.

Three axial sections along the riser were identified as: the entrance influence zone at the very bottom of the riser, the dense region at the base of the riser and the relatively low solids holdup region in the upper sections (as shown in Figures 5.3(e), (f) and (g)). Such axial structures can also be observed in the axial profiles of the average particle velocity shown in Figures 5.3(a), 5.3(b) and 5.3(c).

5.3.2 Radial profiles of particle velocity

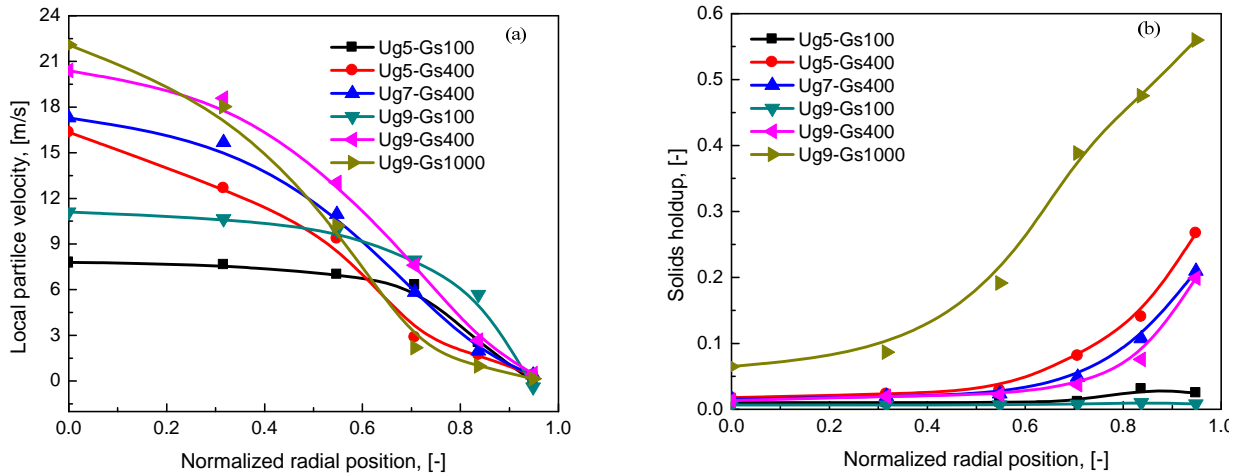


Figure 5.4 Radial profiles of particle velocity and corresponding solids holdup.

The radial profiles of particle velocity and the related solids holdup at $z = 7.78$ m under a wide range of operating conditions are plotted in Figure 5.4. Generally, the particle velocity has its maximum value at the riser axis and decreases with the radial position moving outward toward the wall. A clear change in the shapes of the radial profiles of particle velocity occurs when the solids circulation rate increases. When solids circulation rate is low ($G_s = 100$ kg/m²s), the radial profile of the particle velocity is typically “core-annulus” structure with a wide and rather flat core region. At the radial positions around $0.7 < r/R < 0.85$, the particle velocities decrease sharply as the radial position shifts towards the wall. When r/R is larger than 0.85, particle velocities reverse downward and the negative values are nearly constant around 0.5-1 m/s. The flatter velocity regions in the axis and wall area correspond to the core and annulus region and the steeper velocity zone corresponds to the transition of the two regions. This kind of radial distributions is similar to the corresponding radial profiles of solids holdup shown in Figure 5.4 (b).

Increasing G_s up to 400 kg/m²s, the radial profiles of particle velocity show a great change from the “core-annulus” structure to a more parabolic shape with a maximum value at the centerline and decreases monumentally outer toward to the wall. The same trend was also observed by

Pärssinen and Zhu (2001). Further increasing G_s to extremely high G_s up to $1000 \text{ kg/m}^2\text{s}$, the parabolic shape is transformed to a steeper and approximately linear radial profile. The same trend of change in shape with increasing G_s is consistent with profiles reported by Liu (2001). The particle velocities are higher in the center of the riser for extremely high solids flux compared to the low fluxes at a constant U_g of 9 m/s . The reason could be that more solids occupy the wall region and restrict the gas flow under high flux conditions. In order to maintain the superficial gas velocity of 9 m/s , the gas velocity has to be correspondingly higher in the riser center (Martin *et al.*, 1992 and Liu *et al.*, 1999) leading to higher particle velocity in the center. In addition, the particle velocity at each radial position of the riser is positive under high solids circulation rate which is totally different from that under low flux conditions where net negative particle velocities are often seen near the wall. The similar results had also been reported by other researchers (Grace *et al.*, 1999 and Pärssinen and Zhu, 2001). Finally, the particle velocities at the wall region are all very small in magnitude at high G_s , no doubt affected by the non-slip condition on gas velocity.

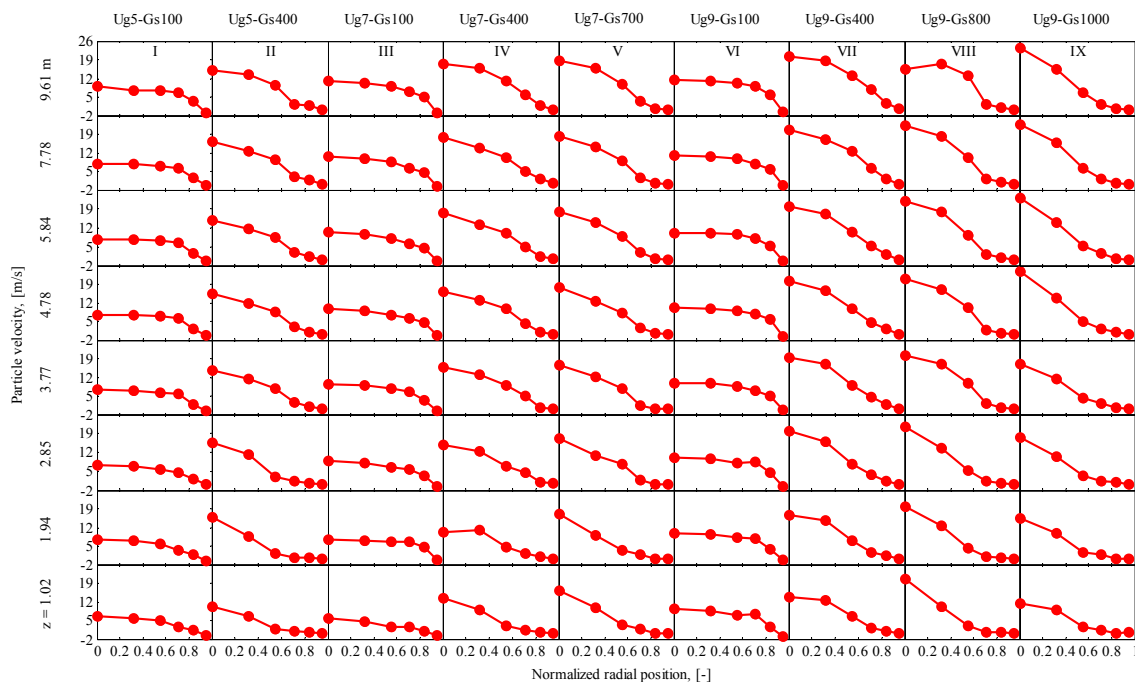


Figure 5.5 Radial particle velocity distribution for various operating conditions.

Figure 5.5 presents more details of radial profiles of particle velocity on different axial elevations under a wide range of operating conditions. As discussed above, the particle velocity is lower at the bottom than in the upper sections. Additionally, Figure 5.5 displays axial development with respect to the radial profiles of particle velocity under each operating condition. Clearly, the solids flow structures are different under various operating conditions. When solids circulation rate is the lowest ($G_s = 100 \text{ kg/m}^2\text{s}$), the flow development of particle velocity is faster with only slight changes in the shape of radial profiles up the riser. When solids circulation rate is $400 \text{ kg/m}^2\text{s}$, the development of particle velocity can be divided into three regions. In the “distributor controlled” region (below 2 m), the radial profiles vary without specific trend, showing either parabolic shape or approximately linear structure. In the middle elevations (2-4 m), the acceleration of solids leads to a steeper linear radial velocity profile. In the upper levels (above 4 m), the linear-shaped profile of radial particle velocity distribution changed into parabolic-shaped structure. Increasing G_s further, particularly higher than $700 \text{ kg/m}^2\text{s}$, the linear-shaped radial profiles cover the whole riser elevations. The axial development of the radial particle velocities is almost independent of the height under such high solids fluxes. Moreover; the maximum in the axis and minimum particle velocities near the wall region of the column is nearly unchanged along the riser. The area of the low particle velocity region near the wall shrinks slightly as the axial elevation increases. Similar results were reported by Wei *et al.* (1998) in their high density riser.

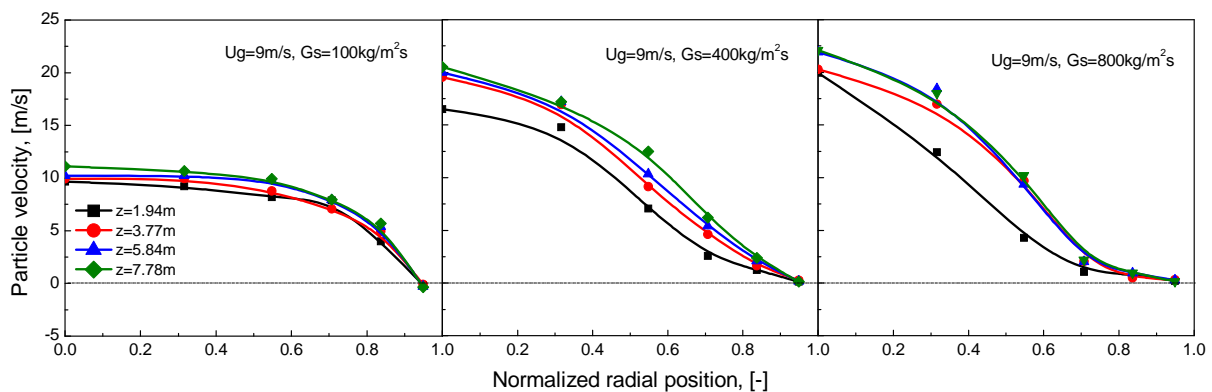


Figure 5.6 Development of radial profiles of local particle velocities.

To further investigate the flow development of the radial profiles of particle velocity under low and high flux operating conditions, Figure 5.6 compares the flow structure at four heights under the same superficial gas velocity of 9 m/s. It is clear that under low solids flux, the radial profile is more uniform than that under higher G_s . When G_s is higher than 400 kg/m²s, the particle velocities at each radial positions are unchanged with the riser heights except the very bottom part ($z = 1.94$ m). On the other hand, negative velocities occurred near the wall, although the magnitudes were generally small (< 1 m/s) under low solids flux. With further increase in solids flux, the negative velocities at the wall disappear, as also shown in Figure 5.4 (a). The reason for this difference may be that the solids holdups in the high flux/density riser are higher than in the low flux/density system. The previous results (Grace *et al.*, 1999; Liu *et al.*, 1999; Zhu and Zhu, 2008 and Qi *et al.*, 2009) confirmed that higher solids holdup results in higher effective viscosity of the rising gas-solids suspension. Higher viscosity would impose more shear stress on the possible descending particles. Meanwhile, higher solids holdup would also provide more upward momentum to reduce the tendency for the descending particles by particle-particle interactions (Qi *et al.*, 2009). No net downward flow near the wall is one of the most important advantages of the high flux/density riser over the conventional low flux/density reactor, leading to a reduction in axial dispersion of gas carried by the downflowing particles.

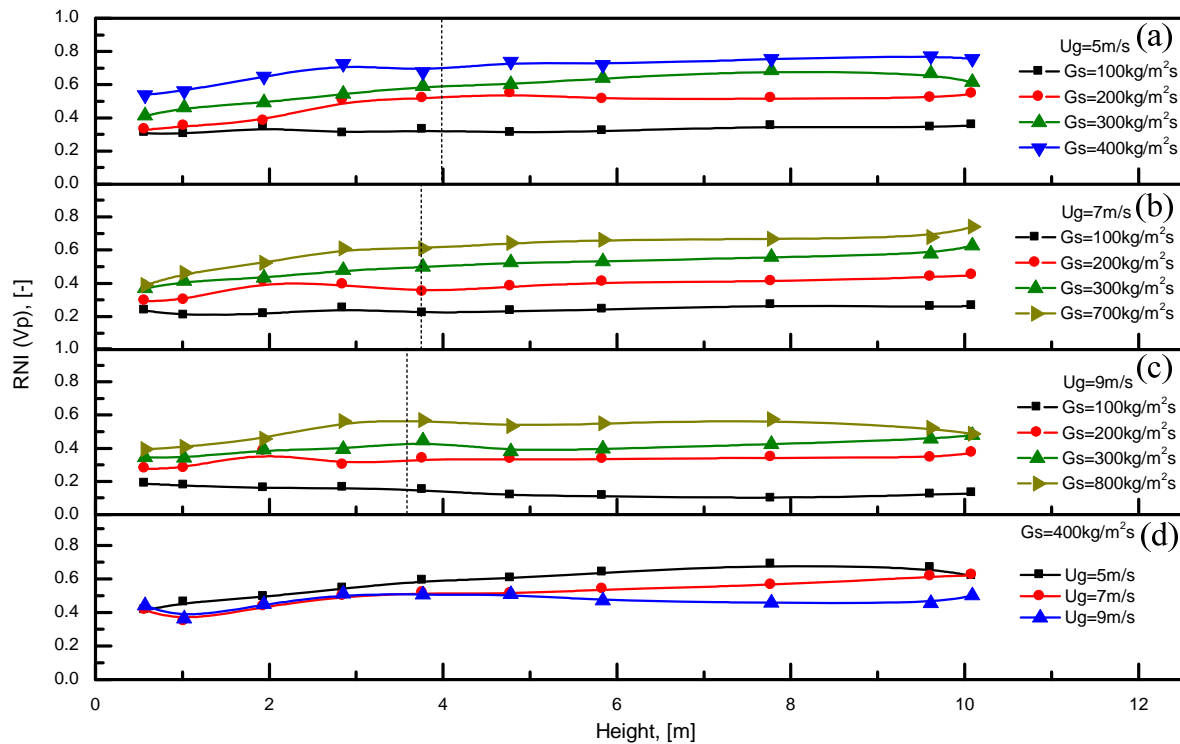


Figure 5.7 RNI's of particle velocity the riser under different operating conditions.

The axial development of radial particle flow can also be described by the radial nonuniformity index (RNI) which was proposed by Zhu and Manyele (2001). The *RNI* is defined for each given parameter as the standard deviation of its values in the radial direction, normalized by the maximum possible standard deviation for the same parameter with the same average cross-sectional value. Meanwhile, the *RNI* can be used to distinguish exactly the structure of radial profiles on a quantitative basis at different planes and/or operating conditions. The values of RNI (V_p) along the axial direction in the riser are given in Figure 5.7.

In general, the profiles had similar trend indicating two regions along the riser height with RNI (V_p) values between 0.1-0.75. Under a wide range of operating condition, RNI (V_p) increases sharply from the solids entry section and thereafter, the profiles start to be gradually flat. RNI (V_p) values were lower in the entrance region, probably because the particles were to be accelerated so that the particle velocities were low and didn't vary much along the radial positions. Towards higher levels, the RNI (V_p) value tends to increase slightly with low superficial gas velocity or remain constant for high superficial gas velocity. It also shows that

increasing U_g at a given G_s lowers the RNI (V_p), but increasing G_s at constant U_g raises RNI (V_p). This is because higher U_g and /or lower G_s lead to flatter radial profiles of particle velocities. In addition, the length of the acceleration zone at the bottom (shown in the left of the dash line in Figure 5.7) becomes shorter when U_g is increasing and/or G_s is decreasing, which indicates a lengthy process for the radial flow structure to be fully developed in the riser.

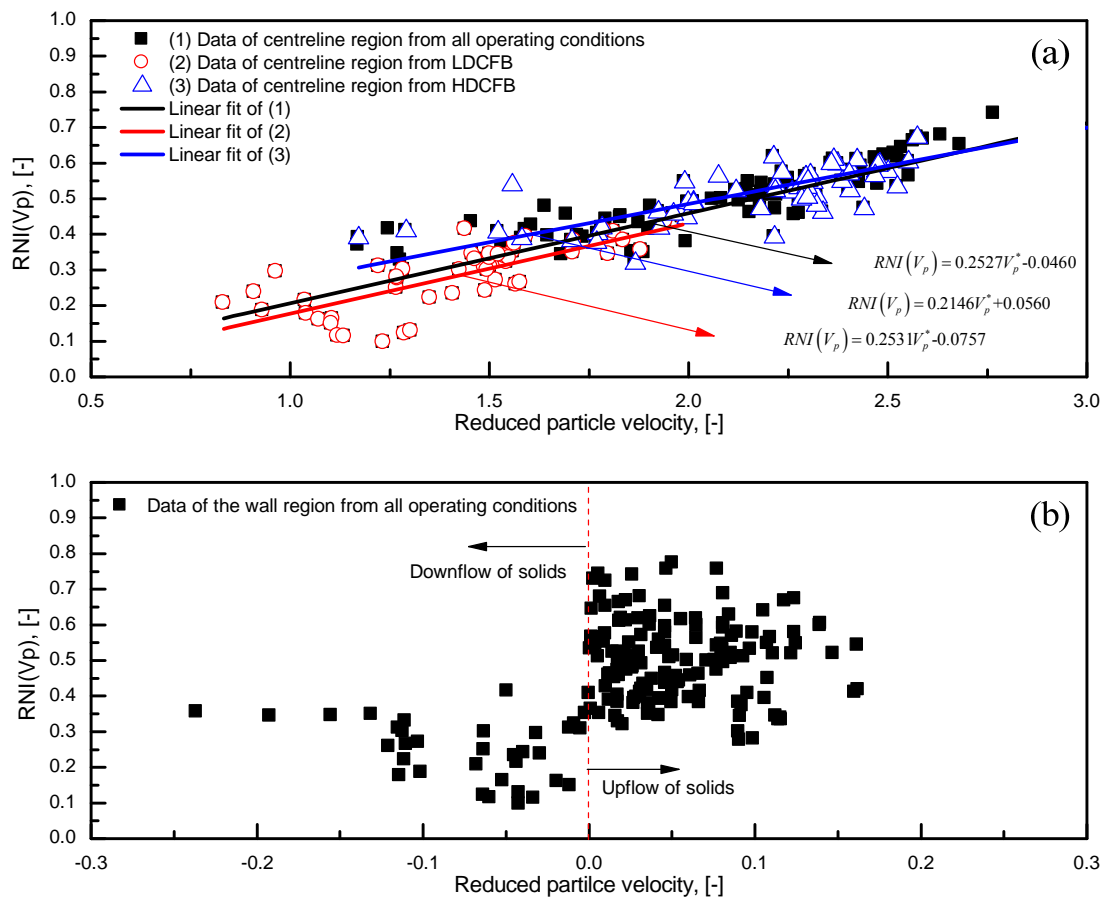


Figure 5.8 Variation of RNI (V_p) with (a) reduced centerline particle velocity and (b) reduced wall particle velocity in the riser at different operating conditions.

As discussed above, a strong velocity gradient with a maximum at the center and a minimum at the wall in the riser is the typical radial distribution of the particle velocity especially at high solids fluxes. In order to examine the changes of RNI (V_p) with particle velocity, Figure 5.8 shows the relationships between RNI (V_p) and the particle velocity at the axis ($r/R = 0.0$) and near the wall ($r/R = 0.950$). Figure 5.8(a) displays the variation of RNI (V_p) with the reduced

centerline velocity, V_{pc}^* , ($V_{pc}^* = V_{pc}/U_g$), for different operating conditions. It shows that the RNI (V_p) values increase with V_{pc}^* . The reason is that when the reduced centerline particle velocity increases, the radial profile of particle velocity becomes steeper leading to a high RNI (V_p). Meanwhile, the relationship between RNI (V_p) and V_{pc}^* is linear with slightly affected by changing operating conditions. It can be concluded that RNI (V_p) is essentially proportional to the reduced centerline particle velocity. On the other hand, the variation of RNI (V_p) with the reduced wall velocity, V_{pw}^* , ($V_{pw}^* = V_{pw}/U_g$), is shown in Figure 5.8(b). The effect of both upward velocity and downward velocity near the wall on the RNI (V_p) is indicated clearly by a dotted vertical line through $V_{pw}^* = 0$. However, a universal relationship could not be found between RNI (V_p) and V_{pw}^* probably because of the wall effects on particle velocity in this region.

5.3.3 Flow development profiles of solids flux

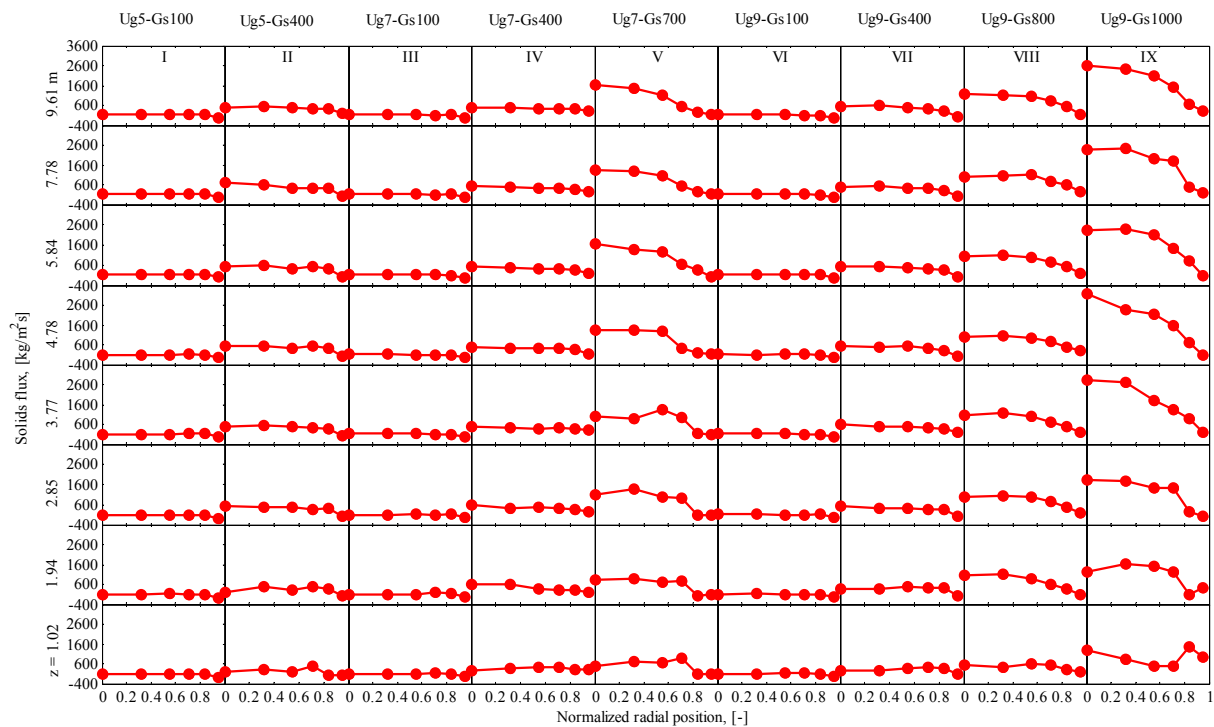


Figure 5.9 Radial profiles of local solids flux under different operating conditions.

Figure 5.9 presents the results of the solids flux at eight axial positions under different operating conditions. Overall, the shape of the radial solids flux distribution can be divided into two types: the flatly radial uniform profile and the parabolic-shaped profile. When G_s is low ($< 400 \text{ kg/m}^2\text{s}$), the profile is relatively flat occupies more than 80% of the total cross-sectional area of the riser. The solids flux then decreases continuously towards the wall. Near the wall for low solids flux conditions, solids flux is negative because particles in the wall region move downward. When G_s increases to $700 \text{ kg/m}^2\text{s}$, the profiles are roughly parabolic and an increase in G_s is accompanied by an increase in the solids flux in all radial positions. On the other hand, the net solids flux near the wall falls to close to zero, and changes the direction to upflow and continues to increase with the solids circulation rate once the solids flux is high up to $400 \text{ kg/m}^2\text{s}$. The observed profiles are consistent with the early results of other researchers at lower G_s (Herb *et al.*, 1992). However, they are different from the solids flux profiles in the dense region of the riser reported by Wei *et al.* (1997). The no slip condition at the wall means that the gas velocity approaches zero towards the wall. There is therefore a tendency for particles to fall downwards near the wall, especially when they form cluster or streamers. However, the high solids holdup found near the wall for high flux/density conditions results in increased momentum transfer from the upflow suspension in the interior of the column, meaning that there is relatively little downflow in the vicinity of the wall (Issangya *et al.*, 1998).

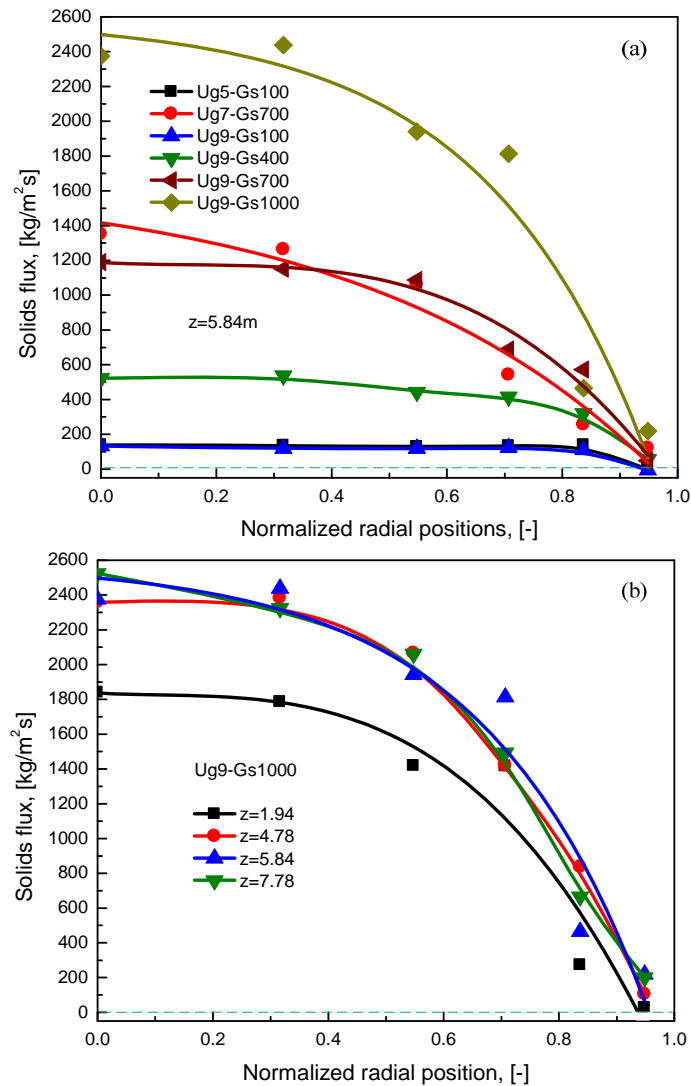


Figure 5.10 Typical radial profile of solids flux under low and high flux/density operating conditions.

Figure 5.10 shows typical radial profiles of local solids flux. Again, the solids flux is highest at the axis, decreasing towards the wall. Toward the wall, the local solids flux decreases with different magnitudes with a wide range of flat area then gradually decreasing under low solids flux conditions and a more significant drop when G_s is high.

The radial solids flux profiles presented in Figure 5.10(a) show clearly a transition in the shape of the profiles. At the lowest flux of $100 \text{ kg/m}^2\text{s}$, the local solids flux profile is flat. The value of

solids flux remains nearly constant up to a dimensionless radial location of about 0.8. Local solids flux in this range is slightly higher than at the wall where solids were flowing downward at the wall. At the intermediate solids flux of $400 \text{ kg/m}^2\text{s}$, the mass flux profile became slightly parabolic. Radial solids flux was constant from the centerline to a dimensionless radial position of about 0.6. Beyond that point, the solids flux decreased gradually becoming almost zero near the wall. When G_s rises to $700 \text{ kg/m}^2\text{s}$, the local solids flux profile was roughly parabolic. At this G_s , the solids flux showed a steeply decrease from the column axis to the wall region. The sharp decrease of solids flux with radial location corresponds to a sharp decline of local particle velocity as discussed in the above section. Moreover, the measured local solids flux at the center was about two times higher than external solids circulation rate when the parabolic-shaped radial profiles occurred.

Figure 5.10(a) also illustrates the effects of superficial gas velocity on local solids flux distribution. Firstly, the superficial gas velocity has barely any effects on the shape of radial profiles when G_s is $100 \text{ kg/m}^2\text{s}$. Secondly, at a higher G_s ($= 700 \text{ kg/m}^2\text{s}$), the shape of the radial profile changes greatly with superficial gas velocity. Higher superficial gas velocity results to a much flatter and less parabolic shaped radial profile. At $U_g = 9 \text{ m/s}$, the profile is flat across the riser with a small variation at $r/R = 0.5$. When U_g is decreased to 7 m/s , the magnitude of the local solids flux is much higher in the central region of the riser and undergoes a dramatic decrease at around $r/R = 0.3$. In addition, the profile indicates that under high gas velocity and high flux/density operating conditions, solids travel rapidly upward in the central region, while they move slowly upwards or nearly stagnant near the wall.

From the above discussion, there is a trend that higher superficial gas velocity and lower solids circulation rate (low solids/gas loading) generate the more uniform radial (local solids flux remain constant within a wide cross-sectional area) profiles of local solids flux while high solids/gas loading produce parabolic-shaped radial profile of solids flux. The nature of the radial solids mass flux profiles could be attributed to the different interaction mechanisms between the gas and solids phases in the two sets of operating conditions.

Generally, the way solids are dispersed in a carrier gas is mainly affected by two factors including (1) particle-particle interaction (collisions and inter-particle forces) and (2) gas-solid interaction (Li, 2003; Li and Kwauk, 2003; Sundaresan, 2003 and Li *et al.*, 2007). As discussed earlier, gas particle interactions (drag forces) play a more important role under low solids/gas loading conditions. If particles are fed into the gas stream at a low rate, particles can be carried up easily by gas and have little effect on the motion of the gas resulting in a velocity profiles very similar to that of the gas across the whole radial positions, only lagging by a certain “slip velocity” at the wall. Hence, the flat radial uniform profile occurs. On the other hand, if the solids flux is high enough, relatively high solids holdup would cover the entire cross-sectional area (same authors), affecting the motion of gas. Typical turbulent profiles of gas velocity for single gas phase flow would become more distorted with more gas tending to flow through the central region of the column (Zhu and Zhu, 2008). Besides, when solids in a large amount cannot be completely carried by the gas, solids downflow begins to form at the wall, leading to a parabolic shape in the radial solids flux distributions. Moreover, high solids concentration would tend to promote particle-particle interactions (collisions) which would control particle motion. Higher collision frequency is responsible for higher shear on the descending particles reducing the tendency for solids downflow. Considering the two reasons on the particles near the wall, it is found that particle velocity near the wall is positive as stated earlier. As a result, there is no negative solids flux under high solids/gas loading conditions. No net downward solids flux near the wall is another important advantage of the high flux/density riser reducing solids backmixing.

Figure 5.10(b) compares local solids flux profiles at different axial elevations at $U_g = 9$ m/s and $G_s = 1000$ kg/m²s. It is obvious that the radial solids flux profiles overlap essentially. Such an independence of solids flux on the axial level seems to be understood by considering that gas-solids suspension reached some kinds of “an equilibrium state”, or “a force balance” in the macro-scope. In addition, the improved collision (particle-particle interactions) under such extremely high flux leads to more uniform distribution of solids holdups and particle velocities along the column, and thereafter a more uniform axial solids flux distribution as suggested by Zhu and Zhu (2008).

5.3.4 Relationship between solids holdup, particle velocity and solids flux

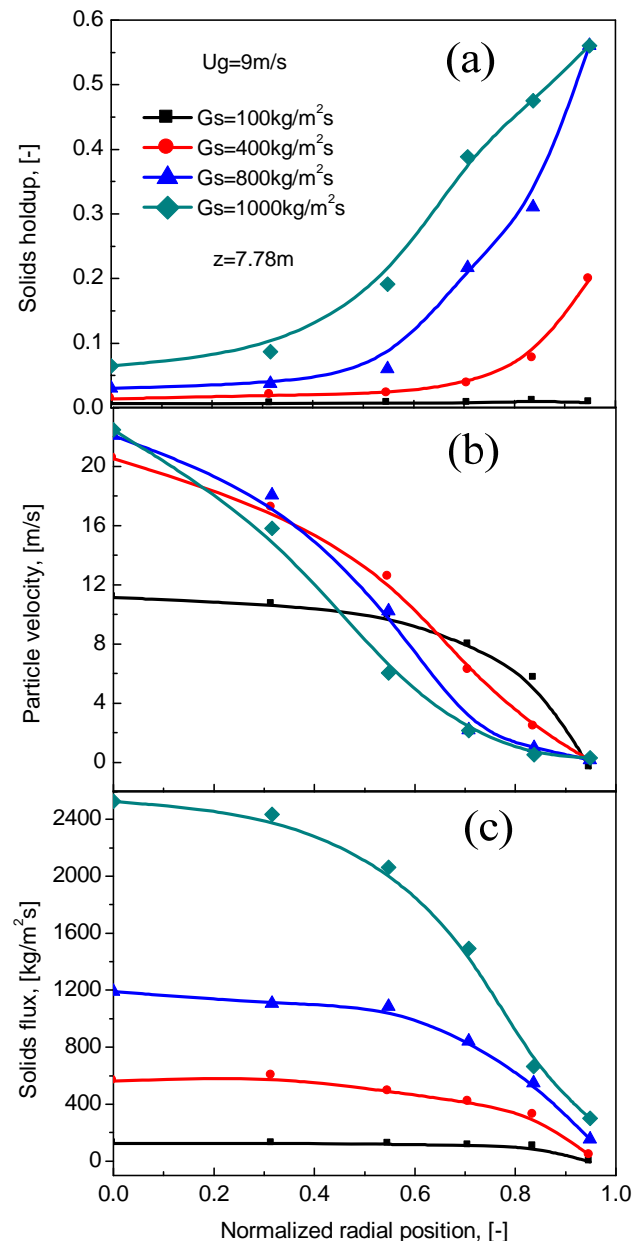


Figure 5.11 Radial profiles of (a) solids holdup, (b) particle velocity, and (c) solids flux.

According to the study, the three main hydrodynamic parameters in circulating fluidized bed systems were closely related to each other. Typical radial profiles of solids holdup, local particle velocity and solids flux based on Eqs. (5.3), (5.5) and (5.6) at $z = 7.78 \text{ m}$ under different operating conditions are plotted in Figure 5.11. Overall, higher solids holdup usually corresponds

to lower particle velocity under each operating conditions. Under low solids flux/density conditions, the curves of these three parameters are relatively flat. With increasing G_s , the shapes of the three parameters become steeper. Moreover, the shape of solids flux is not only influenced by solids holdup profile but also by particle velocity distribution. For $U_g = 9$ m/s and $G_s = 400$ kg/m²s, the solids holdup profile remains relatively flat over a wide radial region before sharply increasing near the wall. The corresponding particle velocity profile is roughly parabolic in shape with a maximum at the centerline and decreasing toward to the wall. The corresponding solids flux profile is again relatively uniform in the core over a considerable radial distance, and then decreases gradually toward the wall.

To further investigate the relationship between the local solids holdups, particle velocities and solids fluxes, Figures 5.12-5.15 compare the particle velocities against solids holdups, solids fluxes against solids holdups and particle velocities, under a wide range of operating conditions.

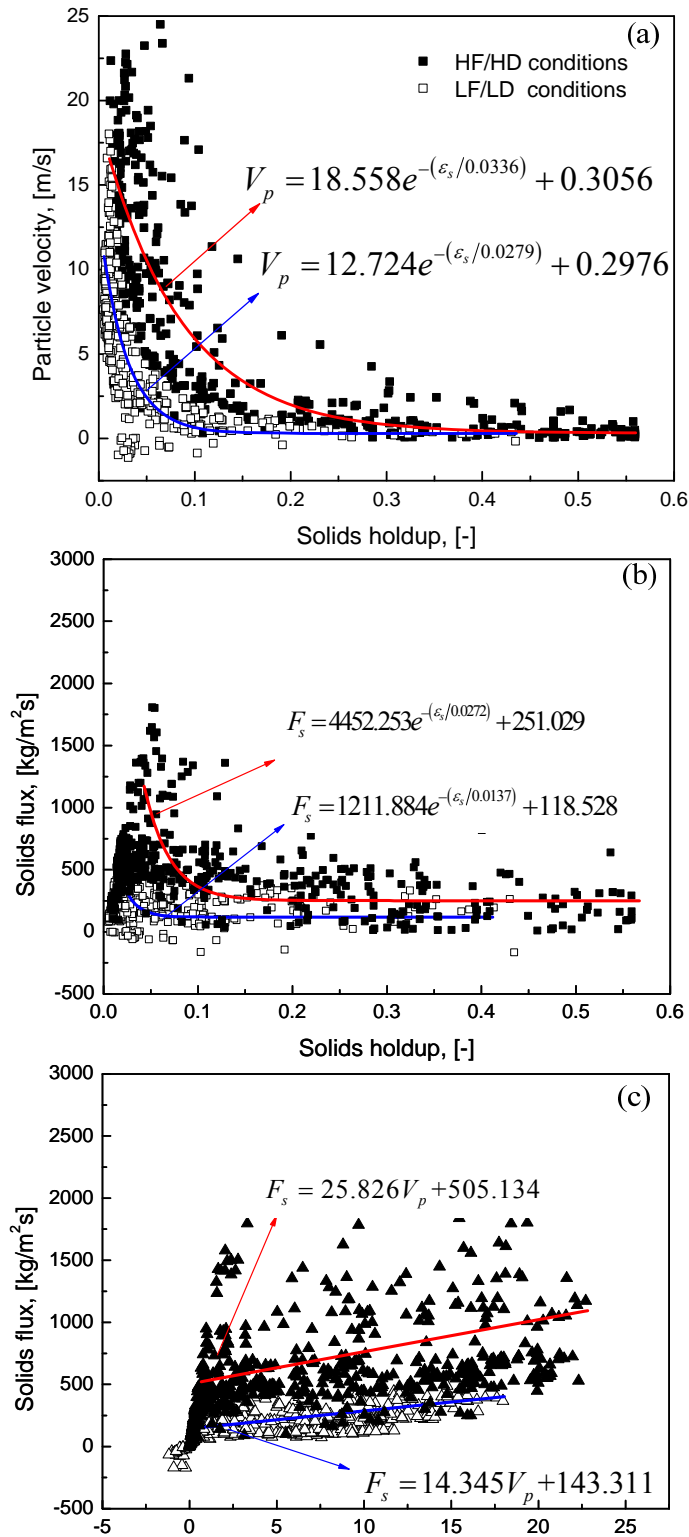


Figure 5.12 Relationship between solids holdup and particle velocity under low and high solids flux operating conditions.

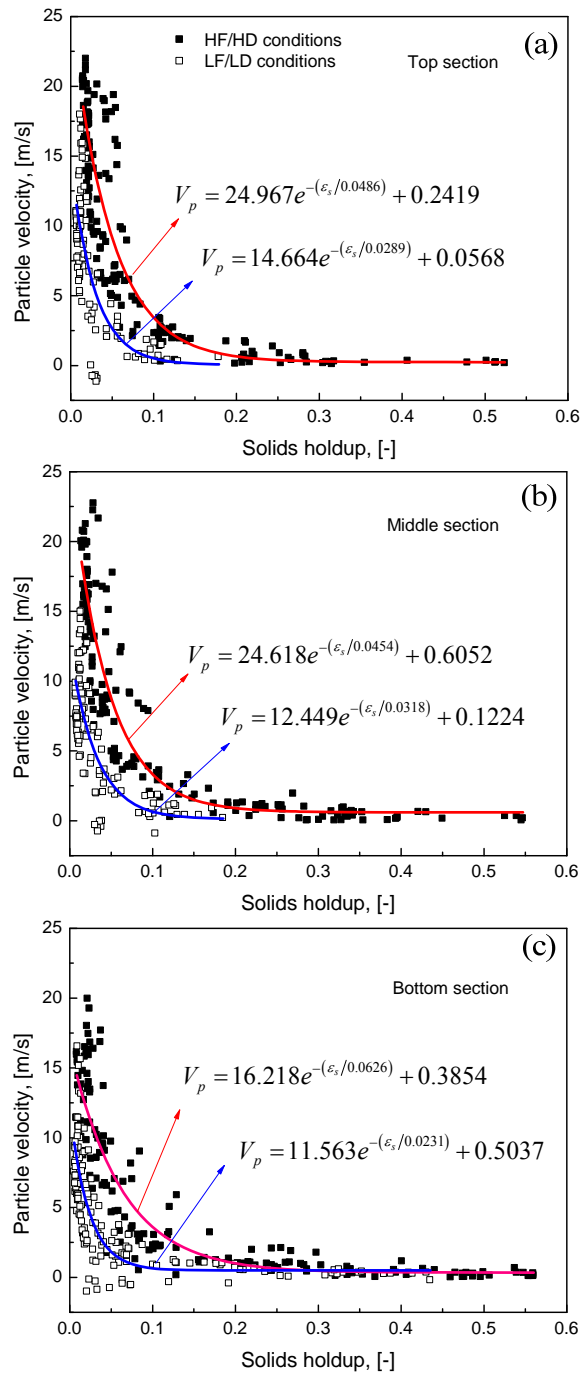


Figure 5. 13 Relationship between solids holdup and particle velocity in the three axial sections along the riser.

Figure 5.12 shows the relationship between solids holdup, particle velocity and solids flux comparing the low flux (where solids flux is lower than $500 \text{ kg/m}^2\text{s}$) and high flux conditions. Figure 5.13 presents the relationship between particle velocity and solids holdup in three different axial regions according to the above discussion on the development of solids flow. As shown in Figures 5.12 and 5.13, local particle velocity and solids flux were exponentially related to the corresponding solids holdup. Local solids flux to some extent has a linear relationship with the particle velocity. Figures 5.12 and 5.13 also demonstrate the relationship between the main hydrodynamic parameters under low solids flux/density (LF/LD) and high solids flux/density (HF/HD) conditions. Figures 5.12 and 5.13 show the same trend that the particle velocity against solids holdup is well correlated under LF/LD conditions. Such a strong dependence under LF/LD conditions indicates that solids motion is mainly controlled by the gas-solids interactions in low flux/density CFB systems. However, the correlation is not good when solids flux/solids holdup is high especially under the lower part of the column. As is clearly shown in Figure 5.13, both solids holdups and particle velocities have wide distributions in HF/HD conditions. This suggests that a higher solids concentration could lead to stronger particle-particle interactions, as a result, the particle movement is to some extent controlled by the collisions between particles in the dense conditions. Meanwhile, it is clear that the correlation hardly varies with the height of the column except in the “distributor controlled zone” at the very bottom of the riser according to Figure 5.13, which suggested an inherent relationship between particle velocity and solids holdup.

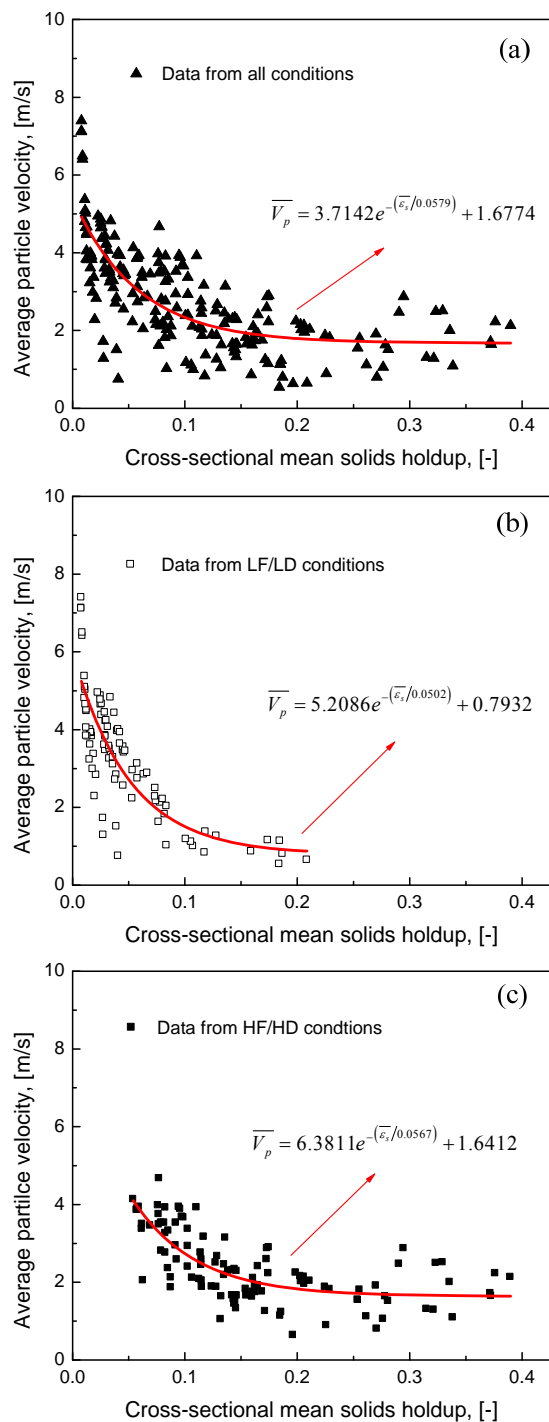


Figure 5.14 Relationship between cross-sectional average solids holdup and particle velocity for different operating conditions.

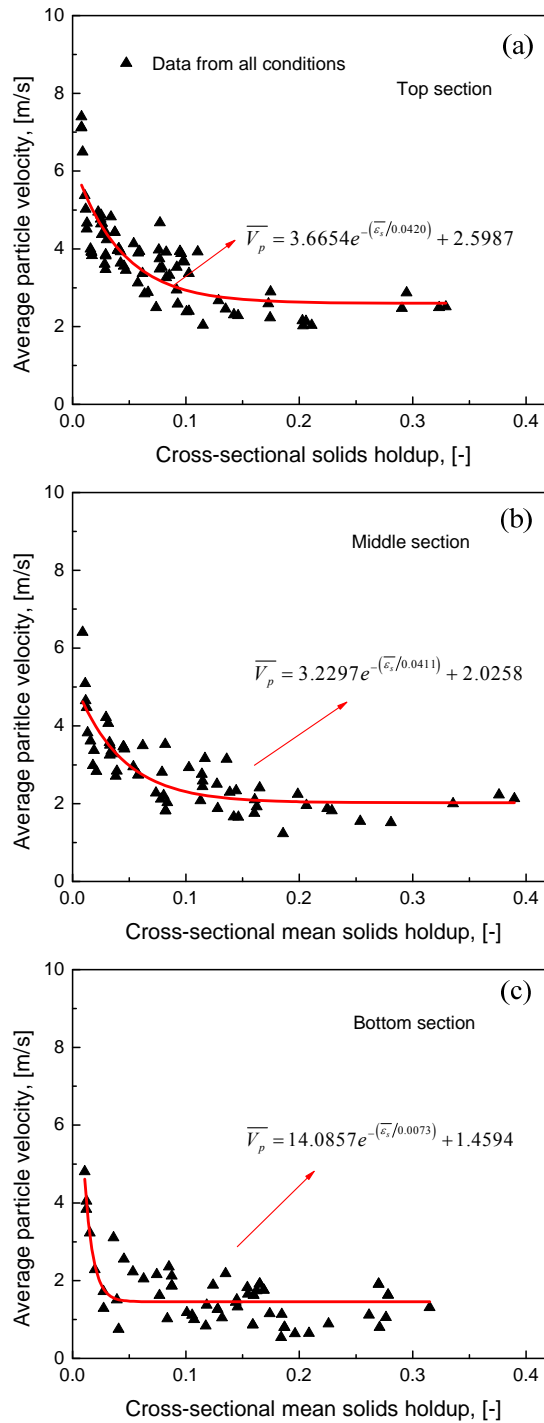


Figure 5.15 Relationship between cross-sectional average solids holdup and particle velocity in the three axial sections along the riser.

Figures 5.14 and 5.15 present the cross-sectional average particle velocity against the cross-sectional average solids holdup under different operating conditions. Similar results are observed where high average solids holdup lead to low average particle velocity. Under low solids flux/density, the relationship between average solids holdup and particle velocity is more correlated than that for high solids flux/density operating conditions. For different axial positions, Figures 5.15(a), (b) and (c) describe the approximate pattern in three axial sections showing decreasing of the average particle velocity with the average solids holdup. The independence of the variation with the heights indicates again that the particle-particle interaction play a significant role on particle motions in the dense conditions.

5.4 Conclusions

Detailed knowledge about flow structure and properties is crucial in better understanding of the hydrodynamics in a high flux/density circulating fluidized bed. Local flow structures and hydrodynamics were investigated for the first time at high solids fluxes up to $1000 \text{ kg/m}^2\text{s}$ using multipurpose optical fiber probes, which could measure the solids concentration and velocity at the same time.

The shape of the axial particle velocity profiles depends on the operating conditions. When solids flux is lower than $700 \text{ kg/m}^2\text{s}$, three axial sections are formed along the riser: “distributor controlled” zone at the very bottom, acceleration section at the base of the column, and the upper section with constant average particle velocity. Under extremely high solids flux of $800 \text{ kg/m}^2\text{s}$, the axial profile of the particle velocity became more uniform. The axial particle velocity is affected more significantly by superficial gas velocity especially under high solids flux/density conditions.

Radial profiles of particle velocity and solids flux had unique shapes under different operating conditions with radially uniform structure under low solids flux/density and roughly parabolic-shaped under high solids flux/density conditions. No net downward flow near the wall is one of the most important advantages of the high flux/density riser over the conventional low flux/density reactor, leading to a reduction of solids backmixing.

Relationships between solids holdups, particle velocity, and solids flux were studied. Correlation between particle velocity and solids holdup was stronger for low solids flux/density conditions than that of high/solids flux conditions. The results revealed that gas-particle interactions dominated in low solids flux/density CFBs while particle-particle interactions played a key role for the motion of particles in the high solids flux CFB systems.

Nomenclature

f	calibration function for optical fiber probe
F_s	solids flux [kg/(m ² ·s)]
\bar{G}_s	cross-sectional average solids flux [kg/(m ² ·s)]
$\bar{G}_{s,L}$	time mean local solids flux [kg/(m ² ·s)]
G_s	solids circulation rate [kg/(m ² ·s)]
L_e	effective distance between light-receiving fiber A and B [m]
r/R	reduced radial sampling positions
t	time [s]
T	time interval [s]
U_g	superficial gas velocity [m/s]
v_p	particle velocity [m/s]
\bar{v}_p	cross-sectional average particle velocity [m/s]
V	voltage [volt]
$V(t)$	voltage time series [volt]
z	axial coordinate, or distance from gas distributor [m]

Greek letters

ε_s	solids holdup [-]
$\varepsilon_s(t)$	local instantaneous solids holdup [-]
$\bar{\varepsilon}_s$	average solids holdup in the entire column [-]

Subscripts

1, 2	subprobe 1 and 2 of optical fiber probe
g	gas
p	particle
s	solids

References

- Bai DR., Jin Y., Yu ZQ. and Zhu JX., (1992), The axial distribution of the cross-sectionally averaged voidage in fast fluidized beds, *Powder Technology* 71, 51-58
- Du B., Warsito W. and Fan LS., (2003), Bed non-homogeneity in turbulent gas-solid fluidization, *AIChE Journal* 49, 1109-1126
- Ellis N., Bi HT., Lim CJ. and Grace JR., (2004), Influence of probe scale and analysis method on measured hydrodynamic properties of gas-fluidized beds, *Chemical Engineering Science* 59(8-9), 1841-1851
- Grace JR., Issangya AS., Bai DR., Bi HT. and Zhu JX., (1999), Situating the high density circulating fluidized bed, *AIChE Journal* 45, 2108-2116
- Herbert PM., Gauthier TA., Briens CL. and Bergougnou MA., (1994), Application of fiber optic reflection probes to the measurement of local particle velocity and concentration in gas-solid flow, *Powder Technology* 80, 243-252
- Issangya AS., Bai DR., Bi HT., Lim KS., Zhu J. and Grace JR., (1999), Suspension densities in a high-density circulating fluidized bed riser, *Chemical Engineering Science* 54, 5451-5460
- Issangya AS., Bai DR., Grace JR., Lim KS. and Zhu J., (1997), Flow behaviour in the riser of high-density circulating fluidized bed, *AIChE Symposium Series* 93, 25-30
- Issangya AS., Grace JR., Bai DR. and Zhu JX., (2000), Further measurements of flow dynamics in a high-density circulating fluidized bed riser, *Powder Technology* 111, 104-113
- Johnsson H. and Johnsson F., (2001), Measurements of local solids volume-fraction in fluidized bed boilers. *Powder Technology*; 115,13-26
- Kathleen S. and Jan B., (2001), Hydrodynamic modeling of the axial density profile in the riser of a low-density circulating fluidized bed. *The Canadian Journal of Chimerical Engineering* 79(3), 422-429
- Kunii D. and Levenspiel O., (1991), *Fluidization Engineering*. Butterworth-Heinmann, London
- Li J., (2003), Euler-Lagrange simulation of flow structure and evolution in dense gas-fluidized beds. . Ph.D. Diss., University of Twente, Enschede
- Li JH. and Kwauk M., (2003), Exploring complex systems in chemical engineering-the multi-scale methodology. *Chemical Engineering Science* 58, 521-535

- Li J., JAM. and Kuipers., (2007), Effect of competition between particle-particle and gas-particle interactions on flow patterns in dense gas-fluidized beds. *Chemical Engineering Science* 62, 3429-3442
- Li Y. and Kwauk M., (1980), The dynamics of fast fluidization. In, Grace JR, Matsen JM, editors. *Fluidization*. New York, Plenum Press, 537-544
- Li DB., (2010), Investigation of circulating fluidized bed riser and downer reactor performance for catalytic ozone decomposition. Ph.D. Diss. Western University
- Liu JZ., Grace JR., Bi HT., Morikawa H. and Zhu JX., (1999), Gas dispersion in fast fluidization and dense suspension upflow, *Chemical Engineering Science* 54(22), 5441-5449
- Liu JZ., (2001), Particle and gas dynamics of high density circulating fluidized beds. Ph.D. Diss. University of British Columbia, Vancouver, BC
- Liu JZ., Grace JG. and Bi HT., (2003a), Novel multifunctional optical-fiber probe, development and validation, *AIChE Journal* 49(6), 1405-1420
- Liu JZ., Grace JG. and Bi HT., (2003b), Novel multifunctional optical-fiber probe, high-density CFB measurements, *AIChE Journal* 49(6), 1421-1432
- Martin MP., Turlier P., and Bernard JR., (1992), Gas and solid behavior in cracking circulating fluidized beds,. *Powder Technology* 70, 249-258
- Nieuwland JJ. and Meijer R., (1996), Measurements of solids concentration and axial solids velocity in gas-solid two-phase flows, *Powder Technology* 87(2), 127-139
- Pärssinen JH. And Zhu JX., (2001), Particle velocity and flow development in a long and high-flux circulating fluidized bed riser, *Chemical Engineering Science* 56,5295-5303
- Qi XB., Zhu HY. and Zhu J., (2009), Demarcation of a new circulating turbulent fluidization regime, *AIChE Journal* 55(3),594-611
- Qi MZ., Barghi S. and Zhu J., (2012), Detailed hydrodynamics of high flux gas-solid flow in a circulating turbulent fluidized bed, *Chemical Engineering Journal* 209,633-644
- Qi MZ., Zhu J. and Barghi S., (2012), Particle velocity and flux distribution in a high solids concentration circulating turbulent fluidized bed, *Chemical Engineering Science* 84,437-448
- Smolders K, and Baeyens J., (2001), Hydrodynamic modelling of the axial density profile in the riser of a low-density circulating fluidized bed, *The Canadian Journal of Chemical Engineering* 79(3), 422-429
- Sundaresan and Sankaran, (2003), Instabilities in fluidized beds, *Annual Review of Fluid Mechanics*, 35,63-88

van Der Hoef MA. and Van Sint Annaland M., (2004), Computational fluid dynamics for dense gas-solid fluidized beds a multi-scale modeling strategy, *Chemical Engineering Science* 59, 5157-5165

Wei F., Lu FB., Jin Y., and Yu ZQ., (1997), Mass flux profiles in a high density circulating fluidized bed, *Powder Technology* 91(3), 189-195

Wei F., Lin H., Cheng Y., Wang Z. and Jin Y., (1998), Profiles of particle velocity and solids fraction in a high-density riser, *Powder Technology* 100, 183-189

Werther J., (1999), Measurement techniques in fluidized beds, *Powder Technology* 102(1), 15-36

Zhang H., Johnston PM., Zhu JX., de Lasa HI., and Bergougnou MA., (1998), A novel calibration procedure for a fiber optic solids concentration probe, *Powder Technology* 100,260-272

Zhu JX. and Bi HT., (1995), Distinctions between low density and high density circulating fluidized beds. *The Canadian Journal of Chemical Engineering* 73,644-649

Zhu JX. and Li GZ., (2001), Direct measurements of particle velocities in gas-solids suspension flow using a novel five-fiber optical probe, *Powder Technology* 115,184-192

Zhu JX. and Manyele SV., (2001), Radial nonuniformity Index (RNI) in fluidized beds and other multiphase flow systems, *The Canadian Journal of Chemical Engineering* 79, 202-211

Zhu JX. and Cheng Y., (2005), Fluidized-Bed Reactors and Applications, Chapter 5.3 in *Multiphase Flow Handbook*, ed. Clayton Crowe, CRC Press, New York, pp 5.55-5.93

Zhu HY. and Zhu J., (2008), Gas-solids flow structures in a novel circulating-turbulent fluidized bed, *AIChE Journal* 54(5), 1213-1223

CHAPTER 6

Hydrodynamics in a High Flux CFB Downer

6.1 Introduction

Circulating fluidized bed (CFB) reactors have found extensive applications in the field of chemical, petrochemical, environmental and energy industries (Grace and Bi, 1997 and Zhu and Cheng, 2005). Compared to the conventional bubbling and turbulent bed reactors, CFB risers have such advantages as high gas-solids contact efficiency, high turndown ratios, high gas and solids throughput, etc (Wang *et al.*, 1992; Zhu *et al.*, 1995 and Zhang *et al.*, 2001). However, the riser still suffers from non-uniform flow structure such as core-annulus flow structure, severe solids backmixing as well as radial segregation of gas and solids (Zhu *et al.*, 1995 and Zhang *et al.*, 2001). These disadvantages of the risers may be resulted from the flow of gas and solids against gravity. Thus, a concurrent downflow CFB reactor (downer) has been devised recently. In the downer reactor, both gas and solids flow in the direction of the gravity, and thus the radial gas and solids distributions are much more uniform than those in the risers. As a novel reactor, downer has drawn much attention in the past two decades (Wang *et al.*, 1992; Wei and Zhu 1996; Herbert *et al.*, 1999; Johnston *et al.*, 1999; Ma and Zhu, 1999; Schiewe *et al.*, 1999; Zhang *et al.*, 1999, 2000 and 2001; Deng *et al.*, 2004; Luo *et al.*, 2007; Wu *et al.*, 2007; Qi *et al.*, 2008; Abbasi *et al.*, 2013 and Li *et al.*, 2013). In spite of numerous advantages, it suffers a serious shortcoming: very low volumetric solids holdup (mostly less than 1%) which may result in severe problems for reactions where a high solids/gas ratio is required (Wang *et al.*, 1992; Johnston *et al.*, 1999 and Zhang *et al.*, 1999). Although many studies on the hydrodynamics of downers have been carried out, only a few researches focus on the high density/flux CFB downer (Luo *et al.*, 2001; Li *et al.*, 2004 and Chen *et al.*, 2004, 2005, and 2006). Certainly, studies are needed on high density/flux CFB downer to get a detailed and clear understanding of the flow structures in downer reactors. A comprehensive study of hydrodynamics in a high flux CFB downer under a wide range operating conditions is conducted in this study.

6.2 Experimental details

6.2.1 CFB experimental setup

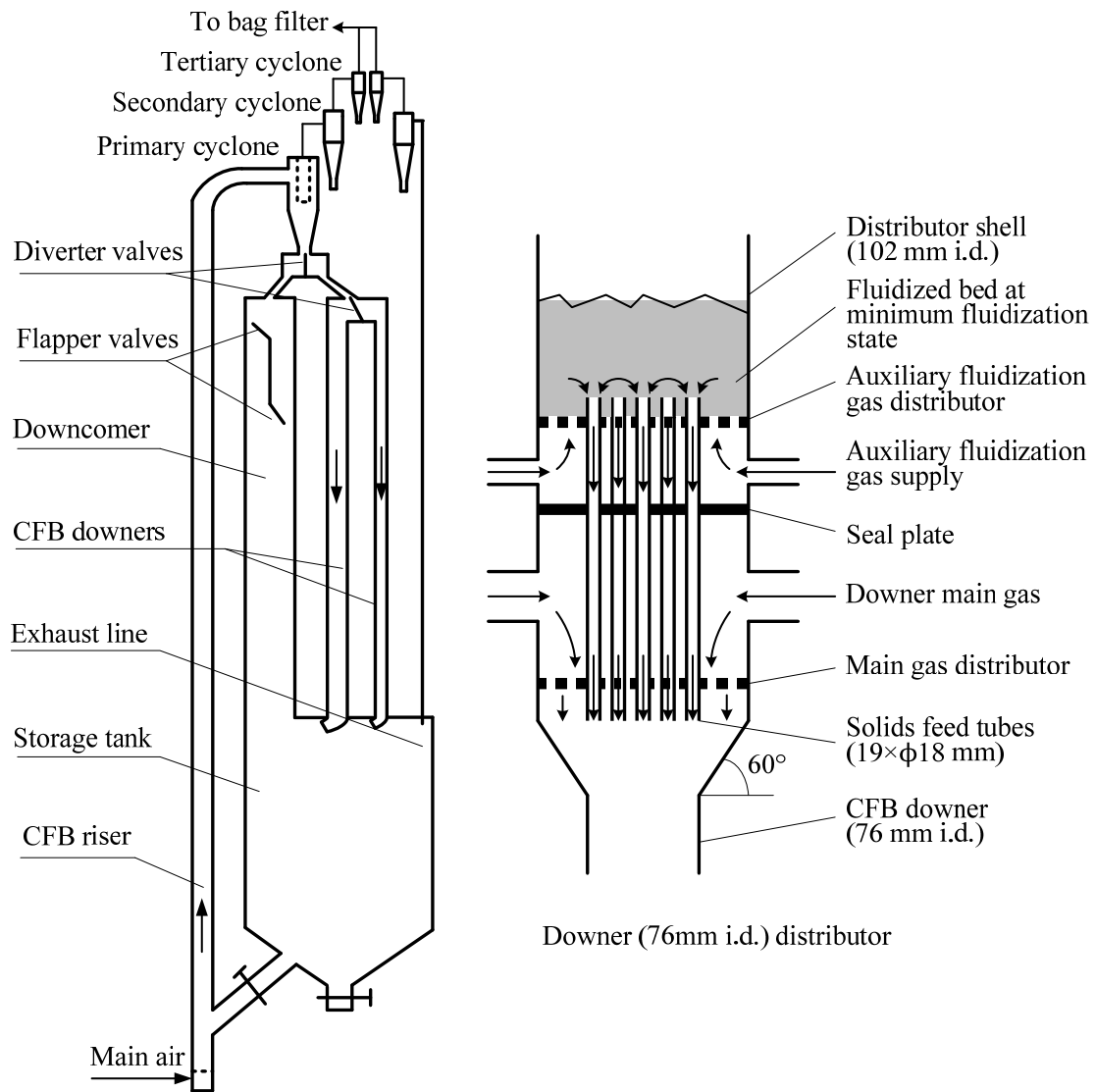


Figure 6.1 Schematic diagram of the multifunctional CFB system.

All experiments were conducted in a multifunctional circulating fluidized bed (MCFB) system, schematically shown in Figure 6.1. The system includes three circulating fluidized bed loops, the left hand fluidized bed loop serves as a high flux/density circulating fluidized bed riser with an inner diameter of 76 mm and the height of 10 m. The right hand fluidized bed loops are two circulating fluidized beds downer (co-current downflow circulating fluidized beds) of different diameters (76 mm i. d. and 5.8 m high and 50 mm i.d. and 4.9 m high, respectively). A downcomer with an inner diameter of 203 mm for solids return during riser operating and at its bottom a solids storage tank with an inner diameter up to 457 mm were used as general solids storage for the entire system. Total solid inventory of FCC particles in the downcomer and storage tank could be up to 450 kg, equivalent to a solids height of approximately 6.0 m. This high solids level ensures high back pressure in the downcomer and enables high solids circulation rates and high solids concentrations in the CFBs. In order to obtain higher flux and steadier operating conditions, other modifications had been carried out in this CFB system (details can be found in the chapter 4). The multifunctional circulating fluidized bed (MCFB) can be operated as a CFB riser and downer. For CFB riser operations, particles in the storage tank fluidized by aeration air entering into the bottom of the riser and obtained momentum from the air passing through the riser gas distributor made of perforated plates (2 mm×176 holes, 12% opening area). The particles are carried upward by the riser air along the column. At the top of the riser, particles and gas are separated by primary, secondary and tertiary cyclones and most of the particles return to the downcomer and further down to the storage tank. Fine particles leaving from the cyclones are trapped by the bag filter and returned periodically to the downcomer.

When the MCFB is under downer operating mode, solid particles are first lifted through the riser, separated by the primary cyclone fixed at the top of the downcomer and then fed into the downers. At the top of either one of the downers is a gas-solids distributor (details shown in Figure 6.1) where the particles are uniformly distributed along with the downer air to flow downward concurrently. After fast separation by gravity at the exit of either downer column, most particles are retained in the storage tank, with the remaining particles captured by two cyclones installed in series at the top of the exhausted pipeline and the common bag filter. To eliminate the effects of solids inventory and other influencing parameters on the hydrodynamic

characteristics, the whole experimental work in this study was carried out with a constant particle mass of 400 kg stored in the downcomer and the storage tank.

The entire fluidized bed system uses aluminum as the main construction material with small portions made of Plexiglas for visual observation. In order to minimize possible electrostatic charges formed in the columns during the experiments, the whole fluidized bed system is electrically grounded. A measuring device for solids circulation rate is installed in the top section of the downcomer. By regulating the ball valve located in the solids feeding line connecting the storage tank and the riser column, the solids circulation rate can be adjusted and maintained at the desired level during each experiment. The fluidization gas used in this study is air at ambient temperature, supplied by a large compressor capable of delivering 1000 SCFM at 100 psi. Equilibrium FCC catalyst particles loaded with ferric oxide (Fe_2O_3) are used in this study and other catalytic ozone decomposition experiments. The Sauter mean diameter and the particle density is $76 \mu\text{m}$ and 1780 kg/m^3 respectively. The particle size distribution is given in Table 6.1.

Table 6.1 Size distribution of the FCC particles

Particle Size (μm)	Volume Fraction (%)
0-20	0.61
20-40	9.72
40-60	26.32
60-80	22.80
80-130	33.24
>130	7.31

6.2.2 Measurements of solids holdup and particle velocity

Experimental measurements include differential pressure, local solids concentration (solids holdup) and particle velocity. Twenty pressure taps are installed along the CFB downer column and connected with 19 differential pressure transducers (Omega PX162) to measure the axial profiles of the pressure gradient. The pressure gradient is mainly used to double check the solids holdup measured by an optical fiber probe. Local solids holdup and particle velocity are measured simultaneously using a novel reflective-type optical fiber probe, which has been shown to be effective and accurate for measuring the local solids concentration and particle velocity in high velocity fluidized beds and thus has been widely used by many investigators (Herbert *et al.*, 1994; Johnson *et al.*, 2001; Liu *et al.*, 2003 and Ellis *et al.*, 2004). It yields high signal-to-noise ratios and is nearly free of interference by temperature, humidity, electrostatics and electromagnetic field. Moreover, its small size does not significantly disturb the overall flow structure in CFB systems with proper design. The optical fiber probe used in this work is model PV6D, developed by the Institute of Processing Engineering, Chinese Academy of Sciences, Beijing, China. The probe and measurement procedure are schematically shown in Figure 6.2. The outer diameter of the probes is 3.8 mm and there are with two subprobes. Each of the subprobes consists of 8000 fine quartz fibers. The effective distance of the two vertically aligned subprobes is 1.51 mm, and the active tip area of each subprobe is 1×1 mm. Each subprobe consists of many quartz fibers with a diameter of 15 μm, for light-emitting and receiving, arranged in alternating arrays. In order to prevent particles from occupying the blind zone, a glass cover of 0.2 mm thickness is placed over the probe tip. The underlying theory was elaborated by Liu *et al.* (2003).

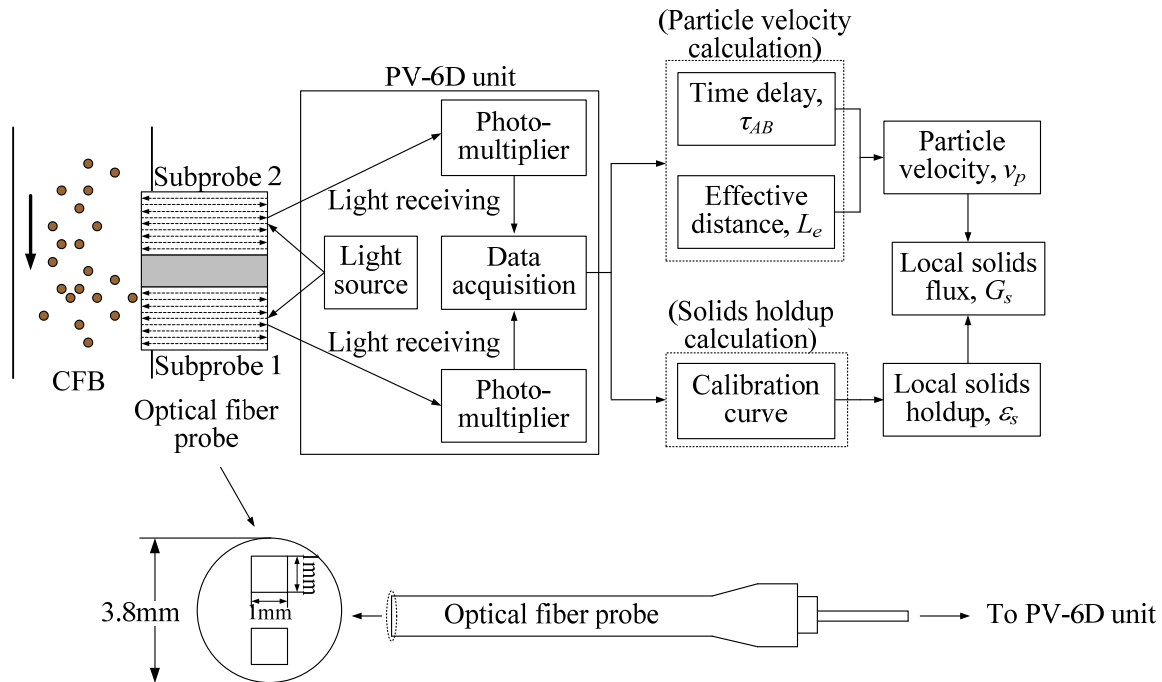


Figure 6.2 Schematic diagram of the novel optical fiber probe and its working principle.

As shown in Figure 6.2, light from the source illuminates a measuring volume of particles through the light-emitting fibers. The received light reflected by the particles is captured by light receiving fibers and processed by a photo-multiplier. The light intensity is then converted into voltage signals and the voltage signals are further amplified and fed into a PC. The voltage signal obtained by the probe is converted to volumetric concentration using a calibration equation. The relationship between the output signals of the optical fiber probe and the local solids holdup (non-linear) is first established through proper a calibration based on the method developed by Zhang *et al.* (1998).

From the voltage time series $V(t)$ and the calibration equation, local instantaneous solids holdup, $\epsilon_s(t)$, can be calculated:

$$\epsilon_s(t) = f[V(t)] \quad (6.1)$$

where, f is the calibration function. The time-mean solids concentration ε_s can be given by integrating $\varepsilon_s(t)$ over the time period, T :

$$\varepsilon_s = \frac{1}{T} \int_0^T \varepsilon_s(t) dt \quad (6.2)$$

The cross-sectional average solids holdup $\bar{\varepsilon}_s$, can be calculated as follow:

$$\bar{\varepsilon}_s = \frac{1}{\pi R^2} \int_0^R 2\pi r \varepsilon_s dr = \frac{2}{R^2} \int_0^R \varepsilon_s r dr \quad (6.3)$$

On the other hand, the particle velocity can also be measured simultaneously with solids holdups. When particles pass through the tips of the two subprobes, they would produce two similar signals with a time delay τ , which can be calculated by cross-correlation method. Combining the time delay τ with the effective distance between two subprobes, L_e , the instantaneous particle velocity, V_p can be calculated as follow:

$$v_p = \frac{L_e}{\tau} \quad (6.4)$$

To obtain the particle velocities, an integration time of 12.80 ms is set after the optimization optimization (Liu *et al.*, 2003). Because of the turbulent nature of gas-solids suspension in fluidized beds, a particle passing through the upstream subprobe may not be detected by the downstream subprobes, due to possible particle-particle and/or particle-probe interactions. This may lead to low or even indeterminate cross-correlation coefficients. Such poorly or uncorrelated data need to be eliminated. The correlation coefficients are set to be higher than 0.6 as the criteria to collect the acceptable results. The direction of the particle motion is determined based on the maximum cross-correlation coefficient from the positive and negative correlation of the two channel signals (Nieuwland *et al.*, 1996; Werther, 1999 and Zhu *et al.*, 2001).

The cross-sectional average particle velocity weighed by the local solids concentrations can be calculated as follow:

$$\bar{v}_p = \frac{2}{R^2 \bar{\varepsilon}_s} \int_0^R v_p \varepsilon_s r dr \quad (6.5)$$

By combining the results of local solids holdup and particle velocity obtained as mentioned above, the time-mean local solids fluxes can be expressed as:

$$\bar{G}_{s,L} = \rho_p \int_0^T v_p(t) \varepsilon_s(t) dt \quad (6.6)$$

where $\bar{G}_{s,L}$ is the time-mean local solids flow rate, $V_p(t)$ is the instantaneous particle velocity and $\varepsilon_s(t)$ is the instantaneous solids holdup measured by the probe. Similarly, cross-sectional average solids fluxes can be defined as:

$$\bar{G}_s = \rho_p \int_0^R 2\pi r \bar{G}_{s,L} dr \quad (6.7)$$

By comparing the G_s measured by the flapper valves installed in the measurement tank and the \bar{G}_s calculated by Eq. (6.7), this measurement accuracy has been verified by Zhu and Zhu (2008).

In order to map the entire cross-section of the downer, nine axial measuring ports ($z = 0.22, 0.61, 1.12, 1.63, 2.13, 2.64, 3.26, 4.02, \text{ and } 4.99$ m below the gas distributor) are installed along the column. Measurements are conducted at six radial positions ($r/R = 0, 0.316, 0.548, 0.707, 0.837$ and 0.950 , where r is the distance from the center and R is the downer radius) on each axial level of the CFB downer system. These positions are determined by dividing the column cross-section into five equal areas and determining the mid-point of each of these areas. For the hydrodynamic experiments in the current study, voltage signals from the optical fiber probe are sampled at a high frequency of 100 kHz with 1,638,40 data points for each measurement under a wide range of operating conditions so that detailed dynamic nature of the flow structure can be fully collected. To get the valid and repeatable data, all measurements are repeated at least 5 times.

6.3 Results and discussion

6.3.1 Radial profiles of solids flow

Figure 6.3 shows the radial profiles of solids holdup at nine axial elevations under various operating conditions. The solids circulation rate are 100, 200, 300 kg/m²s and the superficial gas velocity 1, 3, 5, 7 m/s.

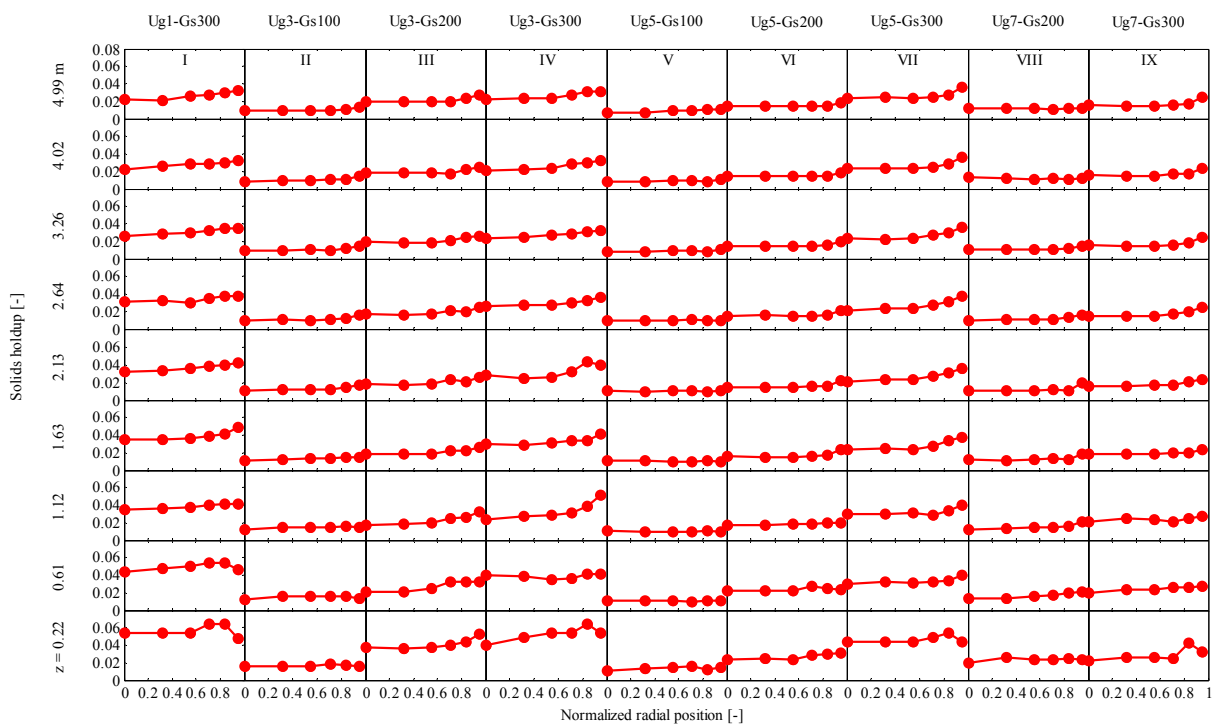


Figure 6.3 Radial profiles of solids holdup along the downer under different operating conditions.

In general, solids holdup is higher near the solids entrance region than that further down the column and is lower in the center compared to the wall region. Near the distributor (0.61 m below the distributor), the solids holdup is gradually increase towards the wall with a maximum value at the radial position $r/R \approx 0.8$ and then decreases at the wall. Above this region, the shape of the radial solids holdup profile does not change significantly. A more uniform distribution of

the solids holdup covers a wide region of the cross sectional area from the centerline to $r/R \approx 0.6-0.8$ and thereafter solids holdup reaches the highest value right at the wall. In the fully developed region (2.64 m below the distributor), the profiles of solids holdup are normally characterised by a fairly uniform radial distribution. A similar trend was also reported by other researchers (Zhang *et al.*, 1999; Johnston, 1999; Chen and Li, 2004 and Li *et al.*, 2013).

The uniform distribution of solids holdup in the downer reactor is one of the key advantages over the upflow riser reactor. This is mainly because particles are not supported by the gas flow, but flow down due to the gravity, either reinforced or resisted by the drag force between gas and solids in the downer reactor. In addition, the aggregation of particles at the wall region can also be prevented in the downer. When particle clusters are formed, the effective drag force on the cluster is reduced so that the slip velocity becomes higher leading to a high particle downwards velocity (Yang *et al.*, 1993 and Zhang *et al.*, 1999). The increased particle velocity in turn increases the instability of the clusters because of the increased shear force on the particles. Large particle cluster is easily broken down into smaller ones or even isolated particles.

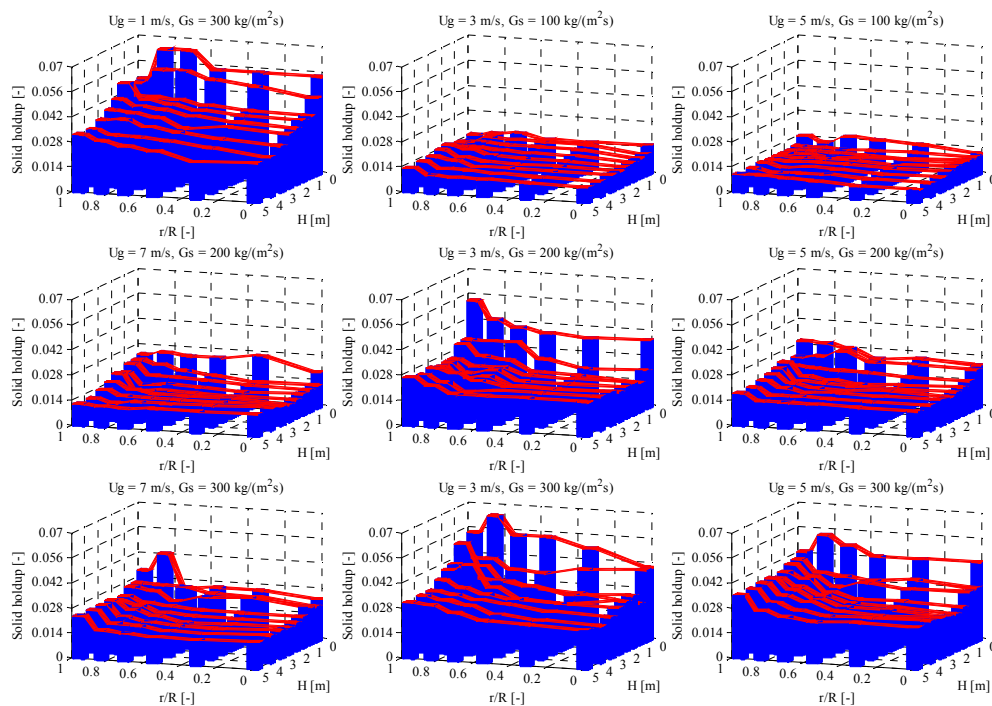


Figure 6.4 Overview of solids holdup along the downer under different operating conditions.

An overview of radial solids holdup profiles under different operating conditions are illustrated in Figure 6.4 where x and y axes are the radial and axial positions in the column, and z -axis is the solids holdup. The solids flow structure is clear to see that there is a “distributor controlled” region at the top of the downer where solids holdup is relatively high and fluctuation occurs. Further down the column, the flow structure becomes more uniform. It is also obvious that the distributions of solids holdup are significantly affected by the operating conditions. In general, higher solids flux and/or lower superficial gas velocity leads to higher solids holdup.

At a fixed superficial gas velocity, increase solids circulation rate increases the solids holdup at all the radial position along all the axial levels. An increase of solids holdup in the development region (especially in the entrance of the column) is more significant than that in the developed zone. Maximum values of the solids holdup in the entrance of the downer often occur in the radial position of $r/R \approx 0.8-0.85$. Compared with the low solids flux condition ($G_s = 100 \text{ kg/m}^2\text{s}$), the solids holdup can be greatly increased both in the central region and near the wall when solids flux is up to $300 \text{ kg/m}^2\text{s}$. Therefore, it is possible to obtain a high density downer by improving the solids circulation rate.

At a constant solids circulation rate, the increase in superficial gas velocity decreases the solids holdup in all radial and axial positions. In addition, with increase of U_g , the distribution of the radial solids holdup becomes more uniform. This is reasonable because the higher gas velocity leads to the higher acceleration rate and particle velocity move faster under the high gas velocity conditions. Moreover, the superficial gas velocity has different affects on the distribution of solids holdups under different circulation rate. Under low solids flux, superficial gas velocity has less influence on the profiles of the solids holdup where solids holdup in all position has a fairly uniform distribution. On the other hand, when solids flux is higher up to $300 \text{ kg/m}^2\text{s}$, the shapes of the radial profiles of solids holdup are significantly changed. The non-uniform radial distribution covers the entire column when U_g is 1 m/s while the profiles are more uniform when U_g is up to 7 m/s .

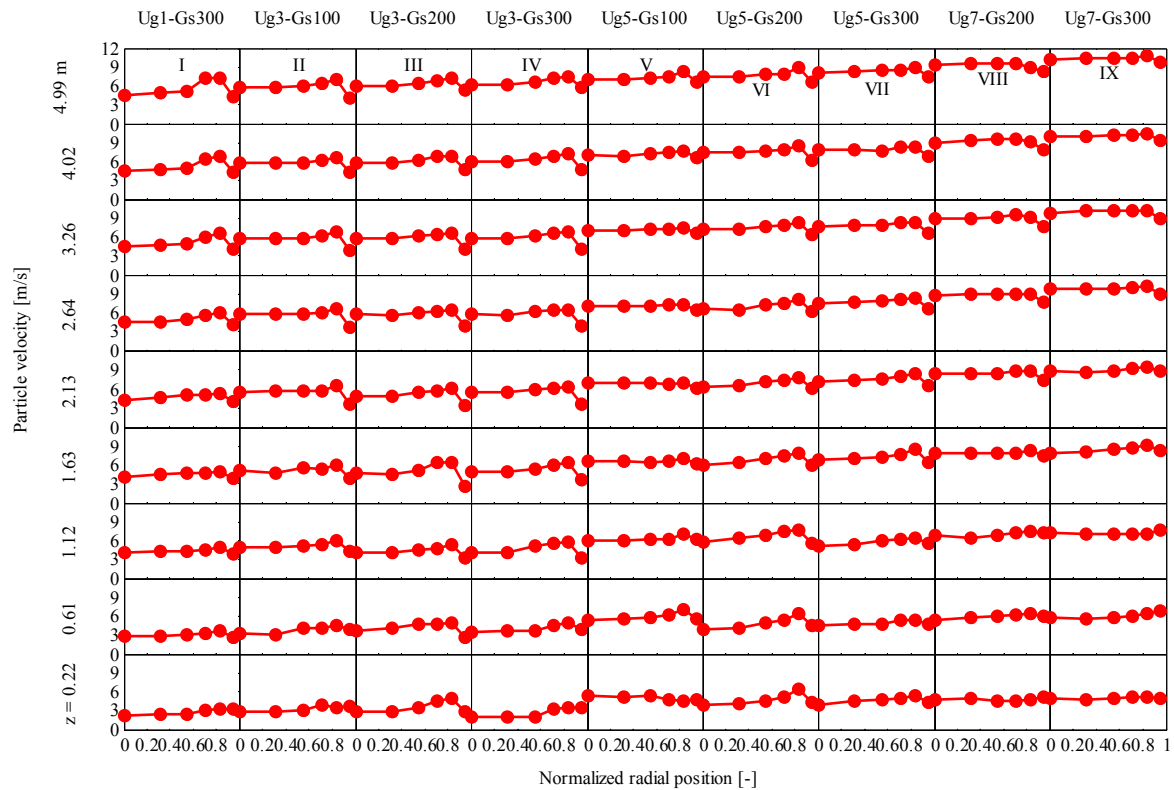


Figure 6.5 Radial profiles of particle velocity along the downer under different operating conditions.

All the radial profiles of particle velocity taken under the same operating conditions with the solids holdup discussed in the above section are shown in Figure 6.5. Generally, particle velocity is relatively low in the central region and increases slightly toward the wall followed by a decrease right at the wall under all operating conditions. With increasing distance from the entrance, radial profiles of the particle velocity further develop and remain almost unchanged. Relatively low particle velocity covers a wide cross-sectional area corresponding to $0 < r/R < 0.6-0.8$. The maximum particle velocity usually appears in the region of $r/R \approx 0.8$. The same results had also been reported by others (Bai *et al.*, 1990; Zhu *et al.*, 1995; Cheng *et al.*, 2008 and Li *et al.*, 2013). This radial profile of particle velocity is quite different from that in the riser. In the riser, the radial profiles of the particle velocity are characterized by the parabolic-shaped distribution with the highest particle velocity at the center and the lowest value near the wall. At

the wall region in the riser reactors, the formulation of clusters results in the slow motion of the collected particles, and even causes the backflow along the wall.

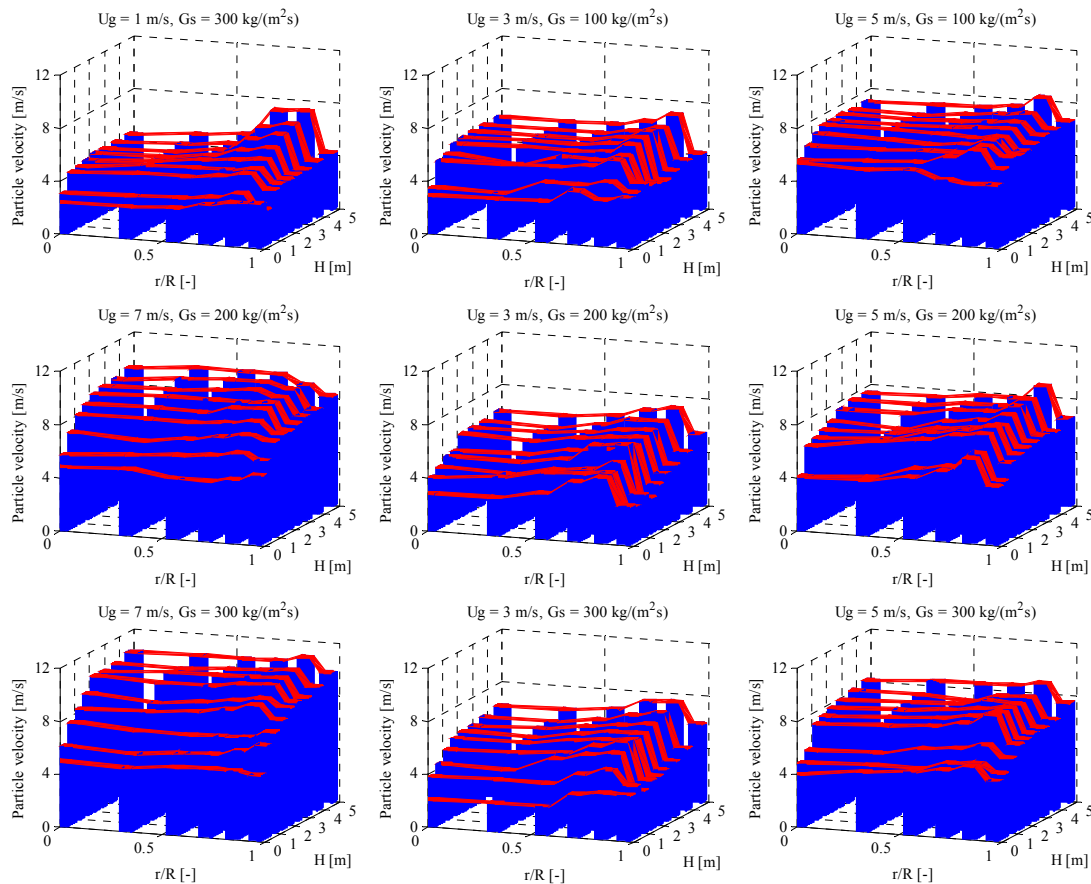


Figure 6.6 Overview of particle velocity along the downer under different operating conditions.

Figure 6.6 provides an overview of the particle velocity profiles along the downer under different operating conditions where x and y axes are the radial and axial positions in the column, and z -axis is the particle velocity. Obviously, particle velocities are significantly affected by the operating conditions. Particle velocity increases with the increase of superficial gas velocity at a fixed solids circulation rate. The distribution of particle velocity across the column becomes more uniform when U_g is higher showing the same trend as solids holdup. On the other hand, solids circulation rate has only a minor effect on the radial profile of the particle velocity especially under high superficial gas velocity.

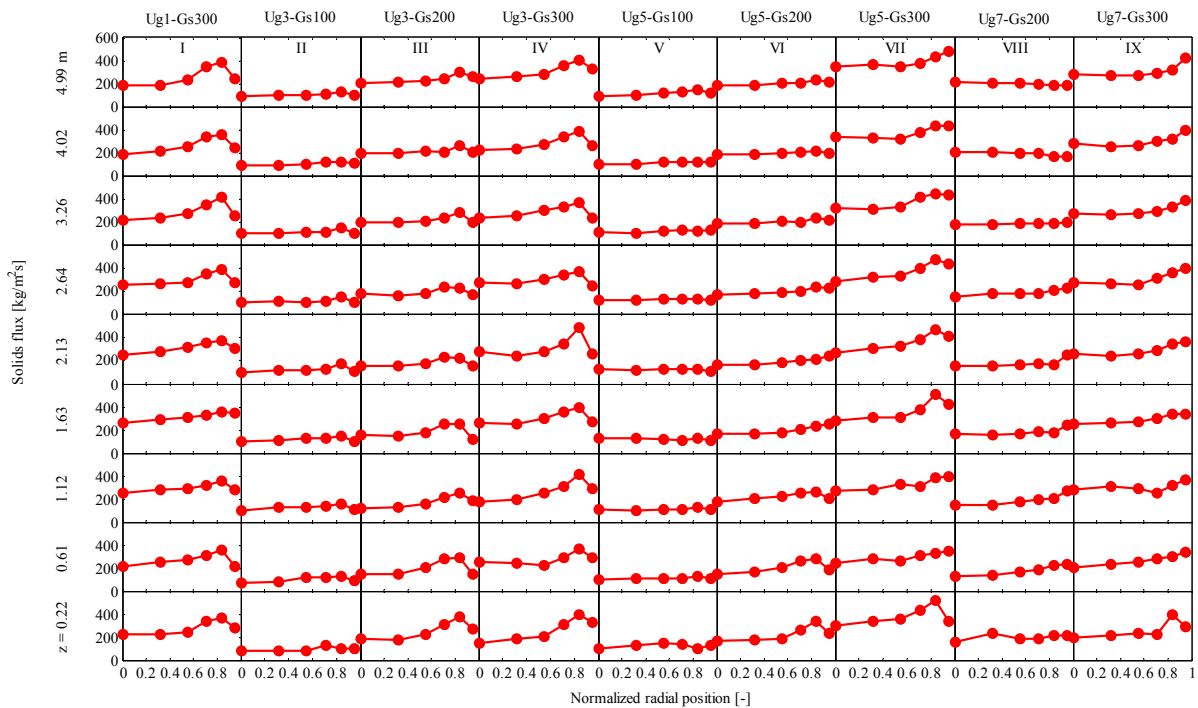


Figure 6.7 Radial profiles of solids flux along the downer under different operating conditions.

Local solids flux is calculated based on Equation (6.7) shown in Figure 6.7. Solids flux distribution is affected dramatically by the operating conditions. Under low solids flux ($G_s = 100 \text{ kg/m}^2\text{s}$), the shape of the radial solids flux profiles change hardly along the column except in the distributor region. The shape of solids flux under such low solids circulation rate is flat in a wide range of radial positions, and reaches to a maximum value at the wall even at the relatively low superficial gas velocity of 3 m/s.

Under high G_s (higher than $200 \text{ kg/m}^2\text{s}$), on the other hand, the distribution of the solids flux becomes less uniform. Both the operating conditions and axial positions affect the shapes of the local solids flux. For example, taking $G_s = 300 \text{ kg/m}^2\text{s}$, when U_g is relatively low ($U_g = 1$ and 3 m/s), local solids fluxes are comparatively low in the central region with a slight increase out towards the wall, and a maximum value appears in the region of $r/R \approx 0.8$. With increase of the superficial gas velocity under such high G_s , the solids flux profiles begin to change as the

measuring position is moved downwards along the column. The peak of the solids flux disappears at $r/R \approx 0.8$ and the maximum value is right at the wall further downer the column. The phenomena indicate that the gas-solids flow is being developed. The development of the solids flow in terms of the solids flux distribution is faster for low G_s and high U_g .

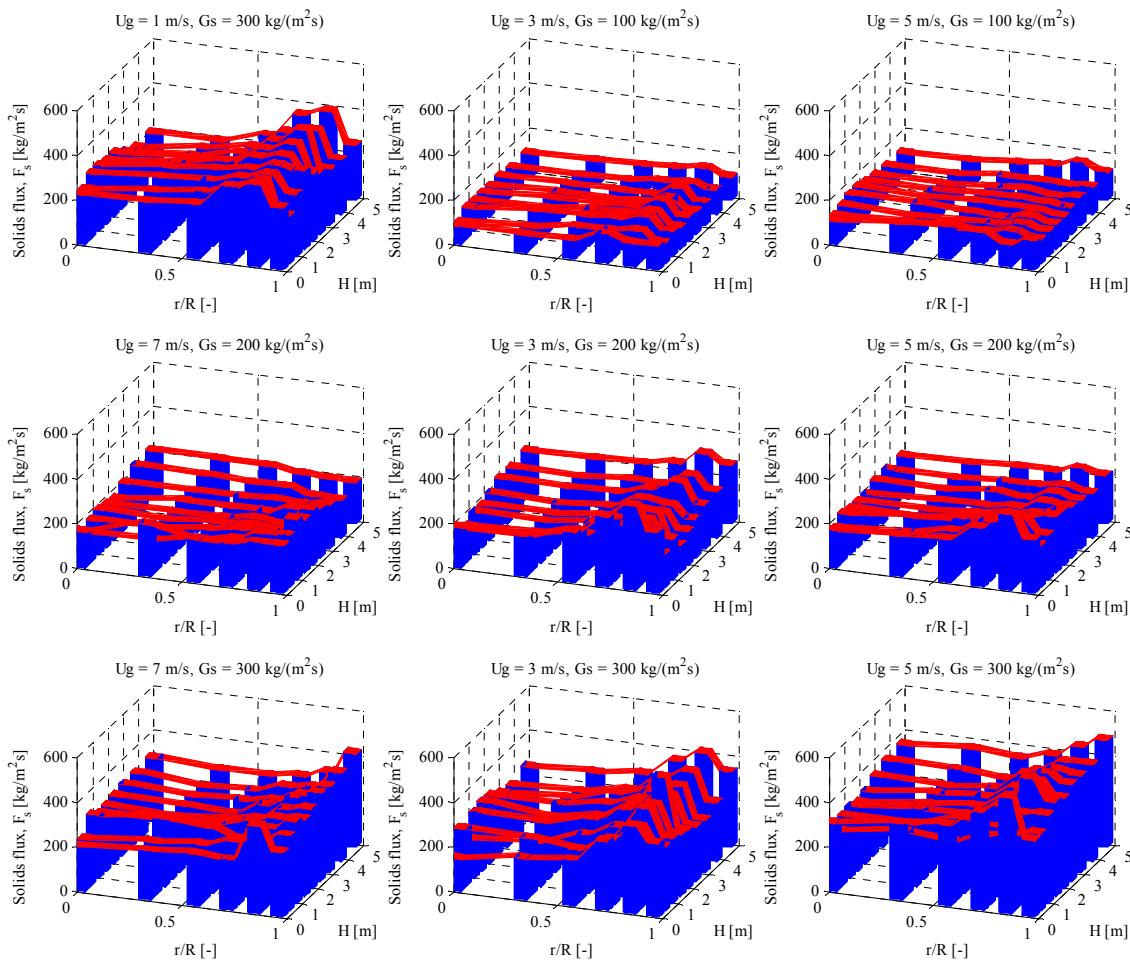


Figure 6.8 Overview of solids flux along the downer under different operating conditions.

Figure 6.8 provides an overview of the local solids flux profiles along the downer under different operating conditions where x and y axes are the radial and axial positions in the column, and z -axis is the local solids flux. As mentioned above, the local solids flux is relatively constant in the center, and thereafter changes begin to occur near the wall region depending on both operating conditions and axial locations. This trend of radial solids flux is quite different from that reported

in the riser. In the riser reactor, the shape of the radial solids flux is considered as a parabolic curve where the solids flux is highest at the center of the column and then decreases towards the wall. The general shape of the profiles does not change greatly with axial elevations in the riser.

6.3.2 Development of solids flow

As mentioned earlier, the flow structure in the downer is affected significantly by the operating conditions. The flow structure becomes more uniform when G_s is low and/or U_g is high. In order to further analyze the influence of the operating conditions on the development of the flow structure, based on Figures 6.3, axial development of radial profiles of solids holdup are plotted in Figure 6.9.

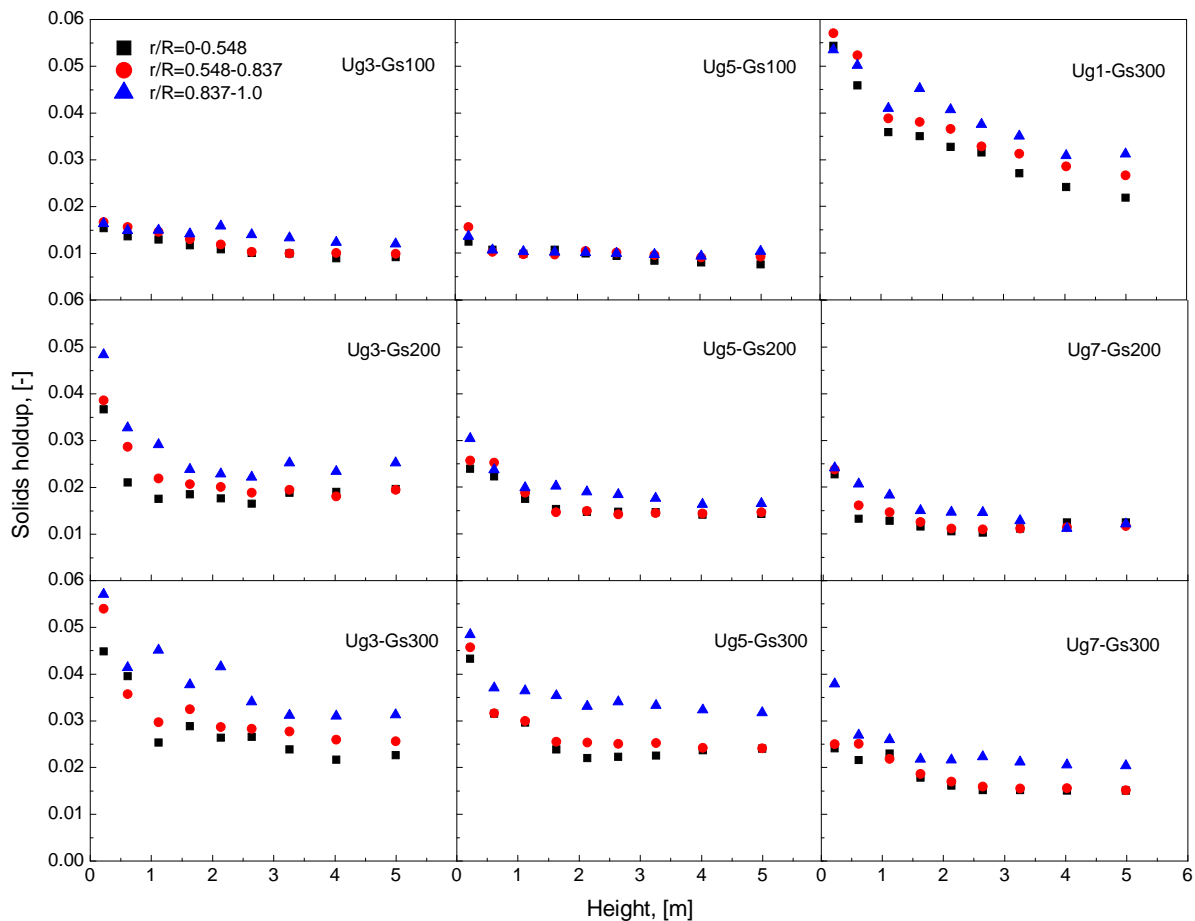


Figure 6.9 Axial development of radial solids holdup along the downer under different operating conditions.

Figure 6.9 shows the axial profiles of the solids holdup in the three radial regions (the central region, $r/R = 0.0-0.548$, the middle region, $r/R = 0.548-0.837$, and the wall region, $r/R = 0.837-1.0$) along the downer under a variety of operating conditions. This figure reveals the difference in the flow development in the three radial regions. The flow developments of different radial regions are not simultaneous and the effects of the operating conditions on the flow development in the three regions are also different.

At a constant $U_g = 3$ m/s, under low solids flux of 100 kg/m²s, the difference of the flow development in the three radial region is not obvious. The length of the development for the central and the wall regions is about 2.5 m and 3 m, respectively. The length of the development extends with increase of G_s . For example, when G_s is enlarged from 100 to 300 kg/m²s, the length of the development for the central and the wall regions extends to around 3 m and 4 m, respectively. It can be concluded that increasing G_s slows down the development of solids holdup profiles in both the core and the wall regions. The reason may due to the contribution of the gas momentum to the total solids flow in the downer. Increasing G_s , the gas momentum contribution on particles becomes smaller leading to a long particle acceleration length.

On the other hand, for a fixed G_s of 300 kg/m²s, under very low superficial gas velocity (e.g. 1 m/s), the length of the development for the central and the wall regions can extend beyond the downer column itself. With increase of the superficial gas velocity, the development length would reduce. Similar results can also be obtained under other operating conditions. Based on the discussed above, it is concluded that increasing G_s and/or decrease U_g can slow down the development of the solids holdup in downer reactors.

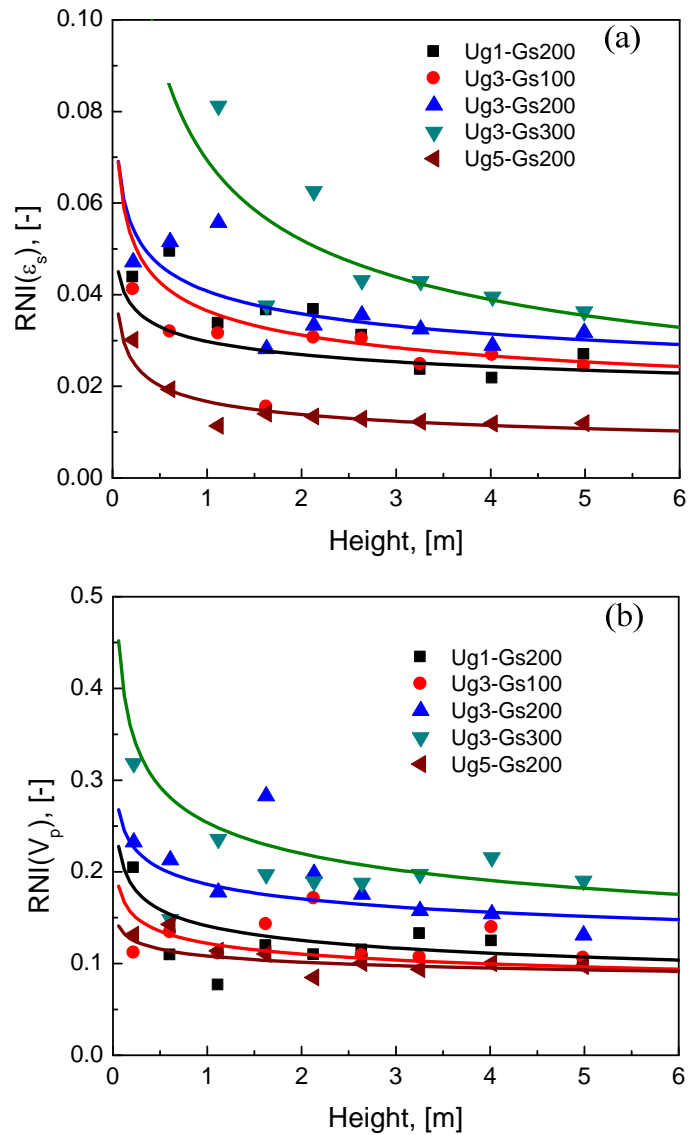


Figure 6.10 Axial development of $RNI(\epsilon_s)$ along the downer under different operating conditions.

To quantify the flow development analysis, the following radial nonuniformity indices (RNIs) proposed by Zhu and Manyele (2001) are employed. The radial nonuniformity indices of solids holdup ($RNI(\epsilon_s)$) and particle velocity ($RNI(V_p)$), are defined as follow.

For RNI (ε_s),

$$RNI(\varepsilon_s) = \frac{\sigma(\varepsilon_s)}{\sigma(\varepsilon_s)_{\max}} = \frac{\sigma(\varepsilon_s)}{\sqrt{\bar{\varepsilon}_s(\varepsilon_{s,mf} - \bar{\varepsilon}_s)}} \quad (6.8)$$

where $\sigma(\varepsilon_s)$ is the standard deviation of the radial solids holdup, $\sigma(\varepsilon_s)_{\max}$ is the normalizing parameter, $\bar{\varepsilon}_s$ is the cross-sectional average solids holdup, and $\varepsilon_{s,mf}$ is the solids holdup at minimum fluidization. RNI (ε_s) is actually the normalized standard deviation for a particular cross-sectionally averaged solids holdup given that the solids holdup can only have values of either 0 or $\varepsilon_{s,mf}$. Therefore, RNI (ε_s) must vary between 0 and 1, with larger values indicating less uniform flow structure.

For RNI (V_p),

$$RNI(V_p) = \frac{\sigma(V_p)}{\sigma(V_p)_{\max}} = \frac{\sigma(V_p)}{\sqrt{(\bar{V}_p - V_{p,\min})(V_{p,\max} - \bar{V}_p)}} \quad (6.9)$$

where $\sigma(V_p)$ is the standard deviation of the particle velocity at different radial positions, $\sigma(V_p)_{\max}$ is the normalizing parameter, \bar{V}_p is the cross-sectional average particle velocity, $V_{p,\min}$ is the minimum particle velocity ($V_{p,\min} = G_s/(\rho_p \varepsilon_{s,mf})$), and $V_{p,\max}$ is the maximum possible particle velocity (taken $2U_g$ by Zhu and Manyele, 2001). Again, RNI (V_p) varies between 0 and 1.

Figure 6.10(a) provides a comparison of RNI (ε_s) as a function of the axial distance from the downer top. Generally, the maximum values of RNI (ε_s) occurs in the entrance region and thereafter gradually decrease down the column to constant values indicating that the solids flow becomes more uniform along the axial elevations. The result corresponds to the higher solids holdup in the wall region in the entry of the downer and gradual transition to the uniform distribution of solids holdup in the fully developed region. This Figure also shows the influence of the operating conditions on RNI (ε_s). At constant U_g , higher values of G_s result in higher RNI (ε_s) intensifying the nonuniformity of the solids flow. As U_g increases, the RNI (ε_s) decreases for all G_s . Thus, a highly uniform flow structure occurs at a high U_g and low G_s . Figure 6.10(b) provides the RNI (V_p) values as a function of height under different operating conditions. In

general, the values of RNI (ε_s) decrease exponentially along the column with constant values near the exit of the downer illustrating that a transition from a nonuniform flow structure in the entrance to a relatively uniform solids flow close to the downer exit. It is also clear from Figure 6.10 that the two RNIs can be used to characterize the flow development. The effects of the operating conditions on the flow development are comparable to the results discussed in the above sections.

6.3.3 Axial profiles of solids flow

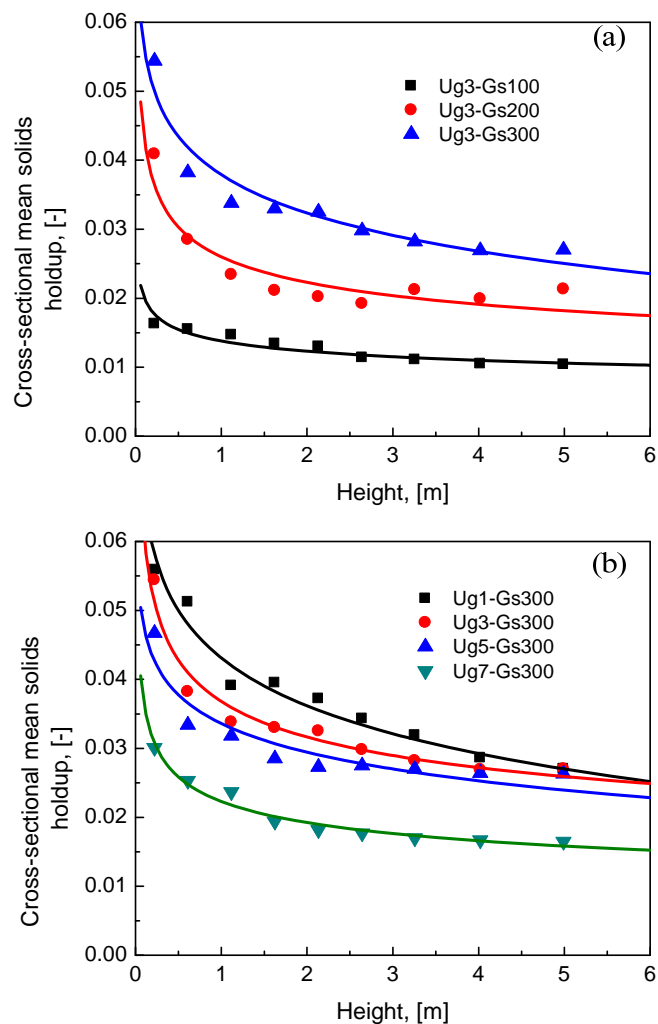


Figure 6.11 Axial profiles of cross-sectional mean solids holdup along the downer under different operating conditions.

Figure 6.11 shows the axial distribution of the cross-sectional average solids holdup along the downer. The cross-sectional average solids holdup profiles decrease dramatically at the top of the downer column (1-2 m below the distributor), then decrease gradually and finally approaches a constant value further down the column. Similar trend had been reported by Zhang et al. (1999). As discussed in their paper, the cross-sectional average particle velocity increases rapidly in the 1-2 m below the downer distributor due to the high drag force resulting from the large initial difference between the gas velocity and the particle velocity. Then the acceleration slows down and finally the particle velocity approaches a constant further down the downer. For most of the operating conditions in this study, the axial profiles of the cross-sectional average solids holdup have the same trends described above, except for the conditions where a very high solids circulation rate ($G_s = 300 \text{ kg/m}^2\text{s}$) combined with relatively low superficial gas velocity ($U_g = 1$ and 3 m/s).

As shown in Figure 6.11, the profiles of the cross-sectional average solids holdup are greatly affected by the operating conditions. Increase G_s at constant U_g significantly increases the solids holdup along the entire downer. Further increase in G_s from $200 \text{ kg/m}^2\text{s}$ to $300 \text{ kg/m}^2\text{s}$ would lead to an extension of the acceleration zone covering the whole axial elevations. From Figure 11(a), it is clear that as G_s increases to $300 \text{ kg/m}^2\text{s}$ at superficial gas velocity of 3 m/s , the cross-sectional average solids holdup decreases monotonically over the entire length of the column. The probable reason is that the cluster forming at high G_s reduces the effective gas drag on particles and thus slows down the particle acceleration (Zhang *et al.*, 1999). In addition, the enhanced clustering probably results in a higher constant particle velocity in the fully developed zone which needs a longer acceleration section for particles to reach.

For a constant solids circulation rate of $300 \text{ kg/m}^2\text{s}$ shown in Figure 6.11(b), an increase in U_g decreases the solids holdup along all axial elevations. Compared to the effect of G_s , the influence of U_g on the cross-sectional average solids holdup is less significant. This is probably because the particle velocity is not proportional to the superficial gas velocity but is the combination of the gas velocity and the effective gas-solids slip velocity. A doubled U_g does not double the particle velocity and thus does not reduce the cross-sectional average solids holdup by half, since

the gas-solids slip velocity does not increase with U_g because the clusters broken under high U_g (Zhang *et al.*, 1999).

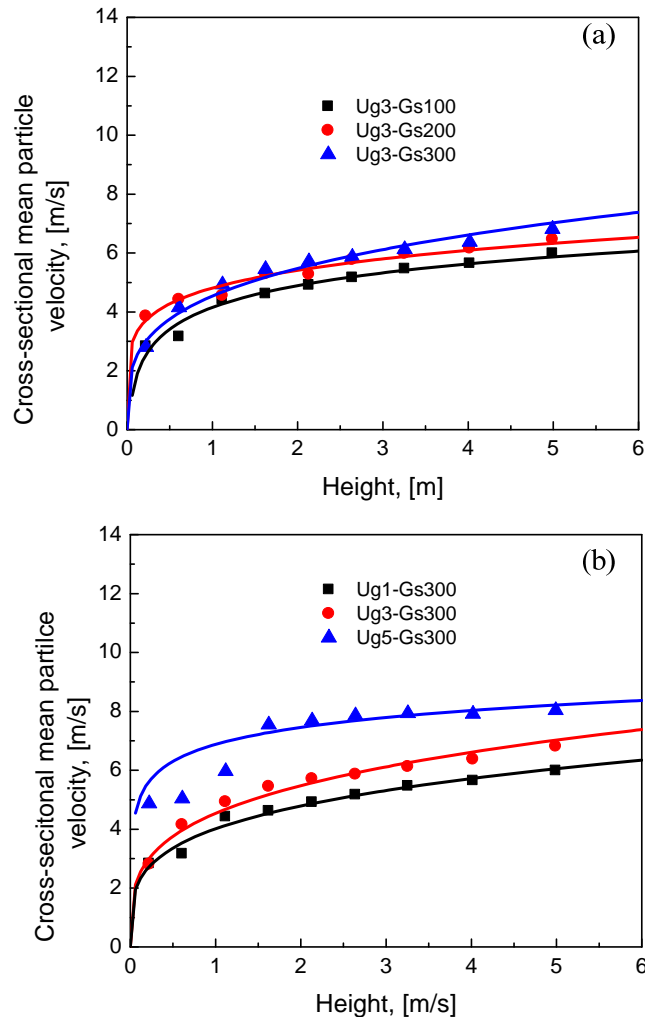


Figure 6.12 Axial profiles of cross-sectional mean particle velocity along the downer under different operating conditions.

Figure 6.12 shows the axial profile of the cross-sectional average particle velocity along the column under different operating conditions. The particle velocity increases rapidly in the entrance region of 1-2 m below the distributor, indicating a high solids acceleration rate in this section due to the large initial difference between the gas velocity and particle velocity as

mentioned before. The acceleration extends gradually further down the column. Effects of operating conditions on the cross-sectional average particle velocity follow the same trend as in cross-sectional average solids holdup. Increasing solids circulation rate and/or decreasing superficial gas velocity slow down the particle velocity in the entire downer column. Comparing with the effect of G_s , the influence of U_g on the cross-sectional average solids holdup is more significant.

It has been reported by many researchers that there are three hydrodynamic flow regions along the axial directions in the downer: the first acceleration section, the second acceleration section and the constant velocity section (Kwauk, 1964; Yang *et al.*, 1991; Zhu *et al.*, 1995; Ma and Zhu, 1999 and Zhang *et al.*, 1999 and 2001). In the first acceleration region near the distributor, gas velocity is high while particle velocity is near zero. Solids are accelerated by both gravity and gas drag force until the particle velocity is equal to the gas velocity. In the second acceleration, particles are farther accelerated by gravity, but resisted by the gas drag (in the upward direction against gravity). Particle velocity then over-takes the gas velocity and increase further until gas drag on the particle counter-balances the gravity. After this region, both particle and gas velocities remain constant downstream where particles travel faster than gas, but with a constant slip velocity between the two. The axial solids holdup and particle velocity variations also follow this three-section axial flow structure as shown in Figures 6.11 and 6.12. Both solids holdup and particle velocity decrease sharply in the first acceleration section (1-2 m at the entrance region of the downer), then the trend becomes much flatter further downer the column. In the constant velocity section, the solids holdup and particle velocity remain almost constant. Again, in very high flux up to 300 kg/m²s conditions, the acceleration sections can extend beyond the downer reactor itself.

6.4 Conclusion

Hydrodynamics of a high flux gas-solids circulating fluidized bed downer were experimentally studied at superficial gas velocities of 1-7 m/s and solids circulation rates from 100 to 300 kg/m²s.

Radial distribution of solids holdup in the downer is much more uniform compared to the riser reactor. Radial solids holdup distribution is characterized by a flat shape covering a wide region of the column cross section and a relatively high value near the wall in the fully developed region. The uniform radial distribution of solids flow provides a nearly plug flow condition in the downer reactor.

The radial solids holdup distribution is affected by the operating conditions. Under low solids circulation rate, the shape of the radial profiles is nearly unchanged along the entire downer. With increasing solids circulation rate, the shape of the radial solids holdup distribution changes along the column. Solids holdup usually reaches the highest value at $r/R \approx 0.8-0.9$ under high solids circulation rates.

Particle velocity in the downer reactor is characterized by a relatively flat core and an annulus where the particle velocity slightly increases towards the wall. Compared to the riser reactor, radial profile of particle velocity in the downer reactor is more uniform.

Radial profiles of the local solids flux in the downer are significantly influenced by operating conditions. The shape of the local solids flux is characterized by a relatively flat core and an annulus where the particles velocity slightly increases towards the wall. Increasing U_g and/or decreasing G_s lead to a more uniform distribution of radial solids flux.

The flow development in the downer reactor is also significantly affected by operating conditions. Increasing G_s or decreasing U_g extends the length of the particles acceleration zone.

Nomenclature

f	calibration function for optical fiber probe
F_s	solids flux [kg/(m ² ·s)]
\bar{G}_s	cross-sectional average solids flux [kg/(m ² ·s)]
$\bar{G}_{s,L}$	time mean local solids flux [kg/(m ² ·s)]
G_s	solids circulation rate [kg/(m ² ·s)]
L_e	effective distance between light-receiving fiber A and B [m]
r/R	reduced radial sampling positions
$RNI(\varepsilon_s)$	radial nonuniformity index of solids holdup
$RNI(V_p)$	radial nonuniformity index of particle velocity
t	time [s]
T	time interval [s]
U_g	superficial gas velocity [m/s]
v_p	particle velocity [m/s]
\bar{v}_p	cross-sectional average particle velocity [m/s]
V	voltage [volt]
$V(t)$	voltage time series [volt]
z	axial coordinate, or distance from gas distributor [m]

Greek letters

ε_s	solids holdup [-]
$\varepsilon_s(t)$	local instantaneous solids holdup [-]
$\bar{\varepsilon}_s$	average solids holdup in the entire column [-]

Subscripts

1, 2	subprobe 1 and 2 of optical fiber probe
g	gas

p particle
 s solids

References

- Abbasi A., Islam MA., Ege PE. and de Lasa H., (2013), CPFD flow pattern simulation in downer reactors, *AIChE Journal* 59(5), 1635-1647
- Chen H., Li H., and Tan S., (2006), Mechanism of achieving a dense downer, modeling and validation, *Industrial and Engineering Chemistry Research* 45, 3488-3495
- Chen H., and Li H., (2004), Characterization of a high density downer reactor, *Powder Technology* 146, 84-92
- Cheng Y., Wu C., Zhu JX., Wei F. and Jin Y., (2008), Downer reactor, from fundamental study to industrial application, *Powder Technology* 183, 364-384
- Deng R., Liu H., Wei F. and Jin Y., (2004), Axial flow structure at the varying superficial gas velocity in a downer reactor, *Chemical Engineering Journal* 99(1), 5-14
- Deng R., Liu H., Gao L., Wang L., Wei F. and Jin Y., (2005), Study on the FCC process in a novel riser-downer-coupling reactor (ii), Simulation and hot experiments, *Industrial and Engineering Chemistry Research* 44(5), 1446-1453
- Ellis N., Bi HT., Lim CJ., and Grace JR., (2004), Influence of probe scale and analysis method on measured hydrodynamic properties of gas-fluidized beds, *Chemical Engineering Science* 59(8-9), 1841-1851
- Grace JR. and Bi H., (1997), Introduction to circulating fluidized beds in *Circulating Fluidized Beds* (editor(s), Grace JR.; Avidan AA. and Knowlton TM.), Engineering Foundation, New York, 1-19
- Herbert PM., (1999), Hydrodynamics study of a downflow circulating fluidized bed. Ph.D. Diss., The University of Western Ontario, London Canada.
- Johnston PM., de Lasa HI. and Zhu JX., (1999), Axial flow structure in the entrance region of a downflow fluidized bed-effects of the distributor design, *Chemical Engineering Science* 54, 161-217
- Johnsson H. and Johnsson F., (2001), Measurements of local solids volume-fraction in fluidized bed boilers, *Powder Technology* 115, 13-26
- Liu W., Luo KB., Zhu JX. and Beeckmans JM., (2001), Characterization of high density gas-solids downward fluidized flow, *Power Technology* 115, 27-35
- Liu JZ., Grace JG. and Bi HT., (2003a), Novel multifunctional optical-fiber probe, development and validation, *AIChE Journal* 49(6), 1405-1420

Liu JZ., Grace JG. and Bi HT., (2003b), Novel multifunctional optical-fiber probe, high-density CFB measurements, *AIChE Journal* 49(6), 1421-1432

Luo BL., Yan D., Ma YL., Barghi S. and Zhu J., (2007), Characteristics of gas-solids mass transfer in a concurrent downflow circulating fluidized bed reactor, *Chemical Engineering Journal* 132, 9-15

Ma Y. and Zhu JX., (1999), Experimental study of heat transfer in co-current downflow fluidized bed (downer), *Chemical Engineering Science* 54, 41-50

Ma Y. and Zhu JX., (2000), Heat transfer between gas-solids suspensions and immersed surface in a upflow fluidized bed (riser), *Chemical Engineering Science* 55, 981-989

Wang Z, Bai DR. and Jin Y., (1997), Hydrodynamics of concurrent downflow circulating fluidized bed (CDCFB), *Powder Technology* 70, 271-275

Wei F. and Zhu JX., (1996), Effect of flow direction on axial solid dispersion in gas-solids cocurrent upflow and downflow systems, *The Chemical Engineering Journal and the Biochemical Engineering Journal* 64(3), 345-352

Yang WC. and Knowlton TM., (1993), L-valve equations, *Powder Technology* 77, 49-54

Zhang H., Johnston PM., Zhu JX., de Lasa HI., and Bergougnou MA., (1998), A novel calibration procedure for a fiber optic solids concentration probe, *Powder Technology* 100, 260-272

Zhang H., Zhu JX. and Bergougnou MA., (1999a), Flow development in a gas-solids downer fluidized bed, *The Canadian Journal of Chemical Engineering* 77(2), 194-198

Zhang H., Zhu JX. and Bergougnou MA., (1999b), Hydrodynamics in downflow fluidized beds (1), solids concentration profiles and pressure gradient distributions, *Chemical Engineering Science* 55, 4367-4377

Zhang H. and Zhu JX., (2000), Hydrodynamics in downflow fluidized beds (2), Particle velocity and solids flux profiles, *Chemical Engineering Science* 55, 4367-4377

Zhang H., Huang WX. and Zhu JX., (2001), Gas-solids flow behavior: CFB riser vs. downer. *AIChE J.* 47(9), 2000-2010

Zhu JX., Yu ZQ., Jin Y., Grace JR. and Issangya A., (1995), Cocurrent downflow circulating fluidized bed (downer) reactors-A state of the art review, *The Canadian Journal of Chemical Engineering* 73(5), 662-677

Zhu JX. and Li GZ., (2001), Direct measurements of particle velocities in gas-solids suspension flow using a novel five-fiber optical probe, *Powder Technology* 115, 184-192

Zhu JX. and Manyele SV., (2001), Radial nonuniformity Index (RNI) in fluidized beds and other multiphase flow systems, *The Canadian Journal of Chemical Engineering* 79, 202-211

Zhu JX. and Cheng Y., (2005), Fluidized-Bed Reactors and Applications, Chapter 5.3 in *Multiphase Flow Handbook*, ed. Clayton Crowe, CRC Press, New York, pp 5.55-5.93

CHAPTER 7

Catalytic Ozone Decomposition in a High Density CFB Riser

7.1 Introduction

Circulating fluidized bed reactors are efficient gas-solid reactors and have been utilized widely in various commercial processes such as gasification of biomass, catalytic cracking of crude oil and coal combustion (Kunii and Levenspiel, 1991; Grace *et al.*, 1997; van der Hoef *et al.*, 2004 and Zhu and Cheng 2005). A number of fundamental researches have been conducted on the hydrodynamics (Li, Kwauk. 1980; Bai *et al.*, 1992; Smolders; Nieuwland *et al.*, 1996 and Baeyens, 2001) and heat transfer (Glicksman 1988; Wu *et al.*, 1989; and Ma and Zhu 1999, 2000 and 2001) in circulating fluidized beds. The major hydrodynamic features of gas-solids CFB risers have been delineated with axial dense/dilute transition solids flow and a core-annulus structure in the radial direction. This kind of nonuniform flow structure and the relatively dilute solids holdup (usually less than 0.10) hampers the CFB systems' application to processes, which require high solids processing capacities and high heat transfer rates (Zhu and Bi, 1995; Grace *et al.*, 1999; Du *et al.*, 2003; and Zhu and Zhu, 2008). The overall efficiency of a riser can be improved when the distribution of the solids particles becomes uniform. Issangya *et al.* (1997, 1999 and 2000) reported that the axial homogenous flow with no downward flow near the wall could be achieved under high superficial gas velocity and high solids circulation rate. Liu *et al.* (1999) thereafter pointed out that gas backmixing became small for the same high density operating conditions. Zhu and Zhu (2008) proposed a novel circulating-turbulent fluidized bed (C-TFB), which operated in a special mode with low superficial gas velocity and high solids circulation rate, resulting in a high-density flow with cross-sectional mean volumetric solids concentration of more than 0.25 through the entire C-TFB. The axial solids distribution profile was nearly uniform ranging from 0.25-0.29, and the uniformity of radial solids distribution had also been improved with local solids holdup around 0.15 at the axis and 0.44 at the wall. There was no net downflow of solids and a good gas solids mixing was observed.

Solids flow structure especially the solids holdup distribution in the CFB riser play a major role on reactor performance both when a catalyst is employed in a chemical reactor, or coal is combusted, and an inert solids is circulated as a heat carrier (Ouyang *et al.*, 1995). Study of chemical reactions can provide direct information on reactor performance compared to other methods. Limited results have been reported on mass transfer dealing with catalytic reaction in circulating fluidized bed systems (Jiang, *et al.*, 1990, 1991; Ouyang *et al.*, 1993, 1995; Fan *et al.*, 2008 and Li *et al.*, 2011 and 2013). Because of its simplicity in reaction kinetics (first order reaction) and negligible heat effect, catalytic ozone decomposition is usually employed as the model reaction in the study of reactor performance. However, the experiments of ozone decomposition reported in the literature were carried out under very low solids circulation rates (less than 200 kg/m²s). The purpose of this paper is to analyze the axial and radial ozone concentration profiles in a high density CFB riser with extremely high solids circulation rates up to 800 kg/m²s. The correlation between solids flow structure and reactor performance is also studied.

7.2 Experimental details

7.2.1 CFB experimental setup

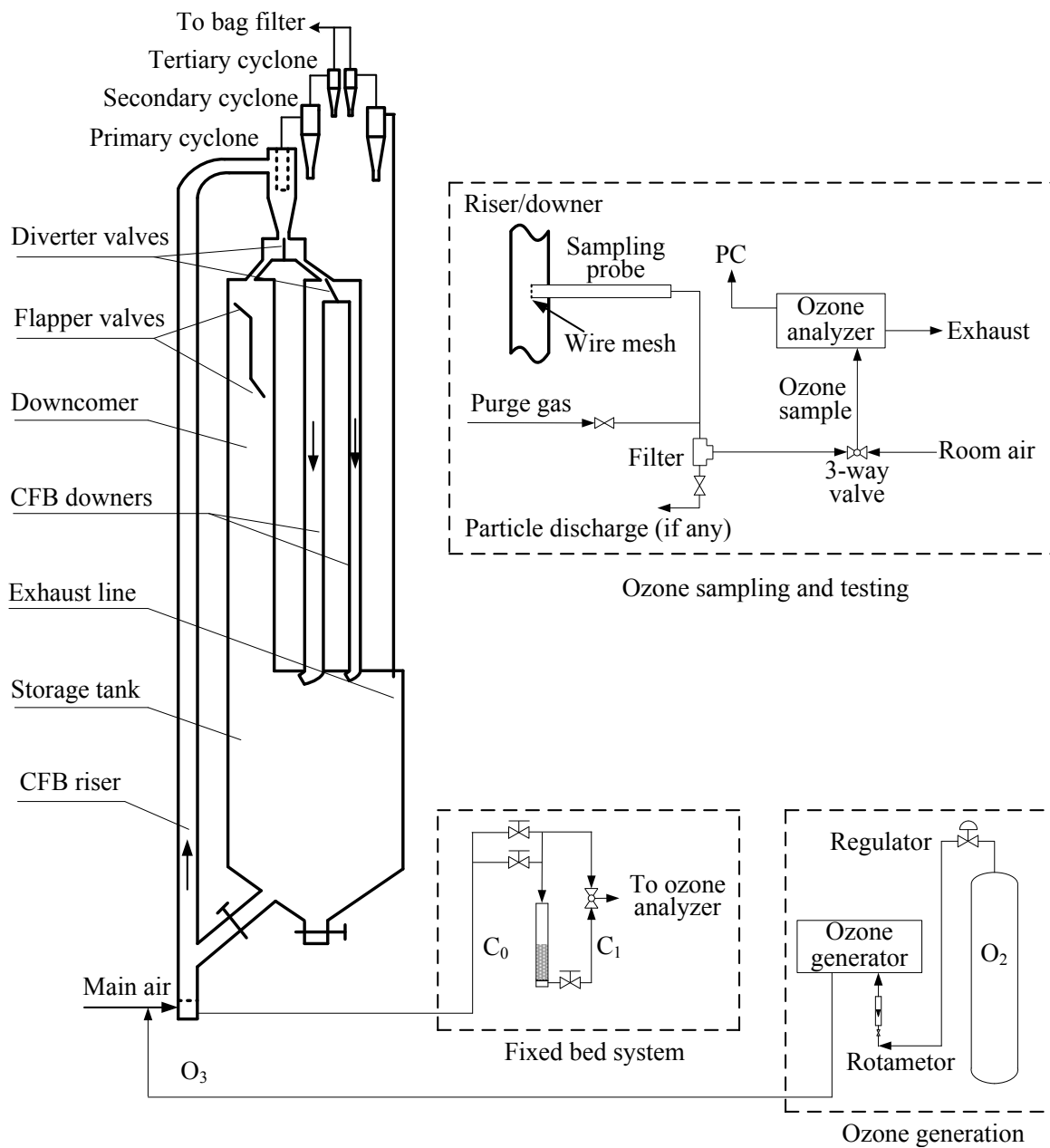


Figure 7.1 Schematic diagram of the multifunctional CFB and ozone testing system.

The circulating fluidized bed reactor facility used in this study is shown schematically in Figure 7.1. The system includes three circulating fluidized beds: the left hand fluidized bed serves as a high flux/density circulating fluidized bed riser (76 mm i. d. and 10 m high), and the right hand fluidized beds are two circulating fluidized beds downer (co-current downflow circulating fluidized beds) of different diameters (76 mm i. d. and 5.8 m high and 50 mm and 4.9 m high, respectively). A large downcomer with an inner diameter of 203 mm returns solids during riser operation. At its bottom a solids storage tank with an inner diameter up to 457 mm were used as general solids storage for the entire system. Total solids inventory of FCC particles in the downcomer and storage tank could be up to 450 kg, equivalent to a solids height of approximately 6.0 m. This high solids level ensures high back pressure in the downcomer and enables high solids circulation rates and high solids concentrations in the CFB riser. To aid the fluidization of the downcomer, aeration points were provided at 2 m and 5 m above the distributor. In order to obtain higher flux and steadier operating conditions, other modifications had been carried out in the CFB system (details can be found in the chapter 4).

The multifunctional circulating fluidized bed (MCFB) can be operated as a CFB riser and downer. For CFB riser operations, particles in the storage tank fluidized by aeration air entering into the bottom of the riser and obtained momentum from the air passing through the riser gas distributor made of perforated plates (2 mm×176 holes, 12% opening area). The particles are carried upward by the riser air along the column. At the top of the riser, particles and gas are separated by primary, secondary and tertiary cyclones and most of the particles returned to the downcomer and further down to the storage tank. Fine particles leaving from the cyclones are trapped by the bag filter and returned periodically to the downcomer. The gas is then discharged into the atmosphere. When the MCFB is under downer operating mode, solid particles are first lifted through the riser, separated by the primary cyclone fixed at the top of the downcomer and then fed into the downers. At the top of either one of the downers is a gas-solids distributor (details shown in Figure 7.1) where the particles are uniformly distributed along with the downer air to flow downward concurrently. After fast separation by gravity at the exit of either downer column, most particles are retained in the storage tank, with the remaining particles captured by two cyclones installed in series at the top of the exhausted pipeline and the common bag filter.

To eliminate the effects of solids inventory and other influencing parameters on the hydrodynamic characteristics, the whole experimental work in this study was carried out with a constant particle mass of 400 kg stored in the downcomer and the storage tank.

The entire fluidized bed system uses aluminum as the main construction material with small portions made of Plexiglas for visual observation. In order to minimize possible electrostatic charges formed in the columns during the experiments, the whole fluidized bed system is electrically grounded. A measuring device for solids circulation rate is installed in the top section of the downcomer. By regulating the ball valve located in the solids feeding line connecting the storage tank and the riser column, the solids circulation rate can be adjusted and maintained at the desired level during each experiment. The fluidization gas used in this study is air at ambient temperature, supplied by a large compressor capable of delivering 1000 SCFM at 100 psi.

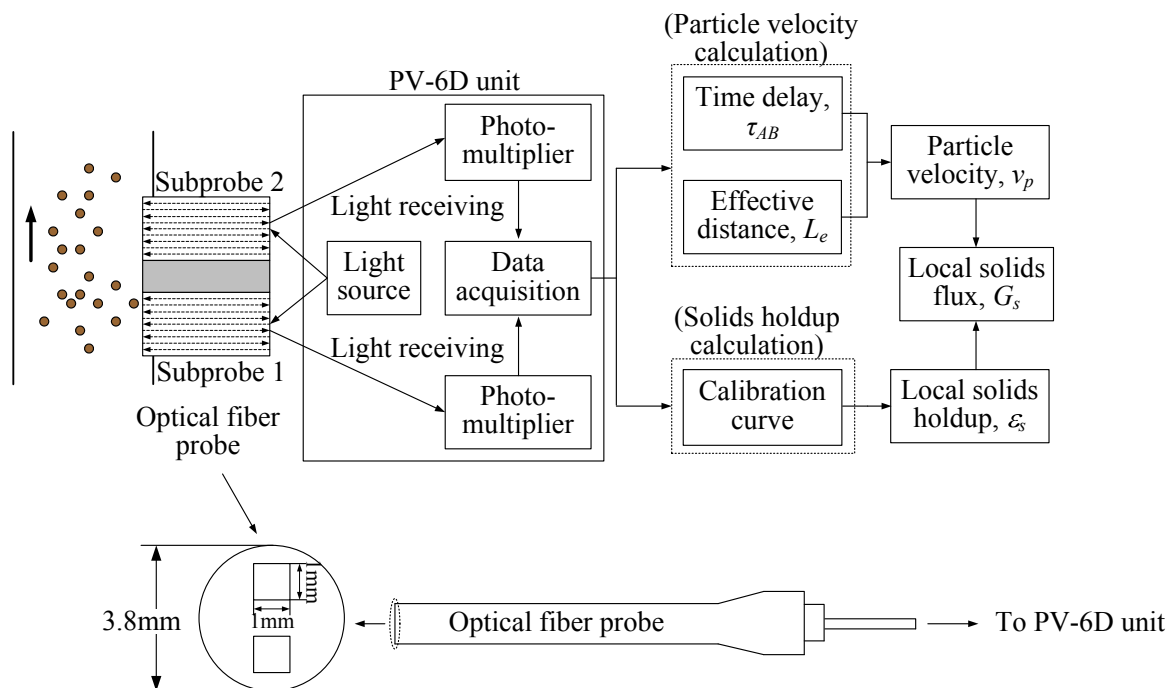


Figure 7.2 Schematic diagram of the novel optical fiber probe and its working principle.

7.2.2 Measurements of solids holdup

Experimental measurements include differential pressure, solids concentration (solids holdup) and ozone concentration. Twenty pressure taps were installed along the CFB column and connected with 19 differential pressure transducers (Omega PX162) to measure the axial profiles of the pressure gradient. The pressure gradient is mainly used to double check the solids holdup measured by an optical fiber probe mentioned below. Local solids holdup and particle velocity are measured simultaneously using a novel reflective-type optical fiber probe which has been shown to be effective and accurate for measuring the local solids concentration and particle velocity in high velocity fluidized beds and thus has been widely used by many investigators (Herbert *et al.*, 1994; Johnsson *et al.*, 2001; Liu *et al.*, 2003 and Ellis *et al.*, 2004). It yields high signal-to-noise ratios and is nearly free of interference by temperature, humidity, electrostatics and electromagnetic field. Moreover, its small size does not significantly disturb the overall flow structure in CFB systems with proper design. The optical fiber probe used in this work are model PV6D, developed by the Institute of Processing Engineering, Chinese Academy of Sciences, Beijing, China. The probe and measurement procedure are schematically shown in Figure 7.2. The outer diameter of the probe is 3.8 mm. There are two subprobes of the probe. Each of the subprobes consists of 8000 fine quartz fibers. The effective distance of the two vertically aligned subprobes is 1.51 mm, and the active tip area of each subprobe is 1×1 mm. Each subprobe consists of many quartz fibers with a diameter of $15 \mu\text{m}$, for light-emitting and receiving, arranged in alternating arrays. In order to prevent particles from occupying the blind zone, a glass cover of 0.2 mm thickness is placed over the probe tip. The underlying theory is elaborated by Liu *et al.* (2003).

As shown in Figure 7.2, light from the source illuminates a measuring volume of particles through the light-emitting fibers. The received light reflected by the particles is captured by light receiving fibers and processed by a photo-multiplier. The light intensity is then converted into voltage signals and the voltage signals are further amplified and fed into a PC. The voltage signal obtained by the probe is converted to volumetric concentration using a calibration equation. The relationship between the output signals of the optical fiber probe and the local solids holdup

(non-linear) is first established through proper a calibration based on the method developed by Zhang *et al.* (1998).

From the voltage time series $V(t)$ and the calibration equation, local instantaneous solids holdup, $\varepsilon_s(t)$, can be calculated:

$$\varepsilon_s(t) = f[V(t)] \quad (7.1)$$

where, f is the calibration function. The time-mean solids concentration ε_s can be given by integrating $\varepsilon_s(t)$ over the time period, T :

$$\varepsilon_s = \frac{1}{T} \int_0^T \varepsilon_s(t) dt \quad (7.2)$$

The cross-sectional average solids holdup $\bar{\varepsilon}_s$, can be calculated as follow:

$$\bar{\varepsilon}_s = \frac{1}{\pi R^2} \int_0^R 2\pi r \varepsilon_s dr = \frac{2}{R^2} \int_0^R \varepsilon_s r dr \quad (7.3)$$

7.2.3 Catalyst preparation

Ozone decomposition is a thermodynamically favoured process. It decomposes slowly at room temperature in the absence of catalysts, so catalysts are necessary for ozone decomposition at lower temperatures (Cotton and Wilkinson, 1972; Dhandapani and Oyama, 1997; Lin and Nakajima, 2002 and Wojtowicz, 2005). The noble metals such as Pt, Pd Rh and transition metal oxides such as MnO₂, Co₃O₄, CuO, Fe₂O₃, NiO and Ag₂O etc, are the active catalysts for ozone decomposition reaction, (Dhandapani and Oyama, 1997). In view of the high cost of noble metals, the metal oxide catalysts are usually preferred for ozone decomposition reactions. Catalyst supports include γ -Al₂O₃, SiO₂, TiO₂, zeolite, activated carbon (or carbon fibrous materials) or a combination of these (Dhandapani and Oyama, 1997 and Kirschner, 2000).

The equilibrium FCC particles, impregnated with ferric nitrate are used as catalysts. FCC particles, which are primarily composed of porous amorphous aluminum hydrosilicate are activated by impregnating in a 40% (*w*t) solution of ferric nitrate overnight. The soaked particles are then dried and calcinated in an oven with a hood at 450°C for 4 hours until no NO₂ is

released. During the calcinations, the ferric nitrate is converted to ferric oxide, which is the active component for the ozone decomposition reaction. The agglomerates formed during this process are then grinded by a ball mill and sifted using a standard sieve with 250 μm pore size. The Sauter mean diameter and the particle density is 76 μm and 1780 kg/m^3 respectively. The particle size distribution is listed in Table 7.1.

Table 7.1 Size distribution of the FCC particles.

Particle Size (μm)	Volume Fraction (%)
0-20	0.61
20-40	9.72
40-60	26.32
60-80	22.80
80-130	33.24
>130	7.31

7.2.4 Ozone generation and testing

An ozone generator using the corona discharge method (Model AE15M, manufactured by Absolute Ozone Inc.) is used in this study. Using bottled oxygen as gas supply, it produces up to 30 g/h of ozone depending on the oxygen flow rate and electrical current settings. Its working pressure is 5-50 psig, with oxygen flow rate of 0.1-10 standard liter per minute (SLPM). The oxygen flow rate into the generator was controlled by two rotameters (VWR, Catalog Number: 97004-648) ranging from 0 to 10 liter per minute (LPM). The ozone/oxygen mixture exiting from the ozone generator is mixed with the main fluidization air before entering the CFB riser or downer. With a fairly long flow path and several L-bends in the main air feeding lines, the mixing process is thorough. To ensure that the ozone stream can be easily and smoothly injected into main air flow of the CFB riser/downer with a pressure of less than 30 psig (for safety reasons, the 100 psig air source is reduced to a maximum feeding pressure of 30 psig), an output pressure of 50 psig is used for the regulator installed on the oxygen gas cylinder, maintaining a

much higher pressure for the ozone flowing from the ozone generator. The resulting initial ozone concentration (C_0) in the main air before ozone decomposition in the CFB columns is set to 80-100 ppm.

An ozone analyzer (Model 49i, Thermo Electron Inc.) that employs the UV photometric method of measurement is used to measure the amount of ozone in the ozone-air sample. It is a dual-cell photometer, having both sample and reference air flowing at the same time. Each cell has a length of 37.84 cm and an inner diameter of 0.91 cm, with the internal surfaces coated with polyvinylidene fluoride (PVDF) to ensure that ozone undergoes no decomposition upon exposure to the internal surface of the cells (Thermo Electron Inc., 2004 and 2005). The ozone analyzer has a measuring range of 0.0001-200 ppm with a resolution of 0.0001 ppm. The response time of the apparatus is 4 s. The ozone concentration output is displayed on an LCD screen. The UV source in the ozone analyzer is a 254 nm mercury lamp.

Considering the fact that ozone is highly oxidative, to reduce ozone loss in the sampling pathway to ozone analyzer, ozone-inert materials (e.g. stainless steel, copper, aluminum and Teflon) are used for the sampling probes, valves, and piping lines (Teflon, 3 mm i.d., 6 mm o.d.). Gas samples are continuously drawn from the CFB column through a sampling system shown in Figure 7.1 using the brass tubes (6 mm o.d. and 0.36 mm wall thickness) as the sampling probes. The tip of the probe is covered with a fine stainless steel mesh to prevent particles from being entrained into the sampling system. The velocity of gas sucked for sampling is 1.5 LPM which is low enough to assure minimal disturbance of the flow structure in CFB system. A high pressure purging air stream of 100 psig is introduced to blow away any particles potentially caked in the sampling probes.

When measuring ozone concentration in the CFB riser/downers, 4-5 g of particles are taken out from the column for catalytic activity check using the fixed bed reactor before and after each experiment. No significant change is observed in reaction rate constant (k_r) before and after several hours of CFB run, so that the ozone concentration profiles obtained under the experimental period is assumed to be under the same particle catalytic reactivity. The average value from these two tests is taken as the reaction rate constant.

In order to map the entire cross-section of the riser, ten axial measuring ports ($z = 0.59, 1.02, 1.94, 2.85, 3.77, 4.78, 5.84, 7.78, 9.61, \text{ and } 10.09$ m above the gas distributor) are installed along the column. Measurements were conducted at six radial positions ($r/R = 0, 0.316, 0.548, 0.707, 0.837$ and 0.950 , where r is the distance from the center and R is the riser radius) on each axial level of the CFB riser system. These positions are determined by dividing the column cross-section into five equal areas and determining the mid-point of each of these areas. For the hydrodynamic experiments, voltage signals from the optical fiber probe were sampled at a high frequency of 100 kHz with 1,638,40 data points for each measurement. To get the valid and repeatable data, all measurements are repeated at least 5 times. For the catalytic ozone decomposition, measurement is started after steady state has been reached in the CFB systems, which usually takes about at least 1 hour (Li, 2010). Ozone sampling is conducted for 1 min where the ozone concentration is fairly stable.

7.3 Results and discussion

7.3.1 Axial and radial profiles of ozone concentration

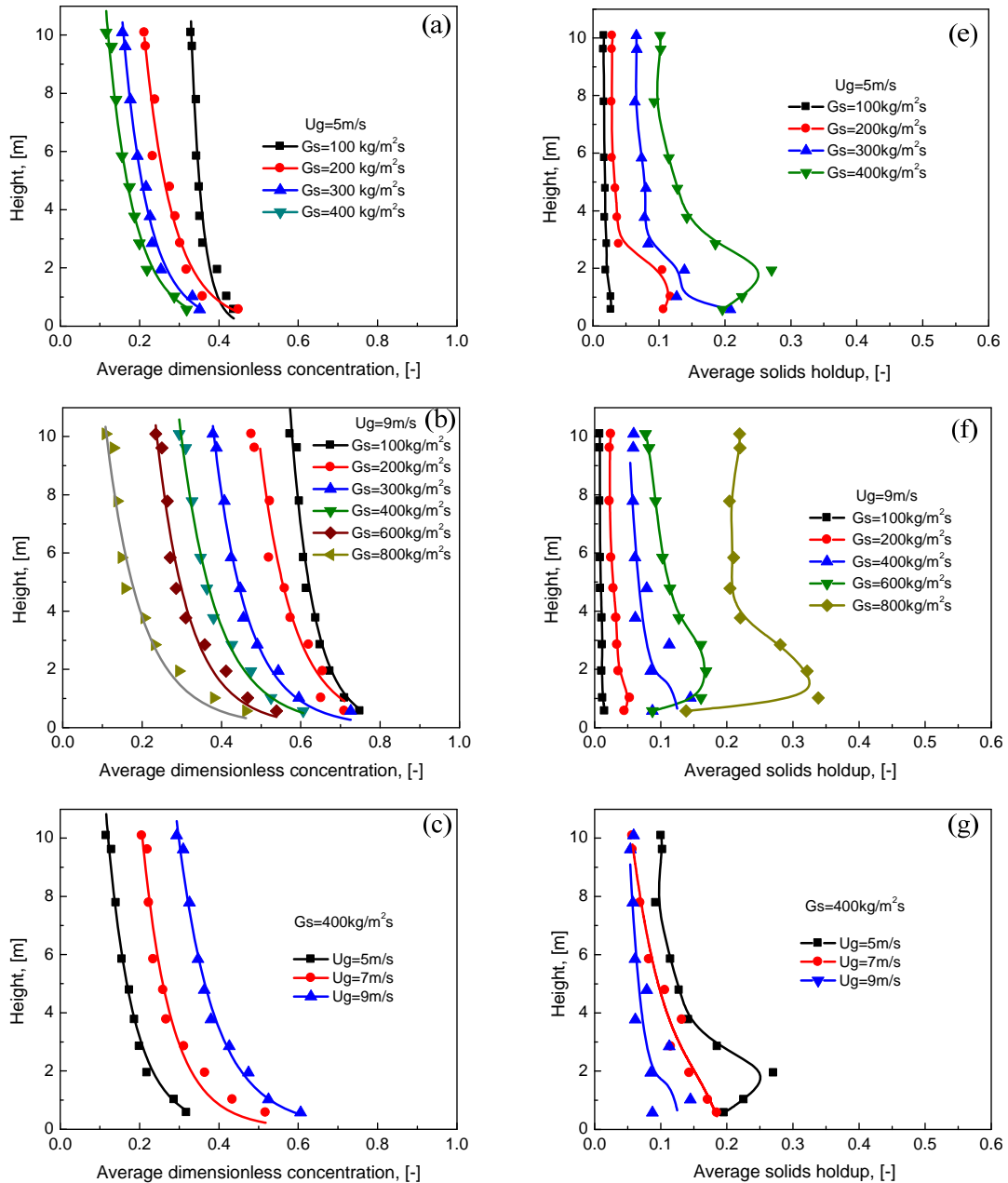


Figure 7.3 Axial distributions of the average dimensionless ozone concentration and the corresponding solids holdup.

The cross-sectionally averaged ozone concentration profiles under different operating conditions in the riser are shown in Figures 7.3 and 7.4. The average ozone concentrations are obtained by averaging the ozone concentration at six radial positions for each axial level. Ozone concentrations in all figures are presented in the form of “dimensionless concentration” which is defined by dividing the actual ozone concentration by initial concentration at the riser inlet. The corresponding solids holdup profiles obtained from optical fiber probe measurements are given in Figures 7.3 (e), 7.3 (f) and 7.3 (g).

From the axial distribution profiles of the ozone concentration, it is shown that the ozone concentration always decreases with increasing distance from the distributor. For all the operating conditions, the axial distribution profiles of the ozone concentration have a similar trend: except for the entrance region of the column where the ozone concentration decreases quickly, the ozone concentrations change more gradually and even have almost no change along the axial elevations. In other words, the conversion of ozone in the entrance section may account for most of the total conversion while the upper section of the riser contributes much less to overall ozone conversion. This indicates that the reaction is much faster in the acceleration region than that in the developed region, possibly due to the higher solids holdup and high gas-solids contact efficiency as well as higher reactant concentration, in the entrance region (shown in Figures 7.3 (e), 7.3 (f) and 7.3(g)). It should be pointed out that a dramatic change in the ozone concentration near the entrance region for all operating conditions may also be attributed to the entrance effect which is dependent on the design associated with this region.

In addition, there is a clear difference in the axial distributions of ozone concentration between low and high solids concentrations. When G_s ($G_s = 100 \text{ kg/m}^2\text{s}$) is low, the axial profiles have a more uniform axial distribution with a very short entrance-section (less than 2 m) where the ozone concentration drops sharply. Above this region, the ozone concentration remains relatively constant. When G_s is higher than $200 \text{ kg/m}^2\text{s}$, the dramatic decrease of ozone concentration covers much longer length which can be up to 6 m for G_s of $800 \text{ kg/m}^2\text{s}$, leading to higher ozone conversion. The obvious reason is that the average solids holdup is much higher for high solids flux conditions than that for low solids flux cases. Under high solids concentration conditions, there would be more opportunity of contacting between gas and solids so that the reactant can be

converted as much as possible. It can also be seen that the operating conditions (superficial gas velocity and solids circulation rate) affect the values of the dimensionless ozone concentration. Low superficial gas velocities and/or high solids circulation rates lead to low ozone concentration (i.e. high ozone conversion) and vice versa.

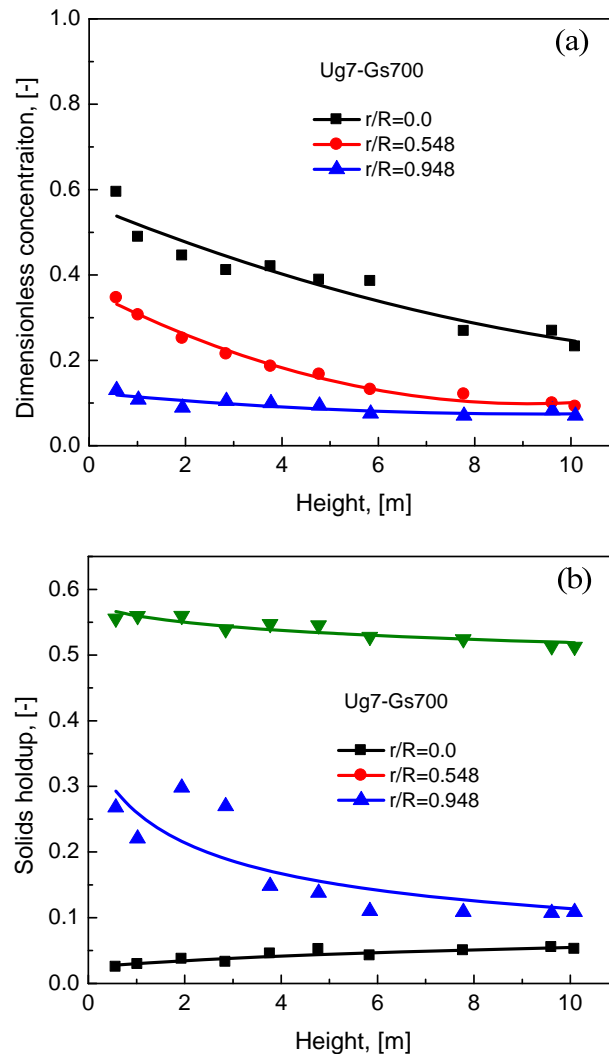


Figure 7.4 Axial distributions of the dimensionless ozone concentration and the corresponding solids holdup at different radial positions.

Figure 7.4 shows the typical axial ozone concentration profiles at different radial positions under U_g of 7 m/s and G_s of 700 kg/m²s. The corresponding solids holdup profiles are also given in the Figure. Different trends are observed for different radial positions. Ozone concentration in the

centreline of the riser is nearly linear and is almost constant along the riser height. In the middle section of the radial position ($r/R = 0.548$), the ozone concentration distribution becomes less uniform with a sharp decrease up to 5-6 m and thereafter remains almost unchanged in the upper sections. On the other hand, a significantly lower ozone concentration has been measured near the wall. The above trend is related to the solids holdup distributions, which are shown in Figure 7.4 (b). At the central region, the solids holdup is low and remains nearly unchanged, so that the unconverted ozone concentration is relatively high and hardly changes with the axial elevations. In the middle section, the solids holdup changes dramatically with the axial level leading to the various ozone concentrations along the riser. However, the solids concentration near the wall is much higher up to 0.55 so that the conversion in this region is higher up to 90%.

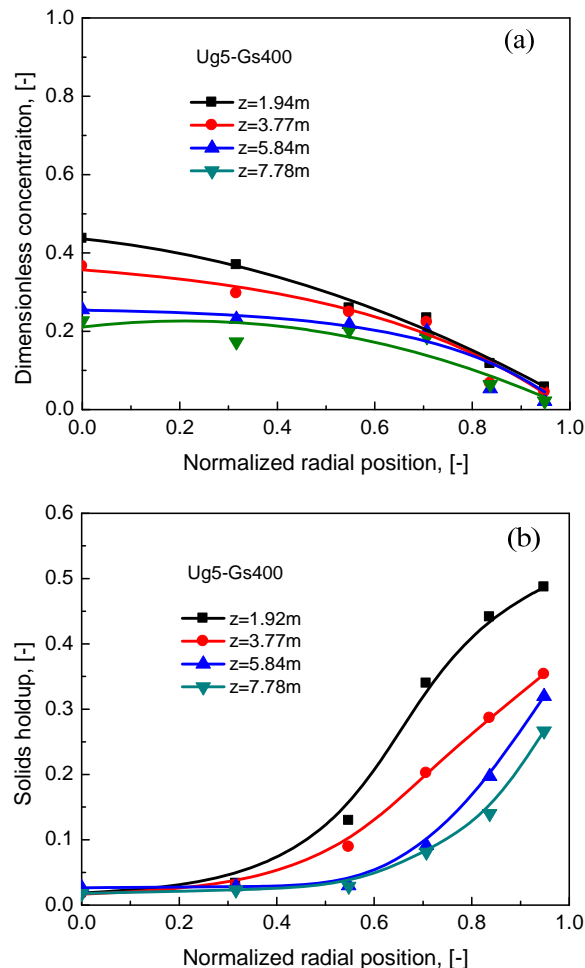


Figure 7.5 Radial distributions of the average dimensionless ozone concentration and the corresponding solids holdup.

Typical radial distribution profiles of the ozone concentration at different axial bed positions under superficial gas velocity of 5 m/s and solids circulation rate of 400 kg/m²s in the column are shown in Figure 7.5 (a). The Figure shows that the distribution of the ozone concentration is not uniform along the radial direction, consistent with those profiles in Figure 7.4. At the lower bed section, ozone concentration changes more rapidly with the radial positions. The ozone concentration is highest at the axis, decreasing sharply towards the wall. With increasing bed height, the profiles of ozone concentration become more uniform across the bed, but still show a small decrease near the wall. The trends of the radial distributions are understandable, and can be explained by the radial flow structure. The radial distribution of solids holdup is shown in Figure 7.5 (b). At the center of the riser, the solids concentration is low and uniform since solids can be easily carried up by the high-velocity gas. Near the wall, as the gas velocity is lower, the solids concentration remains at high values. This causes the radial distribution of unconverted ozone concentration to be high and more uniform in the central region and to have a significant decrease near the wall. The radial distribution of concentration is consistent with that reported by Li *et al.* (2011 and 2013). Moreover, the difference in ozone concentration between the core and wall region seems to decrease with the axial elevations reflecting the decrease in solids holdups.

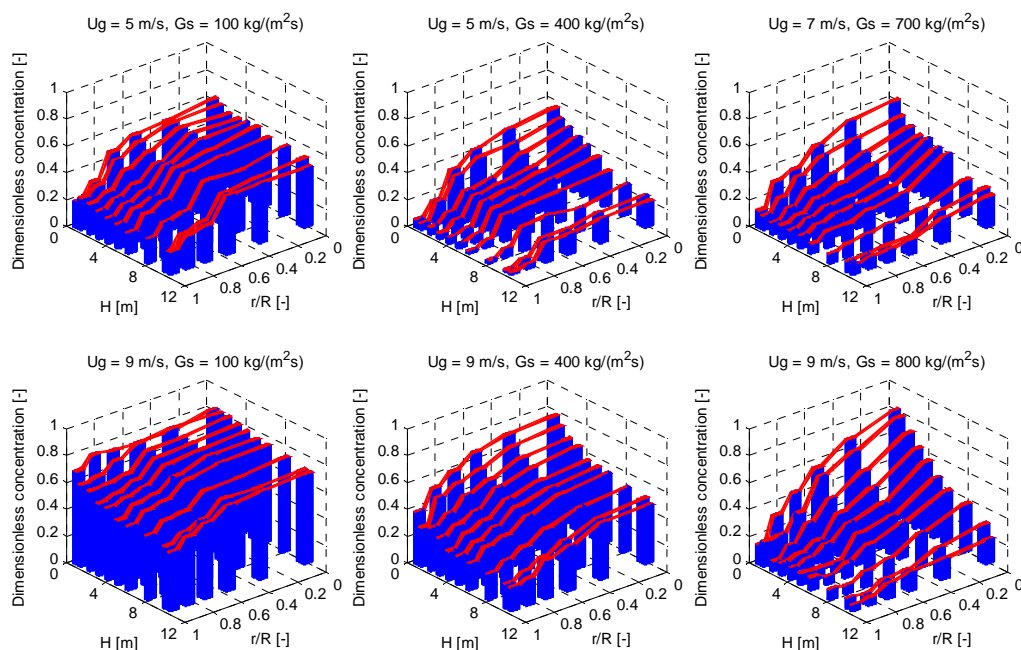


Figure 7.6 Overall view of the dimensionless ozone concentration under different operating conditions.

Based on the above discussion, Figure 7.6 provides an overview of the ozone concentration profiles in the CFB riser under various operating conditions, where x and y axes are the radial and axial positions in the column, and z -axis is the dimensionless ozone concentration. It is observed that with the increase of riser elevations, more ozone reactants are converted due to its extended contact with the catalyst particles, giving decreased ozone concentrations. Ozone concentration in the center region is higher than that in the near wall region, giving a parabolic radial profile of the concentration. The radial ozone concentration distribution also becomes uniform in the upper region of the reactor.

The distribution of ozone concentration is affected by the operating conditions. Higher U_g and/or low G_s results in more uniform distribution of ozone concentration in both axial and radial directions. For example, at low solids circulation rate ($G_s = 100 \text{ kg/m}^2\text{s}$) and high superficial gas velocity ($U_g = 9 \text{ m/s}$), the ozone concentration profiles are nearly constant along the column. The axial profiles become less uniform with increasing G_s . Moreover, an increase in G_s increases the ozone concentration difference between the central and wall region. Next we examine the effects of operating conditions on ozone concentration distributions.

7.3.2 Effect of operating conditions on ozone concentration

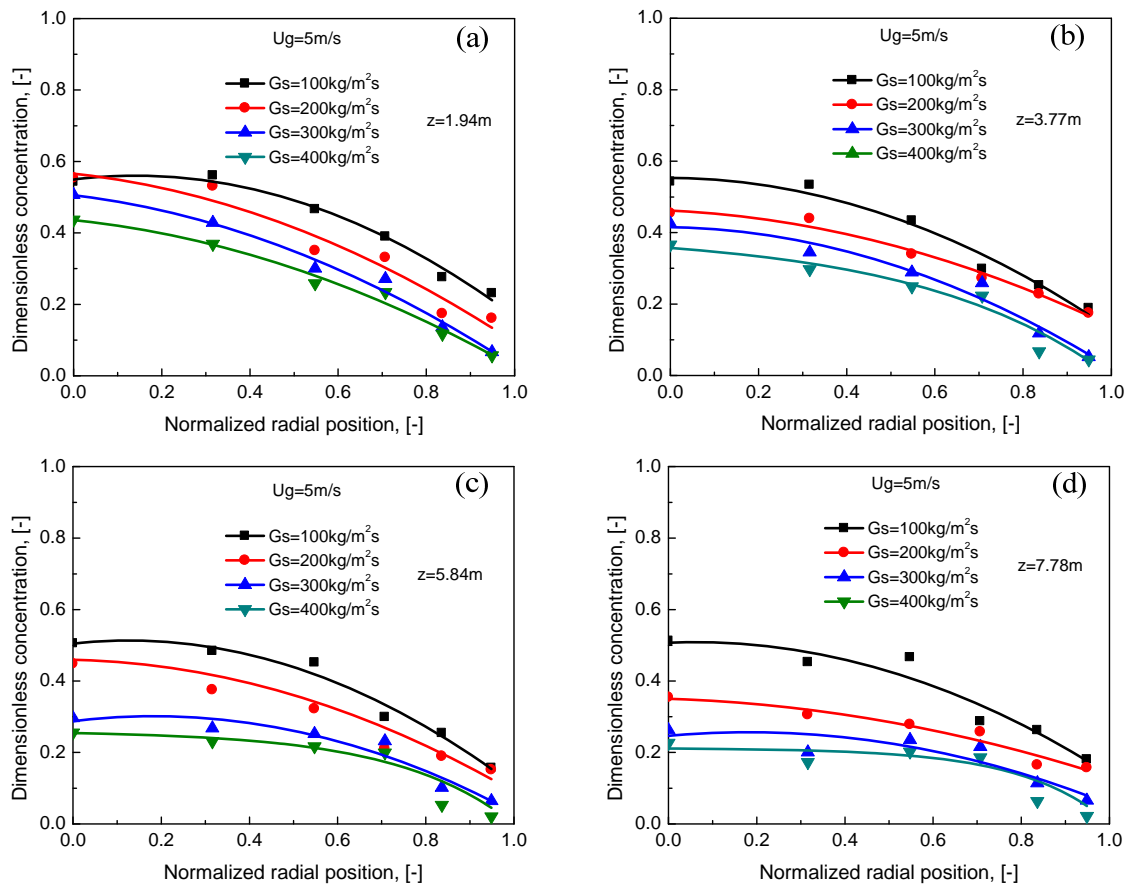


Figure 7.7 The effect of solids circulation rate on the local dimensionless ozone concentration.

The effect of solids circulation rate on radial profiles of dimensionless ozone concentration at four axial levels at $U_g = 5$ m/s with solids circulation rates ranging from 100 kg/m²s to 400 kg/m²s is plotted in Figure 7.7.

As discussed before, the radial profiles of ozone concentrations are parabolic-shaped, corresponding to the radial distribution of solids concentrations. At all axial levels, the dimensionless ozone concentration (unconverted ozone concentration) decreases with an increase in solids circulation rate for the same superficial gas velocity of 5 m/s. This is due to the solids holdups increase with increasing solids circulation rate. Under the high density operating conditions, the total gas-solids contacting area for reaction and mass transfer between gas and solids will also increase leading to significant rise of the ozone conversion. Therefore, ozone

concentration becomes much lower as solids circulation rate increases. At the same bed height, the radial distribution of the ozone concentration becomes more uniform with reduced G_s due to the increased radial uniformity of the solids flow structure.

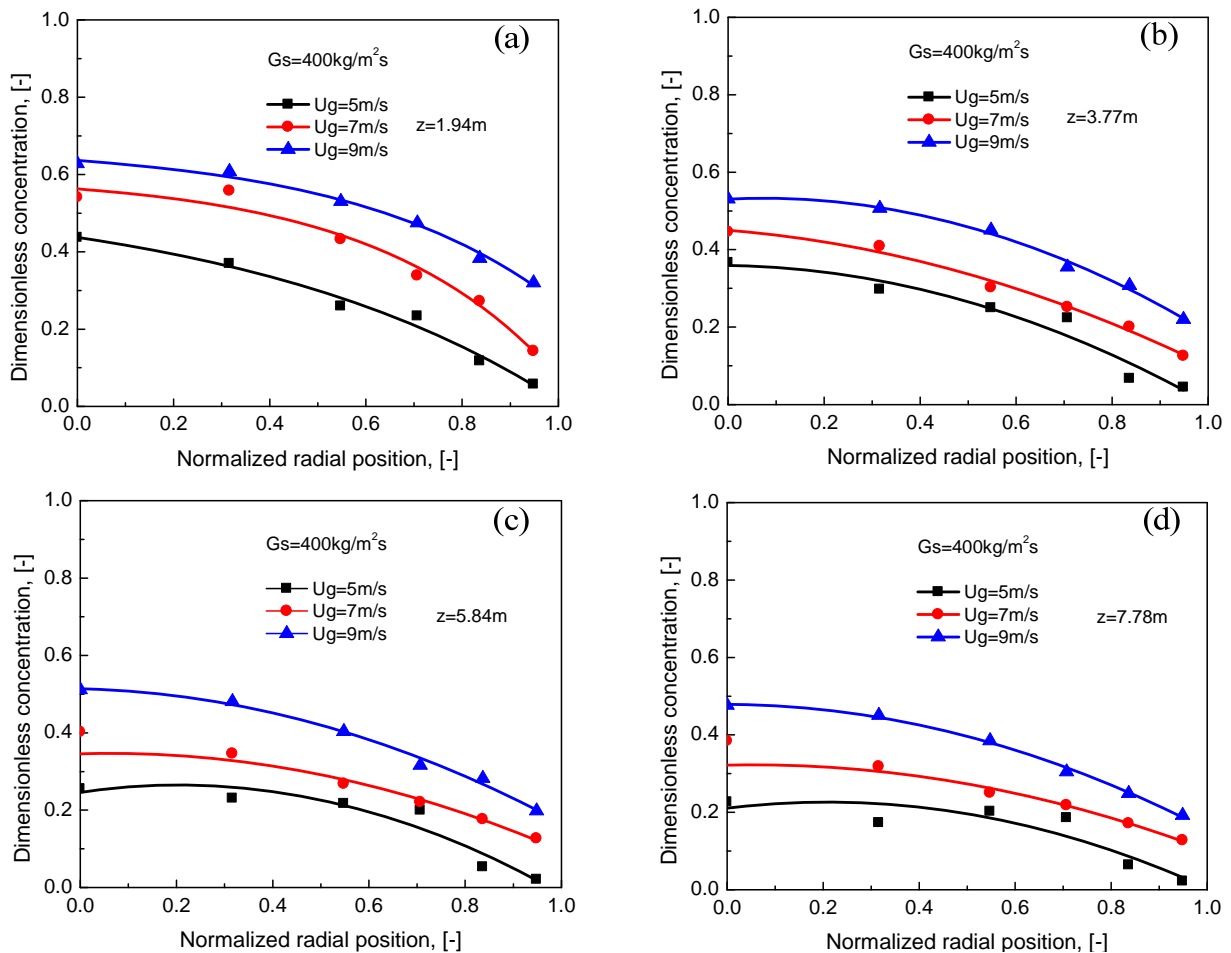


Figure 7.8 The effect of superficial gas velocity on the local dimensionless ozone concentration.

The effect of the superficial gas velocity on radial profiles of dimensionless ozone concentration at four axial levels at $G_s = 400 \text{ kg/m}^2\text{s}$ with superficial gas velocities ranging from 5 m/s to 9 m/s is plotted in Figure 7.8.

Generally, the concentration of the unconverted ozone increases with increasing superficial gas velocity, at a fixed solids circulation rate. This may be attributed to the following mechanisms: when solids circulation rate remains constant, increasing superficial gas velocity reduces the

solids holdups. The decreased solids holdup would result in the decrease of total gas- solids contacting area which is not favourable for the reaction. On the other hand, increasing superficial gas velocity leads to a short residence time of both gas and solid phases, which is not beneficial to the total conversion of ozone. Considering the above two factors, the increase of superficial gas velocity will cause the decrease of the ozone conversion. In addition, increasing U_g can lead to a more uniform radial profile of ozone concentrations.

7.3.3 Relationship between ozone concentration and solids holdup

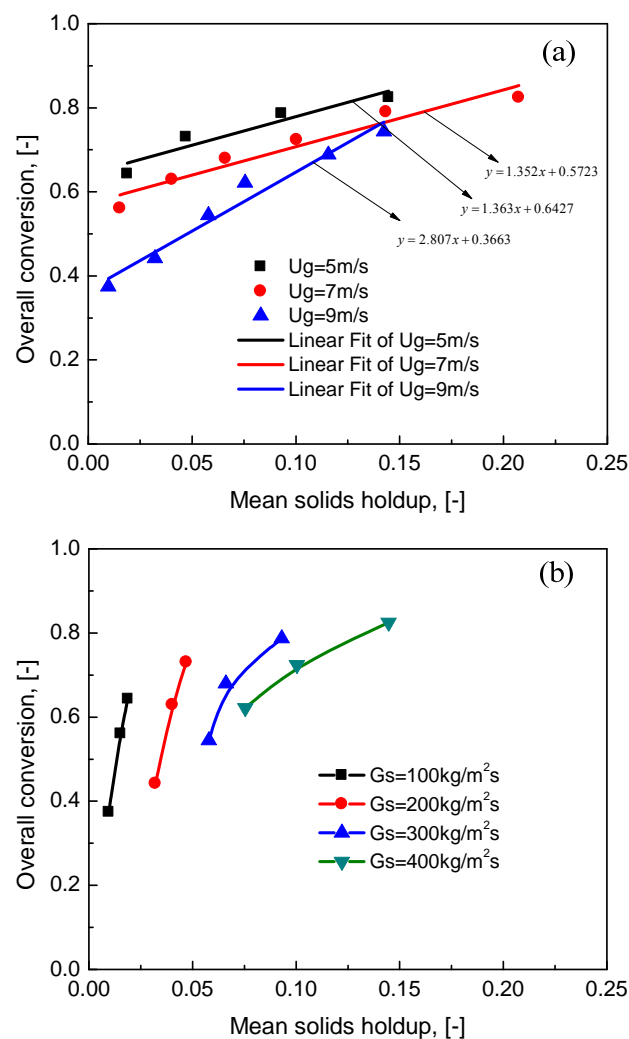


Figure 7.9 Relationship between the conversion and solids holdup.

As stated before, the distribution of ozone concentration is essentially dominated by the flow structure, which can be partially represented by the solids holdup profiles in the CFB reactors. To further evaluate the effects of the solids holdup on ozone concentration, the overall conversion of ozone are plotted against the mean solids holdup in the entire column as shown in Figure 7.9.

In general, the conversion of ozone increases with the solids holdup, as has been confirmed by other researchers (Jiang *et al.*, 1991 and Li *et al.*, 2011 and 2013). There appears to be a linear relationship between total ozone conversion and mean solids holdup as shown in Figure 7.9 (a). The influence of solids holdup on ozone conversion is nearly the same for $U_g = 5$ m/s and 7 m/s with almost the same slope of the fitting lines. On the other hand, effects of solids holdup on ozone conversion is more significant under high superficial gas velocity ($U_g = 9$ m/s). Higher solids holdup under higher superficial gas velocity plays a significant role in overall conversion. The reason is that at low superficial gas velocity, the increase of solids holdup probably leads to the increase of formation of clusters. The gas-solids mass transfer within the clusters is not as good as that between dispersed particles and the gas flow. Under high superficial gas velocity conditions, the high gas velocity can break down the clusters in addition to enhance the gas-solids contacting efficiency. Therefore, the overall conversion of reactant can be increased rapidly with solids holdup under high superficial gas velocity.

Figure 7.9 (b) shows the solids holdup influence on overall conversion under different solids circulation rates. Firstly, the increase of the overall ozone conversion with solids holdup seems to have different trends under different solids circulation rates. The relationship between overall conversion and solids holdup is almost linear under relatively low G_s (less than 300 kg/m²s). Secondly, the variation of the overall conversion with solids holdup also appears to follow different trends for low and high solids flux conditions. The overall conversion of ozone increases significantly under such low G_s . While under high G_s the changes of overall conversion becomes slower. As discussed above, the increase of G_s will lead to the increase of solids holdup causing easy cluster formation. The cluster formation results in the decrease of the gas-solids mass transfer, which leads to the overall conversion at high G_s being less sensitive to the variation of solids holdup. Overall, it seems that at higher superficial gas velocity and lower

solids circulation rate, the increase of solids holdup leads to more significant increase in overall reactant conversion than that at lower gas velocity and higher solids flux. These phenomena have not been well illustrated in the previous studies.

7.3.4 Performance of the CFB reactor

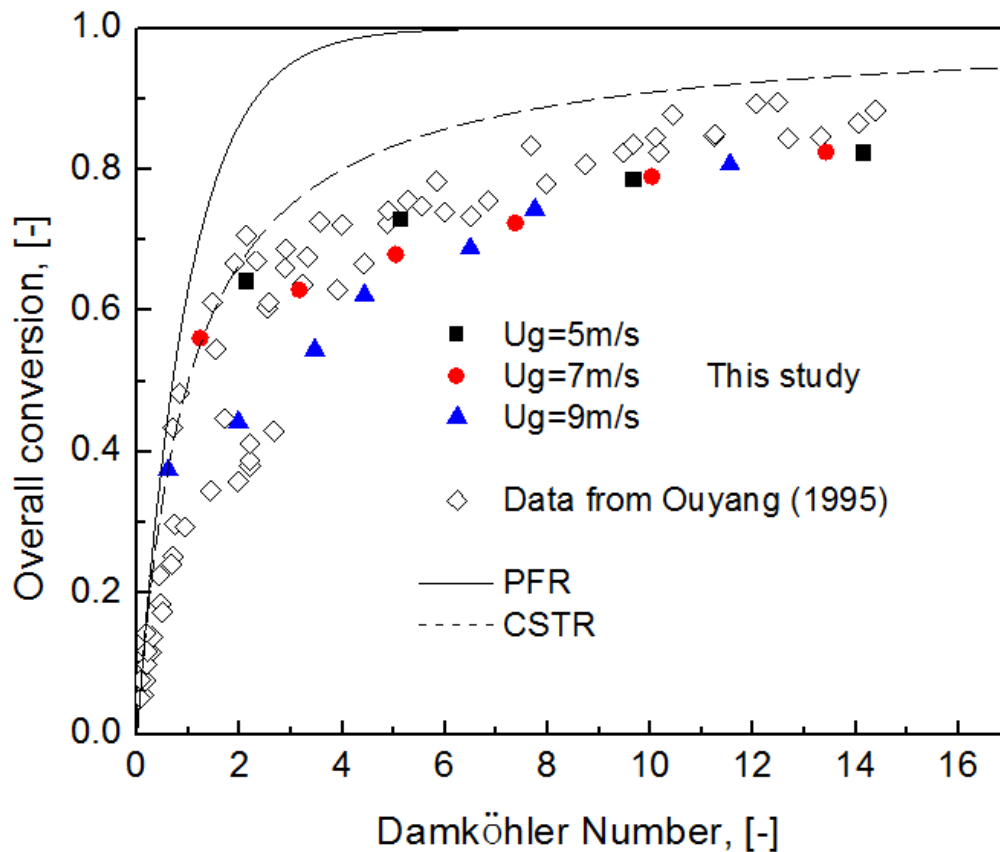


Figure 7.10 Effects of Damköhler number on overall ozone conversion.

The performance of the CFB reactors is related to both hydrodynamics and the chemical reactions. To determine how strong the effects of hydrodynamics have on the chemical reaction, it is better to plot the results of two typical models: a plug-flow reactor (PFR) and the continuous stirred-tank reactor (CSTR). Both of the two model reactors have been idealized in hydrodynamics with perfect mixing between gas and solids phase. Formulas for the conversion in PFR and CSTR can be derived as follows (Levenspiel, 1998).

Plug flow reactor

$$X_{PFR} = 1 - \exp(-k_r') \quad (7.4)$$

Continuous stirred-tank reactor

$$X_{CSTR} = \frac{k_r'}{1 + k_r'} \quad (7.5)$$

where k_r' is the Damköhler number ($= k_r \varepsilon_s (1 - \varepsilon_s) H / U_g$).

The overall conversion of ozone for the entire riser is plotted against Damköhler number in Figure 7.10. The calculated curves of PFR and CSTR are also shown in Figure 7.10. It seems that the conversion in the CFB system is generally lower than that in the two ideal reactor models. This demonstrates that the two models, which idealize bed hydrodynamics, cannot well predict the observed conversions, which implies in turn that hydrodynamics affects the chemical reaction in the CFB riser. Moreover, it is noted that the effects of Damköhler number on overall conversion are consistent with the effect of solids holdup on overall conversions. This indicates that the solids holdup is the main factor affecting the ozone reaction and increasing solids holdup would increase reactant conversion. In addition, the extent of the deviation of the conversion can be attributed to the different gas-solids contact efficiency which will be the subject of the future study.

7.4 Conclusions

The axial and radial distributions of the ozone concentration and the effect of the operating conditions on ozone concentration are studied in a high density circulating fluidized bed riser with various superficial gas velocities and high solids circulation rate up to $800 \text{ kg/m}^2\text{s}$. The key conclusions of this study are as follows.

The axial and radial distribution profiles of the ozone concentration are consistent with the corresponding profiles of the solids holdups which indicate that ozone reaction in the riser is controlled by the gas-solids flow structure.

High ozone conversion in the entrance of the riser indicating that the initial gas-solids contacting plays a key role in the reaction process and more attention need to be paid on the entrance design.

Ozone conversion increases with the solids circulation rate under the same superficial gas velocity due to the increase of solids holdup. The conversion decreases with gas velocity at a fixed solids circulation rate due to the associated reduction in solids holdup.

Solids holdup affects the overall ozone conversion with various trends. There is much more significant influence of solids holdup on overall reactant decomposition under higher superficial gas velocity and/or lower solids circulation rate.

The values of calculated overall conversion are to some extent smaller than those obtained based on the two ideal reactor (plug flow reactor and continuous stirred tank reactor) models indicating that hydrodynamics affects the chemical reaction in the CFB riser reactor. The extent of the deviation of the conversion can be attributed to the different gas-solids contact efficiency.

Nomenclature

C	ozone concentration [ppm]
C_0	initial ozone concentration [ppm]
C/C_0	dimensionless ozone concentration [-]
G_s	solids circulation rate [$\text{kg}/(\text{m}^2 \cdot \text{s})$]
H	height of the reactor [m]
k_r	reaction rate constant based on particle volume, first-order [s^{-1}]
k'_r	Damkoehler number, $k_r \bar{\varepsilon}_s (1 - \bar{\varepsilon}_s) H / U_g$ [-]
r	radial coordinate [m]
R	column radius [m]
r/R	reduced radial sampling position [-]
U_g	superficial gas velocity [m/s]
z	axial coordinate, or distance from the gas distributor [m]

Greek letters

ε_s	solids holdup [-]
$\bar{\varepsilon}_s$	average solids holdup for the entire reactor column [-]

Subscripts

g	gas
p	particle
s	solids

References

- Bai DR., Jin Y., Yu ZQ., and Zhu JX., (1992), The axial distribution of the crosssectionally averaged voidage in fast fluidized beds, *Powder Technology* 71: 51-58
- Cotton FA. and Wilkinson G., (1972), *Advanced Inorganic Chemistry*, Wiley, New York
- Dhandapani B., and Oyama S., (1997), Gas phase ozone decomposition catalysts, *Applied Catalysis B: Environmental* 11(2): 129-166
- Du B., Warsito W. and Fan LS., (2003), Bed non-homogeneity in turbulent gas-solid fluidization, *AIChE Journal* 49: 1109-1126
- Ellis N., Bi HT., Lim CJ. and Grace JR., (2004), Influence of probe scale and analysis method on measured hydrodynamic properties of gas-fluidized beds, *Chemical Engineering Science* 59(8-9): 1841-1851
- Fan C., Bi X., Lin W. and Song W., (2008), Mass transfer and reaction performance of the downer and its hydrodynamic explanation, *The Canadian Journal of Chemical Engineering* 86(3): 436-447
- Fan C., Zhang Y., Bi X., Song W., Lin W. and Luo L., (2008), Evaluation of downer reactor performance by catalytic ozone decomposition, *Chemical Engineering Journal* 140(1-3): 539-554
- Glicksman LR., (1988), Circulating fluidized bed heat transfer. *Circulating fluidized bed technology II*, Basu P and Large JF, eds., Pergamon, Oxford, P13
- Grace JR., Issangya AS., Bai DR., Bi HT. and Zhu JX., (1999), Situating the high density circulating fluidized bed, *AIChE Journal* 45: 2108-2116
- Grace JR., Avidan A. and Knowlton T., (1997), *Circulating Fluidized Beds*, Chapman & Hall
- Herbert PM., Gauthier TA., Briens CL., and Bergougnou MA., (1994), Application of fiber optic reflection probes to the measurement of local particle velocity and concentration in gas-solid flow, *Powder Technology* 80: 243-252
- Issangya AS., Bai D., Bi HT., Lim KS., Zhu J. and Grace JR., (1999), Suspension densities in a high-density circulating fluidized bed riser, *Chemical Engineering Science* 54: 5451-5460
- Issangya AS., Bai D., Grace JR., Lim KS. and Zhu J., (1997), Flow behaviour in the riser of high-density circulating fluidized bed, *AIChE Symposium Series* 93: 25-30
- Issangya AS., Grace JR., Bai DR. and Zhu JX., (2000), Further measurements of flow dynamics in a high-density circulating fluidized bed riser, *Powder Technology* 111: 104-113

Jiang P., Bi H., Jean RH. and Fan LS., (1991), Baffle effects on performance of catalytic circulating fluidized bed reactor, *AIChE Journal* 37(9): 1392-1400

Jiang P., Inokuchi K., Jean RH., Bi H. and Fan LS., (1990), Ozone decomposition in a catalytic circulating fluidized bed reactor, in *Circulating Fluidized Bed Technology III* (editor(s): Basu P.; Horio M. and Hasatani M.), Pergamon Press, Oxford, pp557-562

Johnsson H. and Johnsson F., (2001), Measurements of local solids volume-fraction in fluidized bed boilers, *Powder Technology* 115: 13-26

Smolders K. and Baeyens J., (2001), Hydrodynamic modelling of the axial density profile in the riser of a low-density circulating fluidized bed, *The Canadian Journal of Chemical Engineering* 79(3): 422-429

Kirschner MJ., (2000), Ozone, in *Ulmann's Encyclopedia of Industrial Chemistry*, Wiley-VCH Verlag GmbH & Co. KGaA

Kunii D, and Levenspiel O., (1991), *Fluidization Engineering*. Butterworth-Heinmann, London

Li DB., Ray AK., Ray MB., and Zhu J., (2013), Catalytic reaction in a circulating fluidized bed riser: Ozone decomposition, *Powder Technology* 342(15): 65-73

Li DB., Zhu J., Ray MB. and Ray AK., (2011), Catalytic reaction in a circulating fluidized bed downer: Ozone decomposition, *Chemical Engineering Science* 66 (20): 4615-4623

Li DB., (2010), Investigation of circulating fluidized bed riser and downer reactor performance for catalytic ozone decomposition, Diss. The University of Western Ontario

Li Y. and Kwauk M., The dynamics of fast fluidization. In: Grace JR, Matsen JM, editors. *Fluidization*. New York: Plenum Press, 1980; 537-544

Lin J. and Nakajima T., (2002), An AM1 study of decomposition of ozone on a Cu(110) surface, *Ozone: Science & Engineering: The Journal of the International Ozone Association* 24(1): 39-47

Liu JZ., Grace JR. and Bi HT., (2003a), Novel multifunctional optical-fiber probe: development and validation, *AIChE Journal* 49(6): 1405-1420

Liu JZ., Grace JR. and Bi HT., (2003b), Novel multifunctional optical-fiber probe: high-density CFB measurements, *AIChE Journal* 49(6): 1421-1432

Liu JZ., Grace JR., Bi HT., Morikawa H. and Zhu JX., (1999), Gas dispersion in fast fluidization and dense suspension upflow, *Chemical Engineering Science* 54(22): 5441-5449

Nieuwland JJ. and Meijer R., (1996), Measurements of solids concentration and axial solids velocity in gas-solid two-phase flows, *Powder Technology* 87(2): 127-139

Ouyang S., Lin J. and Potter OE., (1993), Ozone decomposition in a 0.254 m diameter circulating fluidized bed reactor, *Powder Technology* 74(1): 73-78

Ouyang S., Li XG. and Potter OE., (1995), Circulating fluidized bed as a catalytic reactor: experimental study, *AIChE Journal* 41(6): 1534-1542

Wu RL., Grace JR., Lim CJ. and Bereton CMH., (1989), Suspension to surface heat transfer in a circulating fluidized bed combustor, *AIChE Journal* 35: 1685

Wojtowicz JA., (2005), Ozone, in *Kirk-Othmer Encyclopedia of Chemical Technology*, John Wiley & Sons

Ma Y. and Zhu JX., (1999), Experimental study of heat transfer in a co-current downflow fluidized bed (Downer), *Chemical Engineering Science* 54(54): 41-50

Ma Y. and Zhu JX., (2000), Heat transfer between gas-solids suspension and immersed surface in an upflow fluidized bed (riser), *Chemical Engineering Science* 55: 981-989

Ma Y. and Zhu JX., (2001), Heat transfer in downer and the riser of a circulating fluidized bed-A comparative study, *Chemical Engineering Technology*, 1: 85-90

Zhang H., Johnston PM., Zhu JX., de Lasa HI. and Bergougnou MA., (1998), A novel calibration procedure for a fiber optic solids concentration probe, *Powder Technology* 100: 260-272

Zhu HY. and Zhu J., (2008), Gas-Solids Flow Structures in a Novel Circulating-Turbulent Fluidized Bed, *AIChE Journal* 54(5): 1213-1223

Zhu JX. and Bi HT., (1995), Distinctions between low density and high density circulating fluidized beds, *The Canadian Journal of Chemical Engineering* 73:644-649

Zhu JX. and Cheng Y., (2005), Fluidized-Bed Reactors and Applications, Chapter 5.3 in *Multiphase Flow Handbook*, ed. Clayton Crowe, CRC Press, New York, pp 5.55-5.93

CHAPTER 8

Catalytic Ozone Decomposition in a High Flux Gas-solids CFB Downer

8.1 Introduction

Gas-solid reactors have been utilized widely in many industrial operations such as coal combustion, fluid catalytic cracking (FCC) and Fischer-Tropsch process. Circulating fluidized bed (CFB) is one of the efficient reactors employed to handle a variety of gas-solids processes. There are two basic flow modes: co-current upflow in a riser and co-current downflow in a downflow CFB or downer. For the riser reactor, both gas and solids are fed at the bottom and flow upwards. Compared to the conventional fluidized beds (bubbling and turbulent fluidized beds), risers have such advantages as high gas-solids contact efficiency, high solids throughput, flexible operation and unique heat and mass transfer characteristics. On the contrary, relatively significant axial dispersion of solids, which can greatly influence selectivity and irregular distribution of the desired products, is the main disadvantage of the CFB riser. It has been suggested that the axial back mixing in the riser is largely due to the particle aggregation which, in turn, is due to the gas and solids flow against gravity (Zhu and Wei, 1995 and Wei and Zhu, 1996).

The downer reactor, in which gas and solids move downward in a concurrent fashion, has drawn much attention in recent years due to its unique features such as shorter residence time, narrow residence time distribution, little or no solids backmixing (Zhu *et al.*, 1995 and Cheng *et al.*, 2008). These features of downer reactors can potentially lead to its application for ultra rapid reactions such as the highly selective and fast catalytic conversion of residual oil or other hydrocarbons (Bassi *et al.*, 1994; Shaikh *et al.*, 2008 and Guan *et al.*, 2011 and Abbasi *et al.*, 2012), biomass and coal pyrolysis.

In chemical reactors, reactor performance is determined both by the process itself and by the hydrodynamics. The design, optimization and scale-up of a downer reactor require more precise

and quantitative understanding of both the flow behavior and the chemical reaction. Many studies on the hydrodynamics of downers have been carried out in recent years (Wang *et al.*, 1992; Wei and Zhu, 1996; Herbert *et al.*, 1999; Johnston *et al.*, 1999; Ma and Zhu, 1999; Schiewe *et al.*, 1999; Zhang *et al.*, 1999, 2000 and 2001; Deng *et al.*, 2004; Luo *et al.*, 2007; Wu *et al.*, 2007; Qi *et al.*, 2008; Abbasi *et al.*, 2013 and Li *et al.*, 2013). However, few researches have been reported on heat transfer, mass transfer and chemical reactions (Ma and Zhu, 1999 and 2000; Fan *et al.*, 2008 and Li *et al.*, 2011). Study of chemical reactions in the downer can provide direct information on reactor performance. In this study, the objective is to obtain the axial and radial ozone concentration profiles and investigate the downer reactor performance at high flux operating conditions. Because of the simplicity of reaction kinetics and negligible heat effect of reaction, the ozone decomposition reaction is chosen as a model reaction in the current work. In order to explain the ozone profiles in the downer reactor, the flow structure of the downer under corresponding operating conditions is also determined.

8.2 Experimental details

8.2.1 CFB experimental system

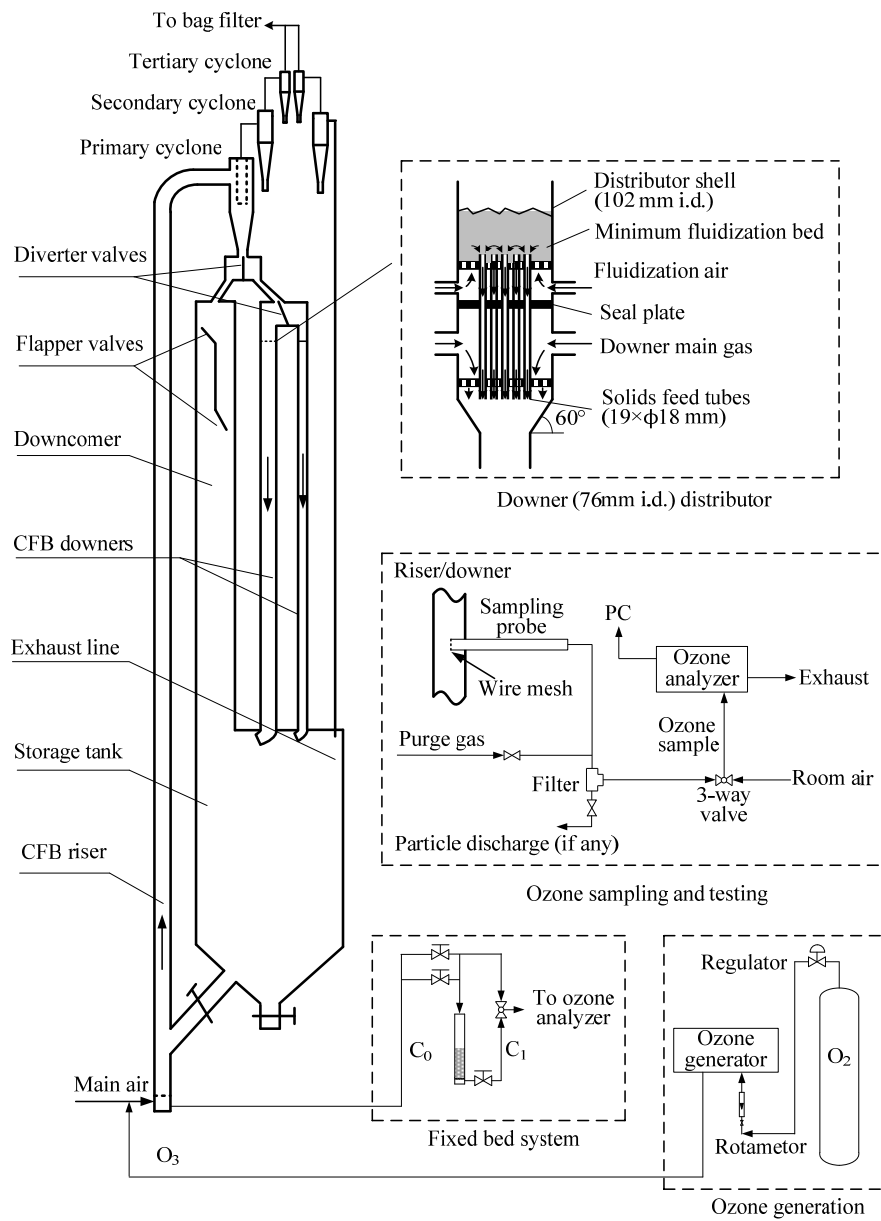


Figure 8.1 Schematic diagram of the multifunctional CFB and ozone testing system.

The circulating fluidized bed reactor facility used in this study is shown schematically in Figure 8.1. The system includes three circulating fluidized beds: the left hand fluidized bed serves as a high flux/density circulating fluidized bed riser (76 mm i. d. and 10 m high), and the right hand fluidized beds are two circulating fluidized beds downer (co-current downflow circulating fluidized beds) of different diameters (76 mm i. d. and 5.8 m high and 50 mm and 4.9 m high, respectively). A large downcomer with an inner diameter of 203 mm returns solids during riser operation. At its bottom a solids storage tank with an inner diameter up to 457 mm were used as general solids storage for the entire system. Total solids inventory of FCC particles in the downcomer and storage tank could be up to 450 kg, equivalent to a solids height of approximately 6.0 m. This high solids level ensures high back pressure in the downcomer and enables high solids circulation rates and high solids concentrations in the CFB riser. To aid the fluidization of the downcomer, aeration points were provided at 2 m and 5 m above the distributor. In order to obtain higher flux and steadier operating conditions, other modifications had been carried out in the CFB system (details can be found in the chapter 4).

The multifunctional circulating fluidized bed (MCFB) can be operated as a CFB riser and downer. For CFB riser operations, particles in the storage tank fluidized by aeration air entering into the bottom of the riser and obtained momentum from the air passing through the riser gas distributor made of perforated plates (2 mm×176 holes, 12% opening area). The particles are carried upward by the riser air along the column. At the top of the riser, particles and gas are separated by primary, secondary and tertiary cyclones and most of the particles returned to the downcomer and further down to the storage tank. Fine particles leaving from the cyclones are trapped by the bag filter and returned periodically to the downcomer. The gas is then discharged into the atmosphere.

When the MCFB is under downer operating mode, solid particles are first lifted through the riser, separated by the primary cyclone fixed at the top of the downcomer and then fed into the downers. At the top of either one of the downers is a gas-solids distributor (details shown in Figure 7.1) where the particles are uniformly distributed along with the downer air to flow downward concurrently. After fast separation by gravity at the exit of either downer column, most particles are retained in the storage tank, with the remaining particles captured by two

cyclones installed in series at the top of the exhausted pipeline and the common bag filter. To eliminate the effects of solids inventory and other influencing parameters on the hydrodynamic characteristics, the whole experimental work in this study was carried out with a constant particle mass of 400 kg stored in the downcomer and the storage tank.

The entire fluidized bed system uses aluminum as the main construction material with small portions made of Plexiglas for visual observation. In order to minimize possible electrostatic charges formed in the columns during the experiments, the whole fluidized bed system is electrically grounded. A measuring device for solids circulation rate is installed in the top section of the downcomer. By regulating the ball valve located in the solids feeding line connecting the storage tank and the riser column, the solids circulation rate can be adjusted and maintained at the desired level during each experiment. The fluidization gas used in this study is air at ambient temperature, supplied by a large compressor capable of delivering 1000 SCFM at 100 psi.

8.2.2 Measurements of solids holdup

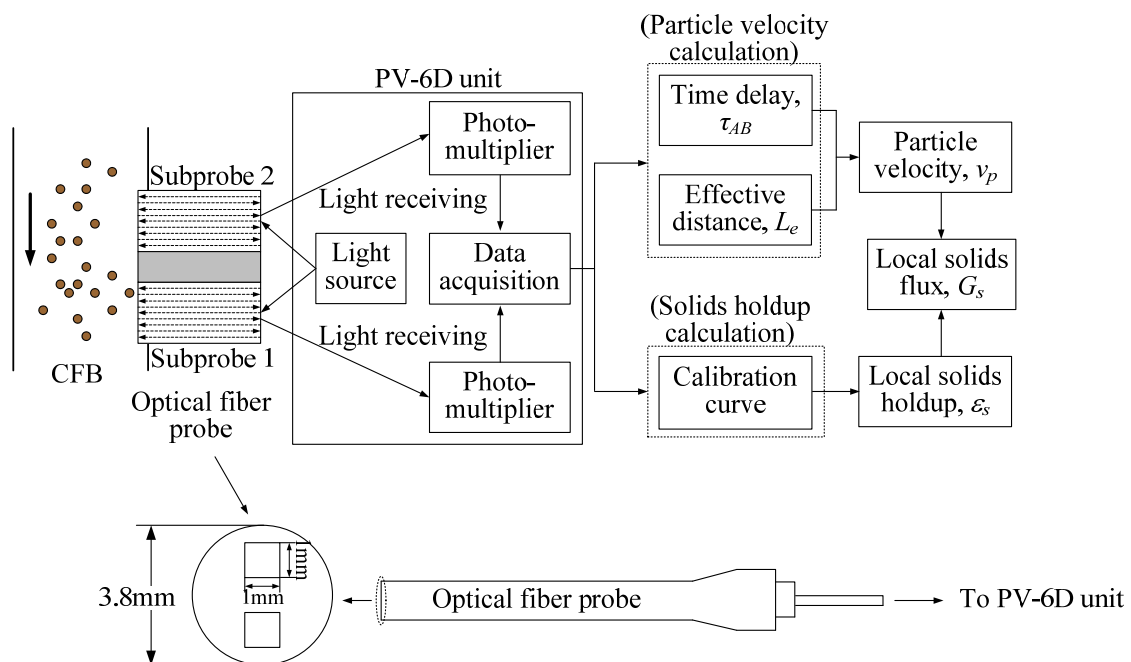


Figure 8.2 Schematic diagram of the novel optical fiber probe and its working principle.

Experimental measurements include differential pressure, solids concentration (solids holdup) and ozone concentration. Twenty pressure taps were installed along the CFB column and connected with 19 differential pressure transducers (Omega PX162) to measure the axial profiles of the pressure gradient. The pressure gradient is mainly used to double check the solids holdup measured by an optical fiber probe mentioned below. Local solids holdup and particle velocity are measured simultaneously using a novel reflective-type optical fiber probe which has been shown to be effective and accurate for measuring the local solids concentration and particle velocity in high velocity fluidized beds and thus has been widely used by many investigators (Herbert *et al.*, 1994; Johnsson *et al.*, 2001; Liu *et al.*, 2003 and Ellis *et al.*, 2004). It yields high signal-to-noise ratios and is nearly free of interference by temperature, humidity, electrostatics and electromagnetic field. Moreover, its small size does not significantly disturb the overall flow structure in CFB systems with proper design. The optical fiber probe used in this work are model PV6D, developed by the Institute of Processing Engineering, Chinese Academy of Sciences, Beijing, China. The probe and measurement procedure are schematically shown in Figure 8.2. The outer diameter of the probe is 3.8 mm. The probe has two subprobes. Each of the subprobes consists of 8000 fine quartz fibers. The effective distance of the two vertically aligned subprobes is 1.51 mm, and the active tip area of each subprobe is 1×1 mm. Each subprobe consists of many quartz fibers with a diameter of $15 \mu\text{m}$, for light-emitting and receiving, arranged in alternating arrays. In order to prevent particles from occupying the blind zone, a glass cover of 0.2 mm thickness is placed over the probe tip. The underlying theory is elaborated by Liu *et al.* (2003).

As shown in Figure 8.2, light from the source illuminates a measuring volume of particles through the light-emitting fibers. The received light reflected by the particles is captured by light receiving fibers and processed by a photo-multiplier. The light intensity is then converted into voltage signals and the voltage signals are further amplified and fed into a PC. The voltage signal obtained by the probe is converted to volumetric concentration using a calibration equation. The relationship between the output signals of the optical fiber probe and the local solids holdup (non-linear) is first established through proper a calibration based on the method developed by Zhang *et al.* (1998).

From the voltage time series $V(t)$ and the calibration equation, local instantaneous solids holdup, $\varepsilon_s(t)$, can be calculated:

$$\varepsilon_s(t) = f[V(t)] \quad (8.1)$$

where, f is the calibration function. The time-mean solids concentration ε_s can be given by integrating $\varepsilon_s(t)$ over the time period, T :

$$\varepsilon_s = \frac{1}{T} \int_0^T \varepsilon_s(t) dt \quad (8.2)$$

The cross-sectional average solids holdup $\bar{\varepsilon}_s$, can be calculated as follow:

$$\bar{\varepsilon}_s = \frac{1}{\pi R^2} \int_0^R 2\pi r \varepsilon_s dr = \frac{2}{R^2} \int_0^R \varepsilon_s r dr \quad (8.3)$$

8.2.3 Catalyst preparation

Ozone decomposition is a thermodynamically favoured process. It decomposes slowly at room temperature in the absence of catalysts, so catalysts are necessary for ozone decomposition at lower temperatures (Cotton and Wilkinson, 1972; Dhandapani and Oyama, 1997; Lin and Nakajima, 2002 and Wojtowicz, 2005). The noble metals such as Pt, Pd Rh and transition metal oxides such as MnO_2 , Co_3O_4 , CuO , Fe_2O_3 , NiO and Ag_2O etc, are the active catalysts for ozone decomposition reaction, (Dhandapani and Oyama, 1997). In view of the high cost of noble metals, the metal oxide catalysts are usually preferred for ozone decomposition reactions. Catalyst supports include $\gamma\text{-Al}_2\text{O}_3$, SiO_2 , TiO_2 , zeolite, activated carbon (or carbon fibrous materials) or a combination of these (Dhandapani and Oyama, 1997 and Kirschner, 2000).

The equilibrium FCC particles, impregnated with ferric nitrate are used as catalysts. FCC particles, which are primarily composed of porous amorphous aluminum hydrosilicate are activated by impregnating in a 40% (wt) solution of ferric nitrate overnight. The soaked particles are then dried and calcinated in an oven with a hood at 450 °C for 4 hours until no NO_2 is released. During the calcinations, the ferric nitrate is converted to ferric oxide, which is the active component for the ozone decomposition reaction. The agglomerates formed during this

process are then grinded by a ball mill and sifted using a standard sieve with 250 μm pore size. The Sauter mean diameter and the particle density is 76 μm and 1780 kg/m^3 respectively. The particle size distribution is listed in Table 8.1.

Table 8.1 Size distribution of the FCC particles.

Particle Size (μm)	Volume Fraction (%)
0-20	0.61
20-40	9.72
40-60	26.32
60-80	22.80
80-130	33.24
>130	7.31

8.2.4 Ozone generation and testing

An ozone generator using the corona discharge method (Model AE15M, manufactured by Absolute Ozone Inc.) is used in this study. Using bottled oxygen as gas supply, it produces up to 30 g/h of ozone depending on the oxygen flow rate and electrical current settings. Its working pressure is 5-50 psig, with oxygen flow rate of 0.1-10 standard liter per minute (SLPM). The oxygen flow rate into the generator was controlled by two rotameters (VWR, Catalog Number: 97004-648) ranging from 0 to 10 liter per minute (LPM). The ozone/oxygen mixture exiting from the ozone generator is mixed with the main fluidization air before entering the CFB riser or downer. With a fairly long flow path and several L-bends in the main air feeding lines, the mixing process was thorough. To ensure that the ozone stream could be easily and smoothly injected into main air flow of the CFB riser/downer with a pressure of less than 30 psig (for safety reasons, the 100 psig air source is reduced to a maximum feeding pressure of 30 psig), an output pressure of 50 psig is used for the regulator installed on the oxygen gas cylinder, maintaining a much higher pressure for the ozone flowing from the ozone generator. The

resulting initial ozone concentration (C_0) in the main air before ozone decomposition in the CFB columns is set to 80-100 ppm.

An ozone analyzer (Model 49i, Thermo Electron Inc.) that employs the UV photometric method of measurement was used to measure the amount of ozone in the ozone-air sample. It is a dual-cell photometer, having both sample and reference air flowing at the same time. Each cell has a length of 37.84 cm and an inner diameter of 0.91 cm, with the internal surfaces coated with polyvinylidene fluoride (PVDF) to ensure that ozone undergoes no decomposition upon exposure to the internal surface of the cells (Thermo Electron Inc., 2004 and 2005). The ozone analyzer had a measuring range of 0.0001-200 ppm with a resolution of 0.0001 ppm. The response time of the apparatus is 4 s. The ozone concentration output was displayed on an LCD screen. The UV source in the ozone analyzer is a 254 nm mercury lamp.

Considering the fact that ozone is highly oxidative, to reduce ozone loss in the sampling pathway to ozone analyzer, ozone-inert materials (e.g. stainless steel, copper, aluminum and Teflon) are used for the sampling probes, valves, and piping lines (Teflon, 3 mm i.d., 6 mm o.d.). Gas samples are continuously drawn from the CFB column through a sampling system shown in Figure 8.1 using the brass tubes (6 mm o.d. and 0.36 mm wall thickness) as the sampling probes. The tip of the probe is covered with a fine stainless steel mesh to prevent particles from being entrained into the sampling system. The velocity of gas sucked for sampling was 1.5 LPM and low enough to assure minimal disturbance of the flow structure in CFB system. A high pressure purging air stream of 100 psig is introduced to blow away any particles potentially caked in the sampling probes.

When measuring ozone concentration in the CFB riser/downers, 4-5 g of particles are taken out from the column for catalytic activity check using the fixed bed reactor before and after each experiment. No significant change is observed in reaction rate constant (k_r) before and after several hours of CFB run, so that the ozone concentration profiles obtained under the experimental period is assumed to be under the same particle catalytic reactivity. The average value from these two tests is taken as the reaction rate constant.

In order to map the entire cross-section of the downer, ten axial measuring ports ($z = 0.22, 0.61, 1.12, 1.63, 2.13, 2.64, 3.26, 4.02, \text{ and } 4.99$ m below the gas distributor) are installed along the column. Measurements were conducted at six radial positions ($r/R = 0, 0.316, 0.548, 0.707, 0.837$ and 0.950 , where r is the distance from the center and R is the downer radius) on each axial level of the CFB downer system. These positions are determined by dividing the column cross-section into five equal areas and determining the mid-point of each of these areas. For the hydrodynamic experiments, voltage signals from the optical fiber probe are sampled at a high frequency of 100 kHz with 1,638,40 data points for each measurement. To get the valid and repeatable data, all measurements are repeated at least 5 times for each location. For the catalytic ozone decomposition, measurement is started after steady state has been reached in the CFB systems, which usually takes about at least 1 hour (Li, 2010). Ozone sampling is conducted for 1 min where the ozone concentration is fairly stable.

8.3 Results and discussion

8.3.1 Radial profiles of ozone concentration

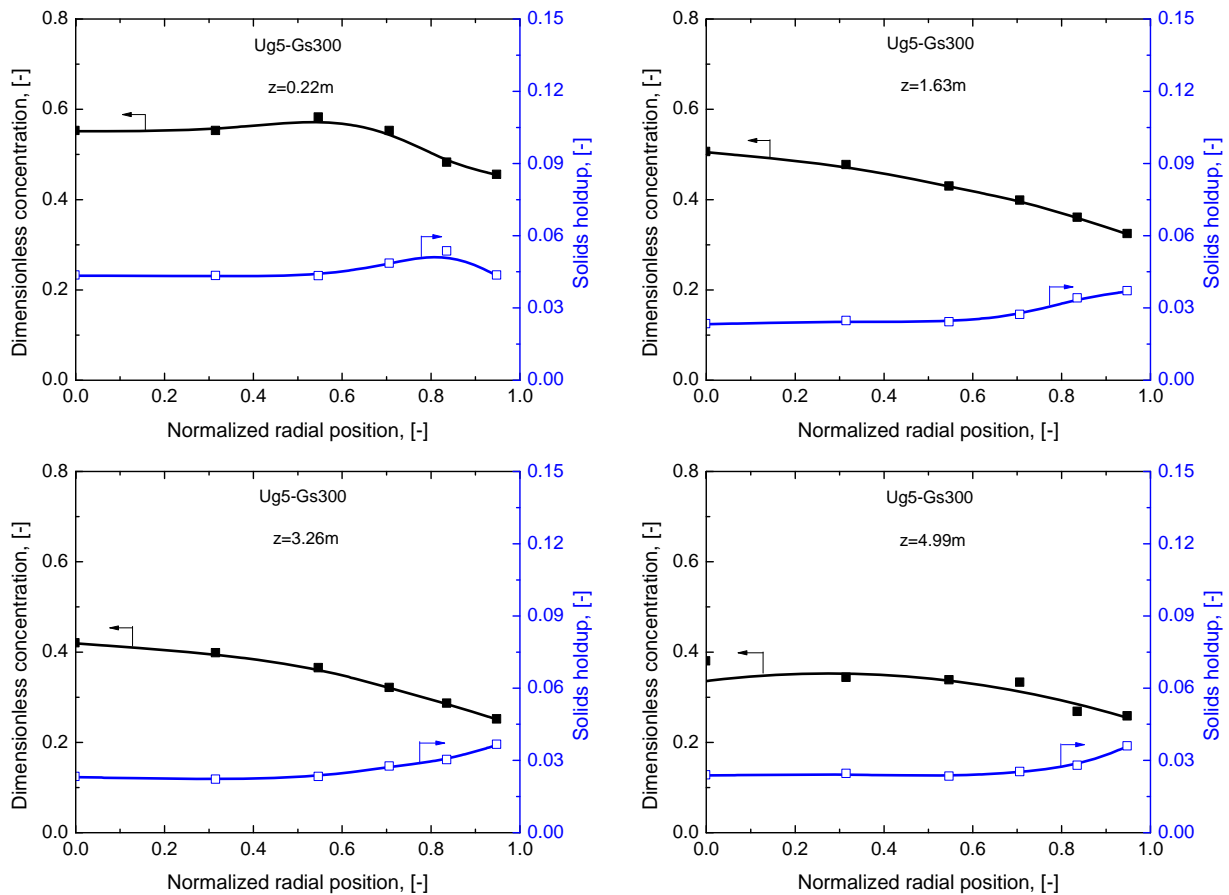


Figure 8.3 Radial profiles of dimensionless ozone concentration and the corresponding solids holdup.

Figure 8.3 shows the typical radial distribution of ozone concentration and the corresponding radial solids holdup profiles along the column at the superficial gas velocity of 5 m/s and solids circulation rate of 300 kg/m²s. Ozone concentrations are presented in the form of “dimensionless concentration” which is defined by ratio of the actual ozone concentration (C) measured at a certain radial position to the initial concentration (C_0) at the downer inlet. Ozone concentration is not very uniform along the radial direction. Near the entrance of the downer, the radial profile of the ozone concentration is almost flat in the central region, and decreases gradually near the wall. With increasing the bed height down the column, the radial profiles become more uniform in the

central region followed by a small decrease near the wall. These radial profiles are well correlated with the radial distribution of solids holdup shown in Figure 8.3. The solids radial flow structure is nonuniform with higher solids holdup near the wall leading to high gas-solids interactions, so that the unconverted ozone concentration is lower near the wall than that in the central region. With the flow development along the column, the radial distributions of the solids holdup become more uniform, consistent with the radial profiles of ozone concentration.

8.3.2 Axial profiles of ozone concentration

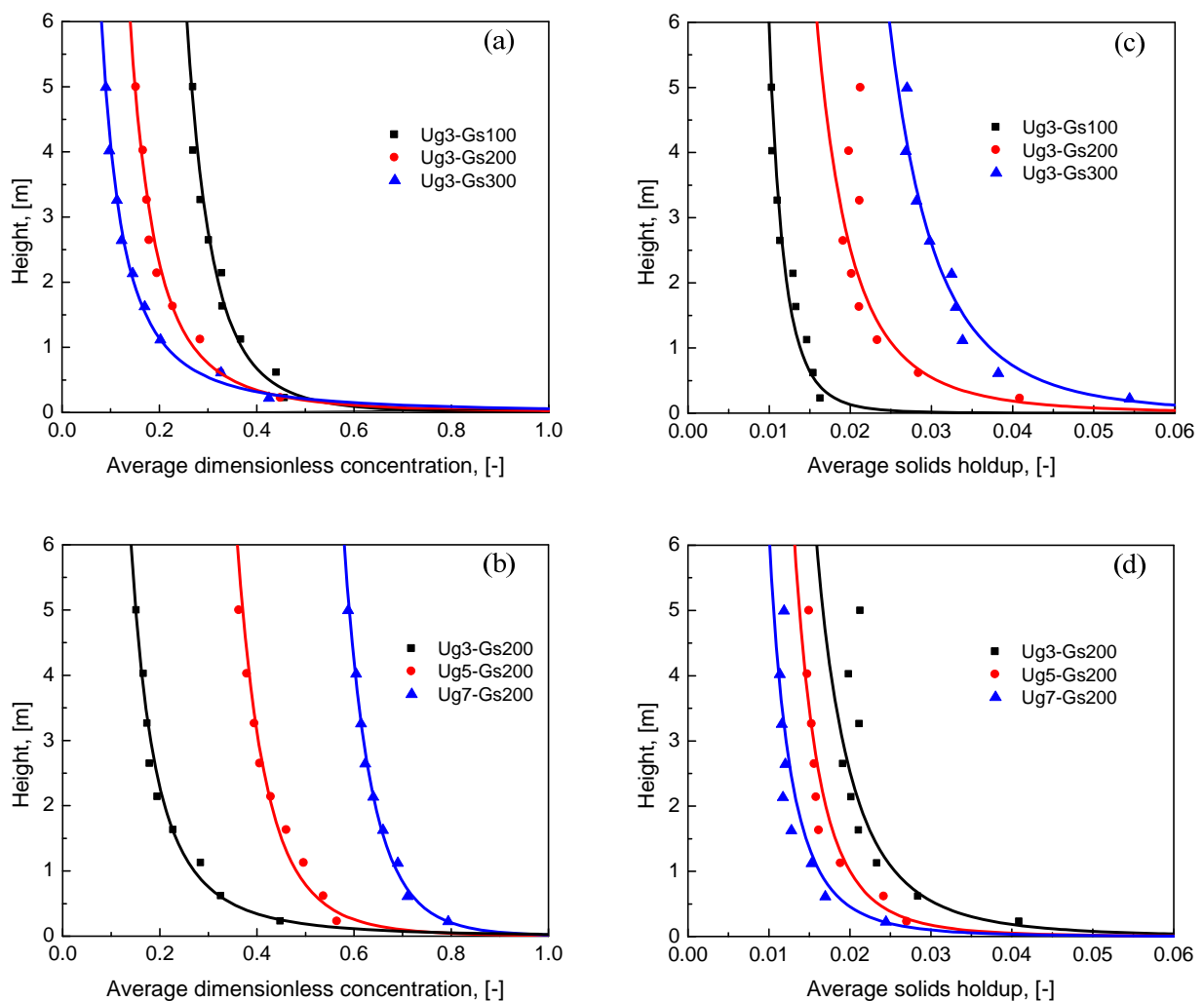


Figure 8.4 Axial profiles of the average dimensionless ozone concentration and the corresponding solids holdup.

The cross-sectionally averaged ozone concentration profiles under different operating conditions in the downer are shown in Figures 8.4 and 8.5. The average ozone concentrations are obtained by averaging the ozone concentration at six radial positions for each axial level. In general, the unconverted ozone concentration decreases significantly near the entrance of the column and gradually approach a nearly constant value further down the downer. These axial distribution profiles are consistent with those of solids holdup. From Figure 8.4, it can also be seen that larger axial gradient of ozone concentration occurs when the solids circulation rates are higher and/or when the superficial gas velocities are lower. This is reasonable since a higher solids circulation rate and/or lower gas velocity can results in higher solids holdup and thus higher ozone conversion.

There are three different solids flow regions along the axial direction in the downer: 1) first acceleration zone, 2) second acceleration zone and 3) the constant velocity zone (Kwauk, 1964; Yang *et al.*, 1991; Zhu *et al.*, 1995; Ma and Zhu, 1999 and Zhang *et al.*, 1999 and 2001). In the first acceleration zone near the distributor, gas velocity is high while particle velocity is near zero. Solids are accelerated by both gravity and gas drag force until the particle velocity is equal to the gas velocity. In the second acceleration, particles are farther accelerated by gravity, but resisted by the gas drag (in the upward direction against gravity). Particle velocity then overtakes the gas velocity and increase further until gas drag on the particle counter-balances the gravity. After this region, both particle and gas velocities remain constant downstream, where particles travel faster than gas, but with a constant slip velocity. The axial ozone concentration and solids holdup variations also follow this three-section axial flow structure as shown in Figure 8.4. Both ozone concentration and solids holdup decrease sharply in the first acceleration zone, then the trend becomes much wider further down the column. In the constant velocity section, the ozone concentration and solids holdup remain almost unchanged.

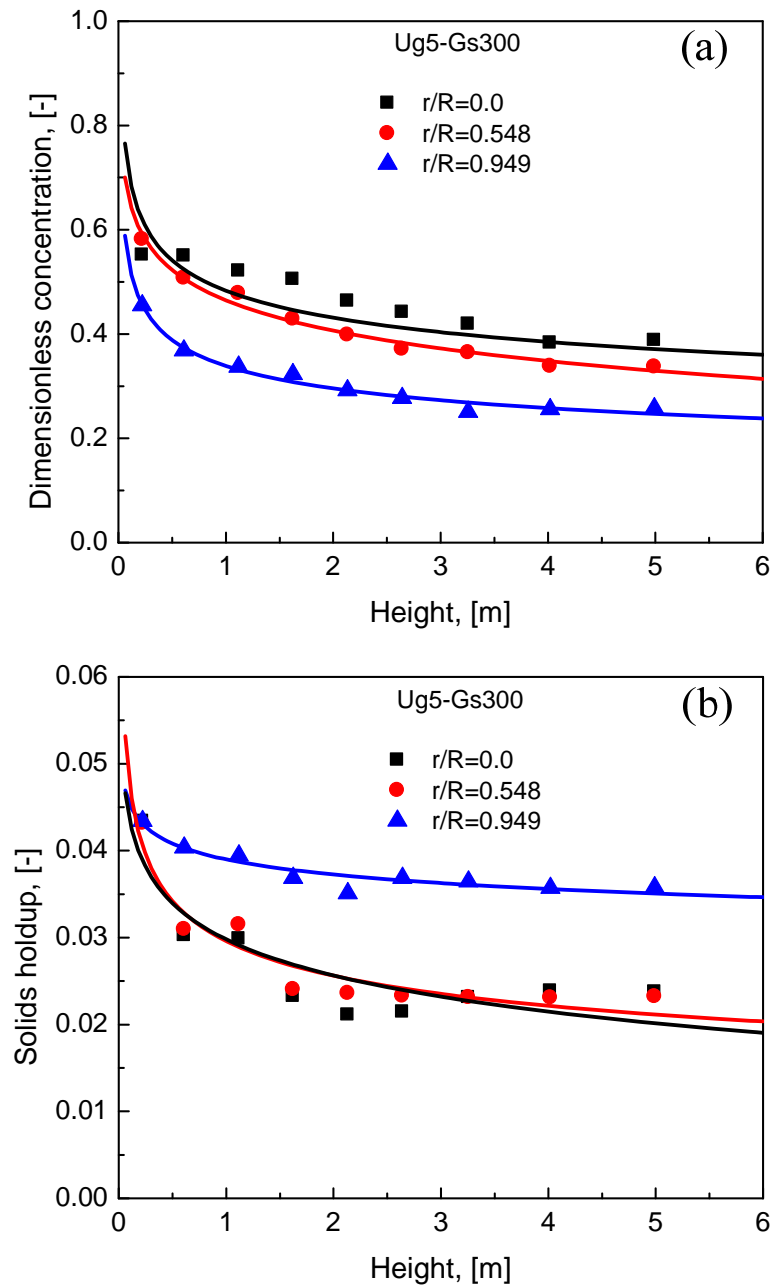


Figure 8.5 Axial profiles of dimensionless ozone concentration and the corresponding solids holdup at different radial positions.

Figure 8.5 shows the axial ozone concentration profiles at different radial positions. The corresponding solids holdup distributions are also given in the Figure. Compared the ozone changes at the three different radial positions, it is seen that smaller differences between the

ozone concentration profiles at $r/R = 0.0$ and $r/R = 0.548$, which correspond to the solids holdup variation against axial elevation. Moreover, ozone concentrations at all radial positions decrease sharply along the axial direction in the first region. The variation becomes less dramatic in the second section and finally becomes nearly negligible in the third section.

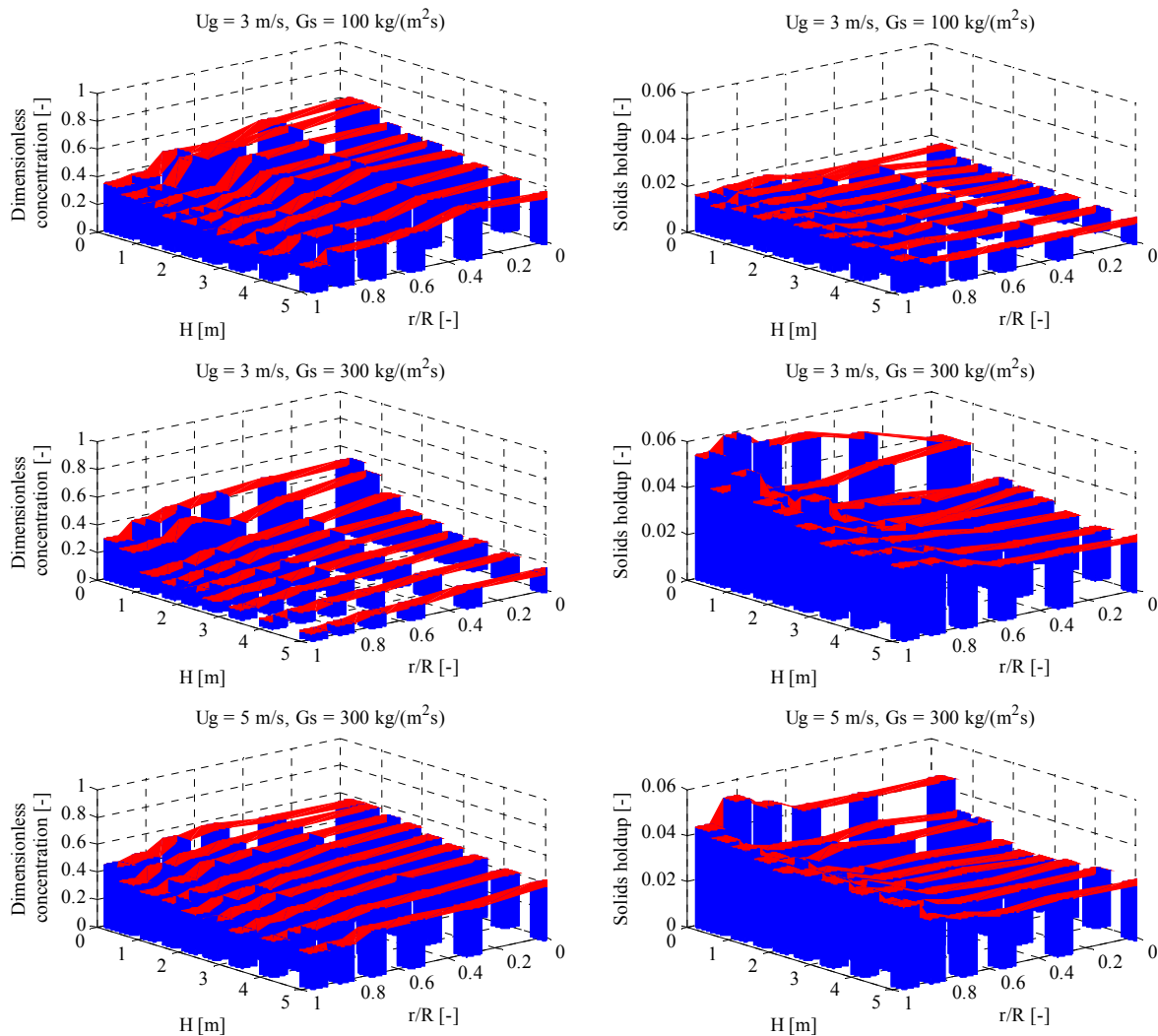


Figure 8.6 Overall view of the dimensionless ozone concentration and the corresponding solids holdup at different operating conditions.

Based on the above discussion, Figure 8.6 provides an overall view of the ozone concentration profiles in the downer under various operating conditions, where x and y axes are the radial and axial positions in the column, and z -axis is the dimensionless ozone concentration. It is observed

that with the increase of downer elevations, more ozone reactants are converted due to its extended contact with the catalyst particles, giving decreased ozone concentrations. Ozone concentration in the central region is a little bit higher than that in the near wall region. The radial ozone concentration distribution also becomes uniform further down along the reactor. The variation of the ozone concentration is consistent with that of the solids holdup shown in the righthand of Figure 8.6.

The distribution of ozone concentration is affected by the operating conditions. Higher U_g and/or low G_s results in more uniform distribution of ozone concentration in both axial and radial directions. For example, at low solids circulation rate ($G_s = 100 \text{ kg/m}^2\text{s}$) and high gas velocity ($U_g = 5 \text{ m/s}$), the ozone concentration profiles are nearly constant along the column.

8.3.3 Effect of operating conditions on ozone concentration

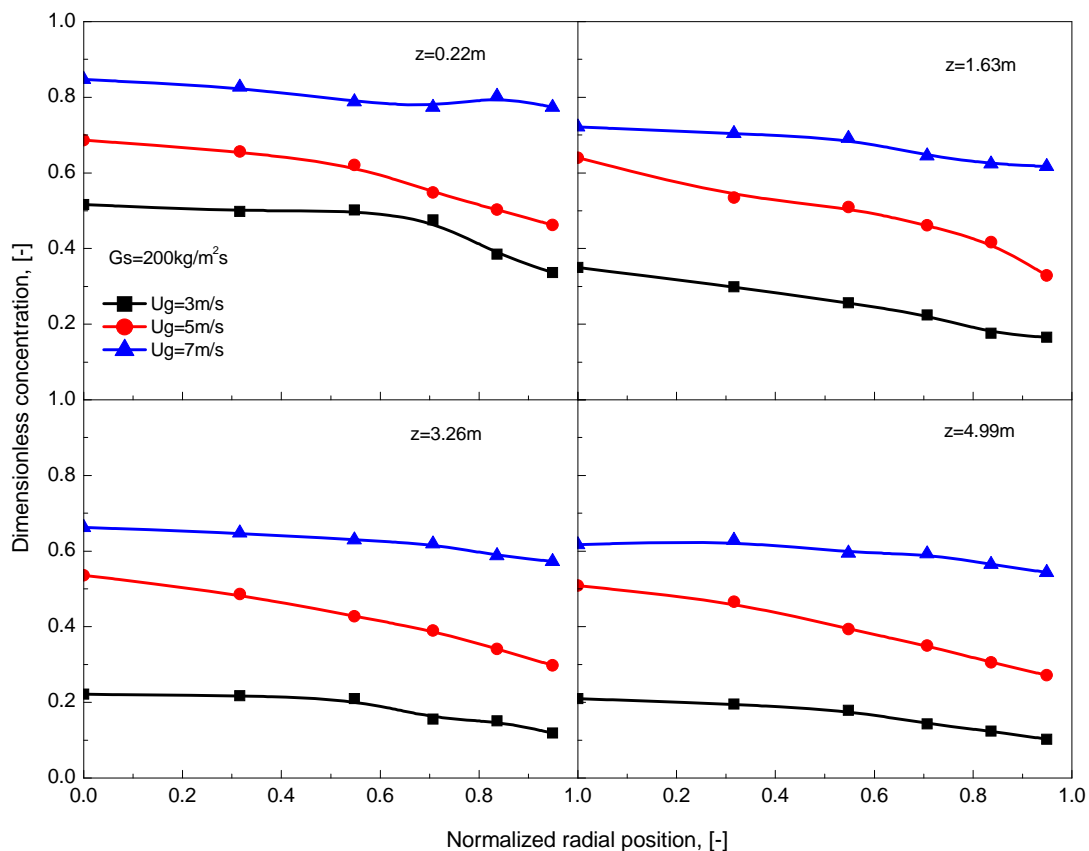


Figure 8.7 Effects of superficial gas velocity on the dimensionless ozone concentration.

The effect of superficial gas velocity on ozone conversion is presented in Figure 8.7. Generally, the concentration of the unconverted ozone increases with increasing the superficial gas velocity, at a fixed solids circulation rate of $200 \text{ kg/m}^2\text{s}$. This may be attributed to the following mechanisms: when solids circulation rate remains constant, increasing superficial gas velocity reduces the solids holdups. The decrease in solids holdup would result in the decrease of total gas-solids contacting area which is not favourable for the reaction. On the other hand, increasing superficial gas velocity leads to a short residence time of both gas and solid phases, which is not beneficial to the total conversion of ozone. Considering the above two factors, the increase of superficial gas velocity will cause the decrease of the ozone conversion. In addition, increasing U_g can lead to a more uniform radial profile of solids holdup and therefore of ozone concentrations.

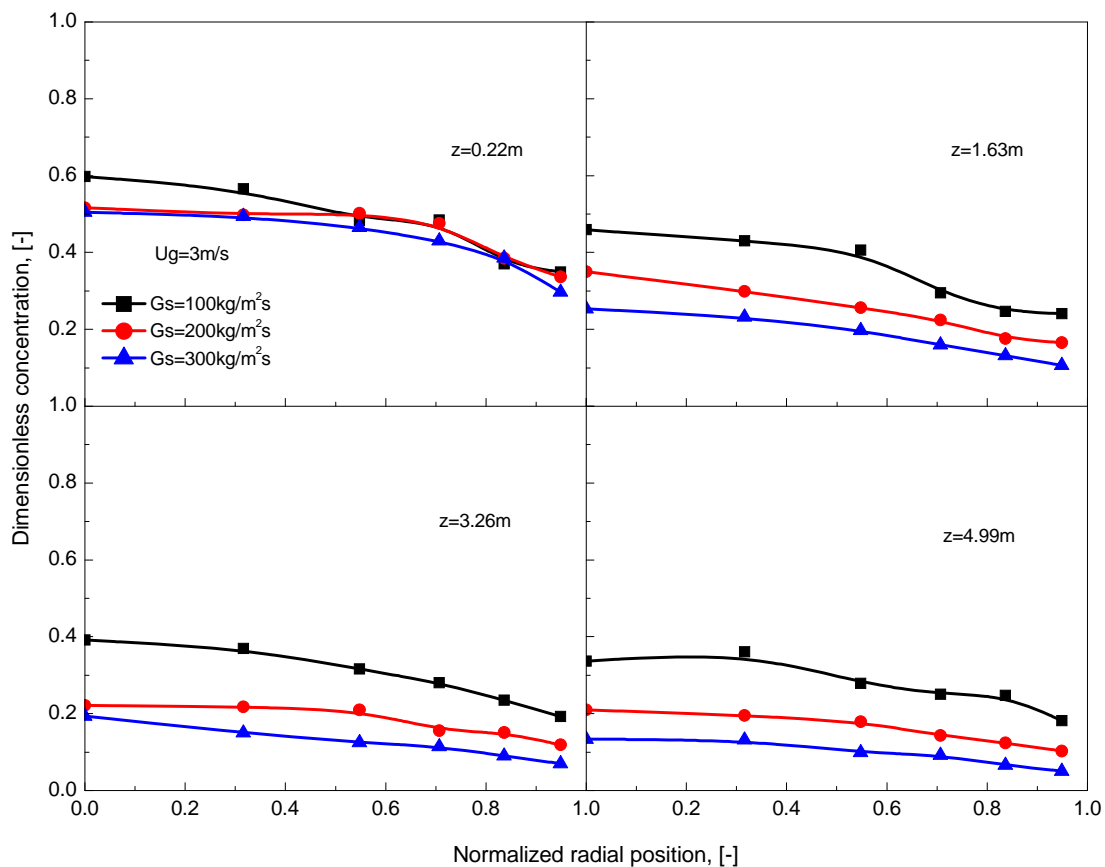


Figure 8.8 Effects of solids circulation rate on the dimensionless ozone concentration.

The effect of solids circulation rate on radial profiles of dimensionless ozone concentration at four axial levels under $U_g = 3$ m/s is shown in Figure 8.8. At all axial levels, the dimensionless ozone concentration decreases with an increase of solids circulation rate under the same superficial gas velocity of 3 m/s. This is due to the solids holdups increase with increasing solids circulation rate. Under the high density operating conditions, the total gas-solids contacting area for reaction and mass transfer between gas and solids will also increase leading to significant rise of the ozone conversion. Therefore, ozone concentration becomes much lower as solids circulation rate increases. At the same bed height, the radial distribution of the ozone concentration becomes more uniform with reduced G_s due to the increased radial uniformity of the solids flow structure. Interestingly, that the effect of solids circulation rate on ozone conversion seems to be much more significant in both second acceleration and fully developed regions than that in the first acceleration zone (near the distributor). The possible reason is that solids holdup is usually relatively high near the distributor. A change in solids circulation rate may not result in a significant change in solids holdup in the first acceleration region. On the other hand, in the following two regions, particle velocity is high and solids holdup is relatively low. Increasing solids circulation rate will lead to a more dramatic increase in solids holdup which in turn causes high ozone conversion in those zones.

8.3.4 Relationship between solids holdup and ozone concentration

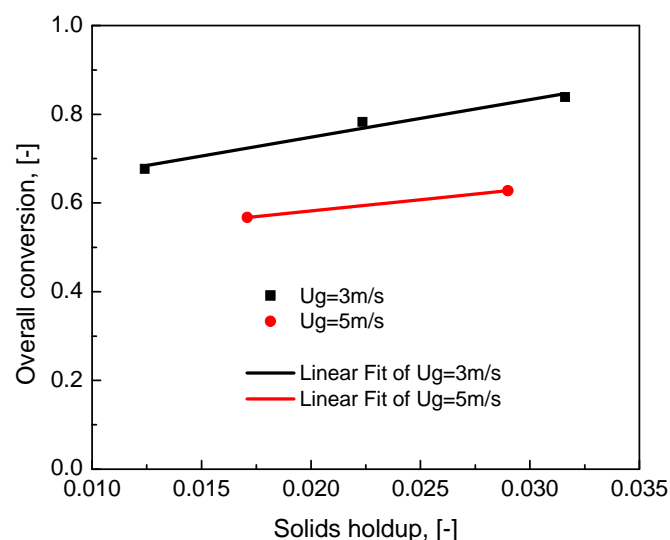


Figure 8.9 Relationship between overall ozone conversion and solids holdup.

As stated before, the distribution of ozone concentration is essentially dominated by the flow structure, which can be partially represented by the solids holdup profiles in the CFB reactors. To further evaluate the effects of the solids holdup on ozone concentration, the overall conversion of ozone is plotted against the mean solids holdup in the entire column as shown in Figure 8.9.

In general, the conversion of ozone increases with the solids holdup, as confirmed by other researchers (Jiang *et al.*, 1991 and Li *et al.*, 2011 and 2013). There appears to be a linear relationship between total ozone conversion and mean solids holdup as shown in Figure 8.9. The influence of solids holdup on ozone conversion is nearly the same with almost the same slope of the fitting lines under different superficial gas velocities. This phenomenon is different from that in the riser, where the effects of solids holdup on ozone conversion are more significant under high superficial gas velocity compared to low gas velocity cases (details can be found in chapter 7). This might be due to the different hydrodynamics in the two kinds of CFB reactors.

In CFB riser, higher solids holdup under higher superficial gas velocity plays a much more significant role in the overall conversion. The reason is that at low superficial gas velocities, the increase of solids holdup probably leads to the increase of cluster formation. The gas-solids mass transfer within the clusters is not as good as that between dispersed particles and the gas flow. Under high superficial gas velocity conditions, the high gas velocity can break down the clusters in addition to enhancing the gas-solids contact efficiency. Therefore, the overall conversion of reactant can be increased rapidly with solids holdup under high superficial gas velocity.

On the other hand, the uniform distribution of solids holdup in the downer reactor is one of the key advantages over the upflow riser reactor. This is mainly because particles are not supported by the gas flow, but flow down due to the gravity, either reinforced or resisted by the drag force from the gas flow. In addition, the aggregation of particles at the wall region can also be prevented in the downer. When particle clusters are formed, the effective drag force on the cluster is reduced so that the slip velocity becomes higher leading to a high particle downwards velocity (Yang *et al.*, 1993; Zhang *et al.*, 1999). The increased particle velocity in turn increases the instability of the cluster because of the increased shear force on them. Large particle cluster

is easily broken down into smaller ones or even isolated particles in CFB downer reactors. Therefore, the increase in solids holdup will enhance the gas-solids contacting efficiency leading to higher reactant conversion.

8.3.5 Reactor performance

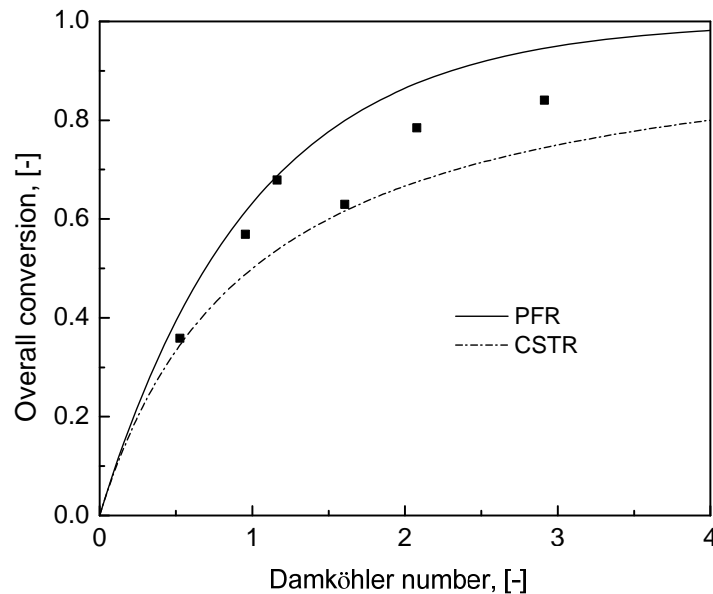


Figure 8.10 Effects of Damköhler number on overall ozone conversion.

The performance of the CFB reactors is related to both hydrodynamics and the chemical reactions. To investigate the effects of hydrodynamics on the chemical reaction, it is better to plot the results of two typical reactor models: a plug-flow reactor (PFR) and the continuous stirred-tank reactor (CSTR) for comparison. Both of the two model reactors have been idealized in hydrodynamics with respect to mixing between gas and solids phases. Equations for the conversion in PFR and CSTR can be derived as follows (Levenspiel, 1998).

Plug flow reactor

$$X_{PFR} = 1 - \exp(-k_r') \quad (8.4)$$

Continuous stirred-tank reactor

$$X_{CSTR} = \frac{k_r'}{1+k_r'} \quad (8.5)$$

where k_r' is the Damköhler number ($k_r' = k_r \varepsilon_s (1 - \varepsilon_s) H / U_g$).

The overall conversion of ozone for the downer is plotted against Damköhler number as well the calculated curves for PFR and CSTR models are shown in Figure 8.10. It seems that the conversion in the CFB system is generally less than that in the ideal plug flow reactor but could be larger than that in the continuous stirred-tank reactor. This demonstrates that the two ideal models, which idealize bed hydrodynamics in the reactor, cannot well predict the observed conversions, which implies in turn that hydrodynamics affects the chemical reaction in CFB downer. Moreover, the overall conversion increases with increasing Damköhler number, which is consistent with the effects of solids holdup on the overall conversion. This indicates that the solids holdup is the main factor affecting the ozone reaction and increasing solids holdup would increase reactant conversion. In addition, the extent of the deviation of the conversion can be attributed to the different gas-solids contacting efficiency requiring more investigation.

8.4 Conclusions

Ozone decomposition is experimentally studied in a high flux gas-solids circulating fluidized bed downer at superficial gas velocity of 3-7 m/s and solids circulation rates from 100 to 300 kg/m²s.

The axial and radial distribution profiles of the ozone concentration are consistent with the corresponding profiles of the solids holdups which indicate that ozone reaction in the downer is controlled by the gas-solids flow.

High ozone conversion at the entrance region of the downer indicating that the initial gas-solids contact plays a key role in the reaction yield and more attention needs to be paid on the downer distributor design, which is important to gas-solids mixing.

Ozone conversion increases with the solids circulation rate under the same superficial gas velocity due to the increase of solids holdup. The conversion decreases with gas velocity at a fixed solids circulation rate due to the associated reduction in solids holdup.

The values of calculated overall conversion are smaller than those obtained based on the ideal plug flow reactor model indicating that hydrodynamics affects the chemical reaction in the CFB downer reactor. The extent of the deviation of the conversion can be attributed to the different gas-solids contacting efficiency.

Nomenclature

f	calibration function for optical fiber probe
F_s	solids flux [kg/(m ² ·s)]
\bar{G}_s	cross-sectional average solids flux [kg/(m ² ·s)]
$\bar{G}_{s,L}$	time mean local solids flux [kg/(m ² ·s)]
G_s	solids circulation rate [kg/(m ² ·s)]
L_e	effective distance between light-receiving fiber A and B [m]
r/R	reduced radial sampling positions
$RNI(\varepsilon_s)$	radial nonuniformity index of solids holdup
$RNI(V_p)$	radial nonuniformity index of particle velocity
t	time [s]
T	time interval [s]
U_g	superficial gas velocity [m/s]
v_p	particle velocity [m/s]
\bar{v}_p	cross-sectional average particle velocity [m/s]
V	voltage [volt]
$V(t)$	voltage time series [volt]
z	axial coordinate, or distance from gas distributor [m]

Greek letters

ε_s	solids holdup [-]
$\varepsilon_s(t)$	local instantaneous solids holdup [-]
$\bar{\varepsilon}_s$	average solids holdup in the entire column [-]

Subscripts

1, 2	subprobe 1 and 2 of optical fiber probe
g	gas

p particle
 s solids

References

- Abbasi A., Islam MA., Ege PE. and de Lasa HI., (2013), CPFD flow pattern simulation in downer reactors. *AIChE Journal* 59(5), 1635-1647
- Bassi AS., Briens CL, and Bergougnou MA., (1994), Short contact time fluidized reactors (SCFTRs). In, Avidan, A. (Ed). *Circulating fluidized bed technology. IV.* AIChE, New York, 15-19
- Chen H. and Li H., (2004), Characterization of a high density downer reactor. *Powder Technology* 146, 84-92
- Chen H., Li H. and Tan, S., (2006), Mechanism of achieving a dense downer, modeling and validation. *Industrial and Engineering Chemistry Research* 45, 3488-3495
- Cheng Y., Wu C., Zhu JX., Wei F. and Jin Y., (2008), Downer reactor, from fundamental study to industrial application. *Powder Technology* 183, 364-384
- Cotton FA. and Wilkinson G., (1972), *Advanced Inorganic Chemistry*, Wiley, New York
- Deng R., Liu H., Wei, F. and Jin Y., (2004), Axial flow structure at the varying superficial gas velocity in a downer reactor, *Chemical Engineering Journal* 99(1), 5-14
- Deng R., Liu H., Gao L., Wang L., Wei F. and Jin Y., (2005), Study on the FCC process in a novel riser-downer-coupling reactor (ii), Simulation and hot experiments, *Industrial and Engineering Chemistry Research* 44(5), 1446-1453
- Dhandapani B, and Oyama S., (1997), Gas phase ozone decomposition catalysts, *Applied Catalysis B, Environmental* 11(2), 129-166
- Ellis N., Bi HT., Lim CJ. and Grace JR., (2004), Influence of probe scale and analysis method on measured hydrodynamic properties of gas-fluidized beds, *Chemical Engineering Science* 59(8-9), 1841-1851
- Fan C., Bi X., Lin W. and Song W., (2008a), Mass transfer and reaction performance of the downer and its hydrodynamic explanation, *The Canadian Journal of Chemical Engineering* 86(3), 436-447
- Fan C., Zhang Y., Bi X., Song W., Lin W. and Luo L., (2008b), Evaluation of downer reactor performance by catalytic ozone decomposition, *Chemical Engineering Journal* 140(1-3), 539-554
- Grace JR. and Bi H., (1997), Introduction to circulating fluidized beds, in *Circulating Fluidized Beds* (editor(s), Grace, JR.; Avidan AA. & Knowlton TM.), Engineering Foundation, New York, 1-19

Guan GQ., Fushimi C. and Ishizuka C., (2011), Flow behaviors in the downer of a large-scale triple-bed combined circulating fluidized bed system with high solids mass flux. *Chemical Engineering Science* 66, 4212-4200

Herbert PM., (1999), Hydrodynamics study of a downflow circulating fluidized bed. Ph.D. Dissertation, The University of Western Ontario, London Canada

Johnston PM., de Lasa HI. and Zhu JX., (1999), Axial flow structure in the entrance region of a downflow fluidized bed---effects of the distributor design. *Chemical Engineering Science*, 54,2161-2173

Johnsson H, and Johnsson F., (2001), Measurements of local solids volume-fraction in fluidized bed boilers, *Powder Technology* 115, 13-26

Kirschner MJ., (2000), Ozone, in *Ulmann's Encyclopedia of Industrial Chemistry*, Wiley-VCH Verlag GmbH & Co. KGaA

Levenspiel. O., (1998), *Chemical Reaction Engineering*. 3rd ed. New York, Wiley

Li DB., Zhu J., Ray MB., and Ray AK., (2011), Catalytic reaction in a circulating fluidized bed downer, Ozone decomposition, *Chemical Engineering Science* 66 (20), 4615-4623

Li DB., (2010), Investigation of circulating fluidized bed riser and downer reactor performance for catalytic ozone decomposition, Ph.D. Diss. The University of Western Ontario

Lin J. and Nakajima T., (2002), An AM1 study of decomposition of ozone on a Cu (110) surface, *Ozone, Science & Engineering, The Journal of the International Ozone Association* 24(1), 39-47

Liu W., Luo KB., Zhu JX. and Beeckmans JM., (2001), Characterization of high density gas-solids downward fluidized flow. *Power Technology*, 115, 27-35

Liu JZ., Grace JR., and Bi HT., (2003a), Novel multifunctional optical-fiber probe, development and validation, *AIChE Journal* 49(6), 1405-1420

Liu JZ., Grace JR., and Bi HT., (2003b), Novel multifunctional optical-fiber probe, high-density CFB measurements, *AIChE Journal*, 49(6), 1421-1432

Luo BL., Yan D., Ma YL., Barghi S. and Zhu J., (2007), Characteristics of gas-solids mass transfer in a concurrent downflow circulating fluidized bed reactor. *Chemical Engineering Journal* 132, 9-15

Ma Y. and Zhu JX., (1999), Experimental study of heat transfer in co-current downflow fluidized bed (downer), *Chemical Engineering Science* 54, 41-50

Ma Y. and Zhu JX., (2000), Heat transfer between gas-solids suspensions and immersed surface in a upflow fluidized bed (riser). *Chemical Engineering Science* 55, 981-989

Nieuwland JJ. and Meijer R., (1996), Measurements of solids concentration and axial solids velocity in gas-solid two-phase flows, *Powder Technology* 87(2), 127-139

Shaikh AA., AlMutairi, EM. and Ino, T., (2008), Modeling and simulation of a downer-type HS-FCC unit. *Industrial and Engineering Chemistry Research* 47, 9018-9024

Wang Z., Bai D. and Jin Y., (1997), Hydrodynamics of concurrent downflow circulating fluidized bed (CDCFB). *Powder Technology* 70, 271-275

Wei F. and Zhu JX., (1996), Effect of flow direction on axial solid dispersion in gas-solids cocurrent upflow and downflow systems, *The Chemical Engineering Journal and the Biochemical Engineering Journal* 64(3), 345-352

Wojtowicz JA., (2005), Ozone, in *Kirk-Othmer Encyclopedia of Chemical Technology*, John Wiley & Sons

Yang YL., Jin Y., Yu ZQ., Wang ZW. and Bai DY., (1991), The radial distribution of local particle velocity in a dilute circulating fluidized bed. In P. Basu, M. Horio and Hasatani, *Circulating fluidized bed technology III*. Toronto, Pergamon Press, 201-206

Yang WC. and Knowlton TM., (1993), L-valve equations. *Powder Technology* 77, 49-54

Zhang H., Johnston PM., Zhu JX., de Lasa HI., and Bergounou MA., (1998), A novel calibration procedure for a fiber optic solids concentration probe, *Powder Technology* 100, 260-272

Zhang H., Zhu, JX. and Bergounou, MA., (1999a), Flow development in a gas-solids downer fluidized bed, *The Canadian Journal of Chemical Engineering* 77(2), 194-198

Zhang H., Zhu JX. and Bergounou, MA., (1999b), Hydrodynamics in downflow fluidized beds (1), solids concentration profiles and pressure gradient distributions. *Chemical Engineering Science* 55, 4367-4377

Zhang H. and Zhu JX., (2000), Hydrodynamics in downflow fluidized beds (2), Particle velocity and solids flux profiles. *Chemical Engineering Science* 55, 4367-4377

Zhang H., Huang WX. and Zhu JX., (2001), Gas-solids flow behavior: CFB riser vs. downer. *AIChE Journal* 47(9), 2000-2010

Zhu JX. and Wei F., (1995), Proc. 8th Int. Conf. on Fluidization, Tours, France, 907-914

Zhu JX., Yu ZQ., Jin Y., Grace JR. and Issangya A., (1995), Cocurrent downflow circulating fluidized bed (downer) reactors - A state of the art review, *The Canadian Journal of Chemical Engineering* 73(5), 662-677

Zhu JX. and Li GZ., (2001), Direct measurements of particle velocities in gas-solids suspension flow using a novel five-fiber optical probe, *Powder Technology* 115, 184-192

Zhu JX. and Manyele SV., (2001), Radial nonuniformity Index (RNI) in fluidized beds and other multiphase flow systems, *The Canadian Journal of Chemical Engineering* 79, 202-211

Zhu JX. and Cheng Y., (2005), Fluidized-Bed Reactors and Applications, Chapter 5.3 in *Multiphase Flow Handbook*, ed. Clayton Crowe, CRC Press, New York, pp 5.55-5.93

CHAPTER 9

Conclusions and Recommendations

9.1 Summary comments on experimental setup and measurements

Hydrodynamics and performance of high density circulating fluidized bed riser/downer reactors are experimentally investigated. Solids fluxes of up to 1000 and 300 kg/m²s are reached in the high density riser and downer, respectively. Ozone decomposition reaction is selected as the model reaction in the experiments. Spent fluid catalytic cracking (FCC) particles impregnated with ferric oxide and activated at high temperature are used as the catalyst for the ozone decomposition reaction. Particles used in this study are the blend of spent FCC particles and activated catalysts. The rate of the reaction can be adjusted by changing the ratio of activated catalyst and spent FCC particles. Catalyst stability can be affected by humidity of the fluidized beds, so that relative humidity and temperature of the feeding air were carefully monitored using a hygrometer, and the air supply was maintained at a constant temperature of 21.9°C and a constant relative humidity of 19%. The reaction rate constant of the catalyst is regularly checked during CFB riser and downer experiments, using a fixed bed reactor installed on side.

All the experiments were carried out in two gas-solids CFB reactors, a CFB riser of 76 mm inner diameter and of 10.2 m high and a 76 mm CFB downer of 5.8 m in height. To minimize ozone loss resulting from contacting with column walls, the main construction materials used for the fluidized bed assembly were ozone-inert aluminum and Plexiglas. The entire fluidized bed system was electrically grounded to remove electrostatic charges formed in the columns.

An optical fiber probe was calibrated and used to measure solids holdup and particle velocity in the riser and downer reactors. To ensure data accuracy, measurements of solids holdup and particle velocity were repeated at least 5 times for each location.

Effort was made to improve ozone sampling and measurement. Brass tubes with fine wire mesh covering the tip were used to extract ozone gas sample from the CFB reactors. Purging by high

pressure air was adopted to blow away particles possibly adhered to the wire mesh, preventing fine particles from blocking it. With these measures taken, data of ozone concentration in the CFB reactor was reproducible and reliable.

Stability of the initial ozone concentration before entering the reactors over a long period of time showed good performance of the ozone generator, and thorough mixing of the main air with O_3/O_2 flow from the ozone generator.

9.2 Conclusions

In this study, a comprehensive investigation was conducted on hydrodynamics and reactor performance in a gas solids circulating fluidized bed system to systematically identify the hydrodynamic characteristics of high density/flux CFB riser and downer on the performance of the CFB reactors, by examining the axial and radial profiles of solids holdup, particle velocity and solids flux and the axial and radial ozone concentration profiles.

To obtain a comprehensive insight into the solids flow structures in a high flux/density (up to 1000 kg/m²s) riser, solids holdup, particle velocity and solids flux distributions and flow development were studied under a wide range of operating conditions.

Solids holdup of up to 0.2-0.3 can be maintained throughout the entire high flux/density riser. A homogenous axial flow structure is observed at $G_s = 1000$ kg/m²s. Radial distributions of the solids holdup in the riser were non-uniform with a dilute region and a dense region. When G_s exceed about 700 kg/m²s, the dilute core region shrinks to less than 20% of the cross-sectional area. Solids holdups thereafter increase monotonically towards the wall which can be up to 0.59. Moreover, the solids holdup remains higher than 0.4 over a wide cross-sectional area ($r/R = 0.7$ -1.0, about 60% of the cross-sectional area) even at the top section of the riser. The radial profile of solids holdup under high G_s is a concave parabolic curve. The solids holdup remains low and relatively constant at the riser center, suggesting very quick solids flow development in the riser center at the bottom section. In the wall region, however, the flow development is slower, with the solids holdup near the wall decreasing slowly toward the riser top. Increasing solids flux prolongs the solids flow development.

Better gas-solids contacting and mixing indicated by standard deviation and intermittency index of local solids holdups at high solids fluxes can lead to vigorous interactions between gas and solids phases, improving the reactor performance.

Particle velocity and solids flux are also the important parameters in the study of hydrodynamics, crucial in the better understanding of the flow structure in a high flux/density circulating fluidized bed. Local particle velocity and solids flux are investigated at $G_s = 1000$ kg/m²s, along

with the study of solids holdup, using an optical fiber probe, which can measure the solids concentration and velocity simultaneously.

For all operating conditions, the cross-sectional average particle velocity increases up the riser. The shape of the axial particle velocity profiles depends on the operating conditions. Three axial sections are formed along the riser: “distributor controlled” zone at the very bottom, acceleration section at the base of the column, and the upper section with constant average particle velocity. When G_s is of up to $800 \text{ kg/m}^2\text{s}$, the axial profiles of the particle velocity become more uniform. Radial profiles of particle velocity and solids flux have unique shapes under different operating conditions with radially uniform structure under low solids flux/density and roughly parabolic shape under high solids flux/density conditions. No net downward flow near the wall is one of the most important advantages of the high flux/density riser over the conventional low flux/density reactor, leading to a reduction of solids backmixing.

Relationships between solids holdups, particle velocity, and solids flux are studied. Correlation between particle velocity and solids holdup is stronger for low solids flux/density conditions than that of high solids flux/density conditions. The results revealed that gas-particle interactions dominated in low solids flux/density CFBs while particle-particle interactions played a key role for the motion of particles in the extremely high solids flux CFB systems.

Studies of hydrodynamics show that better gas-solids contacting is achieved, and the solids backmixing can be reduced under high density operating conditions. Because backmixing in the riser is due to particle aggregation which, in turn, is due to the gas and solids flow against gravity, an alternative to the riser, the downer reactor in which gas and solids move downward in a concurrent fashion, is an also experimentally studied at superficial gas velocity of 1-7 m/s and solids circulation rates from 100 to $300 \text{ kg/m}^2\text{s}$.

As expected, radial distribution of solids holdup in the downer is much more uniform than in the riser reactor. Radial solids holdup distribution is almost flat covering a wide region of the cross section. The uniform radial distribution of solids flow provides a nearly plug flow condition in the downer reactor. The radial solids holdup distribution is affected by the operating conditions. Under low solids circulation rate, the shape of the radial profiles is nearly unchanged along the

entire downer. With increasing solids circulation rate, the shape of the radial solids holdup distribution changes axially. Particle velocity in the downer reactor is characterized by a relatively flat core with slightly increase towards the wall. Compared to the riser reactor, the downer reactor has a much more uniform radial profile of particle velocity. Radial profiles of the local solids flux in the downer are also influenced by operating conditions significantly. Increasing U_g and/or decreasing G_s can lead to a more uniform distribution of radial solids flux.

In both riser and downer reactors, the reactor performance is determined by both the chemical reaction itself and the hydrodynamics. The design, optimization and scale-up of a CFB reactor require more precise and quantitative understanding of both the flow behavior and the chemical reaction. Reactor performance in both riser and downer is investigated using catalytic ozone decomposition reaction.

The axial and radial distribution profiles of the ozone concentration are consistent with the corresponding profiles of the solids holdup, which indicate that ozone reaction in the riser and downer reactors is also controlled by the gas-solids flow structure.

Ozone conversion increases with the solids circulation rate under the same superficial gas velocity due to the increase of the average solids holdup. The conversion decreases with gas velocity at a fixed solids circulation rate due to the associated reduction in solids holdup. Most of the ozone conversion occurs in the entrance region of the reactors indicating that the initial gas-solids contacting plays a key role in the reaction process so that more attention needs to be paid on the distributor design.

The values of calculated overall conversion based on the experiments are to some extent smaller than that obtained based on the ideal plug flow reactor model indicating that hydrodynamics affects the performance of CFB reactors. The extent of the deviation of the conversion can be attributed to the different gas-solids contacting efficiency in the CFBs.

Strong correlation between reactant concentration distribution and hydrodynamics especially the solids holdup is observed in both the riser and downer reactors. Solids holdup affects the overall ozone conversion with various trends. There is much more significant influence of solids holdup on overall reactant decomposition under higher superficial gas velocity and/or lower solids

circulation rate in the riser, while in the downer reactor solids holdup influence on reactor performance follows different trend and needs more investigation.

9.3 Recommendations

This dissertation provides comprehensive experimental results and systematic understanding on hydrodynamics and reactor performance in riser/downer reactors in a wide range of solids flux. However, there are areas which require further work:

Due to the limitation of the storage tank capacity, the solids circulation rate for downer experiments is limited to 300 kg/m²s. It will be useful to study higher flux conditions in the downer reactor.

Hydrodynamics of the CFB riser/downer is greatly influenced by physical properties of solid particles. Particle properties also affect the reactor performance, therefore experiments using different solid particles can provide more insight into their impacts in both CFB riser and downer reactors hydrodynamics and performance.

The results in this study are obtained in a 76 mm CFB riser and downer reactors. Scale-up of fluidized bed reactors is quite challenging and therefore further experimental works may need to be carried out in large size riser/downer reactors.

Riser/downer reactors in this study are cylindrical in shape. Riser/downer reactors of different geometry have been used commercially. Therefore, the effect of geometry of the bed might need to be investigated through additional experiments in non-cylindrical CFB reactors.

In this study, only one type of distributor was employed throughout the experiments, however, in riser/downer reactors distributor region plays a key role in chemical conversion of the gaseous reactants as well as hydrodynamics. Therefore, experiments with different distributors may be carried out to study the effects of distributors on hydrodynamics and reactor performance.

Although ozone decomposition reaction is an ideal choice for experimental work in this study due to its simplicity and compatibility, real world complex reactions may results in gaseous products which may affect the hydrodynamics and reactor performance. Therefore, the results obtained for ozone reaction should be carefully applied for other reacting systems and further experiments with other chemical reactions would be required.

All the experiments were carried out at room conditions, however, experiments at different temperatures and pressures will be useful to investigate their impacts on hydrodynamic and reactor performance.

This study mainly focuses on experimental works, which are labor intensive and time consuming due to the relatively large scale of the experimental setup and the number of variables to be controlled and measured. Therefore, no model was developed. However, the available experimental hydrodynamics and reactor performance data can be used for the purpose of empirical and mathematical modeling in different areas.

Appendix 1. Raw data of solids holdup, particle velocity, and solids flux in the CFB riser

1.1 $U_g = 5.0 \text{ m/s}$, $G_s = 100 \text{ kg/m}^2\text{s}$

Solids holdup, [-]

$U_g 5G_s 100$	r/R=0.0	r/R=0.316	r/R=0.548	r/R=0.707	r/R=0.837	r/R=0.950	Average
z=0.57	0.0071	0.0090	0.0134	0.0286	0.0326	0.0737	0.0274
z=1.02	0.0083	0.0102	0.0132	0.0212	0.0384	0.0744	0.0273
z=1.94	0.0077	0.0081	0.0107	0.0159	0.0283	0.0489	0.0198
z=2.85	0.0080	0.0090	0.0106	0.0139	0.0406	0.0393	0.0212
z=3.77	0.0086	0.0089	0.0101	0.0120	0.0322	0.0342	0.0181
z=4.78	0.0099	0.0103	0.0106	0.0130	0.0316	0.0369	0.0189
z=5.84	0.0101	0.0103	0.0100	0.0116	0.0316	0.0270	0.0173
z=7.78	0.0101	0.0100	0.0105	0.0116	0.0308	0.0249	0.0169
z=9.61	0.0081	0.0103	0.0107	0.0116	0.0216	0.0326	0.0158
z=10.09	0.0081	0.0104	0.0107	0.0116	0.0260	0.0314	0.0167

Particle velocity, [m/s]

$U_g 5G_s 100$	r/R=0.0	r/R=0.316	r/R=0.548	r/R=0.707	r/R=0.837	r/R=0.950	Average
z=0.57	6.12	5.96	4.48	1.19	1.11	-0.57	2.66
z=1.02	6.42	5.91	5.05	2.43	1.49	-0.56	3.16
z=1.94	7.29	6.97	5.60	3.35	1.98	-0.78	3.79
z=2.85	7.45	6.94	5.83	4.67	2.04	-0.02	4.24
z=3.77	7.33	6.89	6.14	5.74	1.95	-0.55	4.46
z=4.78	7.52	7.36	6.86	6.06	2.01	-0.06	4.87
z=5.84	7.72	7.47	7.17	6.44	2.47	-0.04	5.15
z=7.78	7.81	7.63	7.01	6.31	2.51	-0.01	5.13
z=9.61	9.00	7.43	7.21	6.51	3.49	-0.96	5.29
z=10.09	9.41	7.49	7.42	6.62	3.22	-1.18	5.29

Solids flux, [$\text{kg/m}^2\text{s}$]

$U_g 5G_s 100$	r/R=0.0	r/R=0.316	r/R=0.548	r/R=0.707	r/R=0.837	r/R=0.950	Average
z=0.57	77.86	95.73	106.71	60.40	64.18	-75.13	63.07
z=1.02	94.57	107.53	118.54	91.94	101.75	-73.98	83.89
z=1.94	99.26	100.62	106.98	94.42	100.03	-67.46	80.75
z=2.85	106.33	110.78	110.53	115.56	147.55	-1.59	106.81
z=3.77	111.53	108.90	110.72	122.20	111.91	-33.62	96.21
z=4.78	132.46	135.06	128.90	140.55	113.05	-3.74	113.51
z=5.84	138.45	136.36	128.14	133.02	138.94	-2.05	117.89
z=7.78	139.78	136.02	131.06	130.69	137.98	-0.40	117.97
z=9.61	129.23	135.78	137.22	133.87	133.74	-55.70	112.63
z=10.09	136.32	138.96	141.58	136.42	149.00	-66.13	117.06

1.2 $U_g = 5.0 \text{ m/s}$, $G_s = 200 \text{ kg/m}^2\text{s}$

Solids holdup, [-]

$U_g G_s 200$	r/R=0.0	r/R=0.316	r/R=0.548	r/R=0.707	r/R=0.837	r/R=0.950	Average
z=0.57	0.0131	0.0287	0.0396	0.1296	0.1460	0.2547	0.1072
z=1.02	0.0111	0.0235	0.0665	0.0522	0.2409	0.2646	0.1176
z=1.94	0.0128	0.0163	0.0516	0.0380	0.2001	0.3090	0.1055
z=2.85	0.0131	0.0182	0.0204	0.0258	0.0596	0.0975	0.0391
z=3.77	0.0115	0.0159	0.0141	0.0368	0.0550	0.0926	0.0381
z=4.78	0.0125	0.0153	0.0164	0.0263	0.0511	0.0841	0.0342
z=5.84	0.0130	0.0127	0.0147	0.0158	0.0416	0.0871	0.0292
z=7.78	0.0130	0.0129	0.0132	0.0155	0.0442	0.0791	0.0284
z=9.61	0.0118	0.0131	0.0115	0.0154	0.0438	0.0897	0.0292
z=10.09	0.0119	0.0130	0.0159	0.0154	0.0439	0.0828	0.0294

Particle velocity, [m/s]

$U_g G_s 200$	r/R=0.0	r/R=0.316	r/R=0.548	r/R=0.707	r/R=0.837	r/R=0.950	Average
z=0.57	6.39	3.88	2.26	1.02	0.97	0.09	1.75
z=1.02	9.29	5.30	1.62	1.56	0.54	0.03	1.89
z=1.94	9.97	7.95	2.59	2.95	0.67	0.14	2.98
z=2.85	10.75	8.07	6.16	4.09	1.95	0.24	4.41
z=3.77	10.92	8.60	7.66	3.28	1.86	0.61	4.71
z=4.78	10.75	9.10	7.95	4.48	2.16	0.54	5.21
z=5.84	10.94	9.53	8.28	6.97	2.05	0.47	5.90
z=7.78	10.93	9.92	8.74	7.08	2.05	0.56	6.12
z=9.61	10.99	10.38	9.68	7.63	2.58	0.74	6.70
z=10.09	10.93	9.98	8.63	7.64	2.05	0.81	6.26

Solids flux, [kg/m²s]

$U_g G_s 200$	r/R=0.0	r/R=0.316	r/R=0.548	r/R=0.707	r/R=0.837	r/R=0.950	Average
z=0.57	148.49	198.32	159.48	235.94	252.90	40.74	191.29
z=1.02	183.56	221.50	192.38	145.07	231.04	15.89	175.11
z=1.94	227.89	231.38	237.48	199.38	238.79	74.92	208.77
z=2.85	250.12	261.97	224.10	187.73	206.76	42.46	197.80
z=3.77	223.22	243.22	192.58	214.92	182.52	100.78	194.29
z=4.78	239.73	248.25	232.62	209.93	196.72	80.66	204.47
z=5.84	252.88	214.96	217.09	196.66	152.20	72.38	180.37
z=7.78	253.20	227.25	205.76	194.77	160.93	78.40	182.29
z=9.61	230.19	241.51	197.45	209.05	201.46	117.64	200.04
z=10.09	230.91	231.41	244.81	209.26	160.19	119.27	200.32

1.3 $U_g = 5.0 \text{ m/s}$, $G_s = 300 \text{ kg/m}^2\text{s}$

Solids holdup, [-]

$U_g G_s 300$	r/R=0.0	r/R=0.316	r/R=0.548	r/R=0.707	r/R=0.837	r/R=0.950	Average
z=0.57	0.0156	0.0302	0.1258	0.2102	0.3305	0.4310	0.2086
z=1.02	0.0148	0.0268	0.0598	0.1824	0.3201	0.3490	0.1739
z=1.94	0.0185	0.0360	0.0884	0.1846	0.3252	0.3529	0.1846
z=2.85	0.0159	0.0233	0.0393	0.1068	0.1206	0.1563	0.0836
z=3.77	0.0176	0.0248	0.0344	0.0917	0.1289	0.1303	0.0781
z=4.78	0.0214	0.0240	0.0356	0.0982	0.1266	0.1395	0.0803
z=5.84	0.0167	0.0211	0.0331	0.0947	0.1141	0.1239	0.0737
z=7.78	0.0185	0.0213	0.0330	0.0575	0.1100	0.1169	0.0635
z=9.61	0.0147	0.0197	0.0339	0.0574	0.0922	0.1789	0.0667
z=10.09	0.0146	0.0194	0.0332	0.0493	0.1012	0.1019	0.0576

Particle velocity, [m/s]

$U_g G_s 300$	r/R=0.0	r/R=0.316	r/R=0.548	r/R=0.707	r/R=0.837	r/R=0.950	Average
z=0.57	7.95	5.69	1.24	0.51	0.32	0.34	1.62
z=1.02	10.77	7.02	3.72	0.85	0.49	0.33	2.58
z=1.94	10.64	5.09	2.31	1.00	0.56	0.41	1.93
z=2.85	12.15	9.11	5.08	1.85	1.08	0.40	3.67
z=3.77	12.17	9.07	5.99	1.76	1.05	0.41	3.85
z=4.78	12.70	9.49	6.29	1.82	1.17	0.41	4.04
z=5.84	13.53	10.62	6.84	2.18	1.26	0.53	4.51
z=7.78	14.78	11.70	6.45	3.08	1.46	0.41	4.86
z=9.61	14.87	11.71	6.55	3.48	1.82	0.59	5.08
z=10.09	15.40	10.34	6.52	4.37	1.64	0.33	4.94

Solids flux, [kg/m²s]

$U_g G_s 300$	r/R=0.0	r/R=0.316	r/R=0.548	r/R=0.707	r/R=0.837	r/R=0.950	Average
z=0.57	221.28	305.79	276.80	189.16	190.13	257.90	240.77
z=1.02	284.66	334.88	396.21	276.24	279.83	206.67	308.66
z=1.94	350.04	325.98	362.85	329.23	326.32	255.38	327.24
z=2.85	344.66	378.03	355.31	352.07	232.41	111.35	302.51
z=3.77	380.39	400.41	366.67	287.14	241.76	94.28	294.87
z=4.78	483.41	405.11	398.32	318.79	263.76	100.92	316.22
z=5.84	402.66	399.20	403.23	367.92	255.00	116.29	327.24
z=7.78	487.32	444.76	379.35	315.16	286.16	84.57	321.61
z=9.61	390.44	410.72	395.01	355.34	298.10	188.11	342.82
z=10.09	400.53	357.14	385.42	383.55	294.72	59.00	320.64

1.4 $U_g = 5.0 \text{ m/s}$, $G_s = 400 \text{ kg/m}^2\text{s}$

Solids holdup, [-]

$U_g G_s 400$	r/R=0.0	r/R=0.316	r/R=0.548	r/R=0.707	r/R=0.837	r/R=0.950	Average
z=0.57	0.0131	0.0281	0.0794	0.1924	0.3211	0.4747	0.1962
z=1.02	0.0118	0.0400	0.0967	0.2796	0.3917	0.3694	0.2258
z=1.94	0.0184	0.0329	0.1294	0.3395	0.4411	0.4869	0.2708
z=2.85	0.0168	0.0279	0.0891	0.2021	0.3534	0.2863	0.1857
z=3.77	0.0216	0.0280	0.0292	0.1214	0.2536	0.3842	0.1422
z=4.78	0.0201	0.0278	0.0271	0.1066	0.2368	0.3282	0.1280
z=5.84	0.0266	0.0281	0.0297	0.0910	0.1969	0.3195	0.1151
z=7.78	0.0176	0.0230	0.0288	0.0811	0.1404	0.2667	0.0927
z=9.61	0.0249	0.0224	0.0278	0.1134	0.1317	0.3086	0.1027
z=10.09	0.0217	0.0219	0.0255	0.1049	0.1305	0.3151	0.1006

Particle velocity, [m/s]

$U_g G_s 400$	r/R=0.0	r/R=0.316	r/R=0.548	r/R=0.707	r/R=0.837	r/R=0.950	Average
z=0.57	7.79	6.33	1.29	1.34	0.10	0.01	1.85
z=1.02	10.38	6.56	1.92	0.95	0.52	0.01	2.05
z=1.94	15.80	8.57	2.10	0.59	0.50	0.05	2.40
z=2.85	15.47	11.03	3.09	1.24	0.59	0.02	3.27
z=3.77	14.71	11.32	7.92	2.42	0.92	0.04	4.82
z=4.78	15.27	11.68	8.52	2.88	0.98	0.03	5.15
z=5.84	14.62	11.56	8.56	2.75	1.20	0.05	5.16
z=7.78	16.35	12.68	9.35	2.87	1.72	0.39	5.75
z=9.61	14.80	13.48	9.54	2.29	1.92	0.25	5.84
z=10.09	15.89	13.58	9.86	2.33	2.01	0.24	5.96

Solids flux, [kg/m²s]

$U_g G_s 400$	r/R=0.0	r/R=0.316	r/R=0.548	r/R=0.707	r/R=0.837	r/R=0.950	Average
z=0.57	181.82	316.23	183.10	459.03	54.57	12.55	222.27
z=1.02	217.41	467.71	330.38	475.26	360.22	8.26	358.35
z=1.94	517.19	501.16	483.22	355.49	395.74	45.24	386.32
z=2.85	461.47	547.97	489.62	444.50	372.77	7.91	407.47
z=3.77	564.69	564.84	410.84	522.70	413.55	24.29	420.82
z=4.78	547.26	578.41	411.07	546.24	412.30	17.97	427.80
z=5.84	692.90	578.39	452.22	445.69	419.98	29.70	417.88
z=7.78	510.77	519.53	479.75	414.25	430.06	184.49	426.52
z=9.61	655.24	538.51	472.74	462.74	449.21	138.74	438.41
z=10.09	614.06	528.88	447.66	435.28	465.99	132.18	427.36

1.5 $U_g = 7.0 \text{ m/s}$, $G_s = 100 \text{ kg/m}^2\text{s}$

Solids holdup, [-]

$U_g G_s 100$	r/R=0.0	r/R=0.316	r/R=0.548	r/R=0.707	r/R=0.837	r/R=0.950	Average
z=0.57	0.0077	0.0094	0.0214	0.0561	0.0600	0.0642	0.0407
z=1.02	0.0108	0.0120	0.0175	0.0416	0.0695	0.0642	0.0391
z=1.94	0.0072	0.0086	0.0101	0.0068	0.0137	0.0315	0.0124
z=2.85	0.0084	0.0090	0.0112	0.0115	0.0192	0.0385	0.0159
z=3.77	0.0073	0.0074	0.0083	0.0094	0.0171	0.0346	0.0135
z=4.78	0.0075	0.0079	0.0093	0.0106	0.0124	0.0310	0.0126
z=5.84	0.0069	0.0074	0.0083	0.0100	0.0145	0.0306	0.0126
z=7.78	0.0072	0.0077	0.0090	0.0104	0.0144	0.0305	0.0128
z=9.61	0.0074	0.0078	0.0083	0.0091	0.0116	0.0296	0.0116
z=10.09	0.0071	0.0072	0.0080	0.0083	0.0112	0.0268	0.0109

Particle velocity, [m/s]

$U_g G_s 100$	r/R=0.0	r/R=0.316	r/R=0.548	r/R=0.707	r/R=0.837	r/R=0.950	Average
z=0.57	6.38	4.73	2.49	1.47	1.04	-0.20	2.05
z=1.02	5.83	4.49	2.78	2.50	1.09	-0.47	2.28
z=1.94	7.27	6.81	6.67	6.72	4.44	-0.30	5.38
z=2.85	8.88	7.97	6.31	5.51	3.33	-0.44	4.98
z=3.77	9.46	8.95	7.68	6.42	3.37	-0.78	5.67
z=4.78	9.87	9.10	7.40	6.07	4.57	-0.31	5.88
z=5.84	10.44	9.63	7.97	6.01	4.44	-0.27	6.08
z=7.78	10.63	9.96	8.70	6.04	4.54	-0.72	6.29
z=9.61	10.98	10.37	9.08	6.98	5.18	-0.84	6.80
z=10.09	11.05	10.94	9.25	7.71	5.32	-0.77	7.16

Solids flux, [kg/m²s]

$U_g G_s 100$	r/R=0.0	r/R=0.316	r/R=0.548	r/R=0.707	r/R=0.837	r/R=0.950	Average
z=0.57	87.78	78.68	95.10	147.25	110.80	-23.21	93.34
z=1.02	111.67	95.79	86.24	185.40	134.68	-53.82	104.94
z=1.94	93.65	104.83	120.35	81.08	108.05	-16.91	89.49
z=2.85	132.03	127.20	125.96	112.64	113.80	-30.15	102.02
z=3.77	123.05	118.16	113.91	107.36	102.34	-47.77	91.56
z=4.78	131.87	127.31	122.12	114.22	100.51	-17.28	100.01
z=5.84	128.85	127.38	118.41	106.73	114.66	-14.97	100.90
z=7.78	136.30	137.11	139.62	111.62	116.22	-38.93	106.45
z=9.61	145.01	144.57	133.43	112.93	107.27	-44.46	104.04
z=10.09	140.60	141.02	132.57	113.50	106.61	-36.61	104.06

1.6 $U_g = 7.0 \text{ m/s}$, $G_s = 200 \text{ kg/m}^2\text{s}$

Solids holdup, [-]

$U_g G_s 200$	r/R=0.0	r/R=0.316	r/R=0.548	r/R=0.707	r/R=0.837	r/R=0.950	Average
z=0.57	0.0097	0.0185	0.0721	0.1782	0.3174	0.4356	0.1840
z=1.02	0.0101	0.0116	0.0187	0.0349	0.2062	0.1925	0.0837
z=1.94	0.0101	0.0152	0.0203	0.0202	0.2230	0.1203	0.0767
z=2.85	0.0119	0.0138	0.0161	0.0204	0.0415	0.1073	0.0331
z=3.77	0.0109	0.0122	0.0132	0.0229	0.0443	0.1037	0.0329
z=4.78	0.0127	0.0133	0.0124	0.0199	0.0367	0.0960	0.0296
z=5.84	0.0116	0.0125	0.0111	0.0118	0.0305	0.0969	0.0260
z=7.78	0.0129	0.0129	0.0116	0.0111	0.0266	0.0968	0.0252
z=9.61	0.0106	0.0115	0.0125	0.0164	0.0291	0.0901	0.0261
z=10.09	0.0112	0.0129	0.0125	0.0168	0.0238	0.0895	0.0252

Particle velocity, [m/s]

$U_g G_s 200$	r/R=0.0	r/R=0.316	r/R=0.548	r/R=0.707	r/R=0.837	r/R=0.950	Average
z=0.57	6.76	3.50	2.01	1.09	0.28	-0.22	1.44
z=1.02	9.99	7.52	6.75	3.13	0.52	-0.44	3.83
z=1.94	10.08	7.58	6.61	3.04	0.69	-0.34	3.84
z=2.85	11.15	9.61	7.45	6.01	2.65	0.74	5.67
z=3.77	11.98	10.03	9.36	6.53	3.15	-0.92	6.24
z=4.78	12.00	10.86	10.12	7.25	3.54	0.47	6.99
z=5.84	12.69	11.11	10.74	9.94	3.56	0.67	7.82
z=7.78	12.52	11.78	10.10	9.84	3.69	1.12	7.87
z=9.61	13.60	11.91	10.40	8.92	4.12	0.38	7.76
z=10.09	13.90	11.54	10.97	7.94	4.34	0.76	7.69

Solids flux, [kg/m²s]

$U_g G_s 200$	r/R=0.0	r/R=0.316	r/R=0.548	r/R=0.707	r/R=0.837	r/R=0.950	Average
z=0.57	116.95	115.42	258.17	344.98	158.58	-170.65	177.41
z=1.02	180.03	155.32	224.35	194.41	191.87	-150.45	152.74
z=1.94	180.97	204.68	238.83	109.60	273.34	-73.67	173.82
z=2.85	235.79	236.35	213.94	218.56	196.29	142.10	206.85
z=3.77	232.23	216.91	219.72	265.89	248.20	-169.12	190.17
z=4.78	270.99	257.45	223.36	256.64	231.44	79.79	222.34
z=5.84	262.60	247.56	212.41	209.39	192.77	116.04	202.69
z=7.78	288.05	271.45	208.52	195.06	174.80	193.45	208.20
z=9.61	256.90	244.66	231.81	260.91	213.81	60.63	216.63
z=10.09	276.64	264.23	243.24	237.81	183.97	120.45	218.22

1.7 $U_g = 7.0 \text{ m/s}$, $G_s = 300 \text{ kg/m}^2\text{s}$

Solids holdup, [-]

$U_g G_s 300$	r/R=0.0	r/R=0.316	r/R=0.548	r/R=0.707	r/R=0.837	r/R=0.950	Average
z=0.57	0.0107	0.0157	0.0715	0.1996	0.3234	0.4142	0.1869
z=1.02	0.0116	0.0181	0.0687	0.1773	0.2363	0.3880	0.1590
z=1.94	0.0142	0.0233	0.0547	0.1629	0.1282	0.3797	0.1281
z=2.85	0.0127	0.0144	0.0270	0.0543	0.1720	0.1854	0.0821
z=3.77	0.0136	0.0141	0.0293	0.0588	0.1019	0.1014	0.0579
z=4.78	0.0146	0.0133	0.0211	0.0422	0.0629	0.1154	0.0449
z=5.84	0.0111	0.0129	0.0178	0.0366	0.0501	0.1151	0.0398
z=7.78	0.0165	0.0131	0.0161	0.0282	0.0567	0.1297	0.0408
z=9.61	0.0131	0.0146	0.0168	0.0229	0.0572	0.1061	0.0374
z=10.09	0.0125	0.0115	0.0199	0.0215	0.0617	0.0690	0.0338

Particle velocity, [m/s]

$U_g G_s 300$	r/R=0.0	r/R=0.316	r/R=0.548	r/R=0.707	r/R=0.837	r/R=0.950	Average
z=0.57	8.20	8.85	3.04	0.97	0.21	0.26	2.72
z=1.02	13.31	8.96	2.19	0.95	0.39	0.25	2.58
z=1.94	13.13	9.07	3.19	1.05	1.06	0.23	3.01
z=2.85	13.34	12.02	6.46	2.99	0.88	0.19	4.75
z=3.77	14.43	13.63	6.70	3.08	1.22	0.50	5.25
z=4.78	15.04	14.95	9.63	3.67	2.10	0.56	6.54
z=5.84	16.83	16.75	10.60	4.95	2.47	0.57	7.49
z=7.78	15.76	15.87	11.95	5.93	2.74	0.30	7.89
z=9.61	16.95	15.91	12.79	6.70	2.05	0.69	8.17
z=10.09	17.62	17.97	12.03	7.82	1.90	0.59	8.59

Solids flux, [kg/m²s]

$U_g G_s 300$	r/R=0.0	r/R=0.316	r/R=0.548	r/R=0.707	r/R=0.837	r/R=0.950	Average
z=0.57	155.46	246.55	386.48	343.07	119.71	189.66	266.50
z=1.02	274.19	288.98	267.93	301.17	163.29	172.68	244.75
z=1.94	332.11	376.93	309.93	305.65	241.17	158.22	288.47
z=2.85	301.04	307.29	310.09	289.35	268.80	61.58	266.23
z=3.77	350.38	343.09	349.38	322.55	221.35	90.26	282.71
z=4.78	390.49	353.47	362.45	275.15	234.99	115.61	283.12
z=5.84	333.16	384.54	334.83	321.92	220.48	116.10	289.93
z=7.78	463.86	370.60	343.18	297.46	276.69	68.79	290.74
z=9.61	396.24	413.16	381.40	272.63	208.59	131.04	294.41
z=10.09	393.18	366.31	426.56	298.72	208.49	73.01	295.20

1.8 $U_g = 7.0 \text{ m/s}$, $G_s = 400 \text{ kg/m}^2\text{s}$

Solids holdup, [-]

$U_g G_s 400$	r/R=0.0	r/R=0.316	r/R=0.548	r/R=0.707	r/R=0.837	r/R=0.950	Average
z=0.57	0.0165	0.0259	0.0825	0.1630	0.2868	0.4996	0.1851
z=1.02	0.0250	0.0369	0.0726	0.1562	0.2477	0.4746	0.1715
z=1.94	0.0328	0.0219	0.0552	0.1008	0.2442	0.4095	0.1435
z=2.85	0.0192	0.0195	0.0299	0.0536	0.2327	0.3384	0.1153
z=3.77	0.0179	0.0195	0.0261	0.0507	0.2573	0.4503	0.1325
z=4.78	0.0187	0.0208	0.0253	0.0570	0.1920	0.3422	0.1065
z=5.84	0.0175	0.0205	0.0237	0.0519	0.1392	0.2536	0.0826
z=7.78	0.0154	0.0192	0.0234	0.0487	0.1070	0.2096	0.0691
z=9.61	0.0154	0.0164	0.0242	0.0420	0.1069	0.1264	0.0574
z=10.09	0.0153	0.0163	0.0249	0.0449	0.1119	0.1090	0.0573

Particle velocity, [m/s]

$U_g G_s 400$	r/R=0.0	r/R=0.316	r/R=0.548	r/R=0.707	r/R=0.837	r/R=0.950	Average
z=0.57	8.73	8.49	3.04	1.38	0.56	0.35	2.84
z=1.02	13.22	8.89	3.09	1.21	0.75	0.25	2.92
z=1.94	10.20	11.09	4.72	2.29	0.86	0.33	4.00
z=2.85	14.59	12.43	6.84	4.33	0.91	0.53	5.27
z=3.77	15.98	13.12	9.07	4.96	0.79	0.15	6.00
z=4.78	16.19	12.87	9.86	4.24	1.04	0.36	6.06
z=5.84	17.33	13.19	9.96	4.78	1.51	0.54	6.40
z=7.78	17.88	13.92	10.38	5.11	2.24	0.77	6.90
z=9.61	17.29	15.68	10.94	5.84	1.98	0.39	7.43
z=10.09	17.44	16.17	10.77	6.04	1.67	0.26	7.45

Solids flux, [kg/m²s]

$U_g G_s 400$	r/R=0.0	r/R=0.316	r/R=0.548	r/R=0.707	r/R=0.837	r/R=0.950	Average
z=0.57	256.84	391.25	446.99	401.74	286.20	315.15	374.29
z=1.02	587.26	584.17	399.33	336.41	331.02	212.92	383.23
z=1.94	595.92	431.29	464.11	409.97	374.06	237.06	398.47
z=2.85	497.31	432.69	363.79	413.37	375.52	321.16	385.89
z=3.77	510.04	455.27	420.64	447.63	363.24	122.84	385.37
z=4.78	539.59	477.25	444.15	430.29	356.40	217.99	400.94
z=5.84	540.90	482.16	420.88	442.19	374.26	245.32	406.30
z=7.78	488.82	475.64	433.27	443.17	427.25	286.29	424.96
z=9.61	474.93	457.60	470.57	435.99	375.94	88.34	393.84
z=10.09	475.60	470.50	476.40	483.25	331.66	50.89	394.05

1.9 $U_g = 7.0 \text{ m/s}$, $G_s = 500 \text{ kg/m}^2\text{s}$

Solids holdup, [-]

$U_g G_s 500$	r/R=0.0	r/R=0.316	r/R=0.548	r/R=0.707	r/R=0.837	r/R=0.950	Average
z=0.57	0.0111	0.0122	0.0164	0.0456	0.2612	0.4793	0.1319
z=1.02	0.0193	0.0347	0.0508	0.0620	0.2867	0.4096	0.1457
z=1.94	0.0215	0.0217	0.0454	0.0590	0.3354	0.4270	0.1542
z=2.85	0.0219	0.0255	0.0406	0.0782	0.3434	0.4308	0.1604
z=3.77	0.0206	0.0231	0.0407	0.0720	0.3359	0.3407	0.1462
z=4.78	0.0232	0.0220	0.0413	0.0696	0.1512	0.3292	0.1027
z=5.84	0.0226	0.0224	0.0352	0.0679	0.1429	0.3269	0.0988
z=7.78	0.0227	0.0218	0.0330	0.0618	0.1169	0.2810	0.0855
z=9.61	0.0225	0.0227	0.0364	0.0574	0.1101	0.2199	0.0767
z=10.09	0.0223	0.0224	0.0363	0.0500	0.1012	0.2526	0.0769

Particle velocity, [m/s]

$U_g G_s 500$	r/R=0.0	r/R=0.316	r/R=0.548	r/R=0.707	r/R=0.837	r/R=0.950	Average
z=0.57	8.20	8.76	3.14	1.75	1.03	0.31	3.10
z=1.02	9.04	9.94	4.64	2.48	0.40	0.22	3.69
z=1.94	16.26	14.57	6.56	4.74	0.74	0.60	5.67
z=2.85	15.82	13.86	7.70	3.84	0.60	0.60	5.58
z=3.77	15.95	14.20	7.93	3.97	0.62	0.68	5.74
z=4.78	16.19	14.94	8.08	3.86	1.86	0.88	6.19
z=5.84	16.62	14.47	8.95	3.91	2.39	0.98	6.45
z=7.78	17.31	14.24	9.55	4.26	2.33	0.87	6.60
z=9.61	17.86	14.04	8.35	4.83	2.66	0.98	6.50
z=10.09	18.02	14.01	8.44	4.97	2.30	0.87	6.45

Solids flux, [kg/m²s]

$U_g G_s 500$	r/R=0.0	r/R=0.316	r/R=0.548	r/R=0.707	r/R=0.837	r/R=0.950	Average
z=0.57	161.58	190.94	91.43	141.76	478.76	261.67	229.19
z=1.02	310.40	614.31	419.55	273.63	204.51	160.06	344.91
z=1.94	623.39	562.53	529.78	498.04	444.70	456.61	501.10
z=2.85	616.67	628.70	555.76	534.64	369.75	460.73	511.94
z=3.77	585.55	584.57	574.44	509.24	369.08	413.61	496.43
z=4.78	669.83	584.27	593.83	478.27	500.10	513.03	535.16
z=5.84	668.86	576.44	561.72	472.84	608.63	568.13	555.69
z=7.78	698.55	552.94	560.38	468.77	484.62	434.65	506.29
z=9.61	716.31	567.74	541.26	493.28	521.74	382.55	512.35
z=10.09	715.24	557.34	545.82	442.44	413.47	390.81	476.52

1.10 $U_g = 7.0$ m/s, $G_s = 600$ kg/m²s

Solids holdup, [-]

$U_g G_s 600$	r/R=0.0	r/R=0.316	r/R=0.548	r/R=0.707	r/R=0.837	r/R=0.950	Average
z=0.57	0.0126	0.0143	0.0251	0.0903	0.2108	0.4013	0.1240
z=1.02	0.0222	0.0311	0.0651	0.1021	0.1573	0.4659	0.1350
z=1.94	0.0232	0.0244	0.0546	0.0761	0.2836	0.5399	0.1624
z=2.85	0.0211	0.0257	0.0544	0.0759	0.2835	0.5400	0.1626
z=3.77	0.0241	0.0305	0.0436	0.0956	0.2523	0.4211	0.1444
z=4.78	0.0213	0.0294	0.0429	0.0783	0.1916	0.5257	0.1388
z=5.84	0.0216	0.0283	0.0426	0.0722	0.2542	0.4516	0.1424
z=7.78	0.0225	0.0233	0.0397	0.0788	0.2442	0.5022	0.1460
z=9.61	0.0218	0.0232	0.0395	0.0748	0.2118	0.4790	0.1350
z=10.09	0.02092	0.02083	0.04290	0.08452	0.21067	0.40672	0.1288

Particle velocity, [m/s]

$U_g G_s 600$	r/R=0.0	r/R=0.316	r/R=0.548	r/R=0.707	r/R=0.837	r/R=0.950	Average
z=0.57	13.50	10.04	7.26	3.08	0.98	1.14	4.71
z=1.02	13.47	10.51	6.83	3.04	1.06	0.33	4.61
z=1.94	13.98	11.03	7.03	3.66	0.87	0.33	4.86
z=2.85	15.53	13.47	7.06	4.09	1.00	0.33	5.46
z=3.77	16.86	13.16	7.95	3.87	1.11	0.63	5.62
z=4.78	17.51	13.00	8.66	4.53	1.31	0.33	5.92
z=5.84	17.36	13.60	8.92	4.29	1.22	0.46	6.04
z=7.78	17.33	15.63	9.21	4.64	1.35	0.33	6.59
z=9.61	17.68	15.97	9.32	4.91	1.63	0.21	6.79
z=10.09	18.78	17.99	8.84	4.36	1.73	0.33	6.98

Solids flux, [kg/m²s]

$U_g G_s 600$	r/R=0.0	r/R=0.316	r/R=0.548	r/R=0.707	r/R=0.837	r/R=0.950	Average
z=0.57	302.44	254.89	324.74	495.00	367.62	811.85	417.07
z=1.02	532.32	582.88	791.39	552.08	297.89	269.69	524.44
z=1.94	578.58	478.38	683.06	495.49	441.07	312.53	502.99
z=2.85	584.52	616.48	683.32	552.72	503.77	312.56	556.70
z=3.77	722.55	713.51	616.69	657.99	498.68	469.54	600.77
z=4.78	663.68	679.47	661.51	631.37	446.27	304.32	567.56
z=5.84	668.45	684.22	676.25	551.04	553.55	366.68	585.24
z=7.78	692.87	649.32	650.53	651.61	587.89	290.71	593.99
z=9.61	685.43	658.95	655.33	652.96	612.75	180.28	589.85
z=10.09	699.05	667.13	675.00	655.72	648.74	235.44	611.33

1.11 $U_g = 7.0$ m/s, $G_s = 700$ kg/m²s

Solids holdup, [-]

$U_g G_s 700$	r/R=0.0	r/R=0.316	r/R=0.548	r/R=0.707	r/R=0.837	r/R=0.950	Average
z=0.57	0.0250	0.0407	0.1189	0.2677	0.5072	0.5557	0.2765
z=1.02	0.0290	0.0503	0.1205	0.2205	0.4764	0.5594	0.2615
z=1.94	0.0373	0.0851	0.1696	0.2981	0.5541	0.5600	0.3151
z=2.85	0.0324	0.0479	0.0955	0.2698	0.3958	0.3941	0.2287
z=3.77	0.0452	0.0616	0.0900	0.1483	0.3328	0.5473	0.2063
z=4.78	0.0520	0.0628	0.0834	0.1381	0.3161	0.5456	0.1987
z=5.84	0.0423	0.0505	0.0666	0.1099	0.2736	0.5280	0.1743
z=7.78	0.0500	0.0567	0.0684	0.1086	0.2633	0.5241	0.1729
z=9.61	0.0548	0.0572	0.0634	0.1071	0.2834	0.5136	0.1747
z=10.09	0.0523	0.0543	0.0607	0.1085	0.2813	0.5127	0.1733

Particle velocity, [m/s]

$U_g G_s 700$	r/R=0.0	r/R=0.316	r/R=0.548	r/R=0.707	r/R=0.837	r/R=0.950	Average
z=0.57	11.08	9.47	3.01	1.87	0.12	0.09	3.00
z=1.02	16.36	9.71	3.22	1.96	0.03	0.09	3.09
z=1.94	16.84	9.00	3.21	1.76	0.09	0.10	2.93
z=2.85	16.96	10.63	7.84	1.93	0.18	0.13	4.40
z=3.77	16.55	12.06	8.00	1.59	0.35	0.16	4.68
z=4.78	17.75	12.42	8.38	2.61	0.67	0.02	5.13
z=5.84	17.95	14.06	8.99	2.77	0.53	0.13	5.60
z=7.78	18.13	14.34	8.94	2.80	0.54	0.16	5.66
z=9.61	18.44	15.71	9.73	3.39	0.62	0.22	6.27
z=10.09	19.37	16.14	9.89	3.32	0.72	0.19	6.39

Solids flux, [kg/m²s]

$U_g G_s 700$	r/R=0.0	r/R=0.316	r/R=0.548	r/R=0.707	r/R=0.837	r/R=0.950	Average
z=0.57	492.30	686.40	637.98	892.52	107.72	86.73	520.72
z=1.02	845.56	869.16	691.17	769.40	21.98	91.20	521.83
z=1.94	1117.62	1363.26	969.77	931.28	86.00	102.15	735.53
z=2.85	978.43	907.32	1332.40	927.69	127.49	91.99	741.46
z=3.77	1330.44	1321.45	1280.78	419.67	209.66	154.45	719.40
z=4.78	1641.33	1388.08	1245.29	640.31	378.15	15.14	795.28
z=5.84	1351.63	1262.98	1065.34	541.51	256.19	121.13	691.08
z=7.78	1612.83	1447.44	1088.66	540.59	253.85	147.89	734.52
z=9.61	1797.24	1600.05	1098.36	646.65	314.77	199.13	809.98
z=10.09	1802.64	1558.76	1068.09	641.19	360.65	169.59	800.43

1.12 $U_g = 9.0$ m/s, $G_s = 100$ kg/m²s

Solids holdup, [-]

$U_g G_s 100$	r/R=0.0	r/R=0.316	r/R=0.548	r/R=0.707	r/R=0.837	r/R=0.950	Average
z=0.57	0.0072	0.0072	0.0103	0.0151	0.0186	0.0337	0.0154
z=1.02	0.0062	0.0088	0.0076	0.0054	0.0220	0.0211	0.0122
z=1.94	0.0073	0.0070	0.0069	0.0075	0.0151	0.0239	0.0109
z=2.85	0.0077	0.0071	0.0087	0.0069	0.0129	0.0319	0.0117
z=3.77	0.0073	0.0062	0.0077	0.0099	0.0122	0.0270	0.0112
z=4.78	0.0076	0.0068	0.0069	0.0096	0.0106	0.0126	0.0090
z=5.84	0.0073	0.0065	0.0068	0.0087	0.0115	0.0123	0.0089
z=7.78	0.0064	0.0065	0.0069	0.0077	0.0102	0.0081	0.0079
z=9.61	0.0065	0.0069	0.0068	0.0067	0.0102	0.0104	0.0080
z=10.09	0.0061	0.0068	0.0064	0.0065	0.0109	0.0104	0.0080

Particle velocity, [m/s]

$U_g G_s 100$	r/R=0.0	r/R=0.316	r/R=0.548	r/R=0.707	r/R=0.837	r/R=0.950	Average
z=0.57	8.38	7.08	6.60	5.15	2.35	-0.91	4.52
z=1.02	9.38	8.77	6.83	7.57	2.58	-1.02	5.49
z=1.94	9.66	9.23	8.19	7.89	4.00	-0.17	6.39
z=2.85	9.96	9.71	8.06	8.33	4.47	-0.47	6.62
z=3.77	9.94	9.98	8.76	7.05	4.96	-0.10	6.71
z=4.78	10.08	9.97	9.16	7.68	5.72	-0.54	7.06
z=5.84	10.22	10.21	9.77	7.92	5.39	-0.30	7.26
z=7.78	11.12	10.67	9.92	7.95	5.69	-0.38	7.45
z=9.61	11.59	10.88	10.30	8.81	5.69	-0.57	7.75
z=10.09	11.74	11.13	10.68	9.33	6.10	-0.38	8.12

Solids flux, [kg/m²s]

$U_g G_s 100$	r/R=0.0	r/R=0.316	r/R=0.548	r/R=0.707	r/R=0.837	r/R=0.950	Average
z=0.57	107.43	90.67	120.65	138.08	77.59	-54.53	88.48
z=1.02	103.28	137.24	92.84	73.23	101.02	-38.53	83.27
z=1.94	126.33	115.63	100.57	104.91	107.27	-7.25	93.23
z=2.85	136.06	123.15	125.49	101.84	102.35	-26.41	96.54
z=3.77	130.03	109.79	119.44	124.44	107.90	-4.90	101.45
z=4.78	137.07	120.68	112.26	131.11	107.82	-11.96	102.50
z=5.84	132.38	118.28	117.88	122.52	110.75	-6.51	102.73
z=7.78	125.79	123.98	121.85	108.69	103.37	-5.43	100.10
z=9.61	133.98	134.11	125.13	104.66	102.85	-10.58	101.18
z=10.09	127.73	134.16	122.16	108.21	117.88	-7.01	105.09

1.13 $U_g = 9.0$ m/s, $G_s = 200$ kg/m²s

Solids holdup, [-]

$U_g G_s 200$	r/R=0.0	r/R=0.316	r/R=0.548	r/R=0.707	r/R=0.837	r/R=0.950	Average
z=0.57	0.0081	0.0126	0.0389	0.0639	0.0570	0.0541	0.0454
z=1.02	0.0107	0.0107	0.0319	0.0714	0.0694	0.1009	0.0534
z=1.94	0.0096	0.0110	0.0227	0.0264	0.0458	0.1056	0.0362
z=2.85	0.0092	0.0101	0.0229	0.0244	0.0503	0.1011	0.0362
z=3.77	0.0091	0.0107	0.0135	0.0227	0.0458	0.1024	0.0328
z=4.78	0.0089	0.0103	0.0147	0.0227	0.0454	0.0902	0.0315
z=5.84	0.0098	0.0098	0.0129	0.0217	0.0455	0.0850	0.0301
z=7.78	0.0099	0.0098	0.0120	0.0187	0.0322	0.0551	0.0227
z=9.61	0.0099	0.0099	0.0110	0.0171	0.0422	0.0933	0.0289
z=10.09	0.0095	0.0105	0.0108	0.0161	0.0242	0.0954	0.0250

Particle velocity, [m/s]

$U_g G_s 200$	r/R=0.0	r/R=0.316	r/R=0.548	r/R=0.707	r/R=0.837	r/R=0.950	Average
z=0.57	11.43	8.53	3.65	1.71	2.47	0.82	3.55
z=1.02	11.42	10.36	3.84	2.05	1.57	0.89	3.83
z=1.94	16.54	10.77	5.94	4.63	1.94	0.81	5.07
z=2.85	13.46	12.41	6.30	4.87	2.10	0.81	5.56
z=3.77	13.86	11.61	8.67	5.87	2.20	1.04	6.25
z=4.78	13.95	12.23	9.15	6.07	2.90	1.03	6.68
z=5.84	13.52	12.69	9.96	6.09	3.20	1.05	7.03
z=7.78	13.52	13.25	10.88	6.32	3.19	1.02	7.41
z=9.61	13.72	13.70	12.17	6.64	3.76	0.82	7.98
z=10.09	14.08	13.05	12.19	7.20	4.70	0.83	8.20

Solids flux, [kg/m²s]

$U_g G_s 200$	r/R=0.0	r/R=0.316	r/R=0.548	r/R=0.707	r/R=0.837	r/R=0.950	Average
z=0.57	165.67	191.35	253.02	194.71	250.20	78.81	206.74
z=1.02	217.14	197.72	218.05	260.87	193.70	160.39	211.57
z=1.94	282.22	210.33	239.64	217.28	157.84	152.82	200.29
z=2.85	220.72	222.76	257.09	211.64	187.95	146.32	211.55
z=3.77	224.80	221.42	208.23	237.50	179.19	190.05	208.73
z=4.78	221.28	224.60	238.76	245.39	234.45	165.68	227.95
z=5.84	236.04	222.00	228.09	235.03	259.07	158.25	227.22
z=7.78	237.64	230.03	233.28	209.91	182.82	99.70	200.24
z=9.61	240.89	241.23	238.91	201.57	282.44	136.55	228.59
z=10.09	239.20	244.66	235.10	206.01	202.61	141.49	211.98

1.14 $U_g = 9.0$ m/s, $G_s = 300$ kg/m²s

Solids holdup, [-]

$U_g G_s 300$	r/R=0.0	r/R=0.316	r/R=0.548	r/R=0.707	r/R=0.837	r/R=0.950	Average
z=0.57	0.0092	0.0114	0.0215	0.1048	0.2017	0.2071	0.1009
z=1.02	0.0114	0.0167	0.0253	0.1694	0.2070	0.2049	0.1184
z=1.94	0.0135	0.0152	0.0271	0.0278	0.1528	0.2056	0.0743
z=2.85	0.0133	0.0163	0.0300	0.0294	0.1425	0.2087	0.0736
z=3.77	0.0128	0.0139	0.0204	0.0259	0.1047	0.1415	0.0537
z=4.78	0.0128	0.0148	0.0217	0.0300	0.0746	0.1216	0.0460
z=5.84	0.0143	0.0147	0.0200	0.0383	0.0645	0.1239	0.0454
z=7.78	0.0157	0.0187	0.0228	0.0360	0.0652	0.1285	0.0470
z=9.61	0.0153	0.0161	0.0176	0.0374	0.0633	0.1051	0.0424
z=10.09	0.0153	0.0167	0.0177	0.0372	0.0636	0.1034	0.0424

Particle velocity, [m/s]

$U_g G_s 300$	r/R=0.0	r/R=0.316	r/R=0.548	r/R=0.707	r/R=0.837	r/R=0.950	Average
z=0.57	11.45	13.70	6.92	0.99	0.46	0.38	4.66
z=1.02	15.14	11.40	7.08	1.22	0.71	0.15	4.33
z=1.94	15.62	12.23	7.20	5.53	0.99	0.39	5.59
z=2.85	14.83	12.36	6.63	5.33	1.03	0.55	5.46
z=3.77	16.47	14.96	9.93	5.74	1.30	0.35	6.88
z=4.78	15.96	13.70	9.37	5.74	1.41	0.45	6.54
z=5.84	15.50	14.80	10.67	4.83	1.61	0.26	6.87
z=7.78	14.46	12.03	9.12	4.99	1.86	0.10	6.04
z=9.61	15.24	14.82	10.26	5.07	1.10	0.55	6.75
z=10.09	14.77	13.63	11.90	5.16	1.88	0.20	7.07

Solids flux, [kg/m²s]

$U_g G_s 300$	r/R=0.0	r/R=0.316	r/R=0.548	r/R=0.707	r/R=0.837	r/R=0.950	Average
z=0.57	186.97	277.16	265.05	185.32	166.69	141.04	212.53
z=1.02	307.72	338.39	319.01	368.22	261.55	54.27	289.73
z=1.94	375.21	331.58	347.12	273.27	268.90	140.99	285.46
z=2.85	350.90	358.68	354.12	279.12	260.14	202.79	298.98
z=3.77	376.32	370.50	360.68	265.14	242.81	87.04	282.09
z=4.78	364.65	360.04	362.52	306.89	187.78	97.72	278.87
z=5.84	393.92	387.52	379.22	329.15	184.59	57.54	287.72
z=7.78	403.29	400.81	370.27	319.85	215.49	22.16	288.81
z=9.61	414.14	423.55	321.02	337.41	123.48	103.56	274.36
z=10.09	402.86	404.63	374.11	341.02	212.93	37.18	296.45

1.15 $U_g = 9.0 \text{ m/s}$, $G_s = 400 \text{ kg/m}^2\text{s}$

Solids holdup, [m/s]

$U_g G_s 400$	r/R=0.0	r/R=0.316	r/R=0.548	r/R=0.707	r/R=0.837	r/R=0.950	Average
z=0.57	0.0087	0.0109	0.0207	0.1101	0.2033	0.0839	0.0876
z=1.02	0.0143	0.0175	0.0427	0.1044	0.2184	0.4963	0.1449
z=1.94	0.0190	0.0160	0.0328	0.0843	0.1768	0.1291	0.0850
z=2.85	0.0164	0.0177	0.0376	0.0644	0.1740	0.3962	0.1128
z=3.77	0.0153	0.0166	0.0321	0.0538	0.1096	0.1216	0.0620
z=4.78	0.0144	0.0187	0.0253	0.0537	0.0969	0.3010	0.0791
z=5.84	0.0143	0.0175	0.0242	0.0434	0.0863	0.1988	0.0618
z=7.78	0.0154	0.0195	0.0219	0.0373	0.0759	0.1988	0.0580
z=9.61	0.0152	0.0160	0.0202	0.0322	0.0598	0.2152	0.0540
z=10.09	0.0151	0.0202	0.0226	0.0369	0.0753	0.2072	0.0590

Particle velocity, [m/s]

$U_g G_s 400$	r/R=0.0	r/R=0.316	r/R=0.548	r/R=0.707	r/R=0.837	r/R=0.950	Average
z=0.57	16.14	14.41	9.82	2.26	1.01	0.49	5.90
z=1.02	13.79	12.68	6.75	2.34	1.05	0.01	4.81
z=1.94	16.48	14.78	7.07	2.57	1.22	0.14	5.40
z=2.85	19.92	16.11	7.61	3.63	1.22	0.24	6.04
z=3.77	19.54	16.93	9.16	4.63	1.64	0.26	6.88
z=4.78	20.00	16.66	9.99	4.56	2.07	0.05	7.09
z=5.84	20.47	17.22	10.32	5.39	2.08	0.16	7.47
z=7.78	20.51	17.19	12.50	6.23	2.39	0.11	8.24
z=9.61	20.40	18.58	13.04	7.61	2.68	0.48	9.06
z=10.09	20.51	16.48	12.03	6.61	2.08	0.53	8.06

Solids flux, [kg/m²s]

$U_g G_s 400$	r/R=0.0	r/R=0.316	r/R=0.548	r/R=0.707	r/R=0.837	r/R=0.950	Average
z=0.57	250.62	278.60	362.31	442.78	364.42	73.46	330.86
z=1.02	350.76	393.99	512.36	435.17	406.42	12.80	389.30
z=1.94	556.80	421.68	412.11	386.39	383.81	32.28	356.92
z=2.85	579.88	507.35	509.19	416.07	377.73	172.23	418.38
z=3.77	532.41	501.64	522.51	442.83	320.59	55.68	399.91
z=4.78	512.01	553.75	449.50	435.25	357.03	28.29	395.81
z=5.84	522.43	536.86	443.71	416.42	319.95	56.58	381.90
z=7.78	560.72	597.59	487.76	413.55	323.36	38.91	402.10
z=9.61	551.72	529.00	468.22	435.42	285.88	182.77	397.77
z=10.09	551.14	591.37	484.32	433.57	279.56	197.15	413.44

1.16 $U_g = 9.0 \text{ m/s}$, $G_s = 500 \text{ kg/m}^2\text{s}$

Solids holdup, [-]

$U_g G_s 500$	r/R=0.0	r/R=0.316	r/R=0.548	r/R=0.707	r/R=0.837	r/R=0.950	Average
z=0.57	0.0100	0.0104	0.0086	0.0103	0.0749	0.3356	0.0628
z=1.02	0.0205	0.0251	0.0139	0.0850	0.2248	0.5600	0.1440
z=1.94	0.0205	0.0227	0.0521	0.0672	0.2521	0.5598	0.1548
z=2.85	0.0205	0.0216	0.0452	0.0602	0.2329	0.2876	0.1149
z=3.77	0.0179	0.0196	0.0403	0.0548	0.2093	0.3548	0.1148
z=4.78	0.0160	0.0177	0.0402	0.0549	0.1325	0.2254	0.0818
z=5.84	0.0153	0.0164	0.0384	0.0561	0.1227	0.2552	0.0827
z=7.78	0.0154	0.0155	0.0322	0.0515	0.1227	0.3552	0.0918
z=9.61	0.0154	0.0164	0.0215	0.0544	0.1257	0.2539	0.0788
z=10.09	0.0206	0.0213	0.0211	0.0532	0.1354	0.2075	0.0761

Particle velocity, [m/s]

$U_g G_s 500$	r/R=0.0	r/R=0.316	r/R=0.548	r/R=0.707	r/R=0.837	r/R=0.950	Average
z=0.57	15.37	13.74	11.40	5.52	3.49	0.16	7.41
z=1.02	15.95	13.44	11.17	2.78	0.84	0.16	6.08
z=1.94	16.05	13.61	6.14	4.28	0.65	0.29	5.23
z=2.85	17.92	16.29	7.69	4.60	1.18	0.04	6.28
z=3.77	20.68	19.76	8.82	4.80	1.30	0.01	7.28
z=4.78	20.75	20.06	8.41	5.14	1.86	0.78	7.53
z=5.84	20.89	19.65	8.40	5.80	1.93	0.24	7.55
z=7.78	20.55	19.92	10.28	6.14	1.93	0.18	8.13
z=9.61	20.69	20.35	15.53	5.97	1.97	0.16	9.43
z=10.09	18.11	17.24	18.10	6.43	1.95	0.19	9.54

Solids flux, [kg/m²s]

$U_g G_s 500$	r/R=0.0	r/R=0.316	r/R=0.548	r/R=0.707	r/R=0.837	r/R=0.950	Average
z=0.57	272.28	253.65	175.12	101.55	464.78	95.97	229.34
z=1.02	582.41	601.30	275.64	420.45	336.97	158.31	371.06
z=1.94	586.49	550.86	569.34	511.67	291.83	286.72	456.93
z=2.85	654.49	626.48	618.80	493.30	490.66	20.46	492.37
z=3.77	659.77	691.10	632.59	468.31	484.30	6.77	499.36
z=4.78	591.00	630.43	601.29	502.25	437.82	313.34	513.68
z=5.84	569.60	574.15	573.63	579.33	422.10	109.79	486.20
z=7.78	564.54	548.09	589.11	562.79	421.53	115.85	481.71
z=9.61	567.89	594.98	594.85	577.49	441.61	73.66	494.96
z=10.09	664.39	653.89	678.69	609.06	469.11	68.54	538.98

1.17 $U_g = 9.0 \text{ m/s}$, $G_s = 600 \text{ kg/m}^2\text{s}$

Solids holdup, [-]

$U_g G_s 600$	r/R=0.0	r/R=0.316	r/R=0.548	r/R=0.707	r/R=0.837	r/R=0.950	Average
z=0.57	0.0088	0.0098	0.0107	0.1014	0.0607	0.3939	0.0876
z=1.02	0.0251	0.0230	0.0403	0.2162	0.2443	0.3541	0.1598
z=1.94	0.0211	0.0228	0.0427	0.2658	0.2382	0.3413	0.1687
z=2.85	0.0205	0.0217	0.0470	0.1684	0.3311	0.2775	0.1608
z=3.77	0.0213	0.0220	0.0458	0.1082	0.2560	0.2560	0.1275
z=4.78	0.0197	0.0222	0.0400	0.1055	0.2254	0.2175	0.1141
z=5.84	0.0196	0.0218	0.0392	0.0758	0.1882	0.2516	0.1027
z=7.78	0.0185	0.0197	0.0327	0.0558	0.1882	0.2163	0.0921
z=9.61	0.0185	0.0186	0.0278	0.0533	0.1192	0.2853	0.0828
z=10.09	0.0217	0.0217	0.0276	0.0543	0.1240	0.2219	0.0771

Particle velocity, [m/s]

$U_g G_s 600$	r/R=0.0	r/R=0.316	r/R=0.548	r/R=0.707	r/R=0.837	r/R=0.950	Average
z=0.57	15.93	15.51	10.83	2.01	3.32	0.33	6.80
z=1.02	16.80	15.90	9.58	1.07	0.44	0.19	5.70
z=1.94	17.99	17.42	9.07	1.07	0.98	0.29	6.00
z=2.85	19.96	18.87	8.70	2.28	0.94	0.16	6.45
z=3.77	19.92	17.96	8.95	3.13	1.10	0.18	6.56
z=4.78	21.22	17.81	9.71	3.40	1.11	0.33	6.80
z=5.84	20.65	19.76	9.99	4.95	1.60	0.59	7.73
z=7.78	21.47	20.15	11.88	6.15	1.72	0.22	8.51
z=9.61	21.97	21.13	14.10	7.08	2.62	0.21	9.64
z=10.09	19.63	18.88	15.08	7.18	2.72	0.70	9.54

Solids flux, [kg/m²s]

$U_g G_s 600$	r/R=0.0	r/R=0.316	r/R=0.548	r/R=0.707	r/R=0.837	r/R=0.950	Average
z=0.57	249.56	271.49	205.99	362.48	358.81	227.89	291.04
z=1.02	751.66	651.77	686.87	413.02	191.72	117.16	439.39
z=1.94	675.64	707.82	688.57	504.94	413.59	175.31	528.19
z=2.85	729.48	727.57	728.81	683.27	554.46	78.32	602.26
z=3.77	754.12	702.92	729.58	603.92	500.75	81.35	567.98
z=4.78	742.31	703.30	691.84	638.73	444.79	128.91	560.00
z=5.84	722.18	765.43	697.38	667.92	534.98	263.23	616.02
z=7.78	708.90	704.89	691.56	610.42	574.58	85.74	577.91
z=9.61	725.19	701.00	698.38	671.98	555.09	104.99	590.63
z=10.09	757.48	728.98	740.30	693.63	599.94	274.71	641.02

1.18 $U_g = 9.0 \text{ m/s}$, $G_s = 700 \text{ kg/m}^2\text{s}$

Solids holdup, [-]

$U_g G_s 700$	r/R=0.0	r/R=0.316	r/R=0.548	r/R=0.707	r/R=0.837	r/R=0.950	Average
z=0.57	0.0220	0.0242	0.0415	0.1089	0.3039	0.4873	0.1651
z=1.02	0.0413	0.0758	0.1295	0.2443	0.5482	0.4601	0.2784
z=1.94	0.0380	0.0745	0.1210	0.2557	0.5375	0.4070	0.2700
z=2.85	0.0288	0.0442	0.0732	0.1434	0.3061	0.3198	0.1650
z=3.77	0.0352	0.0474	0.0727	0.1085	0.2012	0.3357	0.1359
z=4.78	0.0290	0.0400	0.0567	0.0806	0.1741	0.3242	0.1169
z=5.84	0.0323	0.0390	0.0578	0.0751	0.1533	0.3191	0.1104
z=7.78	0.0324	0.0292	0.0347	0.0605	0.1450	0.3154	0.0974
z=9.61	0.0401	0.0412	0.0471	0.0656	0.1077	0.3183	0.0958
z=10.09	0.0431	0.0432	0.0432	0.0709	0.1071	0.3050	0.0947

Particle velocity, [m/s]

$U_g G_s 700$	r/R=0.0	r/R=0.316	r/R=0.548	r/R=0.707	r/R=0.837	r/R=0.950	Average
z=0.57	19.95	19.24	10.09	2.20	0.86	0.25	6.82
z=1.02	13.70	7.01	5.87	2.06	0.31	0.00	3.28
z=1.94	17.66	8.15	5.03	2.08	0.66	0.17	3.40
z=2.85	22.22	13.49	9.09	3.24	0.28	0.02	5.56
z=3.77	21.63	15.09	9.16	3.61	0.69	0.29	6.09
z=4.78	22.72	16.74	9.31	4.38	0.54	0.38	6.59
z=5.84	20.70	16.61	10.58	5.15	2.10	0.08	7.36
z=7.78	20.12	19.37	13.58	6.47	1.89	0.09	8.86
z=9.61	19.08	18.92	13.33	6.04	1.39	0.28	8.52
z=10.09	18.12	17.61	13.70	6.14	1.54	0.17	8.40

Solids flux, [kg/m²s]

$U_g G_s 700$	r/R=0.0	r/R=0.316	r/R=0.548	r/R=0.707	r/R=0.837	r/R=0.950	Average
z=0.57	780.89	829.38	745.68	426.37	463.65	216.49	563.45
z=1.02	1007.41	946.32	1353.47	895.71	303.30	2.39	775.68
z=1.94	1194.40	1079.80	1084.65	946.85	632.68	120.46	837.01
z=2.85	1137.46	1061.97	1184.04	826.07	151.71	9.99	708.61
z=3.77	1356.52	1273.96	1185.79	696.45	246.30	172.44	760.83
z=4.78	1172.61	1193.04	938.83	628.93	168.50	216.50	658.90
z=5.84	1188.87	1152.47	1088.33	688.14	572.67	48.19	771.14
z=7.78	1159.00	1007.05	838.86	696.53	488.13	51.18	667.07
z=9.61	1362.26	1387.64	1117.36	705.10	265.81	156.11	770.83
z=10.09	1390.02	1353.83	1054.13	774.43	293.30	90.43	763.45

1.19 $U_g = 9.0 \text{ m/s}$, $G_s = 800 \text{ kg/m}^2\text{s}$

Solids holdup, [-]

$U_g G_s 800$	r/R=0.0	r/R=0.316	r/R=0.548	r/R=0.707	r/R=0.837	r/R=0.950	Average
z=0.57	0.0133	0.0126	0.0164	0.1079	0.2644	0.4638	0.1450
z=1.02	0.0288	0.0594	0.1586	0.4370	0.5511	0.5600	0.3383
z=1.94	0.0272	0.0479	0.1263	0.4108	0.5458	0.5600	0.3213
z=2.85	0.0274	0.0479	0.1028	0.2880	0.5147	0.5600	0.2808
z=3.77	0.0281	0.0342	0.0542	0.2171	0.5285	0.5600	0.2537
z=4.78	0.0277	0.0353	0.0552	0.2125	0.4026	0.5600	0.2247
z=5.84	0.0252	0.0331	0.0652	0.2166	0.3458	0.5264	0.2109
z=7.78	0.0303	0.0345	0.0596	0.2166	0.3103	0.5600	0.2058
z=9.61	0.0422	0.0362	0.0432	0.2085	0.3263	0.5496	0.2028
z=10.09	0.0421	0.0388	0.0537	0.2089	0.3287	0.5242	0.2034

Particle velocity, [m/s]

$U_g G_s 800$	r/R=0.0	r/R=0.316	r/R=0.548	r/R=0.707	r/R=0.837	r/R=0.950	Average
z=0.57	22.31	19.93	19.74	2.88	0.64	0.25	9.36
z=1.02	20.79	10.33	3.18	0.75	0.40	0.11	3.02
z=1.94	19.93	12.43	4.29	1.07	0.48	0.19	3.78
z=2.85	21.58	13.75	5.39	1.43	0.52	0.21	4.39
z=3.77	20.28	16.99	9.71	2.04	0.51	0.29	6.19
z=4.78	21.17	17.08	10.05	1.96	0.75	0.21	6.31
z=5.84	21.93	18.04	9.38	2.02	0.95	0.29	6.41
z=7.78	22.09	18.03	10.21	2.19	0.99	0.16	6.63
z=9.61	15.40	17.43	13.18	2.07	1.00	0.11	7.19
z=10.09	15.23	16.13	10.46	2.22	1.01	0.24	6.35

Solids flux, [kg/m²s]

$U_g G_s 800$	r/R=0.0	r/R=0.316	r/R=0.548	r/R=0.707	r/R=0.837	r/R=0.950	Average
z=0.57	528.75	446.71	575.03	552.39	301.20	209.81	440.53
z=1.02	1066.49	1092.38	898.60	584.53	396.76	108.50	658.49
z=1.94	963.46	1060.62	963.72	780.01	468.45	185.04	737.38
z=2.85	1054.29	1172.39	985.91	732.32	479.95	209.72	758.83
z=3.77	1013.60	1034.65	936.96	786.89	479.42	292.47	742.73
z=4.78	1042.34	1071.88	987.17	739.85	535.31	212.22	754.26
z=5.84	982.35	1063.67	1088.80	778.88	587.77	272.24	804.60
z=7.78	1191.28	1105.89	1083.70	842.99	545.55	155.01	802.72
z=9.61	1157.35	1124.33	1012.42	767.67	580.79	104.84	774.22
z=10.09	1140.69	1115.66	999.62	826.58	591.74	227.78	799.85

1.20 $U_g = 9.0$ m/s, $G_s = 1000$ kg/m²s

Solids holdup, [-]

$U_g 9 G_s 1000$	r/R=0.0	r/R=0.316	r/R=0.548	r/R=0.707	r/R=0.837	r/R=0.950	Average
z=0.57	0.0688	0.0568	0.0775	0.2181	0.4921	0.5584	0.2554
z=1.02	0.0607	0.1038	0.3037	0.4422	0.5059	0.5600	0.3724
z=1.94	0.0668	0.1035	0.3026	0.4417	0.5060	0.5600	0.3720
z=2.85	0.0901	0.1457	0.3042	0.4826	0.5057	0.5600	0.3897
z=3.77	0.1049	0.1190	0.2853	0.4347	0.5367	0.5600	0.3762
z=4.78	0.0549	0.0975	0.2315	0.3922	0.4751	0.5593	0.3357
z=5.84	0.0575	0.0993	0.2047	0.3737	0.4921	0.5589	0.3292
z=7.78	0.0649	0.0865	0.1915	0.3883	0.4754	0.5600	0.3233
z=9.61	0.0672	0.0765	0.1246	0.3258	0.4752	0.5550	0.2907
z=10.09	0.0948	0.0908	0.1036	0.3532	0.4753	0.5549	0.2946

Particle velocity, [m/s]

$U_g 9 G_s 1000$	r/R=0.0	r/R=0.316	r/R=0.548	r/R=0.707	r/R=0.837	r/R=0.950	Average
z=0.57	10.49	8.32	3.50	1.24	1.63	0.96	3.19
z=1.02	11.59	8.80	2.78	1.57	0.11	0.45	2.79
z=1.94	15.47	9.69	2.63	1.80	0.30	0.03	2.97
z=2.85	17.60	10.57	3.32	1.54	1.00	0.23	3.42
z=3.77	17.05	11.31	4.21	2.04	0.78	0.09	3.82
z=4.78	23.91	13.72	5.10	2.03	0.99	0.11	4.55
z=5.84	23.20	13.79	5.33	2.73	0.53	0.22	4.68
z=7.78	22.45	15.80	6.05	2.16	0.78	0.30	5.18
z=9.61	23.34	15.38	6.48	2.39	0.72	0.13	5.22
z=10.09	21.27	13.33	6.03	2.39	0.99	0.34	4.80

Solids flux, [kg/m²s]

$U_g 9 G_s 1000$	r/R=0.0	r/R=0.316	r/R=0.548	r/R=0.707	r/R=0.837	r/R=0.950	Average
z=0.57	1285.02	841.18	483.22	480.96	1429.28	949.42	819.34
z=1.02	1252.17	1626.23	1503.75	1236.32	103.24	444.06	1026.58
z=1.94	1838.94	1785.71	1418.33	1415.11	272.65	26.19	1066.26
z=2.85	2821.15	2742.35	1796.46	1325.70	904.05	225.11	1485.37
z=3.77	3181.62	2396.10	2138.98	1577.39	741.52	86.44	1504.47
z=4.78	2335.11	2382.03	2101.83	1418.03	836.13	104.99	1480.24
z=5.84	2375.75	2438.35	1940.96	1813.09	464.93	218.08	1472.28
z=7.78	2594.11	2432.38	2061.27	1492.53	660.32	302.43	1480.93
z=9.61	2793.43	2094.98	1437.82	1385.36	612.49	132.27	1212.57
z=10.09	3590.31	2154.56	1111.49	1501.83	836.53	331.42	1246.71

Appendix 2. Raw data of solids holdup, particle velocity and solids flux in the CFB downer

2.1 $U_g = 1.0$ m/s, $G_s = 300$ kg/m²s

Solids holdup, [-]

U_g1G_s300	R1	R2	R3	R4	R5	R6	Average
z=0.22	0.0543	0.0544	0.0544	0.0596	0.0596	0.0473	0.0559
z=0.61	0.0438	0.0480	0.0504	0.0542	0.0543	0.0460	0.0512
z=1.12	0.0354	0.0363	0.0377	0.0400	0.0408	0.0410	0.0391
z=1.63	0.0347	0.0353	0.0368	0.0393	0.0410	0.0495	0.0395
z=2.13	0.0320	0.0334	0.0353	0.0379	0.0389	0.0424	0.0372
z=2.64	0.0307	0.0324	0.0303	0.0353	0.0370	0.0380	0.0343
z=3.26	0.0262	0.0280	0.0302	0.0323	0.0355	0.0346	0.0319
z=4.02	0.0226	0.0256	0.0280	0.0292	0.0296	0.0320	0.0286
z=4.99	0.0226	0.0212	0.0258	0.0275	0.0296	0.0327	0.0270

Particle velocity, [m/s]

U_g1G_s300	R1	R2	R3	R4	R5	R6	Average
z=0.22	2.29	2.33	2.51	2.96	3.20	3.28	2.82
z=0.61	2.78	2.91	3.03	3.25	3.71	2.63	3.16
z=1.12	4.04	4.28	4.29	4.54	4.86	3.80	4.42
z=1.63	4.20	4.59	4.68	4.69	4.94	3.93	4.64
z=2.13	4.32	4.59	4.99	5.17	5.34	3.99	4.91
z=2.64	4.54	4.61	5.03	5.58	5.92	4.03	5.16
z=3.26	4.55	4.65	5.05	6.06	6.55	4.03	5.42
z=4.02	4.56	4.76	5.05	6.50	6.86	4.23	5.63
z=4.99	4.57	4.91	5.18	7.17	7.27	4.25	5.94

Solids flux, [kg/m²s]

U_g1G_s300	R1	R2	R3	R4	R5	R6	Average
z=0.22	221.10	225.57	242.85	339.09	366.91	276.25	293.20
z=0.61	217.27	248.73	271.72	313.48	357.89	215.31	289.50
z=1.12	254.55	276.88	288.24	323.66	352.66	277.66	307.33
z=1.63	259.41	288.83	306.49	328.00	360.19	346.15	324.73
z=2.13	246.42	273.32	312.89	348.88	369.77	300.72	324.80
z=2.64	248.05	266.11	271.19	350.28	389.92	273.04	315.08
z=3.26	211.94	231.84	271.14	348.45	413.64	248.57	310.51
z=4.02	183.04	216.94	251.40	337.30	361.03	240.94	287.68
z=4.99	183.56	184.97	237.63	350.86	383.45	247.27	287.13

2.2 $U_g = 3.0 \text{ m/s}$, $G_s = 100 \text{ kg/m}^2\text{s}$

Solids holdup, [-]

U_g3G_s100	R1	R2	R3	R4	R5	R6	Average
z=0.22	0.0156	0.0152	0.0155	0.0179	0.0170	0.0157	0.0163
z=0.61	0.0121	0.0153	0.0155	0.0158	0.0165	0.0133	0.0155
z=1.12	0.0117	0.0142	0.0146	0.0146	0.0154	0.0146	0.0147
z=1.63	0.0109	0.0126	0.0127	0.0135	0.0144	0.0140	0.0134
z=2.13	0.0103	0.0114	0.0115	0.0122	0.0148	0.0168	0.0130
z=2.64	0.0099	0.0103	0.0101	0.0105	0.0122	0.0158	0.0114
z=3.26	0.0100	0.0101	0.0102	0.0098	0.0125	0.0142	0.0111
z=4.02	0.0089	0.0091	0.0097	0.0105	0.0105	0.0141	0.0105
z=4.99	0.0090	0.0094	0.0099	0.0099	0.0103	0.0138	0.0104

Particle velocity, [m/s]

U_g3G_s100	R1	R2	R3	R4	R5	R6	Average
z=0.22	2.85	2.93	3.00	3.98	3.43	3.68	3.38
z=0.61	3.20	3.13	4.20	4.18	4.54	3.88	4.03
z=1.12	4.92	4.95	5.06	5.35	5.91	4.21	5.19
z=1.63	5.13	4.69	5.50	5.43	5.93	3.88	5.23
z=2.13	5.58	5.70	5.65	5.76	6.45	3.70	5.64
z=2.64	5.71	5.83	5.80	6.06	6.70	3.60	5.81
z=3.26	5.82	5.83	5.83	6.18	6.78	3.95	5.90
z=4.02	5.84	5.86	5.84	6.20	6.60	4.27	5.91
z=4.99	5.88	5.87	5.94	6.33	6.99	4.19	6.04

Solids flux, [$\text{kg/m}^2\text{s}$]

U_g3G_s100	R1	R2	R3	R4	R5	R6	Average
z=0.22	79.33	79.49	82.78	126.66	103.42	103.03	99.13
z=0.61	68.73	85.38	115.52	117.78	133.01	92.06	111.40
z=1.12	102.24	125.17	131.61	138.88	161.90	109.59	136.24
z=1.63	99.60	104.89	124.26	130.19	151.84	96.76	124.84
z=2.13	102.74	115.96	116.17	125.19	170.36	110.26	129.66
z=2.64	100.54	107.36	104.43	113.76	145.87	101.07	116.03
z=3.26	103.16	104.35	105.69	107.58	151.31	99.78	115.42
z=4.02	92.42	94.80	100.41	115.74	123.68	107.22	108.85
z=4.99	93.95	98.28	104.66	111.84	128.48	102.71	110.19

2.3 $U_g = 3.0 \text{ m/s}$, $G_s = 200 \text{ kg/m}^2\text{s}$

Solids holdup, [-]

U_g3G_s200	R1	R2	R3	R4	R5	R6	Average
z=0.22	0.0372	0.0362	0.0375	0.0397	0.0433	0.0533	0.0409
z=0.61	0.0216	0.0206	0.0244	0.0329	0.0326	0.0328	0.0285
z=1.12	0.0166	0.0185	0.0191	0.0248	0.0262	0.0321	0.0234
z=1.63	0.0187	0.0184	0.0189	0.0224	0.0223	0.0255	0.0211
z=2.13	0.0179	0.0174	0.0175	0.0226	0.0203	0.0254	0.0202
z=2.64	0.0168	0.0163	0.0167	0.0210	0.0194	0.0250	0.0192
z=3.26	0.0192	0.0186	0.0185	0.0206	0.0243	0.0262	0.0212
z=4.02	0.0190	0.0190	0.0189	0.0173	0.0217	0.0251	0.0199
z=4.99	0.0195	0.0198	0.0194	0.0195	0.0232	0.0273	0.0213

Particle velocity, [m/s]

U_g3G_s200	R1	R2	R3	R4	R5	R6	Average
z=0.22	2.74	2.77	3.37	4.42	4.89	2.86	3.78
z=0.61	3.74	4.07	4.67	4.80	5.00	2.56	4.41
z=1.12	4.16	4.01	4.59	4.83	5.47	3.20	4.57
z=1.63	4.66	4.60	5.10	6.32	6.47	2.67	5.30
z=2.13	4.77	4.89	5.45	5.69	6.17	3.37	5.31
z=2.64	5.74	5.56	6.06	6.29	6.42	3.84	5.83
z=3.26	5.83	5.85	6.11	6.46	6.59	4.16	6.02
z=4.02	5.84	5.72	6.26	6.78	6.81	4.65	6.21
z=4.99	6.02	6.03	6.34	6.89	7.19	5.38	6.48

Solids flux, [$\text{kg/m}^2\text{s}$]

U_g3G_s200	R1	R2	R3	R4	R5	R6	Average
z=0.22	181.86	178.93	225.30	312.84	377.28	271.16	275.84
z=0.61	143.65	149.03	203.27	281.45	290.55	149.25	223.83
z=1.12	122.84	132.35	155.58	212.94	254.70	183.06	189.66
z=1.63	154.76	150.92	171.86	251.80	256.23	121.03	198.95
z=2.13	152.08	151.48	169.71	229.20	222.48	152.84	189.58
z=2.64	171.77	161.21	179.71	235.32	221.62	171.15	197.18
z=3.26	199.10	193.87	200.72	236.76	284.72	194.23	225.71
z=4.02	197.99	193.46	209.99	208.31	262.73	208.17	218.08
z=4.99	209.29	212.67	219.30	239.74	297.68	261.29	245.25

2.4 $U_g = 3.0 \text{ m/s}$, $G_s = 300 \text{ kg/m}^2\text{s}$

Solids holdup, [-]

U_g3G_s300	R1	R2	R3	R4	R5	R6	Average
z=0.22	0.0405	0.0491	0.0540	0.0539	0.0600	0.0542	0.0544
z=0.61	0.0405	0.0386	0.0353	0.0362	0.0413	0.0415	0.0382
z=1.12	0.0235	0.0271	0.0281	0.0313	0.0392	0.0511	0.0338
z=1.63	0.0296	0.0280	0.0314	0.0334	0.0343	0.0412	0.0330
z=2.13	0.0281	0.0247	0.0258	0.0315	0.0433	0.0399	0.0325
z=2.64	0.0264	0.0268	0.0273	0.0294	0.0321	0.0360	0.0298
z=3.26	0.0234	0.0243	0.0270	0.0284	0.0305	0.0319	0.0282
z=4.02	0.0212	0.0221	0.0239	0.0280	0.0302	0.0319	0.0269
z=4.99	0.0222	0.0231	0.0238	0.0273	0.0308	0.0317	0.0270

Particle velocity, [m/s]

U_g3G_s300	R1	R2	R3	R4	R5	R6	Average
z=0.22	2.01	2.09	2.09	3.20	3.43	3.38	2.79
z=0.61	3.51	3.59	3.59	4.49	4.93	3.88	4.13
z=1.12	4.15	4.03	5.14	5.64	5.89	3.21	4.98
z=1.63	4.93	5.05	5.29	5.99	6.45	3.70	5.48
z=2.13	5.46	5.48	5.93	6.16	6.31	3.69	5.72
z=2.64	5.70	5.59	6.13	6.44	6.46	3.83	5.90
z=3.26	5.72	5.89	6.28	6.57	6.81	4.12	6.13
z=4.02	5.92	5.94	6.33	6.87	7.19	4.64	6.37
z=4.99	6.19	6.24	6.57	7.33	7.41	5.89	6.79

Solids flux, [$\text{kg/m}^2\text{s}$]

U_g3G_s300	R1	R2	R3	R4	R5	R6	Average
z=0.22	145.25	182.72	200.70	307.21	391.79	325.95	279.17
z=0.61	253.16	246.85	225.41	289.40	362.34	286.38	282.04
z=1.12	173.71	194.43	256.51	314.24	410.69	292.30	296.57
z=1.63	259.81	251.45	295.75	356.67	393.60	271.78	320.23
z=2.13	273.18	241.05	272.83	345.54	486.00	261.63	329.84
z=2.64	267.36	266.33	297.62	336.80	369.71	245.24	310.52
z=3.26	237.64	254.65	302.34	332.39	369.61	233.66	307.01
z=4.02	223.05	233.82	269.40	342.75	386.46	263.21	304.80
z=4.99	244.24	257.16	278.69	356.05	406.82	332.48	327.27

2.5 $U_g = 5.0 \text{ m/s}$, $G_s = 100 \text{ kg/m}^2\text{s}$

Solids holdup, [-]

U_g5G_s100	R1	R2	R3	R4	R5	R6	Average
z=0.22	0.0111	0.0139	0.0150	0.0161	0.0121	0.0151	0.0144
z=0.61	0.0105	0.0109	0.0104	0.0101	0.0106	0.0107	0.0105
z=1.12	0.0105	0.0092	0.0095	0.0100	0.0105	0.0100	0.0099
z=1.63	0.0108	0.0106	0.0100	0.0093	0.0103	0.0101	0.0100
z=2.13	0.0105	0.0094	0.0105	0.0105	0.0100	0.0103	0.0101
z=2.64	0.0095	0.0092	0.0101	0.0102	0.0096	0.0102	0.0099
z=3.26	0.0085	0.0082	0.0093	0.0098	0.0086	0.0106	0.0092
z=4.02	0.0080	0.0080	0.0091	0.0090	0.0085	0.0102	0.0089
z=4.99	0.0076	0.0076	0.0089	0.0095	0.0103	0.0104	0.0093

Particle velocity, [m/s]

U_g5G_s100	R1	R2	R3	R4	R5	R6	Average
z=0.22	5.29	5.13	5.36	4.82	4.62	4.67	4.94
z=0.61	5.29	5.53	5.72	6.30	6.97	5.68	6.09
z=1.12	6.03	6.10	6.29	6.30	6.97	6.27	6.40
z=1.63	6.64	6.56	6.42	6.62	7.12	6.12	6.61
z=2.13	6.99	7.00	6.94	6.82	7.02	6.10	6.84
z=2.64	7.01	7.02	7.14	7.25	7.33	6.35	7.09
z=3.26	7.12	7.06	7.20	7.34	7.46	6.62	7.19
z=4.02	7.03	6.94	7.25	7.46	7.67	6.62	7.26
z=4.99	7.01	7.15	7.24	7.47	8.27	6.63	7.44

Solids flux, [$\text{kg/m}^2\text{s}$]

U_g5G_s100	R1	R2	R3	R4	R5	R6	Average
z=0.22	104.02	127.27	143.50	137.69	99.09	125.14	126.90
z=0.61	99.14	107.65	105.89	113.21	131.22	107.59	113.79
z=1.12	112.41	100.11	106.79	112.55	130.26	111.79	112.68
z=1.63	127.57	124.40	114.36	109.03	130.70	110.16	118.26
z=2.13	130.23	117.38	129.10	127.08	124.80	111.81	123.38
z=2.64	118.96	115.43	127.94	131.81	125.63	114.77	124.34
z=3.26	108.09	103.55	119.33	128.63	114.56	125.14	118.02
z=4.02	99.63	98.85	118.05	118.94	116.22	120.16	114.40
z=4.99	94.83	96.94	114.68	126.34	151.88	123.03	123.27

2.6 $U_g = 5.0 \text{ m/s}$, $G_s = 200 \text{ kg/m}^2\text{s}$

Solids holdup, [-]

U_g5G_s200	R1	R2	R3	R4	R5	R6	Average
z=0.22	0.0232	0.0247	0.0233	0.0282	0.0302	0.0307	0.0271
z=0.61	0.0219	0.0227	0.0228	0.0277	0.0242	0.0231	0.0242
z=1.12	0.0175	0.0175	0.0187	0.0189	0.0195	0.0202	0.0189
z=1.63	0.0158	0.0149	0.0140	0.0154	0.0166	0.0238	0.0162
z=2.13	0.0149	0.0145	0.0145	0.0153	0.0158	0.0222	0.0159
z=2.64	0.0140	0.0154	0.0140	0.0145	0.0162	0.0206	0.0157
z=3.26	0.0148	0.0144	0.0149	0.0140	0.0159	0.0193	0.0153
z=4.02	0.0141	0.0141	0.0143	0.0145	0.0143	0.0182	0.0148
z=4.99	0.0142	0.0143	0.0146	0.0146	0.0146	0.0184	0.0150

Particle velocity, [m/s]

U_g5G_s200	R1	R2	R3	R4	R5	R6	Average
z=0.22	3.98	4.06	4.59	5.24	6.32	4.35	5.00
z=0.61	3.80	4.10	4.99	5.34	6.47	4.53	5.18
z=1.12	5.80	6.44	6.85	7.38	7.59	5.59	6.91
z=1.63	6.07	6.33	7.08	7.46	7.87	5.91	7.06
z=2.13	6.35	6.46	7.09	7.30	7.66	6.10	7.03
z=2.64	6.69	6.45	7.31	7.58	8.15	6.22	7.26
z=3.26	7.22	7.24	7.78	7.85	8.40	6.33	7.66
z=4.02	7.47	7.44	7.78	7.83	8.46	6.16	7.69
z=4.99	7.40	7.46	7.79	7.81	8.86	6.55	7.83

Solids flux, [$\text{kg/m}^2\text{s}$]

U_g5G_s200	R1	R2	R3	R4	R5	R6	Average
z=0.22	164.17	178.85	190.26	262.50	339.14	237.87	243.56
z=0.61	148.25	165.63	202.40	262.76	279.27	186.52	224.44
z=1.12	180.83	201.04	227.68	248.56	263.55	201.33	232.25
z=1.63	171.27	167.50	175.96	203.95	233.14	249.89	202.27
z=2.13	167.97	166.99	182.84	198.75	214.89	240.39	197.40
z=2.64	166.43	177.01	181.82	195.29	235.08	228.14	201.40
z=3.26	189.89	185.80	205.86	195.96	237.07	217.41	208.14
z=4.02	188.01	186.19	197.94	202.67	215.89	199.24	200.94
z=4.99	186.81	190.43	202.86	203.37	229.54	214.94	208.01

2.7 $U_g = 5.0 \text{ m/s}$, $G_s = 300 \text{ kg/m}^2\text{s}$

Solids holdup, [-]

U_g5G_s300	R1	R2	R3	R4	R5	R6	Average
z=0.22	0.0434	0.0432	0.0432	0.0483	0.0534	0.0434	0.0467
z=0.61	0.0302	0.0329	0.0310	0.0323	0.0337	0.0403	0.0334
z=1.12	0.0299	0.0294	0.0315	0.0284	0.0334	0.0394	0.0318
z=1.63	0.0232	0.0245	0.0240	0.0271	0.0339	0.0368	0.0285
z=2.13	0.0211	0.0229	0.0236	0.0271	0.0311	0.0351	0.0273
z=2.64	0.0214	0.0231	0.0233	0.0269	0.0312	0.0369	0.0275
z=3.26	0.0231	0.0220	0.0231	0.0274	0.0301	0.0365	0.0270
z=4.02	0.0239	0.0235	0.0231	0.0253	0.0289	0.0357	0.0264
z=4.99	0.0238	0.0243	0.0232	0.0251	0.0277	0.0358	0.0263

Particle velocity, [m/s]

U_g5G_s300	R1	R2	R3	R4	R5	R6	Average
z=0.22	3.94	4.45	4.70	5.04	5.45	4.42	4.87
z=0.61	4.55	4.72	4.74	5.31	5.40	4.82	5.02
z=1.12	5.19	5.32	5.90	6.13	6.53	5.65	5.95
z=1.63	6.86	7.08	7.31	7.72	8.49	6.41	7.52
z=2.13	7.16	7.38	7.61	7.95	8.40	6.49	7.69
z=2.64	7.47	7.66	7.93	8.19	8.42	6.62	7.89
z=3.26	7.67	7.86	7.96	8.42	8.32	6.67	7.97
z=4.02	7.93	7.96	7.76	8.32	8.38	6.81	7.95
z=4.99	8.12	8.41	8.46	8.53	8.84	7.51	8.44

Solids flux, [kg/m²s]

U_g5G_s300	R1	R2	R3	R4	R5	R6	Average
z=0.22	304.54	342.34	361.52	433.54	517.95	341.22	406.96
z=0.61	245.21	276.50	260.94	305.20	324.11	345.94	298.21
z=1.12	275.89	278.34	330.74	309.74	387.99	396.32	336.52
z=1.63	283.86	309.29	312.79	371.53	512.02	420.20	382.93
z=2.13	269.08	301.24	319.55	383.01	464.84	405.54	373.25
z=2.64	285.08	315.29	328.50	392.13	467.93	434.45	384.26
z=3.26	315.42	307.49	327.48	410.13	445.39	432.96	381.35
z=4.02	336.52	332.64	318.41	374.14	430.64	432.81	372.53
z=4.99	343.24	363.72	349.11	380.85	435.93	478.56	393.92

2.8 $U_g = 7.0 \text{ m/s}$, $G_s = 200 \text{ kg/m}^2\text{s}$

Solids holdup, [-]

U_g7G_s200	R1	R2	R3	R4	R5	R6	Average
z=0.22	0.0193	0.0262	0.0238	0.0237	0.0250	0.0232	0.0244
z=0.61	0.0134	0.0131	0.0153	0.0170	0.0197	0.0216	0.0170
z=1.12	0.0125	0.0131	0.0143	0.0150	0.0154	0.0212	0.0153
z=1.63	0.0119	0.0112	0.0123	0.0127	0.0119	0.0180	0.0128
z=2.13	0.0106	0.0105	0.0109	0.0113	0.0102	0.0191	0.0117
z=2.64	0.0095	0.0111	0.0109	0.0110	0.0128	0.0163	0.0120
z=3.26	0.0112	0.0112	0.0111	0.0112	0.0115	0.0141	0.0116
z=4.02	0.0128	0.0121	0.0114	0.0114	0.0103	0.0120	0.0114
z=4.99	0.0127	0.0122	0.0121	0.0112	0.0117	0.0125	0.0119

Particle velocity, [m/s]

U_g7G_s200	R1	R2	R3	R4	R5	R6	Average
z=0.22	4.69	4.93	4.48	4.46	4.74	5.14	4.70
z=0.61	5.45	5.74	5.98	6.16	6.47	6.02	6.09
z=1.12	6.77	6.50	6.90	7.26	7.53	7.20	7.08
z=1.63	7.82	7.83	7.81	7.98	8.26	7.42	7.91
z=2.13	8.31	8.39	8.29	8.80	8.89	7.37	8.45
z=2.64	8.75	8.94	8.94	8.92	9.03	7.62	8.80
z=3.26	8.97	9.03	9.26	9.49	9.08	7.78	9.05
z=4.02	9.02	9.39	9.57	9.60	9.22	7.82	9.26
z=4.99	9.34	9.64	9.62	9.61	8.95	8.28	9.31

Solids flux, [$\text{kg/m}^2\text{s}$]

U_g7G_s200	R1	R2	R3	R4	R5	R6	Average
z=0.22	161.21	229.87	189.79	188.39	210.50	212.52	204.52
z=0.61	130.27	134.06	162.96	185.85	226.43	231.04	184.91
z=1.12	150.54	151.37	175.00	193.89	205.88	271.84	193.12
z=1.63	166.14	156.35	170.74	181.19	174.29	238.22	179.10
z=2.13	156.33	156.21	161.41	176.56	162.03	250.42	174.49
z=2.64	148.15	176.43	173.87	174.75	205.97	221.30	187.38
z=3.26	178.70	179.77	182.43	189.96	185.44	195.88	185.89
z=4.02	205.77	201.47	193.43	195.52	169.78	167.23	187.04
z=4.99	210.53	209.33	207.64	192.30	186.17	183.69	196.83

2.9 $U_g = 7.0 \text{ m/s}$, $G_s = 300 \text{ kg/m}^2\text{s}$

Solids holdup, [-]

U_g7G_s300	R1	R2	R3	R4	R5	R6	Average
z=0.22	0.0228	0.0255	0.0257	0.0243	0.0430	0.0328	0.0301
z=0.61	0.0200	0.0232	0.0238	0.0264	0.0266	0.0271	0.0253
z=1.12	0.0214	0.0246	0.0233	0.0204	0.0252	0.0268	0.0237
z=1.63	0.0179	0.0178	0.0181	0.0193	0.0203	0.0233	0.0194
z=2.13	0.0162	0.0161	0.0165	0.0174	0.0204	0.0227	0.0182
z=2.64	0.0152	0.0151	0.0145	0.0174	0.0200	0.0246	0.0177
z=3.26	0.0158	0.0146	0.0150	0.0160	0.0182	0.0241	0.0170
z=4.02	0.0157	0.0145	0.0147	0.0166	0.0171	0.0240	0.0167
z=4.99	0.0156	0.0146	0.0148	0.0155	0.0167	0.0241	0.0165

Particle velocity, [m/s]

U_g7G_s300	R1	R2	R3	R4	R5	R6	Average
z=0.22	4.89	4.75	5.05	5.14	5.11	4.91	5.01
z=0.61	5.79	5.57	5.85	5.99	6.41	6.91	6.08
z=1.12	7.29	6.97	6.96	7.03	7.11	7.65	7.09
z=1.63	7.99	8.15	8.43	8.77	9.23	8.25	8.61
z=2.13	8.85	8.50	8.83	9.14	9.40	8.83	8.97
z=2.64	9.87	9.70	9.75	10.06	10.11	8.98	9.80
z=3.26	9.83	10.11	10.15	10.21	10.28	8.92	10.04
z=4.02	9.96	9.93	10.15	10.28	10.42	9.29	10.10
z=4.99	10.26	10.37	10.33	10.39	10.79	9.76	10.39

Solids flux, [$\text{kg/m}^2\text{s}$]

U_g7G_s300	R1	R2	R3	R4	R5	R6	Average
z=0.22	198.58	215.35	230.89	221.79	390.72	286.91	268.40
z=0.61	206.56	230.23	247.87	281.37	303.54	333.88	274.75
z=1.12	278.14	305.05	288.51	254.88	318.71	364.51	299.82
z=1.63	253.85	258.23	270.99	300.82	333.53	342.72	297.83
z=2.13	254.58	243.68	259.75	282.60	341.96	356.89	291.80
z=2.64	267.03	260.99	252.04	310.83	359.05	392.78	307.78
z=3.26	275.70	263.13	271.81	290.88	332.61	383.31	301.30
z=4.02	278.47	256.02	264.95	303.48	316.49	396.46	299.09
z=4.99	284.07	269.83	272.23	287.21	320.25	419.08	303.30

Appendix 3. Raw data of ozone concentration in the CFB riser

3.1 $U_g = 5.0$ m/s

Dimensionless ozone concentration, [-]

$U_g G_s 100$	r/R=0.0	r/R=0.316	r/R=0.548	r/R=0.707	r/R=0.837	r/R=0.950	Average
z=0.57	0.6044	0.5628	0.5448	0.4759	0.3032	0.1985	0.4374
z=1.02	0.5738	0.5619	0.5057	0.4328	0.2894	0.2399	0.4199
z=1.94	0.5433	0.5609	0.4666	0.3896	0.2756	0.2313	0.3966
z=2.85	0.5367	0.5460	0.4143	0.3225	0.2587	0.2080	0.3595
z=3.77	0.5428	0.5336	0.4338	0.2985	0.2520	0.1885	0.3525
z=4.78	0.5489	0.4963	0.4533	0.2996	0.2578	0.1816	0.3506
z=5.84	0.5056	0.4840	0.4516	0.2988	0.2543	0.1567	0.3440
z=7.78	0.5119	0.4529	0.4663	0.2871	0.2624	0.1802	0.3434
z=9.61	0.4924	0.4686	0.4406	0.2845	0.2410	0.1643	0.3331
z=10.09	0.4447	0.4470	0.4400	0.2740	0.2490	0.1740	0.3293

Dimensionless ozone concentration, [-]

$U_g G_s 200$	r/R=0.0	r/R=0.316	r/R=0.548	r/R=0.707	r/R=0.837	r/R=0.950	Average
z=0.57	0.7402	0.6551	0.5652	0.4369	0.3070	0.1793	0.4498
z=1.02	0.6611	0.5849	0.3850	0.3474	0.2286	0.2104	0.3591
z=1.94	0.6537	0.5309	0.3502	0.3314	0.1742	0.1612	0.3188
z=2.85	0.5479	0.4281	0.3589	0.2752	0.2312	0.1745	0.3027
z=3.77	0.5431	0.3947	0.3395	0.2725	0.2282	0.1747	0.2904
z=4.78	0.5011	0.3774	0.3211	0.2565	0.2260	0.1594	0.2768
z=5.84	0.4484	0.3755	0.2214	0.2107	0.1894	0.1514	0.2331
z=7.78	0.3547	0.3060	0.2783	0.2580	0.1649	0.1573	0.2393
z=9.61	0.3407	0.3092	0.2601	0.1682	0.1667	0.1582	0.2156
z=10.09	0.3560	0.3248	0.2456	0.1916	0.1519	0.1175	0.2124

Dimensionless ozone concentration, [-]

$U_g G_s 300$	r/R=0.0	r/R=0.316	r/R=0.548	r/R=0.707	r/R=0.837	r/R=0.950	Average
z=0.57	0.7010	0.5766	0.5030	0.3953	0.1017	0.0723	0.3516
z=1.02	0.5431	0.4712	0.4582	0.3644	0.1955	0.0575	0.3331
z=1.94	0.5067	0.4284	0.3006	0.2714	0.1361	0.0665	0.2540
z=2.85	0.4639	0.3459	0.3000	0.2700	0.1167	0.0535	0.2317
z=3.77	0.4250	0.3447	0.2890	0.2589	0.1181	0.0519	0.2265
z=4.78	0.3746	0.3226	0.2715	0.2462	0.1083	0.0790	0.2162
z=5.84	0.2961	0.2679	0.2519	0.2315	0.1016	0.0645	0.1944
z=7.78	0.2630	0.2009	0.2349	0.2160	0.1142	0.0655	0.1769
z=9.61	0.2443	0.2361	0.1901	0.1878	0.1034	0.0632	0.1639
z=10.09	0.2234	0.2127	0.1773	0.1741	0.1197	0.0627	0.1569

Dimensionless ozone concentration, [-]

$U_g 5 G_s 400$	r/R=0.0	r/R=0.316	r/R=0.548	r/R=0.707	r/R=0.837	r/R=0.950	Average
z=0.57	0.5353	0.4971	0.4336	0.3407	0.1567	0.0623	0.3186
z=1.02	0.4682	0.4062	0.3950	0.3142	0.1685	0.0496	0.2871
z=1.94	0.4368	0.3693	0.2592	0.2340	0.1174	0.0573	0.2189
z=2.85	0.3999	0.2982	0.2586	0.2328	0.1006	0.0461	0.1997
z=3.77	0.3664	0.2971	0.2491	0.2232	0.0673	0.0447	0.1875
z=4.78	0.3229	0.2781	0.2341	0.2122	0.0589	0.0336	0.1745
z=5.84	0.2553	0.2309	0.2172	0.1996	0.0531	0.0211	0.1558
z=7.78	0.2267	0.1732	0.2025	0.1862	0.0640	0.0220	0.1407
z=9.61	0.2106	0.2035	0.1639	0.1619	0.0547	0.0200	0.1295
z=10.09	0.1926	0.1834	0.1529	0.1501	0.0342	0.0195	0.1157

3.2 $U_g = 7.0$ m/s

Dimensionless ozone concentration, [-]

$U_g 7 G_s 100$	r/R=0.0	r/R=0.316	r/R=0.548	r/R=0.707	r/R=0.837	r/R=0.950	Average
z=0.57	0.7443	0.6392	0.5804	0.5894	0.5402	0.4336	0.5674
z=1.02	0.6112	0.6121	0.5609	0.5571	0.4859	0.4019	0.5343
z=1.94	0.6009	0.5907	0.5256	0.4147	0.3617	0.3270	0.4527
z=2.85	0.6193	0.5801	0.5054	0.4143	0.3666	0.3359	0.4479
z=3.77	0.6101	0.5703	0.4852	0.3842	0.3490	0.3163	0.4281
z=4.78	0.6009	0.5907	0.4953	0.4147	0.3617	0.3270	0.4455
z=5.84	0.5994	0.5634	0.4899	0.3867	0.3715	0.3091	0.4327
z=7.78	0.5906	0.5426	0.5021	0.3616	0.3350	0.3141	0.4182
z=9.61	0.5582	0.5584	0.5115	0.3281	0.3037	0.3072	0.4080
z=10.09	0.5315	0.5423	0.5106	0.3161	0.2971	0.2893	0.3984

Dimensionless ozone concentration, [-]

$U_g 7 G_s 200$	r/R=0.0	r/R=0.316	r/R=0.548	r/R=0.707	r/R=0.837	r/R=0.950	Average
z=0.57	0.7141	0.7189	0.6238	0.5578	0.4348	0.3138	0.5480
z=1.02	0.6813	0.6653	0.5593	0.4694	0.3275	0.2761	0.4737
z=1.94	0.6814	0.6769	0.5232	0.4737	0.2622	0.1839	0.4428
z=2.85	0.6365	0.5761	0.5056	0.3893	0.2615	0.1814	0.3996
z=3.77	0.6027	0.5703	0.4299	0.3892	0.2533	0.1743	0.3778
z=4.78	0.5807	0.5664	0.4253	0.3876	0.2423	0.1499	0.3702
z=5.84	0.4881	0.4786	0.4205	0.3656	0.2413	0.1420	0.3460
z=7.78	0.4684	0.4719	0.4148	0.3399	0.2421	0.1269	0.3359
z=9.61	0.4615	0.4288	0.4045	0.3383	0.2188	0.1053	0.3171
z=10.09	0.4274	0.4021	0.3673	0.3180	0.2062	0.1086	0.2960

Dimensionless ozone concentration, [-]

U_g7G_s300	r/R=0.0	r/R=0.316	r/R=0.548	r/R=0.707	r/R=0.837	r/R=0.950	Average
z=0.57	0.6779	0.6152	0.5791	0.5854	0.4203	0.4403	0.5354
z=1.02	0.6345	0.6087	0.5300	0.3618	0.3141	0.3106	0.4325
z=1.94	0.5663	0.5826	0.3954	0.3055	0.2972	0.3039	0.3781
z=2.85	0.5085	0.4038	0.4119	0.2985	0.2948	0.2678	0.3412
z=3.77	0.5085	0.4038	0.3664	0.2985	0.2796	0.2526	0.3252
z=4.78	0.4585	0.3930	0.3506	0.3154	0.2397	0.2399	0.3127
z=5.84	0.5083	0.3505	0.3528	0.3046	0.2201	0.1919	0.2926
z=7.78	0.4261	0.3916	0.3449	0.3096	0.2011	0.1739	0.2934
z=9.61	0.4079	0.3585	0.3216	0.2623	0.2107	0.1539	0.2705
z=10.09	0.3908	0.3518	0.2842	0.2510	0.1867	0.1613	0.2532

Dimensionless ozone concentration, [-]

U_g7G_s400	r/R=0.0	r/R=0.316	r/R=0.548	r/R=0.707	r/R=0.837	r/R=0.950	Average
z=0.57	0.7205	0.7221	0.6099	0.5402	0.3848	0.2077	0.5176
z=1.02	0.6459	0.6132	0.5055	0.4050	0.3630	0.1916	0.4343
z=1.94	0.5410	0.5579	0.4324	0.3386	0.2722	0.1434	0.3651
z=2.85	0.5102	0.4570	0.3868	0.2754	0.2393	0.1376	0.3124
z=3.77	0.4458	0.4090	0.3023	0.2515	0.2008	0.1252	0.2676
z=4.78	0.4148	0.3610	0.3178	0.2442	0.1955	0.1296	0.2597
z=5.84	0.4021	0.3461	0.2679	0.2205	0.1763	0.1264	0.2349
z=7.78	0.3842	0.3183	0.2505	0.2183	0.1713	0.1279	0.2240
z=9.61	0.3842	0.2919	0.2616	0.2100	0.1704	0.1320	0.2199
z=10.09	0.2868	0.2631	0.2571	0.1738	0.1788	0.1237	0.2060

Dimensionless ozone concentration, [-]

U_g7G_s600	r/R=0.0	r/R=0.316	r/R=0.548	r/R=0.707	r/R=0.837	r/R=0.950	Average
z=0.57	0.7495	0.6732	0.5816	0.3686	0.3059	0.1335	0.4360
z=1.02	0.6521	0.5400	0.4561	0.2943	0.2066	0.0645	0.3332
z=1.94	0.6000	0.4752	0.3337	0.1981	0.1659	0.1179	0.2669
z=2.85	0.4964	0.3871	0.2716	0.1870	0.1516	0.1282	0.2307
z=3.77	0.3700	0.3346	0.2039	0.1993	0.1438	0.1096	0.2034
z=4.78	0.3688	0.2901	0.2046	0.1825	0.1463	0.1149	0.1923
z=5.84	0.3522	0.2764	0.2053	0.1656	0.1487	0.1201	0.1872
z=7.78	0.3377	0.2670	0.1916	0.1669	0.1412	0.1095	0.1795
z=9.61	0.3136	0.2449	0.1745	0.1518	0.1288	0.0905	0.1627
z=10.09	0.2889	0.2062	0.1518	0.1443	0.1381	0.0783	0.1488

Dimensionless ozone concentration, [-]

U_g7G_s700	r/R=0.0	r/R=0.316	r/R=0.548	r/R=0.707	r/R=0.837	r/R=0.950	Average
z=0.57	0.5945	0.5597	0.4628	0.3464	0.3059	0.1302	0.3805
z=1.02	0.4888	0.4388	0.3963	0.3063	0.1988	0.1075	0.3056
z=1.94	0.4450	0.3703	0.2960	0.2510	0.1565	0.0886	0.2443
z=2.85	0.4111	0.3165	0.2617	0.2146	0.1376	0.1049	0.2151
z=3.77	0.4197	0.2513	0.1983	0.1856	0.1412	0.0994	0.1811
z=4.78	0.3882	0.2262	0.1849	0.1667	0.1347	0.0940	0.1667
z=5.84	0.3851	0.2092	0.1776	0.1316	0.1272	0.0752	0.1498
z=7.78	0.3268	0.1682	0.1421	0.1203	0.1015	0.0703	0.1246
z=9.61	0.3269	0.2167	0.1011	0.0995	0.0868	0.0825	0.1175
z=10.09	0.3232	0.1826	0.1128	0.0919	0.0855	0.0702	0.1103

3.3 $U_g = 9.0$ m/s

Dimensionless ozone concentration, [-]

U_g9G_s100	r/R=0.0	r/R=0.316	r/R=0.548	r/R=0.707	r/R=0.837	r/R=0.950	Average
z=0.57	0.7979	0.7446	0.7464	0.7567	0.7749	0.6960	0.7488
z=1.02	0.7874	0.7959	0.7717	0.7019	0.6327	0.6133	0.7106
z=1.94	0.7874	0.7548	0.7495	0.6294	0.6077	0.6008	0.6738
z=2.85	0.7633	0.7442	0.7309	0.6190	0.5688	0.5411	0.6492
z=3.77	0.7468	0.7301	0.7102	0.6023	0.5704	0.5388	0.6379
z=4.78	0.7303	0.7284	0.6646	0.5857	0.5596	0.4865	0.6143
z=5.84	0.7214	0.7121	0.6730	0.5752	0.5485	0.4777	0.6073
z=7.78	0.7048	0.6755	0.6669	0.5636	0.5501	0.4796	0.5967
z=9.61	0.6783	0.6627	0.6734	0.5731	0.5243	0.4693	0.5910
z=10.09	0.6743	0.6562	0.6377	0.5636	0.5126	0.4401	0.5730

Dimensionless ozone concentration, [-]

U_g9G_s200	r/R=0.0	r/R=0.316	r/R=0.548	r/R=0.707	r/R=0.837	r/R=0.950	Average
z=0.57	0.8299	0.8426	0.7893	0.7661	0.5917	0.4527	0.7101
z=1.02	0.8052	0.8057	0.7691	0.6789	0.4806	0.4338	0.6512
z=1.94	0.7723	0.7874	0.7744	0.6679	0.5162	0.4414	0.6554
z=2.85	0.7570	0.7482	0.7035	0.6481	0.4937	0.4313	0.6202
z=3.77	0.7501	0.7109	0.6991	0.5274	0.4519	0.4244	0.5744
z=4.78	0.7025	0.6696	0.6687	0.5279	0.4517	0.4285	0.5598
z=5.84	0.6899	0.6137	0.5850	0.5122	0.4354	0.4145	0.5202
z=7.78	0.6740	0.6163	0.5862	0.5180	0.4355	0.4141	0.5223
z=9.61	0.6018	0.5438	0.5105	0.5018	0.4244	0.4141	0.4842
z=10.09	0.5577	0.5363	0.5007	0.4796	0.4219	0.4218	0.4757

Dimensionless ozone concentration, [-]

U_9G_s300	r/R=0.0	r/R=0.316	r/R=0.548	r/R=0.707	r/R=0.837	r/R=0.950	Average
z=0.57	0.8429	0.8461	0.8020	0.7600	0.6364	0.4832	0.7261
z=1.02	0.7840	0.7192	0.6498	0.5830	0.5318	0.4287	0.5953
z=1.94	0.6805	0.6669	0.5740	0.5265	0.4761	0.4393	0.5432
z=2.85	0.5842	0.5659	0.4977	0.4973	0.4553	0.4073	0.4905
z=3.77	0.5770	0.5619	0.4771	0.4490	0.3993	0.3552	0.4552
z=4.78	0.5014	0.5039	0.4253	0.4815	0.4179	0.3875	0.4471
z=5.84	0.4713	0.4841	0.4056	0.4656	0.3806	0.3678	0.4242
z=7.78	0.5806	0.5626	0.4097	0.3783	0.3511	0.3133	0.4074
z=9.61	0.5841	0.5570	0.4967	0.2939	0.2828	0.2697	0.3874
z=10.09	0.5710	0.5548	0.4551	0.3103	0.2799	0.2551	0.3784

Dimensionless ozone concentration, [-]

U_9G_s400	r/R=0.0	r/R=0.316	r/R=0.548	r/R=0.707	r/R=0.837	r/R=0.950	Average
z=0.57	0.7496	0.7352	0.6885	0.6024	0.5264	0.3912	0.6064
z=1.02	0.6872	0.6620	0.5751	0.5302	0.4719	0.2939	0.5252
z=1.94	0.6284	0.6079	0.5302	0.4746	0.3833	0.3200	0.4747
z=2.85	0.6056	0.5653	0.5054	0.3891	0.3358	0.2813	0.4260
z=3.77	0.5305	0.5067	0.4504	0.3548	0.3074	0.2198	0.3801
z=4.78	0.5191	0.4885	0.4359	0.3395	0.2791	0.2168	0.3630
z=5.84	0.5111	0.4809	0.4035	0.3162	0.2824	0.1980	0.3471
z=7.78	0.4763	0.4504	0.3849	0.3048	0.2486	0.1924	0.3260
z=9.61	0.4656	0.4365	0.3588	0.2937	0.2309	0.1867	0.3099
z=10.09	0.4341	0.4225	0.3340	0.2939	0.2025	0.1765	0.2937

Dimensionless ozone concentration, [-]

U_9G_s600	r/R=0.0	r/R=0.316	r/R=0.548	r/R=0.707	r/R=0.837	r/R=0.950	Average
z=0.57	0.7496	0.7242	0.6387	0.5412	0.4067	0.2828	0.5388
z=1.02	0.7071	0.6640	0.5731	0.4379	0.3234	0.2503	0.4656
z=1.94	0.6631	0.5978	0.4967	0.4026	0.2866	0.1931	0.4117
z=2.85	0.6404	0.5411	0.4418	0.3361	0.2217	0.1900	0.3577
z=3.77	0.5707	0.4500	0.3962	0.2690	0.2109	0.1753	0.3099
z=4.78	0.5778	0.4522	0.3282	0.2497	0.1969	0.1683	0.2858
z=5.84	0.5503	0.4382	0.2891	0.2327	0.1980	0.1737	0.2709
z=7.78	0.4882	0.4523	0.2526	0.2241	0.1926	0.1899	0.2636
z=9.61	0.4745	0.4646	0.2402	0.1757	0.1895	0.1782	0.2500
z=10.09	0.3982	0.4020	0.1904	0.1522	0.2614	0.1539	0.2341

Dimensionless ozone concentration, [-]

U_g9G_s700	r/R=0.0	r/R=0.316	r/R=0.548	r/R=0.707	r/R=0.837	r/R=0.950	Average
z=0.57	0.6838	0.6270	0.5855	0.4448	0.4107	0.2993	0.4885
z=1.02	0.6763	0.5818	0.5577	0.3373	0.2898	0.1725	0.4066
z=1.94	0.6028	0.5519	0.4066	0.2655	0.2210	0.1551	0.3311
z=2.85	0.5576	0.5119	0.3566	0.2626	0.2009	0.1567	0.3065
z=3.77	0.5046	0.4355	0.3088	0.2544	0.2173	0.1494	0.2814
z=4.78	0.4479	0.4046	0.2643	0.2326	0.1874	0.1122	0.2488
z=5.84	0.4092	0.3690	0.2232	0.2151	0.1846	0.1051	0.2268
z=7.78	0.3705	0.3350	0.2149	0.1835	0.1607	0.1080	0.2061
z=9.61	0.3728	0.2896	0.2098	0.1502	0.1385	0.1080	0.1836
z=10.09	0.3371	0.2572	0.2065	0.1113	0.1040	0.0619	0.1545

Dimensionless ozone concentration, [-]

U_g9G_s800	r/R=0.0	r/R=0.316	r/R=0.548	r/R=0.707	r/R=0.837	r/R=0.950	Average
z=0.57	0.7931	0.7000	0.5705	0.4445	0.3252	0.1491	0.4619
z=1.02	0.7606	0.6219	0.5270	0.3094	0.1928	0.1856	0.3804
z=1.94	0.6752	0.5081	0.3891	0.2645	0.1494	0.0735	0.2926
z=2.85	0.5931	0.4159	0.3166	0.1697	0.1181	0.0933	0.2314
z=3.77	0.5292	0.3339	0.2729	0.1749	0.1149	0.0894	0.2052
z=4.78	0.4427	0.2785	0.2368	0.0796	0.0833	0.0896	0.1572
z=5.84	0.3873	0.2637	0.1942	0.1126	0.0606	0.0992	0.1478
z=7.78	0.3598	0.2611	0.1514	0.1171	0.0646	0.0781	0.1365
z=9.61	0.2762	0.2172	0.1381	0.1251	0.0674	0.0792	0.1275
z=10.09	0.1800	0.1507	0.1411	0.1130	0.0621	0.0454	0.1075

Appendix 4. Raw data of ozone concentration in the CFB downer

4.1 $U_g = 3.0$ m/s

Dimensionless ozone concentration, [-]

$U_g 3G_s 100$	r/R=0.0	r/R=0.316	r/R=0.548	r/R=0.707	r/R=0.837	r/R=0.950	Average
z=0.22	0.5973	0.5658	0.4834	0.4848	0.3704	0.3490	0.4583
z=0.61	0.5869	0.5478	0.5161	0.4765	0.3105	0.2971	0.4411
z=1.12	0.4923	0.4869	0.4666	0.2954	0.2874	0.2729	0.3685
z=1.63	0.4594	0.4302	0.4067	0.2947	0.2466	0.2406	0.3302
z=2.13	0.4500	0.4244	0.3978	0.2931	0.2562	0.2424	0.3290
z=2.64	0.4273	0.4273	0.3303	0.2555	0.2578	0.2149	0.3020
z=3.26	0.3921	0.3698	0.3161	0.2809	0.2350	0.1920	0.2855
z=4.02	0.3664	0.3495	0.2704	0.2667	0.2526	0.1819	0.2703
z=4.99	0.3364	0.3608	0.2790	0.2509	0.2479	0.1815	0.2699

Dimensionless ozone concentration, [-]

$U_g 3G_s 200$	r/R=0.0	r/R=0.316	r/R=0.548	r/R=0.707	r/R=0.837	r/R=0.950	Average
z=0.22	0.5167	0.4980	0.5015	0.4758	0.3850	0.3362	0.4493
z=0.61	0.4374	0.3854	0.3307	0.3268	0.2964	0.2788	0.3265
z=1.12	0.3884	0.3506	0.2963	0.2619	0.2578	0.2505	0.2848
z=1.63	0.3499	0.2985	0.2563	0.2241	0.1764	0.1653	0.2284
z=2.13	0.2772	0.2570	0.2246	0.1884	0.1564	0.1291	0.1960
z=2.64	0.2639	0.2321	0.2107	0.1781	0.1412	0.1123	0.1802
z=3.26	0.2214	0.2177	0.2100	0.1556	0.1509	0.1187	0.1751
z=4.02	0.2240	0.2093	0.1893	0.1583	0.1429	0.1165	0.1671
z=4.99	0.2098	0.1953	0.1790	0.1434	0.1242	0.1025	0.1527

Dimensionless ozone concentration, [-]

$U_g 3G_s 300$	r/R=0.0	r/R=0.316	r/R=0.548	r/R=0.707	r/R=0.837	r/R=0.950	Average
z=0.22	0.5050	0.4946	0.4650	0.4305	0.3856	0.2965	0.4251
z=0.61	0.4468	0.3910	0.3082	0.3798	0.2732	0.2590	0.3267
z=1.12	0.3381	0.2711	0.2370	0.1944	0.1523	0.1298	0.2022
z=1.63	0.2537	0.2318	0.1970	0.1597	0.1318	0.1066	0.1699
z=2.13	0.2326	0.2017	0.1586	0.1398	0.1120	0.0999	0.1452
z=2.64	0.1876	0.1620	0.1380	0.1141	0.1030	0.0808	0.1225
z=3.26	0.1932	0.1501	0.1250	0.1140	0.0903	0.0700	0.1130
z=4.02	0.1591	0.1391	0.1072	0.0991	0.0740	0.0524	0.0976
z=4.99	0.1336	0.1318	0.0984	0.0923	0.0656	0.0505	0.0904

4.2 $U_g = 5.0$ m/s

Dimensionless ozone concentration, [-]

$U_{g5}G_{s200}$	r/R=0.0	r/R=0.316	r/R=0.548	r/R=0.707	r/R=0.837	r/R=0.950	Average
z=0.22	0.6867	0.6564	0.6206	0.5479	0.5025	0.4619	0.5657
z=0.61	0.6861	0.6425	0.5737	0.5201	0.5054	0.3887	0.5376
z=1.12	0.6462	0.5904	0.5506	0.4971	0.4391	0.3464	0.4969
z=1.63	0.6400	0.5348	0.5094	0.4617	0.4173	0.3286	0.4614
z=2.13	0.5946	0.5295	0.4440	0.4291	0.3815	0.3308	0.4296
z=2.64	0.5745	0.5001	0.4293	0.4022	0.3559	0.3118	0.4064
z=3.26	0.5359	0.4861	0.4275	0.3894	0.3412	0.2977	0.3954
z=4.02	0.5208	0.4843	0.4166	0.3750	0.3074	0.2869	0.3803
z=4.99	0.5086	0.4661	0.3939	0.3500	0.3058	0.2721	0.3636

Dimensionless ozone concentration, [-]

$U_{g5}G_{s300}$	r/R=0.0	r/R=0.316	r/R=0.548	r/R=0.707	r/R=0.837	r/R=0.950	Average
z=0.22	0.5517	0.5516	0.5816	0.5516	0.4815	0.4546	0.5315
z=0.61	0.5498	0.5368	0.5073	0.4757	0.4362	0.3682	0.4734
z=1.12	0.5207	0.5028	0.4780	0.4570	0.3893	0.3372	0.4415
z=1.63	0.5053	0.4761	0.4285	0.3975	0.3594	0.3232	0.4027
z=2.13	0.4633	0.4305	0.3984	0.3587	0.3326	0.2920	0.3682
z=2.64	0.4416	0.4087	0.3710	0.3545	0.3140	0.2773	0.3506
z=3.26	0.4191	0.3972	0.3642	0.3201	0.2854	0.2505	0.3294
z=4.02	0.3828	0.3554	0.3384	0.3024	0.2788	0.2557	0.3103
z=4.99	0.3878	0.3426	0.3372	0.3319	0.2673	0.2573	0.3119

4.3 $U_g = 7.0$ m/s

Dimensionless ozone concentration, [-]

$U_{g7}G_{s200}$	r/R=0.0	r/R=0.316	r/R=0.548	r/R=0.707	r/R=0.837	r/R=0.950	Average
z=0.22	0.8476	0.8270	0.7881	0.7738	0.8024	0.7738	0.7939
z=0.61	0.8284	0.8192	0.7462	0.7079	0.6378	0.6042	0.7104
z=1.12	0.7774	0.7919	0.7031	0.6786	0.6338	0.6307	0.6905
z=1.63	0.7211	0.7045	0.6915	0.6448	0.6242	0.6174	0.6595
z=2.13	0.7011	0.6848	0.6590	0.6332	0.6069	0.6011	0.6396
z=2.64	0.6789	0.6567	0.6363	0.6172	0.6035	0.5894	0.6230
z=3.26	0.6625	0.6478	0.6292	0.6185	0.5879	0.5721	0.6143
z=4.02	0.6492	0.6388	0.6221	0.6102	0.5792	0.5478	0.6042
z=4.99	0.6174	0.6286	0.5950	0.5924	0.5645	0.5440	0.5880

Curriculum Vitae

Name: Chengxiu Wang

Place of Birth Shandong, China

Post-secondary Education: Department of Chemical and Biochemical Engineering,
University of Western Ontario, London, Ontario, Canada
2010-2013 Ph.D Candidate

Department of Chemical Engineering,
China University of Petroleum, Qingdao, Shandong, China
2007-now Ph.D Candidate
2003-2007 B Sc.

Work Experience: Research Assistant and Teaching Assistant
University of Western Ontario, London, Ontario, Canada
2010-2013

Research Assistant
China University of Petroleum
Qingdao, Shandong, China
2007-2010

Honours and Awards: Graduate Student Scholarship, University of Western Ontario, Canada
2010-2013

Chinese Government Scholarship, China
2010-2012

Excellent Graduate Scholarship , China University of Petroleum, China
2009

Excellent Student Scholarship, China University of Petroleum, China
2003-2007

Chinese Government Scholarship, China
2005

Publications:

- Chengxiu Wang, Jesse Zhu, Shahzad Barghi and Chunyi Li, 2013, Axial and radial distribution of solids holdup and flow development in a high density gas-solids circulating fluidized, *AIChE Journal*, submitted.
- Chengxiu Wang, Jesse Zhu, Shahzad Barghi and Chunyi Li, 2013, Axial and radial distribution of particle velocity and solids flux in a high density gas-solids circulating fluidized, *Chemical Engineering Science*, submitted.
- Chengxiu Wang, Shahzad Barghi, Jesse Zhu and Chunyi Li, 2013, A comprehensive study of hydrodynamics in a high flux circulating fluidized bed downer, ready to be submitted.
- Chengxiu Wang, Gang Wang, Shahzad Barghi and Jesse Zhu, 2013, Catalytic ozone decomposition in a high density gas-solids circulating fluidized bed riser, ready to be submitted.
- Chengxiu Wang, Shahzad Barghi and Jesse Zhu, 2013, Catalytic ozone decomposition in a high flux gas-solids circulating fluidized bed downer, ready to be submitted.
- Chengxiu Wang, Shahzad Barghi, Chunyi Li and Jesse Zhu, 2013, Detailed study of hydrodynamics in a high density gas-solids circulating fluidized bed. *CSCHE*, submitted.
- Chengxiu Wang, Shahzad Barghi and Jesse Zhu, 2013, A Comparative study of ozone decomposition in high density circulating fluidized bed riser and downer reactors. *CSCHE*, submitted.
- Jesse Zhu and Chengxiu Wang, 2011, Research progresses in fluid catalytic cracking. *Chemical Engineering and Technology (TAIWAN)*, 221 (8): 98-125.